Final Report

WiFly: An emergency communication network for disaster areas

WiFly Team

Delft University of Technology

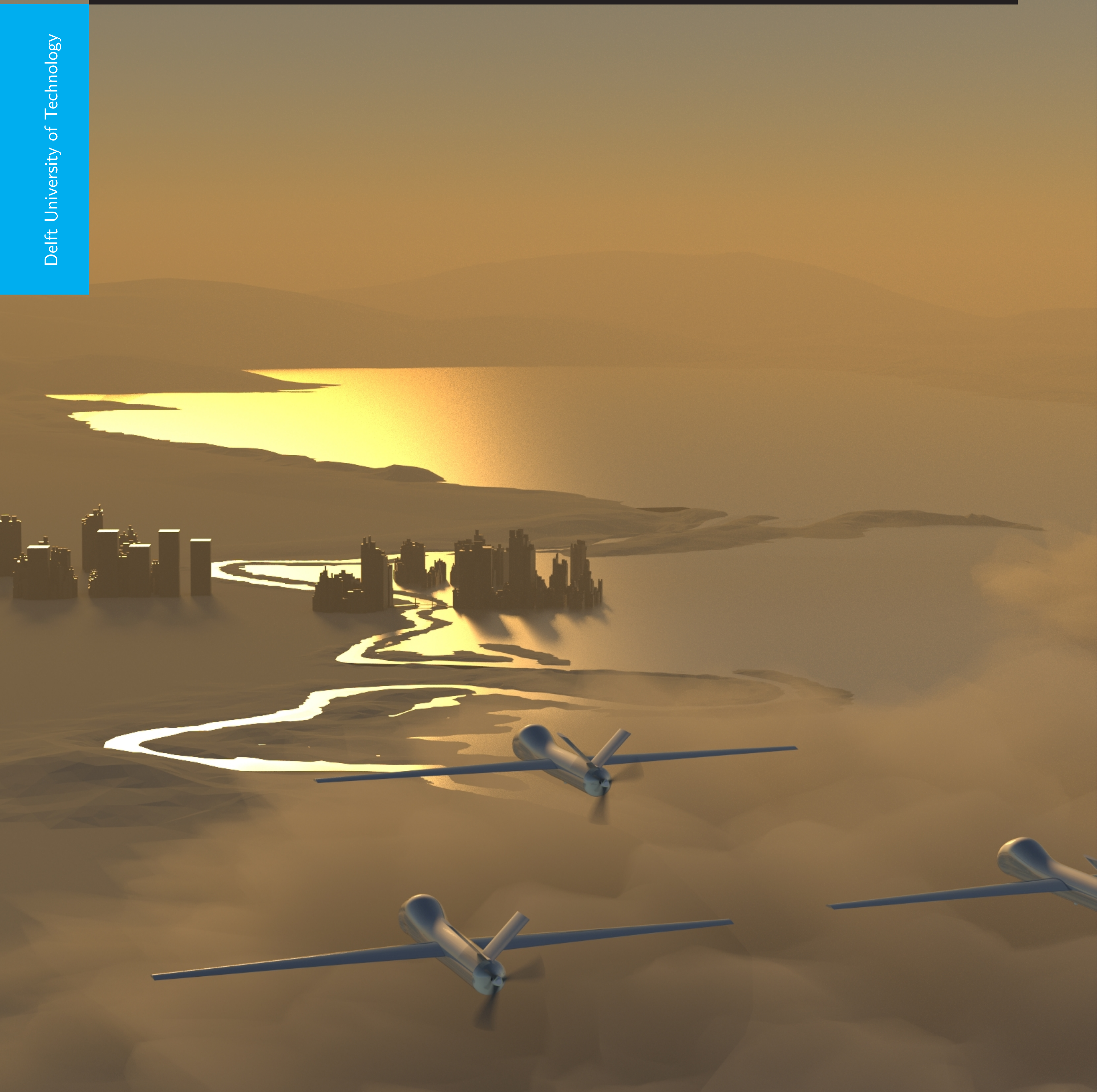

TU Delft Delft University of Technology

Challenge the future

FINAL REPORT

WIFLY: AN EMERGENCY COMMUNICATION NETWORK FOR DISASTER AREAS

by

WiFly Team
L. Bermel - 4278739
H.F.C. Hendrikx - 4156633
A. Jürisson - 4275969
A.J.J. Lagerweij - 4272080
G.H.M. Lebesque - 4304691
V.T. Mateescu - 4273214
N.V. Meima - 4227506
T. Nguyen - 4082249
A.A. Prodan - 4277473
C.A.M. Socci - 4268490

Version 02
June 28, 2016
Delft University of Technology
Cover image made by the WiFly team based upon "Aerial cityscape v1.0" by Hamza CHEGGOUR:
http://www.emirage.org/2014/03/12/free-download-aerial-cityscape-v1-0/

Supervisors:	dr. ir. F.F.J Schrijer
	dr. ir. A.H. van Zuijlen
Coaches:	Z. Whang
	J.D. Brandsen

Preface

Before you lies the Final Report, written for the WiFly Spring DSE. The Spring DSE is a project that takes 10 weeks and is performed by 10 students with the goal of fulfilling the requirements of this Aerospace Engineering Bachelor course at the Delft University of Technology (TU Delft). This report presents the detailed design for the WiFly system, to be used as input for further analysis, prototyping, manufacturing and implementation.

We would like to thank our supervisors Ferry Schrijer and Sander van Zuijlen for their guidance and support during the design process. Furthermore, we would like to express our gratitude to Zi Whang and Jaco Brandsen, who have coached us and provided us with critical, yet supportive, feedback. Also, we would like to explicitly express our gratitude to Martijn Boer from USAR.nl for his input on Search and Rescue operations.

We hope you enjoy reading.

WiFly Team
Leon, Huub, Andres, Bram, Geert, Vlad, Niek, Thang, Alex and Carlo
Delft, June 28, 2016

SUMMARY

The main goal of this report is to offer an overview of the preliminary design of the WiFly system. This consists of a swarm of UAVs that need to provide critical information to disaster affected zones for 24 hours, 24 hours after it occurred. This report starts with an elaborate discussion on the mission analysis which is followed by a complete description of the design procedure. Since the project is done for the aerospace faculty, the discussion focuses manly on the aerospace engineering characteristics of the product. As for this specific project the communication system plays a major role in the development of the design, an extensive chapter about this subsystem is offered as well.

The first chapter of the report offers a complete overview of the mission the system must complete. The main output from this analysis was the amount of people that had to be serviced by the system, set to be 300,000. Additionally an initial loiter altitude of 2 km was selected as well as a swarm size of 45 UAVs. After that the mission profile is displayed, from which initial characteristics of the UAV like the cruise and loiter speed were derived. Those are 200 km/h and 127 km/h respectively.

The core part of the WiFly product consists of the communication system. It consists of three major parts, the links between the UAVs and the people in the disaster area, the links for intra-swarm communications and finally the links between the UAV and ground base. Firstly, the former aspect of this system is treated offering an overview on the communication needs of the people in distress and the potential methods to fulfill those needs. Based on this the sizing of the system is performed. The result is a payload mass of 18.8 kg, with an estimated price of 38,086 Euros, which requires 0.4 kW of power. Afterwards, the non-payload communication system (for links between UAVs, and link between UAVs and base) is sized and designed. All the required hardware is chosen and several link budgets are drawn, to check that each link will close safely with a sufficient margin. The chapter includes elaborate discussions on the choice of each component based on its individual characteristics, as well as an explanation of all the design choices, how the mesh network functionality will work, and the purpose behind each different type of link.

The performed aerodynamic analysis is based on the flight profile selected during the mission investigation. A small discussion on the airfoil selection is offered and the final decision is highlighted. Afterwards, a complete aerodynamics analysis is performed using both XFLR5 and an elaborate empirical method from Roskam [1]. Aerodynamic properties such as the lift, drag and moment coefficients are computed and examined. The discussion moves to tail configuration, where based on an elaborate trade-off, the V-tail was found as the most appropriate for the UAV design. The chapter finishes with the selection of NACA0009 for the tail airfoil.

Next, the structural design is treated. Based on the loads the UAV must cope with, the fuselage and wing are designed accordingly. A complete stress analysis is performed on each component and a specific material is selected. For the fuselage, magnesium was chosen after a material trade off while for the wingbox the common aluminium 6016 was picked. Afterwards, a elaborate discussion on the internal and external layout of the fuselage and wing is performed, offering a complete overview on their integration in the whole UAV design.

From the drag computation performed in the aerodynamic analysis the required power is determined. With this value in mind and using an extensive engine catalogue, it was decided to use Rotron RT300 EFI LCR, which generates the required power with minimum mass and fuel consumption. Based on the engine manufacturer advice and on its worldwide availability, 100 Low Lead (100LL) gasoline was chosen as the fuel for the selected engine. Afterwards, the fuel tanks are sized such that they fit in the wing-box. The generators and battery are then selected and a general layout of the electrical system is offered.

Based on the fuel and payload positions, the center of gravity range is determined for different wing locations. Afterwards, by overlapping the obtained graph on the scissor plot, an optimal ratio of 0.217 between the sizes of the tail and wing was found. The control analysis then sizes the ailerons and the ruddervator, specific for the V-tail configuration. The chapter finishes with a complete stability simulation made in Athena Vortex Lattice program. The result is that the UAVs eigenmotions are dynamically stable except the spiral motion.

In order for the system to be autonomous, specific self-control electrical components have to be selected. The first step consists in conceiving the hardware architecture of the UAV. Based on reference aircraft and technical manuals, the flight computer, the actuators and sensors are picked and integrated in the design. The chapter ends with a detailed description of the power consumption of each chosen component together with a final estimate on the supplementary weight added to the UAV.

With the procedure of designing each subsystem defined, the iteration method combining all these processes together is explained. The class II weight estimation from [2] together with the method of obtaining the necessary layout are discussed. A pie chart displaying the components weights is offered together with a visualisation of the UAV design created in CATIA V5. Both the external and internal layout of the UAV are presented together with a sanity check which guarantees that all the components fit into the fuselage of the aircraft.

The operation of the whole swarm is analysed next. Firstly, the take off and landing system were selected. The bungee chord system was chosen for launching an UAV every three minutes, while the sky-hook was picked for bringing the UAV to the ground. Afterwards, a discussion is offered concerning the accelerations caused by these elements together with their sizing. Next, the swarm formation flying is treated for both cruise and loiter. The best possibility for the cruise phase is the V-formation which is inspired from the birds flight, while for loiter it was decided to fly in circles. The pointing of antenna is afterwards discussed. The shape in which the antenna radiates was considered to be a cone with a 42° angle. The section ends with an elaborate discussion on the influence of the turn radius on the antenna angle.

Furthermore, the flight performance of the UAV is considered. Firstly, the climb characteristics like rate, angle and time to the cruise altitude are determined. The discussions moves to gliding performance of the UAV. This characteristic is manly based on the aerodynamic properties of the UAV as endurance ($C_L^{1.5}/C_D$) and range factors (C_L/C_D). The load factors during maneuvers are then computed and a payload-range diagram is offered in order to complete the performance analysis.

A discussion regarding the impact of varying one parameter is offered in the sensitivity analysis chapter. The cruise speed, payload weight and aspect ratio were selected to be the variables due to their strong dependence on the mission type. Afterwards, a compliance matrix was created in order to check if the final product satisfies the key project requirements. The section ends with a feasibility analysis of the whole design.

Having a final design, the budget breakdown of the system can be defined. This offers a complete overview on the weight, power required and the price of each subsystem. Also, a time budget is defined for the whole mission and an elaborate discussion on the contingency management is offered at the end of the section. Next, the market analysis is performed in order to investigate the competitiveness of the product and the added value in the market. The section is completed by a SWOT analysis in which the strengths and weaknesses are discussed together with the opportunities and threats the system is expected to face.

As the risk of failure during the design procedure must be minimised, verification and validation procedures are defined for each subsystem. Also, in order to ensure that all customer needs are satisfied a RAMS analysis is performed. The investigation regards the reliability, maintainability, availability and the safety of the whole system and the interdependence between these 4 aspects. In order to quantify the uncertainty of the mission, a risk assessment is performed. This offers as output the technical risks map of the project, in which each identified risk is graded. The section finishes with the description of the product development which must satisfy specific principles in order to be sustainable.

At the end of the Final Design, the WiFly system consists of 45 UAVs each with a maximum takeoff weight of 132 kg. The system can fully perform its mission, but it is expected to slightly exceed the assigned budget. The last part of the report offers an overview on the post-DSE activities which must be performed after the scheduled 10 weeks of the project. Actions as testing, certificating and actual producing the system are among the tasks which need to be performed. These are offered schematically in a work flow diagram together with a Gantt Chart which describes the time span required for each one of them.

NOMENCLATURE

Acronyms

AC	Alternating current
Avgas	Aviation Gasoline
CS	Certification Specifications
DC	Direct current
DL	Downlink
EFI	Electronic Fuel Injection
FAA	Federal Aviation Administration
FAR	Federal Aviation Regulation
FMECA	Failure Mode, Effect, and Criticality Analysis
FSPL	Free Space Path Loss
HPBW	Half power beam-width
ISA	International Standard Atmosphere
LiPo	Lithium polymer
MCMT	Mean Corrective Maintenance Time
MDT	Mean Down Time
MPMT	Mean Preventive Maintenance Time
MTBM	Mean Time Between Maintenance
MTOW	Maximum Takeoff Weight
MTTF	Mean Time To Failure
MTTM	Mean Time To Maintain
OEI	One Engine Inoperative
OEW	Operative Empty Weight
PLF	Polarization loss factor
RAMS	Reliability, Availability, Maintainability, Safety
RPM	Revolutions per minute
RPS	Revolutions per second
TEL	Tetraethyl Lead
TRU	Transformer rectifier unit
UAV	Unmanned Aerial Vehicle
UL	Uplink

Variables

α	Angle of attack	°
α	Cellphone penetration	[-]
α	Coefficient for rain attenuation	[-]
$\alpha_{1/2}$	Half power beam-width angle	°
$\bar{c}$	Mean Aerodynamic cord length	m
$\bar{w}$	Control surface loading	$\mathrm{N\,m^{-2}}$
$\bar{x}_{cg}$	Center of gravity location, measured from the leading edge MAC as a fraction of $\bar{c}$	[-]
$\bar{x}_{np}$	Location of the neutral point as a fraction of the $\bar{c}$	[-]
$\bar{x}_{zc}$	Mean aerodynamic cord measured from the nose of the plane as a fraction of $\bar{c}$	[-]
β	Half power beam width	°
β	Pitch angle	°
δ	Antenna tilt angle	°
η	Antenna efficiency	[-]
η_e	Engine efficiency	[-]
η_p	Propeller efficiency	[-]
$\frac{d\epsilon}{d\alpha}$	Downwash gradient	$\mathrm{rad^{-1}}$
$\frac{V_h}{V}$	Relative tail airspeed	[-]
γ	Adiabatic Index	[-]
γ	Flight path angle	°
γ_R	Rain attenuation coefficient	$\mathrm{dB\,km^{-1}}$
λ	Lapse rate	$\mathrm{K\,m^{-1}}$
λ	Signal wavelength	m
μ	Dynamic viscosity	Pa s
μ	Roll angle	°
μ_{cruise}	Cruise dynamic viscosity	Pa s
μ_{loiter}	Loiter dynamic viscosity	Pa s
ν	Poisson ratio	[-]
ϕ	Polarization mismatch angle	°
ρ	Density	$\mathrm{kg\,m^{-3}}$
ρ_0	Sea level density	$\mathrm{kg\,m^{-3}}$
ρ_{cruise}	Cruise density	$\mathrm{kg\,m^{-3}}$
ρ_{loiter}	Loiter density	$\mathrm{kg\,m^{-3}}$
σ	Normal stress	MPa
τ	Shear stress	MPa
A	Area	$\mathrm{m^2}$
A_e	Enclosed area	squarem
a_i	Acceleration in i-direction	$\mathrm{m\,s^{-2}}$
$A_{spinner}$	Spinner area	$\mathrm{m^2}$
AFR	Air to Fuel ratio	[-]
AR	Aspect Ratio	[-]
AR_{tail}	Tail aspect ratio	[-]

AR_{wing}	Wing aspect ratio	[-]
b	Chord length in rest	m
b	Wingspan	m
C	Number of channels	[-]
c	Chord length	m
C_s	Subscriber SMS credit	[-]
$C_{D_{0_f}}$	Fuselage zero lift drag coefficient	[-]
$C_{D_{0_{UAV}}}$	UAV zero lift drag coefficient	[-]
C_{D_0}	Zero lift drag coefficient	[-]
$C_{D_{UAV}}$	UAV drag coefficient	[-]
C_{data}	Number of data channels	[-]
C_D	Drag coefficient	[-]
C_{f_f}	Skin friction coefficient of the fuselage	[-]
c_h	Tail chord length	m
C_{L_α}	Lift gradient	rad^{-1}
$C_{L_{max}}$	Maximum lift coefficient	[-]
$C_{L_{tail}}$	Tail lift coefficient	[-]
$C_{L_{UAV}}$	UAV lift coefficient	[-]
$C_{L_{wing}}$	Wing lift coefficient	[-]
C_L	Lift coefficient	[-]
C_L/C_D	Range factor	[-]
$C_L^{1.5}/C_D$	Endurance factor	[-]
$C_{m_{ac}}$	Moment coefficient at the aerodynamic center	[-]
$C_{M_{tail}}$	Tail moment coefficient	[-]
$C_{M_{UAV}}$	UAV moment coefficient	[-]
$C_{M_{wing}}$	Wing moment coefficient	[-]
C_M	Moment coefficient	[-]
$C_{signalling}$	Number of signalling channels	[-]
C_{sms}	Number of sms channels	[-]
C_{voice}	Reserved voice channels	[-]
D	Diameter	m
D_r	Antenna diameter	m
d_f	Fuselage diameter	m
$DL_{non-payload}$	Total Downlink data-rate for non-payload communications of the whole swarm	$\mathrm{bit\,s^{-1}}$
$DL_{payload}$	Total Downlink data-rate for payload communications of the whole swarm	$\mathrm{bit\,s^{-1}}$
E	Modulus of elasticity	GPa
e	Oswald factor	[-]
e_h	Tail Oswald factor	[-]
f	Signal frequency	s^{-1}
F_e	Force elongation bungee chord	N
F_μ	Friction force launcher	N
$F_{catapult}$	Limit force exerted by catapult	N
F_{prop}	Limit force exerted by propulsive system	N
$f_{sms,p}$	SMS peak factor	[-]
F_{wing}	Force acting between skyhook wire and wing	N
G	Number of survivor groups per cell	[-]
g_0	Gravitational acceleration at sea level	$\mathrm{m\,s^{-2}}$
G_{amp}	Amplifier Gain	[-]
G_t	Gain of the transmitting antenna	[-]
H	Average survivor groups size	[-]
h	Altitude	m
h_{cruise}	Cruise altitude	m
h_{loiter}	Loiter altitude	m
I	Area moment of inertia	m^4
k	Coefficient for rain attenuation	[-]
K_c	Buckling coefficient	[-]
K_t	Torsion coefficient	[-]
l_f	Fuselage length	m
l_h	Distance from the main wing to the horizontal stabilizer	m
l_{fn}	Length from the nose to the front of the wing at the fuselage	m
l_f	Fuselage length	m
l_{ref}	Reference length	m
M	Bending moment	N m
M	Mach number	[-]
m	Mass	kg
m	Technology advancement coefficient	[-]
M_{cruise}	Cruise Mach number	[-]
M_{loiter}	Loiter Mach number	[-]
N	Normal force	N
n	Number of people in the disaster area	[-]
N_c	Number of communication cells	[-]
n_z	Load factor L/W or $a_z/9.81$	[-]
N_{TRX}	Number of transceivers	[-]
P	Average number of mobile phones in a cell	[-]
P	Power	W
P_r	Power received by the receiver	W
P_t	Transmit power of transmitter	W
p_0	Sea level pressure	Pa

P_{BHP}	Break Horse Power	W
p_{cruise}	Cruise pressure	Pa
P_D	Pitch distance	m
p_{loiter}	Loiter pressure	Pa
P_{max_0}	Maximum power at sea level	W
P_{max}	Maximum power	W
P_{prop}	Propulsive power	W
P_{req}	Power required	W
$P_{subsystems}$	Power for subsystems	W
q	Stiffness bungee chord	$\mathrm{N\,m^{-1}}$
q_s	Shear flow	$\mathrm{N\,m^{-1}}$
R	Gas constant (air)	$\mathrm{J\,kg^{-1}\,K}$
R	Leading edge suction parameter	[-]
R	Radius	m
R	Rainfall rate	$\mathrm{mm\,h^{-1}}$
R_x	Radii of gyration	[-]
$R_{cb,i}$	Inbound cell broadcast data rate	$\mathrm{kbit\,s^{-1}}$
$R_{cb,o}$	Outbound cell broadcast data rate	$\mathrm{kbit\,s^{-1}}$
R_{N_f}	Fuselage Reynolds number	[-]
r_{ref}	Reference Radius	m
$R_{sa,i}$	Inbound situational awareness data rate	$\mathrm{kbit\,s^{-1}}$
$R_{sa,o}$	Outbound situational awareness data rate	$\mathrm{kbit\,s^{-1}}$
$R_{sms,i}$	Inbound SMS data rate	$\mathrm{kbit\,s^{-1}}$
$R_{sms,o}$	Outbound SMS data rate	$\mathrm{kbit\,s^{-1}}$
$R_{voice,i}$	Inbound voice data rate	$\mathrm{kbit\,s^{-1}}$
$R_{voice,o}$	Outbound voice data rate	$\mathrm{kbit\,s^{-1}}$
R_{w_f}	Wing fuselage interaction factor	[-]
$R_{wp,r,i}$	Inbound web portal refreshment data rate	$\mathrm{kbit\,s^{-1}}$
$R_{wp,r,o}$	Outbound web portal refreshment data rate	$\mathrm{kbit\,s^{-1}}$
$R_{wp,s,i}$	Inbound web portal serving data rate	$\mathrm{kbit\,s^{-1}}$
$R_{wp,s,o}$	Outbound web portal serving data rate	$\mathrm{kbit\,s^{-1}}$
Re	Reynolds number	[-]
ReF_{cruise}	Reynolds number fuselage in cruise	[-]
ReF_{loiter}	Reynolds number fuselage in loiter	[-]
ReW_{cruise}	Reynolds number wing in cruise	[-]
ReW_{loiter}	Reynolds number wing in loiter	[-]
S	Distance between transmitter and receiver	m
S	Number of inbound and outbound SMS messages per second	$\mathrm{s^{-1}}$
S	Planform area	$\mathrm{m^2}$
S	Shear force	N
S_h	Surface area of the horizontal tail	$\mathrm{m^2}$
S_i	Receiver sensitivity	W
S_h	Tail planform area	$\mathrm{m^2}$
S_{margin}	Link margin	[-]
S_{wet}	Wetted surface area	$\mathrm{m^2}$
SFC	Specific fuel consumption	$\mathrm{kg\,kW^{-1}\,h^{-1}}$
T	Thrust	N
T	Torque	$\mathrm{N\,m}$
t	Skin thickness	m
t	Time	s
T_0	Sea level temperature	K
T_{cruise}	Cruise temperature	K
T_{loiter}	Loiter temperature	K
t_{sa}	Situational awareness refresh interval	s
$t_{sms,d}$	SMS delivery interval	s
T_{static}	Static thrust	N
t_{wp}	Web portal access interval	s
U_l	Airspeed	$\mathrm{m\,s^{-1}}$
$UL_{non-payload}$	Total Uplink data-rate for non-payload communications of the whole swarm	$\mathrm{bit\,s^{-1}}$
$UL_{payload}$	Total Uplink data-rate for payload communications of the whole swarm	$\mathrm{bit\,s^{-1}}$
V	Velocity	$\mathrm{m\,s^{-1}}$
V_s	Hourly cell SMS volume	[-]
V_{cruise}	Cruise velocity	$\mathrm{m\,s^{-1}}$
V_h	Tail airspeed	$\mathrm{m\,s^{-1}}$
V_{loiter}	Loiter velocity	$\mathrm{m\,s^{-1}}$
V_{wp}	Size of web portal	kB
SR	Sink rate	$\mathrm{m\,s^{-1}}$

CONTENTS

1 | Introduction

Lately, mobile phones and Internet connectivity have become of great importance and people have become more and more dependent on them. This, however, poses a threat to the safety of the people when a disaster destroys the existing infrastructure. Telecommunication towers might collapse, cables might break or even a loss of power could cripple the system. During these disasters, communication is crucial. It could allow the victims to communicate with the rescuers, as well as receive vital information about the current state in the disaster area. A reliable means of communication between the rescue teams and organizations involved is critical in a disaster area. In this DSE project the goal is to design a swarm of unmanned aerial vehicles which provides emergency network connectivity to people in disaster areas. The system should provide victims with emergency information and locate them, but should also aid the rescue teams by providing them with an assessment of the situation in the area quickly after the disaster has taken place.

The project consists of multiple phases. This final report succeeds the project plan, baseline report and mid-term report. The project plan provided the project management and planning for the entire course of the project. The baseline report then gave an overview of the project definition phase. It contained an analysis of the mission, requirements and functions which resulted in possible design options. In the mid-term report, the possible design options were investigated in depth. A trade-off was conducted in which a final design option was chosen. This report continues where the mid-term report stopped. It aims at providing a complete overview of how the system was designed, how and how well it will operate, what threats there are to its success and what impact it has on the environment. The subsystems are designed in detail through an iterative process, leading to the complete design of the internal and external layout of the UAVs.

The report starts off with the mission analysis in chapter 2 together with presenting the requirements in a compliance matrix. It is concerned with defining boundaries to the design space for the design of the WiFly system. The aim of the mission is described and the mission profile is analyzed. It also gives a description of the model mission that will be designed for.

Chapter 3 till chapter 10 deal with the design of the UAVs. It begins with the design of the communication system in chapter 3. Communications with the base station, between UAVs, and with the people on the ground in the disaster area are covered. The chapter provides a description of the functional requirements of the communication subsystem, a calculation of the required number of drones for adequate coverage, the hardware selection for payload communications, the design choices and hardware selection of non-payload communications, an explanation of how the mesh network functionality will work, the sizing of all different links (by using link budgets) and finally all hardware budgets for the non-payload communication system (power, mass, cost).

In chapter 4, the aerodynamic properties of the UAVs are analyzed. It begins by calculating the atmospheric properties during the mission, which is followed by the selection of the airfoil of the wing. After this, the lift, drag and moment of the wing, fuselage and tail are analyzed separately and then combined into one analysis of the entire UAV. The chapter finishes with the design of the tail surface.

The structural analysis and design is performed in chapter 5. The design of the fuselage, wing and engine mount is done, taking into account different load cases. Different failure modes are considered during the design. Finally, material is chosen for the design of the fuselage and wing box.

Chapter 6 deals with the propulsion and power subsystem. An engine is selected and the propeller is sized, followed by a calculation of the maximum thrust the engine can deliver. Then, a fuel type is chosen, the fuel system layout is designed and the required fuel tank size is estimated. The chapter finishes with the design of the electrical system, taking into account the different electrical power loads.

The stability and control of the UAVs is covered in chapter 7. Loading diagrams and scissor plots are created, and the control surfaces are designed. Also, the center of gravity range is computed. Finally, a simulation of the stability is performed in order to find out whether the different eigenmodes of the aircraft are stable or not.

Chapter 8 describes the selection and interaction of the different instruments on-board. The hardware is needed to provide reliable and accurate control of the aircraft. Specific flight and mission computers are selected, as well as sensors, actuators and transponders. The hardware architecture is provided to show how the different components interact.

In chapter 9, the iterative process that was applied during the design process is described. It shows how the calculations of different technical characteristics are related to each other. Repeating these calculations until they converge yields a weight estimation and final layout design of the UAVs. The final layout is then presented in chapter 10. CAD models of the UAV were created and drawings of both the internal and external layout are provided. This chapter concludes the design of the UAVs.

The next two chapters describe the operation of the system. First, in chapter 11, the systems for takeoff and landing are described and analyzed. Then, chapter 12 describes the swarm formation during both cruise and loiter. The swarm control algorithm is based on three principles, which are usage of digital pheromones, path planning and collision avoidance. Applying these three principles yields a reliable and accurate control of the swarm.

The following three chapters deal with the performance of the UAVs. In chapter 13 the flight performance is analyzed. The climb and glide performance are investigated and the range and endurance are calculated. Also, the performance of the UAVs in terms of maneuverability is investigated. Finally, a payload-range diagram is provided. A sensitivity analysis is performed in chapter 14. It investigates how sensitive the design is to changes in certain parameters. The parameters that are changed in the analysis are the cruise speed, payload weight and aspect ratio.
The next two chapters cover the economic analysis. Chapter 15 provides the budget break down of the cost, power and weight resources. Furthermore, it includes a description of the contingency management. Then, in chapter 16, a market analysis is conducted in order to investigate how the product fits in the market. Therefore, the potential customers and competitors are analyzed and projections are made regarding the future market and the market share the product will obtain. The chapter is concluded by a SWOT analysis that provides a quick overview of the strengths and weaknesses of the product, and the opportunities and threats in the market.

The design, operational and environmental risks are covered in the next four chapters. First, the numerical models and calculations used in the design process are verified and validated in chapter 17. A RAMS analysis is conducted in chapter 18. It investigates the reliability, availability, maintainability and safety of the system. Chapter 19 provides the risk assessment, in which the threats to the success of the system are identified and assessed. It includes a risk map and risk handling, such that the risks are minimized. Chapter 20 describes the sustainability of the design. The principle of circular economy is explained, and the noise and emissions of the UAVs are investigated in order to estimate the environmental impact of the system.

Finally, chapter 21 covers the tasks that need to be performed after the DSE in order to finalize the design of the system. A work flow diagram and Gantt chart are provided to show the development logic and scheduling of these tasks. The conclusion of the report can be found in chapter 22.

2 | MISSION ANALYSIS

This chapter is dedicated to defining boundaries to the design space for the design of the WiFly system. The mission goals are defined in chapter 2.1, the driving requirements and compliance of the design with them is shown in section 2.2, feasibility of design is discussed in section 2.3 and the operational procedure is described in section 2.4. Section 2.5 shows the functional breakdown and functional flow for the mission.

2.1 MISSION

The primary objective of the WiFly mission is to provide public safety information in disaster areas and to analyze the mobile signals there for situation assessment (impact on the affected zone). Disasters disrupting the correct functioning of communications systems can be of natural cause like hurricanes and earthquakes but also man-made such as terrorist attacks and power outages. A natural first step in the design selection is sizing the different aircraft concepts and picking the best possible compromise. Since vehicle sizing is done around the payload, this must be analyzed first.

One of the driving requirements is the number of people affected by the disaster (or that the swarm aims to connect with). The system is designed so that it covers a city with a population of 300 thousand people. This population can be spread over an area of $100km^2$, but the system will be fully scalable for larger areas and populations (by adding more drones or having a lower endurance time). As a comparison the model city, Rotterdam, has approximately 300 thousand people in a $100km^2$ area.

An estimation of the number of drones is needed for further sizing. Analysis shows that it is more beneficial to have a large number of smaller drones than to have few larger ones, for the following reasons:

- A system with many smaller drones has more flexibility in their positioning and can more easily cover long narrow coastlines without covering a large inhabited area.
- Having more drones results in a higher level of redundancy of the system.
- Since each drone would cover a smaller area, they will be closer to the people they connect with. A smaller power is therefore needed for the antennas.
- The frequency band for the payload and communication subsystem can be reused when the drones are distributed.

The minimum number of drones that can fulfill the mission is approximated to be 45. This is based on the maximum capacity for the communications system that each UAV can provide. It was found the most feasible option for this mission is to use a conventional fixed wing aircraft which can meet the long endurance, have high cruise speed, carry the payload and have good handling in strong winds.

2.2 COMPLIANCE MATRIX

When designing a system set of requirements is needed to give constraints to the performance of the design. In this section the key and driving requirements for the WiFly system are presented that were found in the Mid Term report [3]. In table 2.1 the requirements are presented followed by a "+" if that requirement is met, by a "-" if it is not met and by a "+/-" if it is partially met. The last column provides the chapter in which details about that requirement are obtained. If a requirement is not met its feasibility is discussed in section 2.3 together with the actual values that the design meets instead.

2.3 FEASIBILITY ANALYSIS

Next to the conventional wing tail configuration, other options considered were rotorcrafts which can loiter at a fixed position in the air but unfortunately have very low endurance time and balloons that can have very long endurance time but have very bad handling in strong winds. Rockets have been investigated as well, but their loiter performance is that poor that they were disregarded immediately. A conventional fixed wing - tail configuration was preferred over canard because it has better stability and controllability characteristics which justifies its selection for the final design. For each requirement that is not met or is partially met, a discussion about the reasons and feasibility is given. From table 2.1 it can be seen that this applies for the

Table 2.1: Compliance matrix

	Requirement	Compliance	Reference
1	SR-01.01 The system shall be able to function for at least 24 hours without returning to base.	+	section 6.2.3
2	SR-01.02.1 In case the target area is less than 300 km away, the system shall arrive at the target area in less than 1.5 hours.	+/-	section 2.1
3	SR-01.02.2 In case the target area is more than 300 km but less than 1500 km away, the system shall arrive at the target area in less than 5 hours.	-	section 2.4
4	SR-01.04 The operational envelope shall include wind conditions up to 10Bft.	+	section 5.2
5	SR-01.05 In case the endurance is less than 48 hours, the system shall be able to turn around in less than 2 hours.	+	section 2.4
6	SR-01.06 The noise experienced on the ground during the loiter phase shall not exceed a level of 75 dB.	+	section 20.2
7	SR-01.07.1 The system shall be able to take off without using existing infrastructure.	+	chapter 11
8	SR-02.5 The system shall be visible by surveillance radar equipment of all control towers.	+	section 8.4
9	SR-03.02.3 The Internet connection shall be accessible by all cellphones.	+/-	section 3.1
10	SR-03.04 The Internet connection shall have a data-rate of minimum 9kbps.	-	section 3.1
11	SR-03.06 The network shall be operating in less than 24 hours after the disaster took place.	+	section 2.4
12	SR-03.07 While operating the system shall cover an area of at least 100 km2.	+	section 3.4.3
13	SR-04.02.3 The location of the people transmitting data shall be provided to the rescue teams.	+/-	section 3.1
14	SR-06.01 The prototype design and production costs shall be at maximum of 50k€.	-	section 15.1.1
15	SR-06.02 The full system design and production costs shall be at maximum 3M€.	-	table 15.4
16	SR-06.03 The annual maintenance costs shall not exceed 100k€.	+	section 2.4
17	FR-01.01 The system shall allow for assembly.	+/-	section 5.8
18	FR-04.04 The system shall allow for communication between the rescue teams and the people in distress.	+	section 3.1

following requirements:

SR-01.02.1 Cruise speed
WiFly is able to cruise at a maximum velocity of 200 km/h, which means it can get to a target area 300 km away within 1.5h only without any wind against it. Higher cruise velocity was not selected because it would have resulted in a much higher weight for the UAV. Therefore the system only partially meets the requirement.

SR-01.02.2 System delivery
When the system is more than 300 km away, it needs to be delivered. This can be done using transport aircraft. When they have arrived on the mission site, the UAVs need to be assembled and launched which all together results in 6.5h to get to the mission area from a distance up to 1500 km away. It was decided not to have the UAV fly the 1500km cruise in order to keep its weight lower.

SR-03.02.3 Cellphones
The system uses the GSM standard to connect with the cellphones. This standard is supported by all phones but not all phones support connecting to the Internet and therefore this requirement is partially met.

SR-03.04 Internet connection
The system only provides a local cache of the Internet. Preloaded sites stored on the UAV can be accessed, but there is no direct connection to the Internet. This concept was selected in order to keep the communication data rates low and instead cover a much larger population with essential emergency information service.

SR-04.02.3 Location service
This requirement is partially met because the system can provide the location of the people to the rescue team only when the people choose to share their location themselves.

SR-06.01 Prototype cost
This requirement is not met due to the high price of communications payload components. It is not feasible to reduce this cost because it would seriously affect the service capacity and quality the WiFly is providing. Therefore a higher cost of 64.1 k€ is accepted in order to fulfill the mission.

SR-06.02 System cost
Due to the increased cost of a single UAV also the entire system cost will increase to 3.38 M€ and not fulfill the requirement. In order to be able to fulfill the mission at a desired level again the higher cost is accepted.

FR-01.01 (Dis)assembly
At this point of the design the structure of the UAV is constructed such that it allows for assembly and disassembly but no specific mechanism for the connections has been developed. The development for the (dis)assembly mechanism is planned as a further step in the design process. Because of this the requirement is partially met.

2.4 OPERATIONS ANALYSIS

In this section a view is given on the operations of a typical WiFly mission. The full WiFly system encompasses more than only the UAV. It includes the full set of UAVs for the swarm, the base station including the communication equipment external to it (parabolic dishes), the operations team, the required fuel stored in containers and the launching and recovery systems. During the operation all these things come together and make sure that the communication network can be made operational within 24 hours.

A typical mission consists of several phases. It starts with deployment of the system, then the initial launch, the loiter phase, return to base, check and refuel, relaunch, loiter again, return to base and then finish. A description will be given for all of these phases. Storage could also be considered an important phase. The expectation is that the system will be inactive for long periods it should have a storage system that ensures the durability of all parts and minimize its deployment time.

When the disaster happens the operator of the WiFly will be notified and a decision for the deployment of the system has to be made. If it is decided that the system will be deployed, the number of UAVs will have to be picked based upon the type and location of the disaster. Throughout this report the assumed number of UAVs will be 45 unless stated otherwise. A motivation for this can be found in section 3.5. The other decision that has to be made is deploy at current position or transport the system closer to the disaster. In the latter case all parts of the system will have to be loaded on a means of transport, e.g. trucks or cargo plane.

Before the initial launch can start the launch mechanism and base have to be set up. For the positioning of the base it is important that the parabolic antenna has a line of sight in the direction of the disaster. This means that there should not be any obstruction by buildings and/or trees. The same goes for the launch mechanism. The catapult has to be positioned so that the launch path is unobstructed and that a crash of a malfunctioning UAV during launch cannot cause harm to the crew or surroundings. When everything is set up the UAVs can be unpacked and assembled. After a systems check the UAVs can be launched. The launch requires two people for the operation and will take three minutes per UAV. This means that with three catapults all 45 UAVs can be launched in 45 minutes. The three catapults also assure that three UAVs can be launched at the same time and fly to the disaster area in formation (for drag reduction). The choice has been made to not first launch all UAVs and then let them fly to the disaster area together, because in that way the

UAVs will waste at maximum 45 minutes of endurance on waiting.

After launch the UAVs will start their ascend and then cruise at 4 kilometers altitude to the disaster area. As mentioned before they will do this in a formation, more specific a three UAV V-formation. During cruise no special activity is done by the UAV other than maintaining the formation. The cruise speed will be 200km/h which means that a distance of 300km can be flown in 1.5 hours if there is no wind. On arrival at the disaster site the UAVs will descend to 2 kilometers altitude to start forming the initial coverage pattern (see section 12.2). During all of this the operators at the base station will check if the system is behaving normally and can takeover control if a problem occurs. The UAVs will loiter for 24 hours and then cruise back to the base in the same V-formation as before.

On arrival at the base they will fly into a sky hook recovery system of which there are three in total. The two operators that first guided the launch can now get the UAV out of the sky hook and reload the system in approximately three minutes. A small cart can then be used to move the UAV to the refuel and maintenance station. The UAV weighs too much to be carried by two people (90.5 kg empty weight). After the UAV is refuelled and checked for damage or malfunctioning it can either be relaunched or disassembled and packed.

The described mission profile of the UAV is shown in figure 2.1. If the mission is further than 300km the choice can also be made to let the UAVs cruise further and let them loiter shorter. The loiter phase starts at 2 kilometer, but this is not fixed. When the full swarm is operational the control system will reassign altitudes to each UAV between 2 and 3 km based upon the communication load on each UAV.

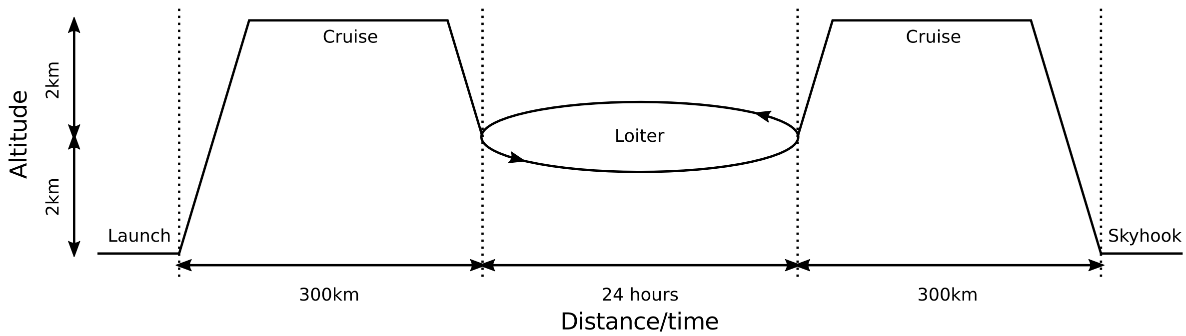

Figure 2.1: Mission Profile. (Elements are not to scale.)

The requirement is that the system has to be up within 24 hours after the disaster. The launch of all the UAVs takes 45 minutes. In case of a 300km cruise an extra one and a half hour is added. The assembly time of each UAV is estimated to be around five minutes. With three teams the assembly takes 75 minutes or 1.25 hours. All this together adds up to three and a half hours from start of assembly to an operational network. This leaves at most 20.5 hours to move the system in case of a far away disaster area and mainly for all organisational tasks that will have to be done. From this it can be concluded that it is likely that the final produced system will meet the 24 hour requirement.

The response time for a disaster of up to 1500km away had the maximum requirement of 5 hours. This requirement cannot be met by the system. If it is assumed that all organisational aspects of the system are already fulfilled and that an airplane is negotiated then the loading of the airplane is estimated to take 1 hour. Then a distance of 1200km will have to be flown to reach the border of the typical cruise range of the system. This 1200km is comparable to a flight from Amsterdam to Barcelona which takes between two and two and a half hours. Then on arrival the system will have to be assembled which was already estimated to take 1.25 hours. And then the launch and cruise will both take 45 minutes and one and a half hours respectively. All this adds up to a response time of 6.5 to 7 hours.

Another requirement is that the system can turn around within two hours. The turn around time is defined as the time between the moment the UAV hits the sky hook and the point where the UAV is released again from the launcher. Exact numbers are hard to calculate without a design of the final system and supporting tools. The launch was already estimated at three minutes. A similar duration will be assumed for the skyhook retrieval. If the three teams need to turn around the whole 45 UAV swarm within two hours then they can spend on average eight minutes on each UAV. This leaves only two minutes for refuelling. With a tank of 41.8 liter this should not lead to any problems. If a UAV detects abnormalities during flight the UAV can be digitally marked and taken out of the swarm during the refuelling phase. That UAV can then later be inspected.

The total fuel volume used by the system and its cost are also part of the operations. Because the fuel will have to be taken with the system during transportation. It cannot be assumed that fuel is available at the place of deployment. A single UAV consumes 41.8 liters of fuel when flying one mission profile round. If each UAV flies the profile twice then $2 \cdot 45 \cdot 41.8 = 3762$L is used by the system. Given the price of one liter AVGAS 100LL is 2.52 € (Price at Lelystad airport, June 2016). This leads to 9480 € of fuel for one complete mission.

After each mission maintenance will have to be performed on the UAVs. If three hours of maintenance are budgeted for every hour flown by the UAV. Then for a deployment where the UAVs will fly two full 24 hour profiles the total flight time per UAV will be $2(24+3) = 54$h (3 hours of cruising). This requires 162 hours of maintenance per UAV or 7,290 hours for the whole swarm. If one hour of maintenance costs 12 € then the maintenance costs for one mission will be 87480 €. These simple calculations are a first order approximation. At this stage it is hard to give an estimate for the required maintenance. This is covered in more detail in section 18.2.

2.5 FUNCTIONAL BREAKDOWN AND FUNCTIONAL FLOW DIAGRAM

This section contains the functional breakdown and functional flow diagrams, shown in figure A.1 and figure A.2, figure A.3 and figure A.4 respectively. Both are updated versions of the diagrams shown in [4].

To avoid taking too much space, as well as avoiding excessive repetitions between the two diagrams, most of the content was included in the functional breakdown. The functional flow is supposed to give an idea of the order in which the "main blocks" illustrated in the functional breakdown will be executed. The actions that compose each single block are analyzed into detail in the breakdown. Moreover, single actions belonging to a block (in the breakdown) are shown (from top to bottom) in a chronological order, giving the reader an idea of what sequence of actions is necessary to provide all the functionalities of a particular block.

There are not very large differences between the updated diagrams and their older counterparts. The mission itself (and how to perform it) is almost identical to the one outlined in the baseline report. The functional flow was simply expanded in the "Loiter" section, and some blocks were rearranged. Most of the changes were applied to the functional breakdown. The biggest changes concern takeoff, landing and loiter. First of all, the UAV's final design only makes use of a catapult for takeoff, and a skyhook system for landing. This means that all of the elements related to conventional takeoff and landing have been removed from the diagrams. Moreover, the communication activities performed during Loiter have now been defined more accurately: two new blocks have been added to the "Loiter & Perform Obj", which accurately detail what kind of communications are used in order to assist the users on the ground. Details have been added to the Communication related blocks in the Loiter section, and the presence of multiple layers of UAVs has been documented. Moreover, the block concerning user safety assessment has been removed, as no particular method (as of the current design stage) has been designed in order to provide that functionality. Some other changes have been applied, but they are considered to be minor in comparison to the ones listed.

3 | COMMUNICATIONS

This chapter will deal with the communication system, its design and the functions it is supposed to perform. First a quick overview is given in section 3.1. After that the information needs for the people in the disaster area are discussed in section 3.2. Then the technical part starts. First the model for estimating the data rates is presented in section 3.3. Second a quick method is presented for determening the number of UAVs needed for a certain disaster in section 3.5. And last the design of the UAV to UAV link and the UAV to base link is discussed in section 3.6.

3.1 COMMUNICATION SYSTEM OVERVIEW

In this section a description will be given on what services the system provides to the users. After several iterations of the communication system the services that could be provided within the given constraints stabilised. At this point it is almost sure that the selected services can be provided with the designed system. A chart depicting the services is added to the appendices and can be found in figure C.1. The services are listed here.

- **SMS-Broadcast** This service will be available to everyone on the ground. It is suitable for sending small text messages to everyone on the ground without the need of an action on their side. This makes it suitable for high priority safety information that is applicable to everyone. The load of this service on the system is limited.

- **Web Portal** The web portal can be accessed by any phone on the ground that is connected to the swarm and that is capable of accessing the internet. The phone should also have a web browser installed, but this is available on most if not all smart phones. A link to the web portal will be broadcasted using the SMS broadcast. The web portal will contain lower priority information compared to the SMS broadcast. The exact information will be presented in the next section. It can be refreshed every hour and can contain simple text and compressed images. A button could be added to let the victim actively send its location obtained from the phone's GPS.

- **Voice Calls** Voice calling is a service limited to the rescue crew only. The access to this service can be coordinated from the base station. This service makes use of the voice protocol in the GSM standard and therefore does not require any special equipment. Which is a major advantage for the rescue crews.

- **Personal SMS** A limited form of personal communciation is also supported by the WiFly system. Unfortunately it is not possible to give the experience that is expected of modern networks. The main reason for this is that all information of the whole system will have to go through one link back to the base. This is a bottleneck for the whole system and requires a limit on the amount of data that can be sent. For this reason only SMS will be available to the users and with hourly quotas. The implementation of the quota is discussed in section 3.3

- **Situational Awareness Map** The amount of phones that are connected to each UAV can be used to judge the situation in the disaster area. It can show where people are concentrated and that can aid in steering the rescue crew to the right places. It has to be noted that this function gives a rough overview of the situation. It will not show the exact location of each phone. This can later be implemented using the web portal, but this requires an action on the users side. The current implementation of the situational awareness map is completely transparent to the user.

Direct internet access will not be given to the users on the ground. While a small portion of the swarm to base link could be reserved for this, this portion would then have to be shared by everyone in the disaster area. If the minimum required 2G data rate (10 kbit s^{-1}) would be provided to everyone and only 10 percent would then access the network, a backhaul link of 300 Mbit s^{-1} would already be required. It is likely that the percentage of people trying to access the internet simultaneously will be even higher because of the disaster. No models could be found for the unpredictable user behavior during disaster situations. With the current design, the largest possible backhaul link with the base measures 3.14 Mbit s^{-1} (section 3.6.4). To have a 300

$\mathrm{Mbit\,s^{-1}}$ backhaul link, it would be necessary to have at least 100 WiFly UAVs in constant contact with the base. This would drive the WiFly system cost to an unacceptable value. On the other hand, increasing the power of the communication system would result in a weight increase that would make it impossible to use the catapult and skyhook systems, which are essential to the quick deployment of the UAV. It was therefore considered unfeasible to have a 300 $\mathrm{Mbit\,s^{-1}}$ backhaul link.

3.2 IMPORTANT INFORMATION FOR USERS IN DISASTER AREAS

This section illustrates what information the WiFly system is going to provide to users in the disaster area, by means of its ad-hoc emergency network. Before identifying what services will be provided to the users, it was of course necessary to identify what they will need the most in case of a disaster: this is done in section 3.2.1. After such an analysis was performed, it was possible to determine what information will fulfill the user needs. This is done in section 3.2.2

3.2.1 USER INFORMATION NEEDS

In order to identify the needs of a disaster survivor, a quick analysis was performed of the possible situations in which one may be involved during a disaster. Assuming the worst case scenario, a disaster survivor may be affected by the following issues:

- The user is injured.
- Someone in close proximity to the user is injured.
- The user is trapped in a confined space.
- The user has no knowledge of its whereabouts.
- No means of transportation are available to the user.
- The user received no warning of the incoming disaster.
- The user was not prepared in any way against the disaster.
- The user has no information about the disaster that happened.
- The user has no information about the current state of events.
- The user has no knowledge on how to behave in case of such a disaster.
- The user has no information about the area surrounding him.
- The user has no information about features of the area surrounding him that may be relevant in case of disaster (shelter, places to avoid, etc.)
- The user has no knowledge concerning the whereabouts and status of people that are of interest to him/her.
- The user has no medical knowledge, including first-aid.
- The user has no knowledge concerning how to survive without external help or assistance, without shelter or basic resources (e.g. food and water).
- The user has no knowledge of how to obtain access to emergency broadcasts (e.g. frequency of emergency radio broadcasts).

It is easy to notice that all the aforementioned issues revolve almost exclusively around the user's lack of information. Only the first items in the list deal with imminent danger. Therefore, the number one priority of the WiFly system is to immediately provide as many users as possible, in the shortest possible time, with all the information necessary to put themselves out of danger, and then all the additional information that is necessary to devise an action plan that will keep them out of harm's way.

3.2.2 INFORMATION NECESSARY TO FULFILL USER NEEDS

In section 3.2.1 it was determined what the user needs are. The information necessary to fulfill the aforementioned needs is listed here below.

1. Information concerning gathering points, as well as which means of transport are safe to use.
2. Information about the disaster. More specifically: type of disaster, affected areas, how to behave (depending on the disaster type), and possibly provide an action plan on what to do in order to attain safety. Updates about the disaster should be given in case the situation changes.
3. Information about shelter and safe areas (to be included in the action plan).
4. Information necessary for survival without external help (how to find food and water, how to make

one's own shelter, how to navigate in an unknown area, etc.).

5. Information necessary to gain access to emergency broadcasts (how to operate a radio, what frequencies to listen to, etc).
6. Any information that the rescuers may have communicate to each other, or to the ground base, for the purposes of the rescue effort.
7. Any information that the user may need to communicate to the external world, be it to the ground base, the rescue crews, or other entities. This may include medical and firefighting services.

The data rate analysis that will be performed in the next section will be based on the information needs found here.

3.3 Modeling Expected Data Rates

Now that the information has been specified it can be used to estimate the size of the data that needs to be sent. With the resulting size the required data rates for each link can be estimated and this is then an important input for the final communication system design.

The total chain of communication links consists of three domains. The cellular domain, this is the part of the communication system that deals with transmitting and receiving data from the end users on the ground using GSM. The mesh domain is the internal communication in the swarm. The backhaul domain is the link that carries the information to the base and the outside world. It would be possible to define a fourth part of the link which is the link from the base to the outside world. This will be an Internet connection, but is outside the scope of this project. It is assumed that the base will have a connection to the internet with enough bandwidth to carry the required traffic. The domains are illustrated in figure C.1.

Each method of communication from section 3.1 will be analysed to come up with an estimate for the required data rate. It has to be noted that a lot of assumptions are made here. The reason for this is the unavailability of models needed to estimate the behavior of the people that are struck by the disaster. This also really depends on the type of disaster. Therefore some rough estimates are made about their access patterns and how they will use the available services. A schematic representation of the data rate model can be found in appendix C figure C.2. First the general parameters will be discussed.

The total volume of data that is produced, for example SMS, depends on the amount of users in the disaster area. The total amount of users in the disaster area will be defined as n and set to 300.000 (taken from the mission parameters). The percentage of the people that posses a mobile phone will be defined as α and set to 0.8 for Europe [5]. The number of cells N_c will be set to 45 (see section 3.5). With these parameters some other useful values can be calculated. First of all an estimate for the amount of mobile phones is $\alpha \cdot n$. With this estimate the amount of phones per cell, P, can be found assuming an equal distribution over all cells. This leads to eq. (3.1).

$$P = \frac{\alpha \cdot n}{N_c} = 5333 \tag{3.1}$$

Starting with the highest priority traffic, the SMS traffic. The estimate for this is based upon SMS credits distributed over the users, C_s. Sending an SMS will cost one credit and the credits are reset every hour. The total SMS volume, V_s, that can be sent in one hour can be calculated (eq. (3.2)). The number of SMS credits is set to 10. It is assumed that all sent SMS messages are outbound traffic of the UAV, in other words messages that are addressed to someone in the same cell will still leave the UAV over the outbound link. The size of an SMS message is 164 bytes. This is the size of an SMS-SUBMIT message in the GSM standard [6]. With this information the average outbound traffic data rate for SMS can be calculated. To account for peaks an extra peak factor, $f_{sms,p}$, is multiplied with the average rate to get the rate for which the system will be sized. The peak factor is set to 3 [7]. The calculation for the final outbound SMS data rate $R_{sms,o}$ is given in eq. (3.2).

$$V_s = C_s \cdot P = 53330 \frac{1}{hr} \Rightarrow R_{sms,o} = \frac{V_s \cdot 164 \cdot 8}{3600} \cdot f_{sms,p} = 56.9\,\mathrm{kbit\,s^{-1}} \tag{3.2}$$

The next value that needs to be calculated is the data rate for the inbound SMS traffic, $R_{sms,i}$. The mechanism applied to limit this is throttling the delivery of messages. For every phone in the cell there is a delivery slot every $t_{sms,d}$ seconds. This is set to 180 seconds. This means that in the worst case everyone receives a SMS message every 3 minutes. It is again assumed that the amount of bytes needed for one message delivery is 164. This leads to eq. (3.3).

$$R_{sms,i} = \frac{P \cdot 164 \cdot 8}{t_{sms,d}} = \frac{5333 \cdot 164 \cdot 8}{180} = 38.0\,\mathrm{kbit\,s^{-1}} \tag{3.3}$$

The SMS broadcast or cell broadcast has a significantly lower data rate. The reason for this is that the message is not addressed to every phone individually, but to all phones at once. The frequency at which the messages can be broadcasted is technically limited to once every 1.833 seconds [8]. This is pessimistically rounded down to one second and it is once more assumed that the data needed for one message is 164 bytes. The cell broadcast inbound data rate, $R_{cb,i}$, can now be calculated using equation eq. (3.4).

$$R_{cb,i} = \frac{164 \cdot 8}{1} = 1.3\,\mathrm{kbit\,s^{-1}} \tag{3.4}$$

The broadcast service does not require interaction from the people on the ground. The phone itself will also not respond to the broadcast. This means that the outbound data rate for the broadcast is zero.

$$R_{cb,o} = 0\,\mathrm{kbit\,s^{-1}} \tag{3.5}$$

Sizing the voice call data rate for the rescue teams cannot be done accurately at this stage. This depends on the client, the amount of rescue teams that will communicate, the disaster and the availability of other communication methods. For now 8 voice channels are reserved in each cell, $C_{voice} = 8$. One voice channel has a bit rate of $13\,\mathrm{kbit\,s^{-1}}$ [9, p. 36]. Two assumptions are made to get from this to a required data rate. First, no calls are made inside the cell. If calls are made inside the cell the required data rate will be lower thus favorable. Second because the calls are two-way the inbound data rate equals the outbound data rate. The data rate, R_{voice}, can now be calculated using eq. (3.6).

$$R_{voice,i} = R_{voice,o} = C_{voice} \cdot 13 = 8 \cdot 13 = 104\,\mathrm{kbit\,s^{-1}} \tag{3.6}$$

The situational awareness information is carried inside the mesh and back haul domain. It is assumed that one situational awareness message is sent for every phone during a refresh interval t_{sa}. For now this is set to 600 seconds. The size of a situational awareness message is estimated to be 18 bytes. This estimate comes from the following content: A 2 byte cell ID, 8 bytes for the phones IMEI, 4 bytes for a timestamp and 4 bytes for extra information. No inbound traffic is needed for the situational awareness. This puts $R_{sa,i}$ to 0 and for the outbound traffic eq. (3.7) can be used.

$$R_{sa,o} = \frac{P \cdot 18 \cdot 8}{t_{sa}} = \frac{5333 \cdot 18 \cdot 8}{600} = 1.3\,\mathrm{kbit\,s^{-1}} \tag{3.7}$$

The last data rate that has to be estimated is the one for the web portal. The first step is determining the size of the web portal. This is done by taking the information requirements from section 3.2.2. Then the size of the text for each point is estimated in amount of words and images. The amount of words is transformed into characters by assuming on average 5 letters per word and one space. Furthermore it is assumed that 1 letter takes up 1 byte, which would be the case if the ISO 8859-1 character encoding is used. The resulting size of the text in bytes is then multiplied by two to account for formatting of text in HTML. It is assumed that each type of information will be one web page. Each page is allocated an extra 1239 bytes (239 for basic HTML tags and 1000 bytes additional formatting). Images are assumed to be in a compressed format and 200kB in size. The result of this is summarized in table 3.1. The total data volume of the web portal, V_{wp}, is found to be 535 kilobyte.
Now the size of the web portal is estimated the next step is estimating by how many people it is accessed and at what frequency. The assumption is made that people cluster together during a disaster and form groups. The average group size, H, is estimated to be 2 based upon the average dutch household size [10]. Then it is assumed that every group downloads the portal at most once every hour, $t_{wp} = 3600$ seconds. From the stakeholder requirements the web portal should be refreshed once an hour and if the portal is accessed again before it is refreshed a cached version is still in the phones browser cache. So this will not trigger a new download. The number of groups per cell of which at least one person in the group possesses a phone is calculated with eq. (3.8).

$$G = \frac{n}{H \cdot N_c} \cdot (1 - (1 - \alpha)^H) = \frac{300000}{2 \cdot 45} \cdot (1 - (1 - 0.8)^2) = 3200 \tag{3.8}$$

Table 3.1: Contents of web portal used for size estimation.

Type of information	Words	Images	Total Size [kB]
Information concerning gathering points	4000	2	448.1
Information about disaster	1000	0	12.9
Shelter and safe areas	1000	0	12.9
Information necessary for survival without external help	3000	0	36.4
Information necessary to gain access to emergency broadcast	2000	0	24.6
Total			535.0

Now the time span, number of downloads and size are known the average required data rate needed to serve the web portal can be calculated. This data rate will be referred to as the outbound web portal serving data rate, $R_{wp,s,o}$. This rate is calculated in eq. (3.9).

$$R_{wp,s,o} = \frac{V_{wp} \cdot G}{t_{wp}} = \frac{535 \cdot 1024 \cdot 8 \cdot 3200}{3600} = 3.7\,\mathrm{Mbit\,s^{-1}} \tag{3.9}$$

The inbound web portal serving data rate,$R_{wp,s,i}$, is the result of the HTTP requests from the phones to get the web portal. Here an average request size of 1000 bytes is assumed and 2 requests for each page and separate requests for the images are assumed. This leads to 12 requests of 1000 bytes each. The average data rate can now be calculated with eq. (3.10)

$$R_{wp,s,i} = \frac{G \cdot 1000 \cdot 12 \cdot 8}{t_{wp}} = \frac{3200 \cdot 1000 \cdot 12 \cdot 8}{3600} = 0.08\,\mathrm{Mbit\,s^{-1}} \tag{3.10}$$

The requirements state that the web portal has to be refreshed every hour. The size of the web portal is already calculated in table 3.1 and given the symbol V_{wp}. Dividing this by 3600 seconds gives the required rate to refresh the portal, $R_{wp,r,i}$. This is done in eq. (3.11).

$$R_{wp,r,i} = \frac{V_{wp}}{3600} = \frac{535 \cdot 1024 \cdot 8}{3600} = 1.2\,\mathrm{kbit\,s^{-1}} \tag{3.11}$$

All data rates for information going into the UAV (inbound) and out of the UAV (outbound) are now estimated. They are summarised in table 3.2.

Table 3.2: Summary of estimated data rates, inbound is data uploaded to UAV and outbound is data downloaded from UAV

Information	**Inbound** [$\mathrm{kbit\,s^{-1}}$]	**Outbound** [$\mathrm{kbit\,s^{-1}}$]
SMS Phone-to-Phone	$R_{sms,i} = 38.0$	$R_{sms,o} = 56.9$
SMS Cell Broadcast	$R_{cb,i} = 1.3$	$R_{cb,o} = 0$
Rescue Voice Calls	$R_{voice,i} = 104$	$R_{voice,o} = 104$
Situational Awareness	$R_{sa,i} = 0$	$R_{sa,o} = 1.3$
Web Portal Serving	$R_{wp,s,i} = 81.9$	$R_{wp,s,o} = 3715$
Web Portal Refreshing	$R_{wp,r,i} = 1.2$	$R_{wp,r,o} = 0$

With these data rates the sizes of each of the link domains can be estimated. The cellular domain data rate will only consist of the web portal serving data rate, $R_{wp,s}$. The SMS and voice are carried over separate channels. This is explained in section 3.4. The data rates that go into the mesh domain are all the rates in table 3.2 except for $R_{wp,s}$. The actual data rate used for sizing will be discussed in section 3.6.4, because this also depends on the possible configuration of the mesh links, as well as the non-payload communications data rate. For the back haul domain one extra assumption has to be made. Namely not all rescue voice calls will go back to the base. 10% of the total voice call data rate will be reserved on the backhaul link. This will lead to eqs. (3.12) and (3.13) for the data rate of the backhaul link.

$$R_{bh,i} = N_c \cdot (R_{sms,i} + 0.1 \cdot R_{voice,o} + R_{sa,i}) + R_{cb,i} + R_{wp,r,i} = 45 \cdot (38.9 + 0.1 \cdot 104 + 0) + 1.3 + 1.2 = 2179\,\mathrm{kbit\,s^{-1}} \tag{3.12}$$

$$R_{bh,o} = N_c \cdot (R_{sms,o} + 0.1 \cdot R_{voice,i} + R_{sa,o}) + R_{cb,o} + R_{wp,r,0} = 45 \cdot (56.9 + 0.1 \cdot 104 + 1.3) + 0 + 0 = 3087\,\text{kbit}\,\text{s}^{-1} \quad (3.13)$$

3.4 THE UAV TO MOBILE PHONES LINK

The load for which one cell has to be sized has been found in section 3.3. With this load the amount of transceivers (TRX) per cell can be determined. The transceivers are the main components of the UAV to mobile phone link. When the amount of transceivers is selected, the next thing will be the selection of the antenna and then finally the link budget can be recalculated to check if the range is sufficient.

3.4.1 TRANSCEIVERS PER CELL

To find the amount of transceivers or carrier frequencies that the cell requires. The first thing to be done is find the amount of physical channels needed for each service. When that is known they can be added and the total number of physical channels required can be found. One transceiver supports 8 physical channels. Dividing the total number of physical channels by 8 and rounding it up to the nearest integer gives the amount of transceivers that is needed. This is shown in eq. (3.14). The channels needed are broken down into the provided services and a number of signalling channels. For the first service, voice, the amount can be directly taken from section 3.3.

$$N_{TRX} = \left\lceil \frac{C}{8} \right\rceil = \left\lceil \frac{C_{voice} + C_{data} + C_{sms} + C_{signalling}}{8} \right\rceil \quad (3.14)$$

For the second one, C_{data}, a quick recap of the contents of the previous report [3] is needed. With EDGE one physical channel can support a 59.2 $\text{kbit}\,\text{s}^{-1}$ data rate. It has to be noted that this is in an ideal case. It is hard to determine the actual throughput of the channels at this point, therefore for now 59.2 $\text{kbit}\,\text{s}^{-1}$ per channel is assumed. Only the download is taken into account for the determination of the channels. Every download slot is always accompanied by at least one upload slot and the required upload rate is a lot lower than the download rate, so this will not lead to any problems. The number of channels is determined in eq. (3.15).

$$C_{data} = \left\lceil \frac{R_{wp,s,o}}{59.2} \right\rceil = \left\lceil \frac{3.8 \cdot 1024}{59.2} \right\rceil = 66 \text{ channels} \quad (3.15)$$

The number of channels required for SMS is calculated in a similar way. But first the average number of text messages per second, S, needs to be determined. The inbound and outbound messages together will determine the amount of channels needed. The sum of the two is calculated in eq. (3.16).

$$S = \frac{P}{t_{sms,d}} + \frac{V_s}{3600} = \frac{5333}{180} + \frac{53330}{3600} = 44.4 \frac{\text{msgs}}{s} \quad (3.16)$$

The text messages are sent over so called standalone dedicated control channels (SDCCH). These are logical channels that can be fit onto the physical channels in several ways. The one that is used in this case is the SDCCH/8 mapping. With this mapping one physical channel can contain 8 SDCCH channels. The last thing needed to complete the picture is the average amount of time the sending of one text message blocks an SDCCH channel. The mean holding time (MHT) of a text messages is assumed to be 6 seconds [11]. This means that one SDCCH/8 channel can support on average $8/6 \approx 1.3$ messages per second. The required amount of channels is found in eq. (3.17).

$$C_{sms} = \left\lceil \frac{S}{8/6} \right\rceil = \left\lceil \frac{44.4}{8/6} \right\rceil = 34 \text{ channels} \quad (3.17)$$

The amount of signalling channels, $C_{signalling}$, will be set to 1 for the broadcast control channel of the cell. All unknowns in eq. (3.14) are now known. The required amount of transceivers is calculated in eq. (3.18).

$$N_{TRX} = \left\lceil \frac{8 + 66 + 34 + 1}{8} \right\rceil = 14 \quad (3.18)$$

In the previous report the concept of frequency reuse was explained. There it was decided to use a frequency reuse ratio of 12 together with the P-GSM band. This gave a maximum of 10 carrier frequencies per cell. Now that the amount of transceivers needed per UAV is calculated this has to be revised. A total of 14 transceivers will require 14 distinct carrier frequencies. This is over the limit. The two possible solutions are lowering the frequency reuse ratio or picking another GSM band. Lowering the frequency reuse ratio would increase the risk of interference and since the system needs a bigger interference margin than conventional cellular systems because of the maneuvering UAVs this option is not considered feasible. Therefore it has been chosen to switch to the E-GSM band. This band has room for 175 carrier frequencies [12]. By keeping the reuse ratio at 12 the amount of carriers per cell, rounded down, now becomes $\lfloor 175/12 \rfloor = 14$. This is enough and leaves 7 carriers unused ($175 - 12 \cdot 14 = 7$).

3.4.2 CONNECTION SETUP AND HANDOVER

When the communication network on the UAVs is turned on, the transceivers will start transmitting on the broadcast channel. The mobile phones will receive this and they will try to connect to the cell with the highest received power. The connection process will require some of the systems communication capacity. This is however not taken into account during the analysis, because during the connection process the phone cannot use the other services like SMS and data yet. The reserved capacity for those services can therefore be used for the connection process.

When a phone is connected to one cell and the phone moves out of that cell. It will try to connect to a new cell that is in reach. This will also use some of the systems capacity. The load of this is assumed to be negligible because during the disaster people will stay within a small area. It is also possible that instead of the phone the cells moves. The cell is connected to the UAV so if the the UAV moves the cell moves with it. This can be a big problem if the UAVs move a lot. If one UAV will move one cell diameter away from its initial position, all the phones in that cell will have to reconnect. This will cause a high and unnecessary load on the system. Therefore it is chosen to let the UAVs loiter in circles above their designated cell. This will keep the handover from one cell to another to a minimum.

3.4.3 HARDWARE

The hardware selection is based upon section 3.4.1 where the amount of transceivers needed is found to be 14. In the previous report an estimate of 20kg was made for the weight of communication payload and 344 watts for the power. This estimate can now be refined. First the link budget is recalculated together with the choice of an antenna. Then the hardware and auxiliary equipment is selected.

The tunable parameters of the link budget are the antenna gain and transmission power. The antenna gain depends on its radiation pattern. For this mission an antenna has to be selected that gives the right radiation pattern on the ground from the altitude at which the UAV is flying. If the system uses 45 cells that together cover at least 100km^2, then one cell should cover $100/45 = 2.2$ km^2. If a circular cell is assumed an average radius of the cell can be calculated with $R = \sqrt{A/\pi} = \sqrt{2.2/\pi} = 0.84$km. The radius of the cell together with the flying altitude determine the required beam angle, β, of the antenna. The relation is given in eq. (3.19).

$$\beta = 2 \cdot \arctan \frac{R}{A} \tag{3.19}$$

Assuming that the UAV's are loitering between 2 and 3 km altitude the optimal beam width would be between 31 and 45 degrees. It has to be noted that it is better to pick a slightly larger beam width because this makes sure that areas do not become uncovered during maneuvering.

There are several antenna designs that can give the required radiation pattern. In the current design a panel antenna was chosen. The reason for this is mainly the form of the antenna that has to fit in the fuselage. Another option would have been a yagi antenna, but this type of antenna is too big in the direction of the maximum gain. This would have meant that a large (>0.5m) pole was sticking outside of the UAV pointing downwards. After discussion with the aerodynamics group this antenna was ruled out. A list of possible panel antenna's is given in table 3.3. From the list the last antenna is selected. This antenna has a gain of 12.5 dBi. This value is used in the recalculation of the link budget.
The last parameter for the link budget is the power. This parameter can be adjusted during operation so only the maximum power is of concern now. This maximum power determines the maximum size of the cell. To calculate the maximum power that is necessary, the distance between the phone and the UAV has to be calculated at the border of the cell. Again assuming the same value for the radius as before and a maximum altitude, h_{max}, of 3 km leads to the maximum distance calculation in eq. (3.20).

$$d_{max} = \sqrt{h_{max}^2 + R_{cell}^2} = \sqrt{3^2 + 0.84^2} = 3.12km \tag{3.20}$$

With the required distance and the antenna gain the link budget was recalculated and this lead to a re-

Table 3.3: Possible antenna's for the GSM communication

Manufacturer	H/V beamwidth [°]	Weight [kg]	Dimensions [mm]	Gain [dBi]
L-com	70/60	1.5	315x315x25	9
Laird Technolgies	55/40	1.36	411x373x36	12
Prosoft	-/-	1	391x391x43	12.5
IteLite	60/55	1.3	345x345x20	10
ARC Wireless	42/42	1.2	391x391x43	12.5

quired transmission power of less than 1 watt. With this lower power than initially thought the selection of transceivers from the previous report can be reconsidered. The model that is now selected as reference for the design is the SatSite model 142 [13]. This device contains 4 transceivers that can transmit with a power of 2 watts each. The weight of this device is 5 kg. The casing of the device is assumed to take up around 2 kg based upon comparing it to similar casings. This will lead to a new estimate of 3 kg for every 4 transceivers. The current design of the communication payload can be found in figure 3.1. It was found before that 14 transceivers were necessary so 4 SatSite model 142 are included in the architecture. They are connected over Ethernet to a central computer. The switch and computer can be standard of the shelf components. A tilting mechanism is also accounted for in the budget. The antenna will have to be pointed and stabilized so that the beam of the antenna is always focused on the center of the cell. The rotation angle of the antenna is analysed in section 12.3.

The refined mass and power budgets can be found in table 3.4. For the computer the PIP39 from the company MPL[1] has been selected as a reference. The reason for this is its ruggedness and powerful processor. The MILTECH 308[2] from techaya was chosen as a reference model for the Ethernet switch also because of its ruggedness and it is marketed for UAV usage. One kilogram of mass has been budgeted for cabling and two kilograms for the combiner/splitter arrangement. The budget for the combiner/splitter is the most uncertain. The traditional design of this is not suitable for usage on a UAV. It uses filters that are too large to carry on the UAV and would require too much of the mass budget. Unfortunately no detailed information could be found on the architecture of this part and the possibilities. In the next phase a cellular communication system expert will have to be consulted. In the worst case scenario this cannot be made light and small. Then a trade off has to be done if it is beneficial to keep the combiner/splitter or use four different antenna's. That means that in the worst case 3 extra antenna's are needed that weigh 1.2 kg each (the 2 kg for the combiner are then removed). The last part in the budget is the tilting mechanism. A general tilting system has been used to get the required budget parameters.[3] A custom mechanism will have to be designed that can interface correctly with the fuselage and supporting structures.

Table 3.4: Payload mass, power and cost budget

Description	Power [W]	Mass [kg]	Cost [$]	Cost [€][4]
Transceivers (4x SatSite 142 without casing)	320	12	39,800	35,260.41
Antenna	-	1.2	40	35.44
Computer (PIP39)	46	1.5	2000	1771.88
Ethernet Switch (MILTECH 308)	2	0.108	200	177.19
Combiner/splitter	-	2	500	442.97
Cabling	-	1	100	310.08
Tilting mechanism (FlyingDream AAT)	30	1	350	88.59
Total	398	18.8	42,990	38,086.56

[1] http://www.mpl.ch/t24f2.html accessed 12-6-2016
[2] http://militaryethernet.com/products/ultra-compact-military-fast-ethernet-unmanaged-switch-8-port/ accessed 12-6-2016
[3] https://www.foxtechfpv.com/flydream-automatic-antenna-v5-12ch-p-367.html accessed on 13-3-2016
[4] Converted from USD to EUR using the exchange rate on 6-16-2016 (0.88594)

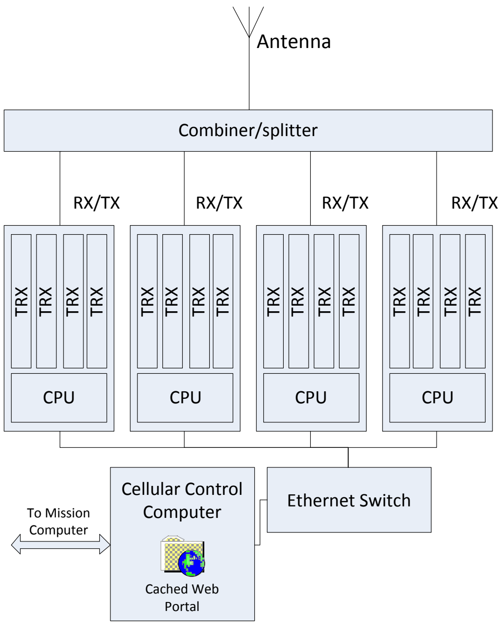

Figure 3.1: UAV to phone communication architecture

3.5 NUMBER OF UAVS

The number of UAVs that need to be deployed depends on the disaster. In this section an estimate is given for the amount of drones that are needed to perform the model mission that was introduced in the mission analysis. The model mission consisted of a square disaster area of 100km^2 and 300.000 people. The main parameters that influence the number of UAVs are the flying altitude, the beam angle of the antenna, maneuverability and the capacity of the mobile communication system. All of these parameters are plotted in figure 3.2. Each parameter will now be discussed.

The flying altitude, h, and beam angle, β, influence the size of the cell. The flying altitudes for three beam angles are plotted as a function of the number of UAVs in figure 3.2. The lines are labeled 40° beam, 50° beam and 60° beam. It is assumed that each UAV is responsible for one cell. The relation shown in eq. (3.21) is used to plot the lines. The total area is equally divided by each cell. Then the radius of the cell is calculated based upon this area. By constructing a right angled triangle with one angle set to half the beam width. The side adjacent to this angle and the right angle is then the flying altitude and can be solved with the tangent function and by setting the other right angled side to the cell radius.

$$h = \frac{\sqrt{\frac{A}{N_c \cdot \pi}}}{\tan \frac{\beta}{2}} \tag{3.21}$$

The dotted vertical lines are the lower limits on the number of UAVs based upon the available channels in the E-GSM and P-GSM band. If less UAVs are used then the load per UAV becomes too high and would require more carrier frequencies than available. The limit is found by executing the model from section 3.3 for all number of UAV's in the plot. The point were the amount of carrier frequencies per UAV (eq. (3.14)) exceeds the number available is marked with the dotted line. The part of the plot on the left side of each line is infeasible.

The solid vertical lines are the upper limits on the number of UAVs based upon the bank angle. The bank angles of 15°, 20° and 25° are plotted in the graph. For each bank angle a corresponding turn radius can be calculated. This is explained in section 13.4. The choice is made to not make the cell radius smaller than two times the turn radius for collision avoidance. With this rule the maximum number of UAVs for a certain bank angle can be calculated. The minimum radius for the cell follows from the turn radius. With the cell radius the cell area can be calculated. And the total area divided by the cell area will result in the maximum number of cells/UAVs. The lines depict the maximum, so the right part of each line is unfeasible.

From the plot, 45 was selected as the default number of UAVs for the design. It was decided that from a cost and operations perspective a lower number of UAVs would be preferable. A total of 45 UAVs is slightly above the E-GSM limit and will lead to flying between 3 and 2 km altitude with a 42 degree beam width antenna.

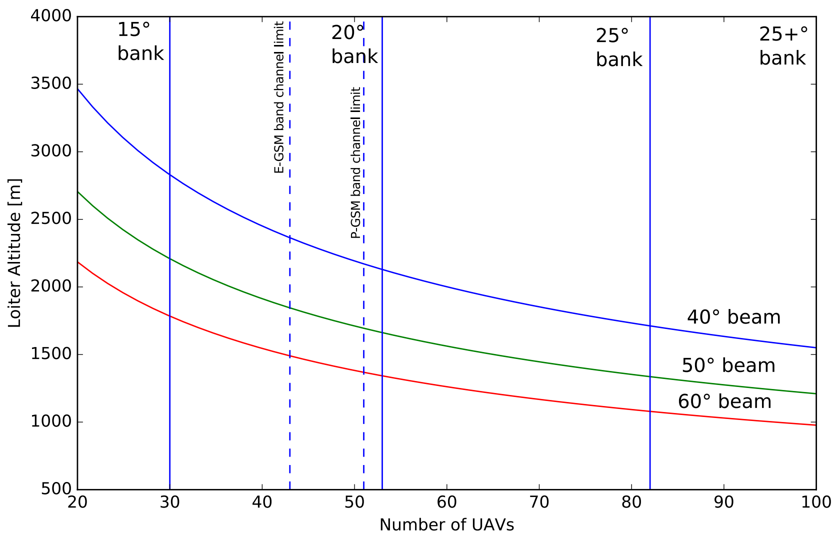

Figure 3.2: Plot for selecting the number of UAVs (Based upon 300.000 people in disaster area of 100km^2)

3.6 COMMUNICATION SYSTEM SIZING FOR NON-PAYLOAD LINKS

In this section, all aspects concerning the sizing of the communication system for non-Payload links will be dealt with. Non-Payload links are defines as all those links that do not directly involve the payload in the link itself. In the case of the WiFly system, it would be any communication link that does not involve the users in the disaster area. Therefore, there are 2 links that belong to this category: links between each UAV (swarm links) and links between a UAV and the ground base (base links). In order to properly size the communication system, it is necessary to take into account all the factors that influence the comms link. This is done by means of a "Link Budget", whose functioning and components are explained in section 3.6.1. The link budget additional losses are estimated in section 3.6.2. The hardware that allows the creation of a mesh network within the swarm is illustrated in section 3.6.3. The choices of radio frequency, radio cards and data rate estimation are then explained in section 3.6.4. Amplifiers and antennas are picked in section 3.6.5, while all the final link budgets are sized in section 3.6.6. Finally, the power, mass and cost budgets for all the communication hardware are shown in section 3.6.7.

3.6.1 INTRODUCTION TO COMMUNICATION LINK BUDGET

The theory behind link budgets was already explained extensively in [3]. This section is meant to give a short summary, to be used for quick reference when reading this report. If more information is needed, please consult [3]. The purpose of the link budget is to check whether a specific communication link closes. It takes into account all aspects that affect the signals along its path, and results in a "margin" being produced at the end of the budget. If the margin is positive, the link can be closed, and communication is possible. The list below quickly illustrates each component of the link budget.

- **Transmit power (P_t):** the power at which the signal is generated from the transmitter.

- **Amplifier Gain (G_{amp}):** the gain that the amplifier adds to the signal. The higher the gain, the more the signal will be amplified.

- **Transmit antenna gain (G_t):** the gain of the transmitting antenna. Gain determines how focused the signal beam is. An omnidirectional antenna will have a gain value of one, since all power is distributed equally. The more directional the antenna, the higher the gain. Antenna gain depends on the antenna type, shape, dimensions, as well as the wave-length of the signal. For parabolic antennas, it can be calculated using eq. (3.22), from [14].

$$G_r = \left(\frac{\pi D_r^2}{\lambda^2}\right)\eta \tag{3.22}$$

  Where D_r is the antenna diameter, λ is the signal's wavelength and η is the antenna efficiency, which depends on the type of antenna selected (0.55 for parabolic ones).
- **Free-Space Path Loss (FSPL):** the decrease in signal power due to the space between the transmitting antenna and the receiving one. It can be calculated using eq. (3.23) from [14]:

$$FSPL = \left(\frac{\lambda}{4\pi S}\right)^2 \tag{3.23}$$

  Where λ is the wave-length of the signal and S is the distance between transmitting and receiving antenna.

- **Additional losses (L_a):** this is the reduction in signal power due to various factors. In the case of the WiFly mission, there are three main factors: **atmospheric losses**, **rain losses** and **airframe interference losses**. The first are losses due to interaction between the signal and the atmosphere. This includes the power that is absorbed by the gases in the atmosphere (which is almost constant), as well as some variable factors, such as rain attenuation. Airframe interference is caused by the body of the UAV interfering with the transmission of the signal (signal is reflected from the aircraft body, or has to go through it).

- **Receiving Antenna Gain (G_r):** it is the same as the transmit antenna gain (G_t), only applied to the receiving antenna.

- **Antenna pointing loss (L_{pr}):** the reduction in received signal power due to pointing errors in the transmitting and receiving antennas. It can be calculated (in dB) using eq. (3.24) from [14]:

$$L_{pr} = -12 \cdot \left(\frac{e_t}{\alpha_{1/2}}\right)^2 \tag{3.24}$$

  Where e_t is the pointing offset in degrees, while $\alpha_{1/2}$ is the antenna half-power beamwidth angle in degrees. The antenna half-power beamwidth angle (or HPBW angle) can be calculated using eq. (3.25), from [14]

$$\alpha_{1/2} = \left(\frac{21}{f \cdot D}\right) \tag{3.25}$$

  Where f is the signal's frequency and D is the transmitting antenna's diameter.

- **Received Power (P_r):** it is simply the amount of power detected by the receiver in the receiving system.

- **Receiver Sensitivity (S_i):** it is the sensitivity of the receiver. In other words, this parameter indicates the minimum signal power that the receiver can detect and read properly. This values depends on a series of factors, mainly the noise generated by the receiver itself, the external noise present on the receiver's frequency and the data rate of the link. If the received power is lower than the receiver sensitivity, the receiver will not be able to properly read the signal.

- **Link Margin (S_{margin}):** it is simply the margin between the received power and the receiver sensitivity. In order for the link to close properly, it needs to be positive. While there is no absolute standard on how large the margin should be, it is considered good practice to close the link with a margin of at least 3dB.

The received power can therefore be written as a function of the aforementioned elements. The result is eq. (3.26).

$$P_r = P_t \cdot G_{amp} \cdot G_t \cdot FSPL \cdot L_a \cdot G_t \cdot L_{pr} \tag{3.26}$$

Where all the parameters are expressed in their standard units. In case dB are used, the conversion shown in eq. (3.27) should be applied to each of the parameters.

$$X\left[dB\right] = 10 \cdot \log_{10}\left(\frac{X}{X_{ref}}\right) \tag{3.27}$$

If dB are used, all multiplications are turned into additions, while all divisions are turned into subtractions. The formula for the received SNR in dB is shown in eq. (3.28).

$$P_{r_{dB}} = P_{t_{dB}} + G_{amp_{dB}} + G_{t_{dB}} + FSPL_{dB} + L_{a_{dB}} + G_{t_{dB}} + L_{pr_{dB}} \tag{3.28}$$

The link margin can be easily calculated through eq. (3.29)

$$S_{margin} = P_{r_{dB}} - S_{i_{dB}} \tag{3.29}$$

3.6.2 ESTIMATION OF LINK BUDGET ADDITIONAL LOSSES

The "Additional Losses" (L_a) component of the link budget depends principally on the environment in which the UAV is operating and the airframe in which it is housed. For the WiFly's communication system, 4 main components of the "Additional Losses" have been estimated: atmospheric attenuation, rain attenuation, airframe interference and antenna polarization mismatch.

Atmospheric attenuation is the loss of signal power caused by the interaction between electromagnetic waves and the gases present in the atmosphere. It can be estimated in dB lost per km that the signal had to travel. Its value will of course depend on the composition of the atmosphere, on the frequency, on the signal and on the distance it has to travel. The calculations required to estimate the dB/km loss can be very complex. Fortunately [15] (a report from the ITU, which is an extremely reputable source in the field of communications) provides all the information necessary to estimate the atmospheric attenuation, depending on the type of communication link. In the case of the WiFly system, the communication link could have a frequency between 1GHz and 6 GHz, as explained in [3]. Moreover, the link's signal will be a low elevation terrestrial one, meaning that the elevation angle of the signal's path is smaller than 5 degrees, and that both the receiver and transmitter are located close to the Earth's surface, implying that the signal will always stay within the lowest layer of the Earth's atmosphere. In [15], the specific attenuation (dB/km) is depicted for low elevation terrestrial signals ranging between 1 and 350 GHZ. The specific atmospheric attenuation coefficients for frequencies between 1GHz and 6GHz are taken from [15], and are listed in table 3.6.

As it is possible to see from the table, the higher the frequency, the higher atmospheric attenuation will be. It is therefore beneficial to choose a frequency as low as possible.

A similar procedure was followed to estimate **rain attenuation losses**. As for the atmospheric losses, a specific rain attenuation coefficient was calculated. In this case, it was determined by means of equations provided in [16]. Equation (3.30) illustrates how to obtain the specific rain attenuation coefficient:

$$\gamma_R = kR^{\alpha} \tag{3.30}$$

Where γ_R is the specific rain attenuation coefficient expressed in dB/km, R is the rainfall rate in mm/h, and k and α are given frequency dependent coefficients for vertical and horizontal polarization. They can be found in [16]. For other types of polarization, k and α have to be determined through eq. (3.31)

$$\begin{aligned} k &= \left[k_H + k_V + \left(k_H - k_V\right)\cos^2(\theta)\cos(2\tau)\right]/2 \\ \alpha &= \left[k_H\alpha_H + k_V\alpha_V + \left(k_H\alpha_H - k_V\alpha_V\right)\cos^2(\theta)\cos(2\tau)\right]/2k \end{aligned} \tag{3.31}$$

Where θ is the path elevation angle, τ the polarization tilt angle relative to the horizontal, and the subscripts "H" and "V" indicate horizontal and vertical antenna polarization. Given that τ is always 45° for circular polarization, the equations in 3.31 simplify to

$$\begin{aligned} k &= \left[k_H + k_V\right]/2 \\ \alpha &= \left[k_H\alpha_H + k_V\alpha_V +\right]/2k \end{aligned} \tag{3.32}$$

All the values of k and α can be found in [16]. In order to obtain the specific rain attenuation coefficient, only the rainfall rate is missing.

The rainfall rate R to be used in eq. (3.30) depends on two factors: the geographic location where the UAV is operating, and the availability that the link should have. The reasons behind the influence of the first factor are obvious: different locations on Earth are subjected to different amounts of rainfall. The second factor is there to ensure that the communication link is designed for the correct amount of rainfall. To make an example, if an availability of 99.9% is required, the chosen rainfall rate should be the rate that is only exceeded during 0.1% of the time in that specific geographic area. Section 3.6.2 shows a list of rainfall rates depending on geographic location and percentage of time (hence probability) of exceeding said rates.

In the case of the WiFly system, an availability of 99.8% is required, as illustrated in [3]. Hence the "0.01" row is selected from section 3.6.2. The design case for the system is a natural disaster in Rotterdam, hence the Netherlands should theoretically be picked as a geographic location.

Table 3.5: Table listing the rainfall rates depending on geographic location and probability of exceeding said rates. Taken from [17]

Percentage of time R exceeded	Zone														
	A	B	C	D	E	F	G	H	J	K	L	M	N	P	Q
1.0	<0.1	0.5	0.7	2.1	0.6	1.7	3	2	8	1.5	2	4	5	12	24
0.3	0.8	2	2.8	4.5	2.4	4.5	7	4	13	4.2	7	11	15	34	49
0.1	2	3	5	8	6	8	12	10	20	12	15	22	35	65	72
0.03	5	6	9	13	12	15	20	18	28	23	33	40	65	105	96
0.01	8	12	15	19	22	28	30	32	35	42	60	63	95	145	115
0.003	14	21	26	29	41	54	45	55	45	70	105	95	140	200	142
0.001	22	32	42	42	70	78	65	83	55	100	150	120	180	250	170

The letters for each Zone in section 3.6.2 are associated to their respective geographic areas in [17]. The Netherlands are located in zone E. Looking at section 3.6.2, it is easy to see that precipitations in zone E are much lower compared to other Zones. Since the WiFly system is being designed for worldwide use, it was decided to design for the most realistic worst case scenario. The communication link for the WiFly system must be available for at least 99.8% of the time, hence the link must be able to cope with rainfalls that occur at least 99.8% of the time, meaning that it is necessary to look at the row with an R value of 0.1. The worst possible rainfall rate would therefore be of 72 mm/h, which corresponds to Zone Q. While Zone Q presents the strongest rains (for that value of R), it only encompasses the coastal area of Cameroon. Zone P, which is the second worse, is much more widespread (central Africa, Philippines, etc). It was therefore decided to design for zone P, making the design rainfall rate 65 mm/h. Now that all parameters of eq. (3.30) are known, it is possible to calculate the specific rain attenuation depending on carrier frequency and antenna polarization. The results are shown in table 3.6:

As it is possible to see from table 3.6, higher frequencies lead to higher losses, for both atmospheric and rain attenuation. Concerning polarization, the lowest losses are achieved by the vertical one, followed by circular polarization, and finally horizontal.

In order to properly estimate **airframe interference**, it would have been necessary to predict how the signal would interact with the airframe in which the antennas are housed. This is a quite complicated and time

Table 3.6: Table showing the specific attenuation factors (in dB/km) for atmospheric attenuation and rain attenuation

Frequency [GHz]	**Specific atmospheric attenuation factor [dB/km]**	**Specific rain attenuation factor [dB/km]**		
		Vert. Polar.	Hor. Polar.	Circular Polar.
1	-0.0055	-0.0278	-0.0370	-0.0316
1.5	-	-0.0603	-0.0778	-0.0668
2	-0.007	-0.131	-0.182	-0.152
2.5	-	-0.246	-0.356	-0.293
3	-0.00767	-0.421	-0.595	-0.480
3.5	-	-0.680	-1.079	-0.747
4	-0.008	-1.124	-2.138	-1.262
4.5	-	-2.0145	-3.959	-2.480
5	-0.00885	-3.631	-6.444	-4.749
5.5	-	-5.897	-9.575	-7.674
6	-0.0095	-8.660	-13.460	-11.053

consuming procedure, which often requires practical tests. Since this was outside the scope of the project, a pessimistic estimate was taken from literature. Specifically, three different values for airframe interference are provided in [18] (page 737). In case a single antenna is used on the UAV, the worst case scenario will induce an airframe attenuation of -28dB (assuming that the antenna is encased in a Radio-Frequency transparent housing). If more than one antenna is used at once, the worst attenuation value will be of -13dB: this technique is called "antenna diversity", and allows for an improvement of 15dB over the previous value. Finally, the loss can be further reduced to -10dB if multiple antennas are also employed on the ground. However, this requires at least 3 different ground antennas, spanning a minimum of 180° of an arc as seen from the UAV. Since the WiFly system has to cover a $100km^2$ area, this would mean that the antennas should be spaced extremely far away from each other. This creates a lot of issues from the point of view of logistics and resource allocation. The 3dB improvement over the previous value simply is not worth the amount of resources necessary to tackle said issues.

Finally, losses due to **polarization mismatch** were taken into account. Polarization losses depend on the orientation between the electromagnetic field of the transmitting antenna and the field of the receiving one. The polarization loss factor (PLF) is defined in eq. (3.33), taken from [19].

$$PLF = \cos^2(\Phi) \tag{3.33}$$

So for example, if one of the antennas is horizontally polarized, and the other is vertically polarized, the angle Φ between them will be of 90°, leading to a PLF of zero, which results in no signal being received. If on the other hand both antennas have vertical polarization, and are at an angle of 30° from each other, the PLF will be $\cos^2(30°) = 0.75$ or -1.25dB. This means that the orientation of the antennas is extremely important in order to ensure low losses. Since antennas with circular polarization do not suffer from polarization mismatch losses (as explained in [19]), in an ideal case both the UAV and the ground station would be equipped with such antennas. However, they also have higher size and worse omnidirectional performance when compared to vertically polarized antennas, thus making their use on a UAV not ideal. A good compromise is obtained by installing a circularly polarized antenna on the ground, and a vertical one in the UAV. Since circular polarization is basically the superposition of an horizontal and a vertical electromagnetic field, the largest angle Φ between the circular field and the vertical one will always be 45°, resulting in a worst case PLF of 0.5, or -3dB, regardless of the antennas' orientations.

To summarize the findings concerning the additional losses, it has been determined that lower frequencies are beneficial for both atmospheric and rain attenuation. It has also been determined that vertical polarization is preferred for rain attenuation, followed by circular and horizontal polarization. It has also been determined that the optimal way of compensating for airframe interference is UAV antenna diversity, but not necessarily ground antenna diversity. Finally, it was found that the best compromise to reduce polarization mismatch losses is equipping the UAV with a vertically polarized antenna, and the ground base with a circularly polarized one. Keeping only these factors into account, the ideal UAV system would make use of low carrier frequencies, have multiple vertically polarized antennas mounted on the UAV, and possible a single high gain circularly polarized antenna mounted on the ground.

3.6.3 MESH ARCHITECTURE HARDWARE

One of the WiFly system's defining traits is the fact that it is composed of a swarm of UAVs. Within the swarm, tasks and information are shared across all members. This means that it is necessary to have each UAV connected to at least another UAV within the swarm at all times, so that no aircraft is left "isolated" from the swarm. While an ad-hoc communication link management system could theoretically be designed from scratch, it would require a considerable amount of time, technical expertise and money. Since it was already decided to implement as many "off-the shelves" components as possible for the WiFly system, it made sense to select and existing commercial solution to implement the mesh functionality in the WiFly network. The selected hardware is the Mesh Dynamics MD4000 mesh node. A mesh node is simply a "unit" which carries out communications within a mesh network.

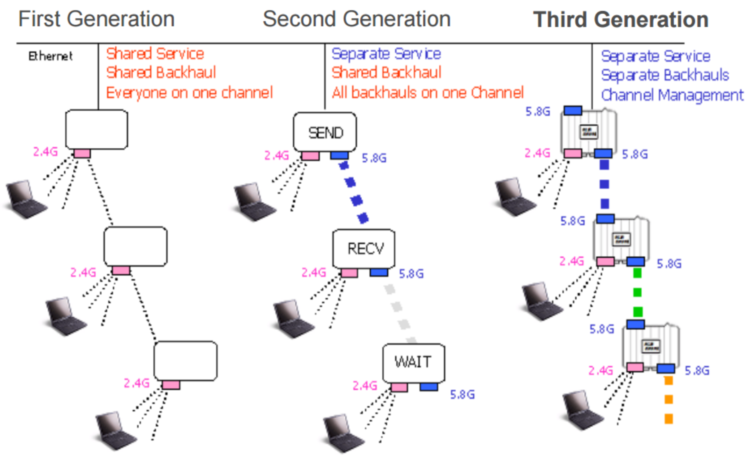

Figure 3.3: Figure showing the different characteristics of 1st, 2nd and 3rd generation mesh nodes. Taken from [20]

Before illustrating the MD4000's characteristics, it is necessary to briefly explain what its purpose is. The MD4000 turns any system it is installed on into a mesh node. It provides multi-radio backhaul links on non-interfering channels. It can house and manage up to four 400mW radios in the same enclosure. Said radios can operate on either 802.11a channels in the 5GHz frequency, 802.11b/g channels in the 2.4GHz frequency and Public Safety band channels in the 4.9GHz frequency. The four separate radio cards that can be integrated in the MD4000 allow for the creation of a "Third Generation mesh network". Information concerning the different generations of mesh networks can be found in figure 3.3. First and second generation networks can only provide "walkie talkie like" functionalities. They are not capable of simultaneously communicating with the user on the ground and maintain multiple uplink and downlink backhaul links. They can only perform one of these actions at a time, as no more than two radios are available for all functionalities, resulting in extremely time consuming and inefficient communications.

Third generation nodes allow for the use of 3 or more radios. This means that each node can now devote one radio to providing user traffic, and two radios to backhaul functionality, allowing for simultaneous backhaul downlink and uplink. Each node is basically free to transmit and receive freely, without having to stop or coordinate with other nodes. This is exactly what the WiFly system needs, as each UAV should be able to communicate both simultaneously and constantly with other UAVs within the swarm. In the case of the WiFly system, user traffic is provided by a separate communication system, described in section 3.2. All four radios to be installed in the MD4000 will hence be used exclusively to communicate with other nodes in the mesh network.

Each radio can handle one link at a time, meaning that every single UAV in the swarm will be able to communicate with four other UAVs simultaneously, in either uplink or downlink. Thanks to the MD4000, mesh nodes will interact automatically among themselves to make sure that every node is connected, and that the swarm as a whole can communicate with the ground base. The ground base can be seen as a "parent node", to which all nodes try to gain access in order to receive and send relevant information. The UAVs are "child nodes": they need to communicate with the parent in order to perform their mission. The MD4000 will always make sure that every child node is connected to the parent one, either directly, or through relays of other child nodes, as illustrated in figure 3.4. If a child node was to move away from the cluster of nodes to which it is currently connected, it would automatically connect to other child nodes within range, so that no node is ever left isolated from the parent, or from the rest of the swarm. In the unlikely case that a cluster of nodes loses contact with the parent, the MD4000 will allow them to automatically form a local mesh network, keeping them in contact and exchanging all necessary information, as shown in figure 3.4

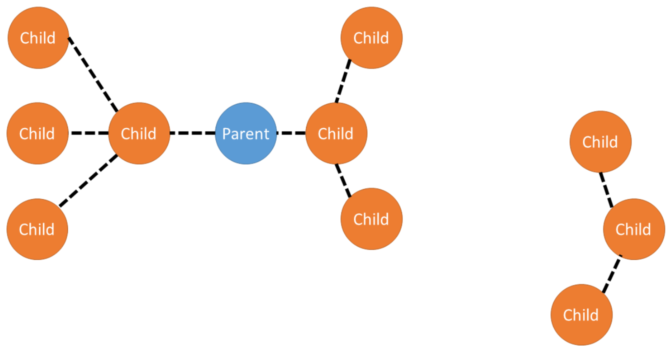

Figure 3.4: Figure showing the links between parent and child nodes within a mesh network.

The MD4000 also comes with its own dedicated software, which allows for easy configuration of both the single nodes, or the whole mesh. The software is called "Network Management System" (NMS), it runs on any Java compatible computer, and it allows for "point and click" management of the whole network. Its user friendliness and wide compatibility add further value to the choice of using the MD4000. More information about the MD4000 can be found in [21]

3.6.4 CHOICE OF RADIO FREQUENCY AND RADIO CARDS, ESTIMATION OF MAXIMUM DATA RATE

As mentioned in section 3.6.3, each UAV can be fitted with up to four 400mW radio cards, with a radio frequency of either 2.4, 4.9 or 5.8 Ghz. Three different models of radio cards were considered, each one operating in one of the aforementioned frequencies. All three cards belong to the "XtremeRange" series of radio modules, designed by "Ubiquiti Networks". The three different radio cards are named XR2, XR4 and XR5. Their technical data sheets are shown in [22], [23] and [24]. The number indicates the frequency at which they operate (respectively 2.4, 4.9 or 5.8 Ghz). Their performance in terms of receiver sensitivity and maximum power consumed is almost identical, with the XR4 performing slightly worse than the rest. The exact values of receiver sensitivity and power consumption can be found in table 3.7

All cards can emit a maximum of 600mW. Given that this is higher than the 400mW supported by the MD4000, their output power will be capped to 400mW, or 26dB. Since the cards all have the same performance, the choice of radio frequency will revolve around the frequency dependant losses estimated in the link budget. These are the free space path loss, the atmospheric attenuation and rain attenuation. The first is illustrated in section 3.4.1, the last two in section 3.6.2. For the sake of comparison, a distance of 100km has been chosen, the antenna is considered to be vertically polarized, and the frequencies are taken to be 2.4Ghz, 4.9Ghz and 5.8Ghz. The different losses for the different frequencies are listed in table 3.8.

It can be easily seen that the 2.4GHz is vastly superior to all other frequencies for both Free space path loss and rain attenuation. In case the receiving antenna is a parabolic one, the higher FSPL of higher frequencies is compensated by higher gains. However, this is not the case for the omnidirectional cylindrical antennas. Hence higher frequencies will often mean higher FSPL. While atmospheric attenuation is more or less the same for all frequencies, rain attenuation presents extremely different values. Given the much higher rain at-

Table 3.7: Table showing the performance of the XR2, XR4 and XR5 radio cards for both transmission (TX) and receival (RX), depending on the Data-rate of the link.

Data	XR2		XR4		XR5	
Rate	**TX Power**	**RX Sensitivity**	**TX Power**	**RX Sensitivity**	**TX Power**	**RX Sensitivity**
1 Mbps	28 dB_{mW}	-97 dB_{mW}	24 dB_{mW}	-	28 dB_{mW}	-
2 Mbps	28 dB_{mW}	-96 dB_{mW}	24 dB_{mW}	-	28 dB_{mW}	-
6 Mbps	28 dB_{mW}	-94 dB_{mW}	24 dB_{mW}	-92 dB_{mW}	28 dB_{mW}	-94 dB_{mW}
9 Mbps	28 dB_{mW}	-93 dB_{mW}	24 dB_{mW}	-90 dB_{mW}	28 dB_{mW}	-93 dB_{mW}
12 Mbps	28 dB_{mW}	-91 dB_{mW}	24 dB_{mW}	-89 dB_{mW}	28 dB_{mW}	-91 dB_{mW}
18 Mbps	28 dB_{mW}	-90 dB_{mW}	24 dB_{mW}	-88 dB_{mW}	28 dB_{mW}	-90 dB_{mW}

Table 3.8: Table depicting different losses for the three frequencies being considered. For the sake of comparison, a distance of 100km has been assumed.

Frequency	Free space path loss [dB]	Atmospheric attenuation [dB]	Rain attenuation [dB]
2.4 GHz	-140	-0.727	-0.986
4.9 GHz	-146	-0.885	-13.2
5.8 GHz	-148	0.00937	-30.2

tenuation values that characterize higher frequencies, it was chosen to use exclusively the 2.4Ghz frequency for all communications. To be precise, the XR2 operates exactly between 2.412GHz and 2.462GHz. It should be noted that these frequencies belong to the "unregulated frequency bands", which means that no license from any organization is required to operate within them. National laws however put limits on the amount of power that unlicensed communication systems can emit at these frequencies. Therefore there will be a very high amount of devices emitting 2.4GHz signals, but their range will be short. As a result, there should be no interference between external devices and the WiFly communications, since the lowest altitude the swarm will fly at is 2km.

Finally, since a radio has been selected , it is possible to determine the receiver sensitivity, once the total data-rate is known. In the worst case scenario, one relay drone will have to relay between the swarm and the base the data for the whole swarm. The maximum data-rate is simply the sum of the non-payload data rate and the payload data-rate, both for the whole swarm. The first had already been calculated in [3]: adapting the calculation to 45 UAVs (instead of the previous value of 50) will yield a non-payload uplink data-rate of 28.425 kbit/s, and a downlink one of 53.117 kbit/s. The maximum uplink data-rate for payload communications is 2178.7 kbit/s, as shown in eq. (3.12), while the downlink one is of 3087 kbit/s, as shown in eq. (3.13). The total maximum uplink data-rate is given in eq. (3.34), while the downlink one is given in eq. (3.35)

$$UL = UL_{payload} + UL_{non-payload} = 28.425 + 2178.7 = 2207.125 kbit/s = 2.25 Mbit/s \tag{3.34}$$

$$DL = DL_{payload} + DL_{non-payload} = 53.117 + 3087 = 3140.117 kbit/s = 3.14 Mbit/s \tag{3.35}$$

Now that the frequency and radio cards have been picked, it is time to select the remaining components of the communication system, namely antennas and amplifiers.

3.6.5 CHOICE OF AMPLIFIER AND ANTENNAS

This section will explain the reasons behind the choice of amplifier and antenna hardware. The amplifier will be analyzed first. The XR2 radio card can output a maximum (signal) power of 600mW, or 27.8dB. This signal however has to go through the MD4000, which instead imposes an upper cap of 400Mw, or 26dB, hence the signal's maximum power could be 26dB. Looking at table 3.9, it is clear that 26dB of output power, as opposed to the current 44dB, would not be enough. The low signal power could have theoretically been fixed by using a omnidirectional high gain antenna, but this would have resulted in a very small HPBW elevation angle, meaning that the UAVs could risk loosing contact every time that they banked. This was clearly not acceptable, hence an amplifier was implemented.

The chosen amplifier model is the TTRM1004-D02, developed by "Triad RF Systems". This particular amplifier was chosen for a variety of reasons. First of all, it has a very high output power, compared to similarly sized competitors. Secondly, it is very lightweight and small in size, resulting in a lighter and smaller communication system. An heatsink is also included within the amplifier design, so the high output powers within the small enclosing of the amplifier will not cause any risk of overheating. Finally, it supports exactly the frequency range of interest. Figure 3.5 shows the most relevant characteristics of the TTRM1004-D02. All other data can be found in the product fact-sheet [25].

TX SPECIFICATIONS				
PARAMETER	MIN	TYP.	MAX	UNIT
Operating Frequency	2400		2500	MHz
PSat Power Output		+44.0		dBm
Gain	24.0	25.0		dB
Gain Flatness		1.0		± dB
Input Return Loss	-12	-16		dB
Operating Voltage	+27	+28	+30	VDC
Current Draw			2.4	A
Tx / Rx Switching Time		1.0	2.0	uS

Figure 3.5: Figure showing the transmission characteristics of the TTRM1004-D02 amplifier. Taken from [25].

The TTRM1004-D02 amplifier has a minimum gain of 24dB, and saturated Power output of 44dB_{mW}, or 25W. This means that the amplifier can output "efficiently" a signal of up to 44dB_{mW} (anything higher than that will result in no improvement, only a waste of energy). This means that the maximum power of the input signal should be limited to 20dB_{mW}. The use of an amplifier (external to the MD4000 system, whose power cap therefore does not apply) allows to output a 44dB signal: 18dB more than a system without an amplifier.

The antennas will now be discussed. The main parameter that influenced antenna choice was gain. As gain increases, so does the directionality (or "focus) of the antenna. An higher gain means that the antenna is able to transmit signals further away, as well as receive them from further away. However the increase in directionality also means that the focus become smaller and smaller. As soon as the receiving system leaves the focus of the transmitting antenna, signal strength drops dramatically.

All the WiFly UAVs are highly mobile transmitters and receivers. Given the variety of scenarios, and given the need to communicate simultaneously with multiple UAVs in a swarm configuration, it is impossible to predict where the receiver will be on the horizontal plane with respect to the transmitter. It is therefore necessary for the antenna to provide a 360 degrees coverage around the UAV. It was decided to use omnidirectional antennas, as they provide equal gain around a 360 degree azimuth angle. In other words, the HPBW angle for the azimuth plane is 360 degrees, as can be seen in figure 3.6. Omnidirectional antennas have however a degree of directionality, which is found in the elevation polar plot, figure 3.7. The gain along the vertical plane is not constant, as it depends on the elevation angle between transmitter and receiver. The higher the overall gain of the antenna, the smaller the HPBW for the elevation plane. Directionality in the vertical plane does not represent a problem for the WiFly system, as the UAVs will be arranged (vertically) in layers, meaning that there will always be some UAVs at the same altitude (zero elevation angle). UAVs at different altitudes (in different layers) can still be contacted, as long as they are not directly above the transmitting one.

It is clear that a trade-off is necessary: higher gain antennas allow for lower transmission power and higher communication range, at the cost of much higher drops in received power when the receiver shifts out of the transmitter's focus. Through numerous iterations of the various link budgets, it was found that a gain of 4.5dB, resulting in an elevation HPBW angle of around 40 degrees, allow for reliable communication in all possible link cases. In order to loiter over their own specific target area, the UAVs will have to bank a maximum of 20 degrees. Thanks to the higher value of the HPBW angle, the link is not cut during banking. Even higher differences in elevation angle, due to different altitudes, would not be enough to interrupt the link.

The chosen antenna for the WiFly system is the OA4-2.5V/9205, created by "Cobham Antennas", its techinical sheet can be found at [26]. It works in a frequency range of 2.4 to 2.7 Ghz, it has a peak gain of 5.9 dB and a

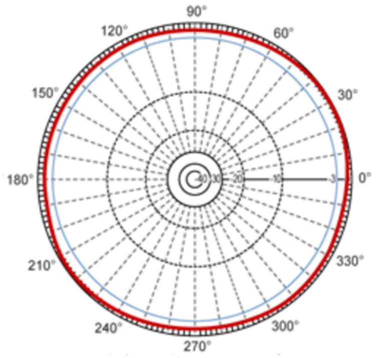

Figure 3.6: Example of a gain polar plot on the azimuth plane.

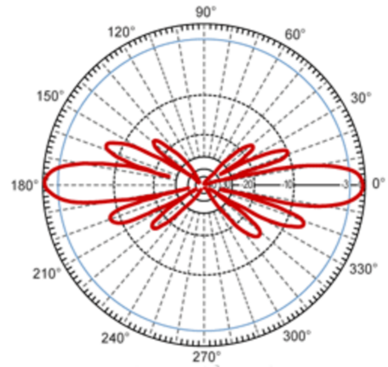

Figure 3.7: Example of a gain polar plot on the elevation plane.

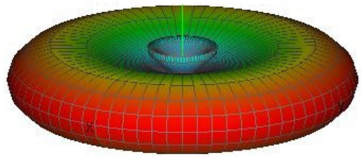

Figure 3.8: Figure showing the 3D pattern of an omnidirectional antenna's gain.

typical one of 4.5 dB. The HPBW angle is of 360° for the azimuth plane, and 42° for the elevation plane. The antenna has vertical polarization, and can output signals of up to 50W (well above the maximum limit of 25W set by the amplifier). More information can be found in the antenna's fact-sheet [27]. It was also decided to install two antennas on each UAV, instead of one. There are two reasons for this: first of all, "antenna diversity" is required to drastically reduce airframe interference losses, as explained in section 3.6.2. Secondly, having two antennas makes the communication system more redundant. One antenna will be placed in the nose of the aircraft, while the other will be located in the back, close to the engine.

While analyzing the redundancy of the communication system, it was realized that two antennas may not be enough. In case of failure of one of them, airframe interference may result in the occurrence of "blind spots", areas where the UAV can neither transmit nor receive any signals. Since this is to be avoided at all costs, two smaller antennas have been implemented in the design. These antennas are only to be used in case the main antennas are not capable of performing adequately. The chosen model is the ABA-2.3V/1964 antenna, produced by "Cobham antennas", its technical sheet can be found at [28]. They will be placed on the UAV, one at each wingtip. The aerodynamic shape of the antenna allows for external mounting without causing any aerodynamic performance degradation. Each of them operates within the 2.2-2.4 Ghz band, has a gain of 2.5 dB, vertical polarization, a HPBW angle of 360° for the azimuth plane and 60° for the elevation plane, and a maximum power output of 10W. More information concerning cost, weight, power consumption and dimensions of any of the aforementioned components can be found in section 3.6.7

3.6.6 FINAL LINK BUDGETS

In this section, the final link budgets are presented. During the design process, several iterations of the link budget were necessary in order to find the hardware components that would satisfy all requirements, and whose implementation in the WiFly system was feasible. The final link budgets for all different link types can be found in table 3.9. All of the link budget components (and how to calculate them) are covered in detail in section 3.6.1.

The links presented in table 3.9 can be split into two categories: links between UAVs (so within the swarm) and links between UAVs and Ground Base.

Before treating each link individually, it is necessary to make some general remarks concerning all links. Whenever the transmitter is a UAV, the transmit power is only 20dB_{mW}, the equivalent of 100mW. Theoreti-

cally the XR2 radio card would be able to output up to 600mW, while the MD4000 could handle only up to 400mW. Such a low transmission power is used because the amplifier can take a maximum input power of 100mW. This has already been explained in section 3.6.5. Looking at table 3.9, it is evident that the use of an amplifier is essential to every single type of link: none of them would "close" if the amplifier was absent, as it provides an additional 18dB (without an amplifier transmit power would be $26dB_{mW}$. The amplifier outputs a max of $44dB_{mW}$), which is more than the margin of any of the links.
It is also possible to notice that, if only the smaller antennas were to be used, an additional loss of 6dB (lower gain plus output power restriction) should be included for downlinks, and a loss of 2dB (lower gain) for uplinks. Since a margin of $3dB_{mW}$ is required in order to properly close the link, it becomes impossible for the damaged UAV to close either the uplink or downlink with a 200 km far base, as well as any uplink or downlink with a 20 km far UAV. The damaged UAV would however still be able to communicate with a 100 km far base, as well as any UAV within a 10 km range. Hence in case the main antennas were to malfunction, a functioning drone would need to escort the impaired one until they are within 100 km of the base.

Looking at table 3.9, one can notice that all receiver sensitives are set to $-95dB_{mW}$. The maximum uplink data rate is 2.2 Mbit/s, while the downlink one is 3.14 Mbit/s, as shown in section 3.6.4. The technical specification sheet for the XR2 radio card gives the receiver sensitivity for data rates of 2 Mbps and 5.5 Mbps, as shown in [22]. It is therefore necessary to use the receiver sensitivity value corresponding to 5.5 Mbps data-rate for both uplink and downlink: said value is exactly $-95dB_{mW}$.

As mentioned before, all links are designed to close with a margin of at least 3dB. While it should be possible to carry out communications as long as the margin stays positive, a margin of 3 dB is required as a contingency for any unexpected losses. All possible pessimistic assumptions have been made: the highest possible banking angle is being used, polarization mismatch losses between UAVs have been exaggerated, as explained in the next paragraph, the worst possible rainfall rate is also being used.

Finally, concerning polarization, all UAV antennas are vertically polarized, while the ground antenna is circularly polarized. This means that the worst possible polarization mismatch loss in UAV-Ground links will always be lower than 3dB, as explained in section 3.6.2. Polarization losses in UAV-UAV links however depend on the orientation of the antennas. Specifically, they depend on the relative pitch angle between the UAVs (if one has a pitch angle of 10°, and another one an angle of −5°, the relative pitch angle between them will be of 15°). Feeding the relative pitch angle in eq. (3.33) would return the actual polarization mismatch loss of two vertical antennas. There are however a multitude of scenarios that may result in different combinations of pitch angles (such as one UAV is climbing and one is cruising, or one is climbing and another one is quickly descending to avoid collision). It was therefore decided to use a worst case scenario relative pitch angle of 45°. This number was chosen for two reasons: firstly, it can be interpreted as the angle between a UAV that is climbing at a 35° angle, and one that is descending at an angle of −10°. The 35° value is the highest possible optimal climb angle, used when climbing immediately after takeoff, at a sea level altitude (shown in figure 13.2). The −10° value can be attributed to a UAV that has to descend in order to avoid a low altitude collision with another aircraft. This is the absolute worst case scenario concerning relative pitch angles, and its likelihood is very low. The second reason for choosing a value of 45° is that it yields a 3dB loss, which is exactly the same polarization loss of all links between UAV and base. Since the communication system design is being driven by the worst case scenarios (long distance links with the base), having the same polarization loss makes the design process easier.

Concerning the specific links, the ones within the swarm will be discussed first: they occupy the second and third column in table 3.9. There are two different instances of UAV - UAV links, one with a distance between UAVs of 10 km, and one with a distance of 20 km. The first link is meant to connect UAVs that are loitering over the disaster area: this is the link that allows the swarm to have information about all UAVs that compose it. A distance of 10 km has been chosen since the network coverage area will measure 100 km^2, so assuming that the area has square-like proportions, a communication range of 10 km would allow contact with most of the swarm. The 20 km distance has been chosen for the "relay UAVs". If the Ground Base is further than 200km from the swarm, the curvature of the Earth will block the line of sight, making direct communication between base and swarm impossible. Hence, it is needed to create a "chain" of relay UAVs (which have the same exact design as any UAV in the swarm).

Starting with the 10km UAV-UAV link, it is possible to see that the same link budget is shared by both Uplink and Downlink. That is because both communication systems on the receiving and transmitting end are identical. The pointing error has been set to 20°, since the maximum banking angle during loiter will be of 20°. Each UAV will have a system that will keep the antenna vertical during banking. It can be imagined as a circle encasing the antenna, resting on a set of ball bearings. If the system is given a low center of gravity, the antenna will stay vertical during banking (perpendicular to the ground). The pointing error angle is still introduced in case the system malfunctions, and the antenna is "stuck" in the vertical position (perpendicular to the wings). As with all other links, the main loss is the free-space path loss. Additional losses are the second largest loss, with the airframe loss being the highest. The link closes with an ample margin: 9.1dB, which is considerably higher than the standard safety margin of 3dB. The reason behind it is that once the amplifier was implemented, it was possible to generate more power than strictly required. Without it however, it would be impossible for the links to close. It is of course possible to output less power, but given that the 10km UAV-UAV link is what allows the swarm to function in the first place, having a larger safety margin only brings benefits.

The 20km UAV-UAV link is mostly identical to the 10km one. The only difference lies in the distance dependent losses, which have been scaled for the new distance. The distance was chosen simply by "stretching" the UAV-UAV link as much as possible, until the distance dependent losses brought the margin down to around 3dB. As mentioned before, the 20km link is needed to form a "chain" of UAVs, which will relay information between the base and the swarm, in case the base is further than 200km from the disaster area, as the line of sight between swarm and base would be blocked by Earth's curvature.

The base-UAV links will be discussed now. Up to 200km distance, the base has line of sight with the swarm. It was therefore decided to design the base's communication system so that it would be able to communicate with UAVs in a 200km radius. Given the relatively small amount of time available, it was not possible to design the base's communication system in the same amount of detail as the UAV's. No "off the shelves" components were picked, but the system was nonetheless properly sized. Since the base system has different hardware from the UAV's, the uplink and downlink present different characteristics, and are presented as separate links. Starting with the 200 km uplink: in this case the transmitter is the ground station. Since no particular hardware was chosen, the amplifier gain has been omitted, and the total output power of the signal is indicated under transmit power. In this case, the output power is 50dB_{mW}, the equivalent of 100W. Using any less power would have required an antenna with a larger gain. However increasing the gain excessively may result in a too small HPBW angle (meaning that the slightest pointing error would cause a loss of contact) as well as an antenna of large dimensions. On the other hand, it is also necessary to keep the power required as low as possible, especially since the ground base may not have easy access to a large and reliable source of electricity. It was therefore decided to make the antenna as "focused" as possible, while keeping its size reasonable, and making sure that most of the swarm would fit within its HPBW angle. Once the antenna size (and therefore gain) was picked, the output power was determined by calculating how much power would be required to close the most challenging link (in this case, the 200 km uplink). The gain of the ground base antenna has a 28.4dB value. Since the antenna is parabolic, this value was calculated using eq. (3.22). To achieve such a gain, an antenna diameter of 2.5 meters was necessary. This diameter resulted in a HPBW angle of 3.5 degrees, calculated using eq. (3.25). As it can be seen in table 3.9, in order for the link to close with a 3dB margin, the pointing error cannot be larger than 3 degrees. This means that no UAV should be further than 3 degrees away from the "focus point" of the antenna. At a distance of 200km, those 3 degrees are the equivalent of $200 \cdot \sin(3°) = 10.47km$. As a very large portion of the swarm will be within a 10 km radius from the antenna's focal point, the HPBW angle was judged to be large enough to allow communications with most of the swarm. Antenna accuracy should however be close to 1 degree, to guarantee that most of the UAVs will be within 3 degrees of the focal point. The maximum polarization loss is -3dB, as the base antenna is circularly polarized, while the UAV antenna is vertically polarized. Receiver sensitivity is the same as all other downlinks, since the ground base is using the same radio cards as the UAV.

The 200 km downlink is almost identical to the 200 km uplink, with the only difference being that now the UAV is transmitting, and the base receiving. This results in different transmit power, the use of an amplifier, and a different pointing loss. The link closes with a margin of 3.7 dB, thanks in great part to the high gain antenna.

The 100km links are included mainly to give an idea of how the link margin scales with distance. Everything that has been said about the 200 km uplink and downlink applies to their 100km counterparts. It can be seen that the margins are much larger, as it was to be expected. The larger margin allows a UAV whose main antennas have been damaged to still communicate with the base, once a distance of 100km has been reached, by using the smaller antennas. The changes in link budgets for the smaller antennas have already been illustrated at the beginning of this section. For a distance of 100km, the ground base antenna's HPBW angle will only cover an area with a radius of 5.23km. This should not be an issue, since a small group of UAVs can easily relay all required information to the whole swarm.

To summarize the contents of this section: it has been proven that, even after making all possible pessimistic assumptions, all links will always close with a safety margin of at least 3dB. This was made possible by the accurate sizing of all components of the communication system, as well as choosing the right hardware for said system. The 10km link will be used by UAVs to communicate with each other within the swarm, during normal operations. The 20km link will be used by the relay UAVs, to relay information between base and swarm, in case the base-swarm distance is higher than 200 km. The 200 km link is the farthest possible link that can be established between UAVs and base, before the curvature of the Earth interrupts the line of sight. Finally, the 100km link represents the farthest distance at which the smaller antennas can communicate with the ground base.

3.6.7 HARDWARE POWER, MASS AND COST BUDGETS

This section will briefly list the power, cost and weight budget of all hardware components of the non-Payload communication system. The power budget can be found in table 3.10, the mass budget in table 3.11 and the cost budget in table 3.12.

Table 3.10: Power budget for the non-payload communication system components

Power Budget	
XR2 radio cards (x4)	
TX max power	4.62 W
RX max power	1.32 W
MD4000 (mesh node hardware)	
Max power required (4 radios)	16.0 W
TTRM1004-D02 amplifier (x4)	
Max power required	67.2 W
Total Max Power per UAV	
4 radios in TX mode	18.5 W
MD4000	16.0 W
4 amplifiers at max output power	268.8 W
Total maximum power required	**303.3 W**

Table 3.11: Mass budget for the non-payload communication system components

Mass Budget	
XR2 radio cards (x4)	0.045 kg
MD4000 (mesh node hardware)	1.36 kg
TTRM1004-D02 amplifier (x4)	0.43 kg
ABA-2.3V/1964 antenna (Low gain, x2)	0.022 kg
OA4-2.5V/9205 antenna (High gain, x2)	0.30 kg
Total mass	**3.88 kg**

Table 3.12: Cost budget for the non-payload communication system components

Costs Budget	
XR2 radio cards (x4)	100 $
MD4000 HW (mesh node hardware)	900 $
MD4000 SW (mesh node software)	720 $
TTRM1004-D02 amplifier (x4)	200 $
ABA-2.3V/1964 antenna (Low gain, x2)	45 $
OA4-2.5V/9205 antenna (High gain, x2)	45 $
Total mass	**3000 $**

3.7 COMMUNICATION FLOW DIAGRAM

An overview of the communication system can be found in the communication flow diagram in figure C.3 in appendix C.

Table 3.9: Table showing the final link budget of all different types of links. The upper half of the table gives the values (in dB) of all components of the link budget for each different link. The second half of the table gives some relevant data concerning the link in question

Link budget table for six different links

Link Component	**UAV - UAV UL & DL 10km**	**UAV - UAV UL & DL 20km**	**UAV - Base DL 200km**	**UAV - Base UL 200km**	**UAV - Base DL 100km**	**UAV - Base UL 100km**
Transmit Power	20 dB_{mW}	20 dB_{mW}	20 dB_{mW}	50 dB_{mW}	20 dB_{mW}	50 dB_{mW}
Amplifier Gain	24 dB	24 dB	24 dB	0 dB	24 dB	0 dB
Transmit Antenna Gain	4.5 dB	4.5 dB	4.5 dB	28.4 dB	4.5 dB	28.4 dB
Free-Space Path Loss	-120 dB	-128 dB	-146 dB	-146 dB	-140 dB	-140 dB
Additional Losses	-16.1 dB	-16.3 dB	-19.4 dB	-19.4 dB	-17.7 dB	-17.7 dB
Atmospheric	(-0.073 dB)	(-0.15 dB)	(-1.45 dB)	(-1.45 dB)	(-0.73 dB)	(-0.73 dB)
Aiframe	(-13 dB)	(-13 dB)	(-13 dB)	(-13 dB)	(-13 dB)	(-13 dB)
Polarization	(-3 dB)	(-3 dB)	(-3 dB)	(-3 dB)	(-3 dB)	(-3 dB)
Rain	(-0.099 dB)	(-0.20 dB)	(-1.97 dB)	(-1.97 dB)	(-0.99 dB)	(-0.99 dB)
Receiving Antenna Gain	4.5 dB	4.5 dB	28.4 dB	4.5 dB	28.4 dB	4.5 dB
Antenna Pointing Loss	-2.7 dB	-2.7 dB	-2.7 dB	-8.8 dB	-2.7 dB	-8.8 dB
Power Received	-85.9 dB_{mW}	-92.1 dB_{mW}	-91.3 dB_{mW}	-91.4 dB_{mW}	-83.6 dB_{mW}	-83.7 dB_{mW}

Closing the Budget (Power received - Receiver Sensitivity = maring)

Power Received	-85.9 dB_{mW}	-92.1 dB_{mW}	-91.3 dB_{mW}	-91.4 dB_{mW}	-83.6 dB_{mW}	-83.7 dB_{mW}
Receiver Sensitivity	-95 dB_{mW}	-95 dB_{mW}	-95 dB_{mW}	-95 dB_{mW}	-95 dB_{mW}	-95 dB_{mW}
Received Power Margin	9.1 dB	2.9 dB	3.7 dB	3.6 dB	11.4 dB	11.3 dB

Link characteristics

Distance	10 km	20 km	200 km	200 km	100 km	100 km
Parabolic Antenna Diameter	-	-	2.5 m	2.5 m	2.5 m	2.5 m
Parabolic Antenna Efficiency	-	-	0.55	0.55	0.55	0.55
HPBW	42 deg	42 deg	42 deg	3.5 deg	42 deg	3.5 deg
Pointing error	20 deg	20 deg	20 deg	3 deg	20 deg	3 deg

4 | AERODYNAMICS

In this chapter the aerodynamic performance of the UAV is analyzed. Firstly the atmospheric conditions experienced during the mission conditions are determined and offered in table 4.1 of section 4.1. Secondly, a discussion on the airfoil selection is offered in section 4.2 summarizing the more elaborate explanation from mid-term report [3]. The chapter ends with a aerodynamic analysis in which the drag, lift and moment coefficients are determined for the main components of the UAV. In the end, the UAV is analysed as a whole and the results are offered and explained in section 4.3.4.

4.1 ATMOSHPERIC PROPERTIES

Before performing the aerodynamics analysis on the system, the properties of the air in which the UAV is flying have to be determined. They consist in physical characteristics as density, temperature or viscosity together with specific parameters which are dependent on the design as speed or Reynolds number. Their values define the aerodynamic scenario in which the UAV is going to operate. In chapter 2 the cruise and loiter characteristics have been determined. The International Standard Atmosphere (ISA) [29] has been used for the determination of atmospheric properties. The ISA describes a set of temperature, density and pressure at every altitude according to eq. (4.1), eq. (4.2) and eq. (4.3).

$$T_{cruise} = T_0 + \lambda \cdot h_{cruise} \tag{4.1}$$

$$\rho_{cruise} = \rho_0 \cdot \left(\frac{T_{cruise}}{T_0} \right)^{\frac{-g_0}{\lambda \cdot R} - 1} \tag{4.2}$$

$$p_{cruise} = p_0 \cdot \left(\frac{T_{cruise}}{T_0} \right)^{\frac{-g_0}{\lambda \cdot R}} \tag{4.3}$$

The Reynolds number and Mach number can be calculated next. The Reynolds number depends on the geometry of the aircraft and on the flight parameters. If in the mid-term report [3] it was enough to consider a reference length during the computation process, for the final analysis this has to be redone in a more accurate way. The approach considered for the computation of the Reynolds number is the following. With the estimate of the geometrical parameters obtained from chapter 9, a wing and tail model are constructed in XFLR5. Introducing the atmospheric parameters in which the UAV is performing the mission, a more accurate estimate of the Reynolds number is found at each location along the wing and tail span. Especially in the analysis of the wing, where the chord length changes throughout the span, having a tool which easily computes the Reynolds number is a great advantage. For the Reynolds number of the fuselage, direct computation using eq. (4.6) is preferred due to the poor modelling of the fuselage possible in XFLR5. The value of the Reynolds number of the wing at the span location of the mean aerodynamic chord together with the Reynolds number of the fuselage are offered in table 4.1. As the Mach number is not dependent on the geometry of the aircraft, its computation is done directly using eq. (4.7) with the atmospheric properties during flight. If the cruise speed is defined by the mission and it is kept constant, the loiter velocity must be changed during the mission. The speed must be modified accordingly such that the UAV will be constantly flying at the highest endurance factor even if the weight is decreasing due to fuel consumption. The formula for loiter velocity is given by eq. (4.4), where W is the weight of the UAV during loiter (which is constantly changing), S is the surface of the UAV, ρ is the density of the air at the altitude where the swarm is performing the loiter stage of the mission and $C_{L_{HE}}$ is the C_L needed for flying at highest endurance factor. It has to be mentioned that the loiter speed slightly changes at each iteration due to change in $C_{L_{HE}}$ which has to be selected after each computation of the endurance factor. A value of 0.9255 was find for this specific lift coefficient at the last iteration. This value was used to compute the loiter speed offered in table 4.1.

$$V_{loiter} = \sqrt{\frac{W}{S} \cdot \frac{2}{\rho \cdot C_{L_{HE}}}} \tag{4.4}$$

When inspecting the Mach number, it can be observed that its value is considerably low (under 0.3). By inspecting Figure 2.10 from [30] it is observed that at this speed no compressibility corrections need to be taken into account in the calculations. This is an important observation, which will be of major significance in further calculations.

$$A = \frac{b^2}{S} = \frac{b}{l_{ref}} \quad (4.5) \qquad Re = \frac{\rho \cdot V \cdot L}{\mu} \quad (4.6) \qquad M = \frac{V}{\sqrt{\gamma \cdot R \cdot T}} \quad (4.7)$$

A complete list of results is found in table 4.1.

Table 4.1: Flight properties

Property	Symbol	Value	Unit
Lapse rate	λ	-0.0065	$\mathrm{K\,m^{-1}}$
Gravitational acceleration	g_0	9.80665	$\mathrm{m\,s^{-2}}$
Gas constant (Air)	R_{air}	287.058	$\mathrm{J\,kg^{-1}\,K^{-1}}$
Adiabatic index	γ	1.4	[-]
Cruise Dynamic viscosity	μ_{cruise}	$1.661 \cdot 10^{-5}$	Pa s
Loiter Dynamic viscosity	μ_{loiter}	$1.726 \cdot 10^{-5}$	Pa s
Cruise altitude	h_{cruise}	4000	m
Loiter altitude	h_{loiter}	2000	m
Cruise velocity	V_{cruise}	55.55	$\mathrm{m\,s^{-1}}$
Loiter velocity (at the start of loiter)	V_{loiter}	35.9	$\mathrm{m\,s^{-1}}$
Sea level temperature	T_0	288.15	K
Sea level density	ρ_0	1.225	$\mathrm{kg\,m^{-3}}$
Sea level pressure	p_0	101325	Pa
Cruise temperature	T_{cruise}	262	K
Cruise density	ρ_{cruise}	0.8194	$\mathrm{kg\,m^{-3}}$
Cruise pressure	p_{cruise}	61660	Pa
Loiter temperature	T_{loiter}	275.15	K
Loiter density	ρ_{loiter}	1.006	$\mathrm{kg\,m^{-3}}$
Loiter pressure	p_{loiter}	79495	Pa
Aspect ratio	AR	20	[-]
Geometric chord of the wing	c	0.326	m
Length of the fuselage	l_f	2.807	m
Reynolds number of the wing during cruise	ReW_{cruise}	893452	[-]
Reynolds number of the wing during loiter	ReW_{loiter}	626761	[-]
Reynolds number of the fuselage during cruise	ReF_{cruise}	7693009.5	[-]
Reynolds number of the fuselage during loiter	ReF_{loiter}	5396688.8	[-]
Mach number cruise	M_{cruise}	0.1712	[-]
Mach number loiter	M_{loiter}	0.10797	[-]

4.2 Airfoil Selection of the Wing

In the Mid-Term report [3] a trade-off was done to find the best suitable airfoil for the WiFly mission. Particularly important for the mission are the range and the endurance factor, which are based on the airfoil in 2D and eventually on the wing in 3D. The higher the endurance factor is, the more time you can loiter with a certain amount of fuel. An increase in range factor, results in a longer range using the same amount of fuel. Endurance and range factors for 3D wing with four airfoils specific for long endurance aircraft are given in table 4.2. Due to its high endurance and range factor, the winner of the trade-off is LA203A. Its specific factors are highlighted in table 4.2. It has to be mentioned that these values were computed during an initial stage of the design, so the values of the endurance and range factors are estimates which can be used only for the sake of comparison between the airfoils. These estimates were computed in the mid-term report [3] and the conversion from 2D data to 3D was based on an aspect ratio of 20, an Oswald factor of 0.9 and a C_{D0} of 0.02. The first of these values is based on reference UAVs while the two latter ones were approximated based on the approach proposed by Anderson in [30]. These were only initial estimates, which have to be updated for the final design. A discussion about computing more accurate estimates for Oswald factor and C_{D0} is offered in section 4.3.4. With these terms more accurately computed, the final version of the drag polar can be more accurately determined.

Table 4.2: Airfoil Selection for the wing-tail UAV.

Airfoil	Endurance Factor $\frac{C_L^{1.5}}{C_D}$	Range Factor $\frac{C_L}{C_D}$	$C_{L_{max}}$
LA203A	30.96	26.587	1.58
NACA4415	30.24	26.587	1.39
NLF1015	27.07	26.579	1.04
FX61-184	24.4	26.088	0.88

4.3 AERODYNAMIC ANALYSIS

For the final design it was decided to use XFLR5 because it offers the opportunity to investigate both the 2D and 3D wing from an aerodynamics perspective. Furthermore, a tail and a fuselage can be added and a complete rough aerodynamic analysis is possible. It has to be mentioned that XFLR5 is not reliable in predicting the drag coefficient for the whole UAV due to its poor capability of integrating different components together. In order to calculate this interdependence, the approach proposed by Roskam in [1] is used. His method offers an accurate estimate for the drag coefficient of the whole UAV. Section 4.3 is separated in four different categories, each of them treating the aerodynamic analysis of a main UAV component. In the last subsection an analysis of the whole UAV is implemented and the final results are further discussed.

4.3.1 WING ANALYSIS

The main lift generator of the UAV is the wing. Therefore, it deserves special attention regarding its aerodynamic properties. XFLR5 was used to implement a 3D wing analysis with the chosen airfoil LA203A and the geometrical wing planform parameters given in table 4.3. An illustration of the wing planform in XFLR5 is shown in figure 4.1. The computation process of XFLR5 uses the lifting-line theory. For the designed wing, which is unswept with a high aspect ratio flying at a low mach number (M<0.3), the results provided by this theory are expected to be accurate. The specific plots, $C_L - \alpha, C_D - \alpha, C_m - \alpha$ and $C_L - C_D$ are offered in figures 4.2 to 4.5. The $C_m - \alpha$ is offered at the span location of the MAC (mean aerodynamic chord). Based on the geometry of the wing, this value is found to be 1.375 m with the center of fuselage as datum point. This location is kept as reference also when generating the $C_m - \alpha$ for the whole UAV.

Table 4.3: Wing Geometry Parameters

Parameter	Value
Wing Area	2.127 m^2
Root Chord	0.54 m
Tip Chord	0.195 m
Wing Span	6.522 m

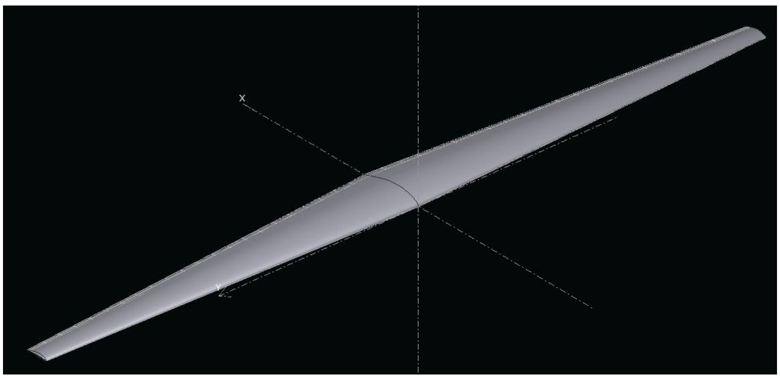

Figure 4.1: Wing model in XFLR5

From figure 4.2 and 4.3 it can be seen that only for the wing, the maximum C_L is 1.7, while the C_{D_0} is 0.014. For a sanity check, this value is compared with the C_{D_0} of 0.0123 obtained by using the method suggested

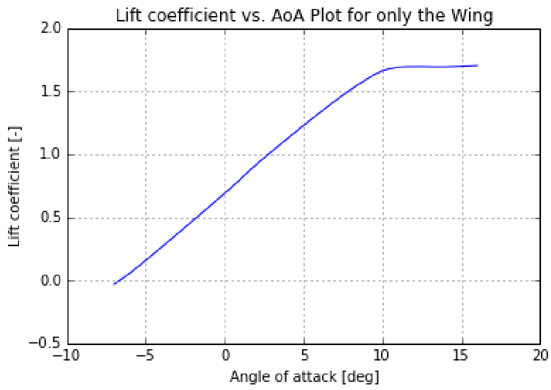

Figure 4.2: 3D Wing $C_L - \alpha$ plot

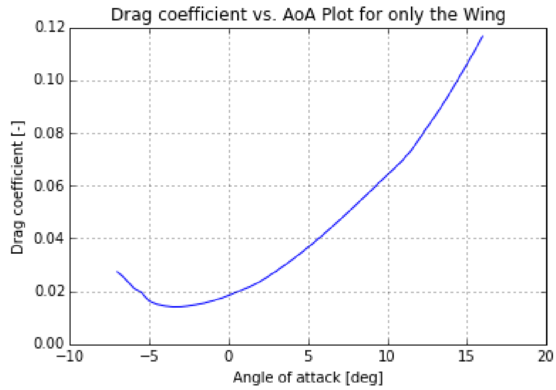

Figure 4.3: 3D Wing $C_D - \alpha$ plot

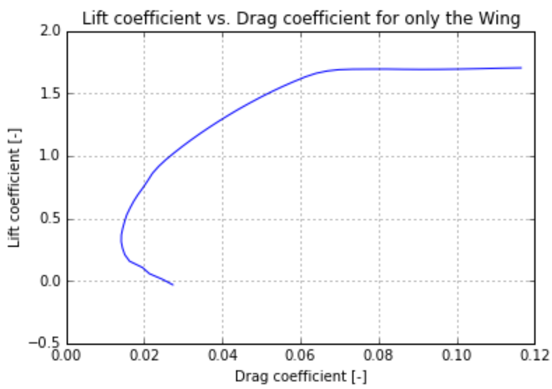

Figure 4.4: 3D Wing Drag Polar ($C_L - C_D$) plot

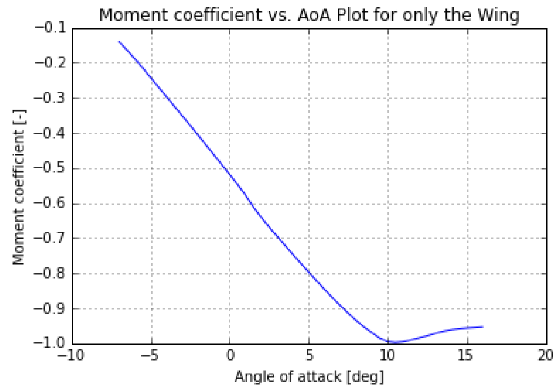

Figure 4.5: Wing $C_m - \alpha$ plot at the location of the MAC along the span

by Roskam in [1]. The small difference between the 2 values (<15%) confirms the reliability of the XFLR5 results. In the later subsections, when the tail and the fuselage will be added, it is very interesting to analyse the difference in these parameters. It is anticipated that the C_L will slightly increase due to contribution of the tail and the C_{D_0} is expected to rise considerably especially due to the interaction with the fuselage. Figure 4.4 shows the drag polar. It can be seen that the slope is considerable big, which points out to a high range and endurance factors. These terms are expected to decrease later on, when both the tail and the fuselage will be added. Also it is noticed that the minimum drag does not occur at 0 lift. The reason behind this may be the computation procedure used by XFLR5 to compute the drag. It probably uses a more accurate estimate of the drag than the standard drag polar equation, which influences the overall shape of the graph and the position of the point of minimum drag. Furthermore it can be observed that the slope of the $C_m - \alpha$ curve is strongly negative. This reveals a stable static behaviour for a wide range of angles of attack. For the angle of attack higher than 10 degrees, the aircraft become slightly statically unstable. It is anticipated that this issue will disappear when the tail will be added and the whole UAV will be analysed.

4.3.2 FUSELAGE ANALYSIS

The fuselage is not optimized for aerodynamic efficiency because its main purpose is to carry payload, fuel and other subsystems. Therefore, it causes a significant amount of drag. This drag consists of multiple contributions, namely:

- Zero-Lift Drag Coefficient
- Base Drag Coefficient
- Induced Drag Coefficient

In the following, all three contributions are discussed and the method to calculate the value of every component is shown.

Zero-Lift Drag Coefficient: The zero-lift drag coefficient of the fuselage can be determined empirically by eq. (4.8). This equation is given by Roskam [1].

$$C_{D_{0_f}} = R_{wf} \cdot C_{f_f} \cdot \left(1 + \frac{60}{(l_f/d_f)^3} + 0.0025 \cdot (l_f/d_f)\right) \cdot \frac{S_{wet}}{S} \tag{4.8}$$

In eq. (4.8) R_{wf} is the wing-fuselage interaction factor, C_{f_f} is the turbulent flat plate skin-friction coefficient of the fuselage, l_f/d_f is the fuselage fineness ratio, S is the fuselage area and S_{wet} is the wetted area of the fuselage. While l_f/d_f, S and S_{wet} are purely geometric parameters, R_{wf} and C_{f_f} are dependent on the Mach number and the Reynolds number of the fuselage and they are given by eq. (4.9) and eq. (4.10).

$$R_{N_f} = \frac{\rho \cdot U_1 \cdot l_f}{\mu} \tag{4.9}$$

$$C_{f_f} = \frac{0.455}{(log_{10} \cdot R_{N_f})^{2.58}(1 + 0.144 \cdot M^2)^{0.58}} \tag{4.10}$$

In eq. (4.9) ρ is the air density at the specific altitude, U_1 is the air speed, l_f is the fuselage length and μ is the dynamic viscosity of air in that condition. In eq. (4.10) R_{N_f} is the Reynolds number of the fuselage and M is the Mach number. As it can be seen, C_{f_f} is obtained immediately from eq. (4.9) wher as R_{wf} is given in as a graph versus the fuselage Reynolds number in figure 5.11 of [1].

Base Drag Coefficient: Base drag is generated in case the fuselage is designed such that it still has a cross sectional area at the very aft of the fuselage. However, for the WiFly UAV, which is anticipated to have a pusher at the end of the fuselage, the base area can be assumed zero while the engine is running as suggested by Roskam in section 5.2 of [1]. As the aerodynamic analysis is of interest only when the UAV is operating, so with the engine running, it can be assumed that the base area is zero and no base drag is generated.

Induced Drag Coefficient: Induced drag is produced as soon as a body generates lift. Therefore, when the fuselage of the aircraft is flying at a positive angle of attack it will generate both lift and drag. However, as for the designed UAV the fuselage is not highly integrated with the wing (as in Burnelli airplanes for example), it can be considered that both the lift and the induced drag generated by the fuselage is negligible as suggested by Roskam in section 5.2 of [1].

4.3.3 TAIL ANALYSIS

As discussed in section 4.4 the optimal tail configuration is a V-tail. Furthermore, it was decided in section 4.5 to use the NACA0009 airfoil for the tail. The geometrical aspects like taper, aspect ratio and tail area are determined in 7.1.3. The resulting geometry is shown in figure 4.6. For stability analysis it is particularly important to accurately compute how much lift the ruddervator produces at a range of angle of attacks the aircraft will experience during its mission. Therefore, lift and drag coefficients are shown in figures 4.7 to 4.8. Figure 4.7 shows the lift curve of the V-tail. It can be seen that the tail generates no lift at zero angle of attack. This is due to the symmetric shape of the airfoil. Furthermore, the slope of the lift curve is constant from -5 to 15 degrees angle of attack. In figure 4.8 the drag coefficient of the V-tail for angles of attack between -7 and 14.5 degrees is shown. The zero lift drag coefficient is 0.00486 which is considerably small with respect to reference values from [1]. The reason for that can be due to the use of V-tail configuration. As it can be seen table 4.4 this configuration has a better aerodynamic performance, generating less drag than the conventional ones which are manly used as reference in [1]. This may be also the reason for why when making the sanity check with the method suggested by Roskam in [1], a C_{D_0} of 0.01226 was found which is considerably higher than the value provided by XFLR5. From this short discussion it can be retrieved that the NACA0009 airfoil used on a V tail configuration is beneficial for the aircraft aerodynamic performance.

4.3.4 AERODYNAMIC ANALYSIS OF THE WHOLE UAV

To analyze the drag generated by the whole UAV, it was decided to use the method offered by Roskam in [1]. For the whole UAV this approach proved to be more reliable than the XFLR5 results due to fact that the simulation software poorly integrates the components (wing, tail, fuselage) together. The procedure for creating the specific plots for the whole UAV follows the next procedure. Firstly, as the fuselage does not

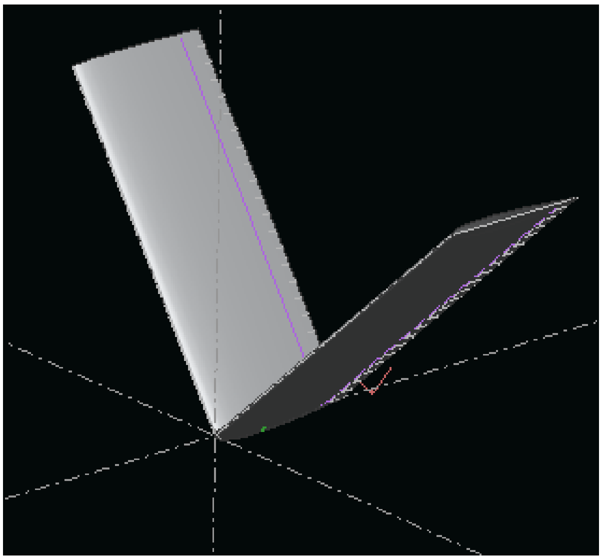

Figure 4.6: Tail model in XFLR5

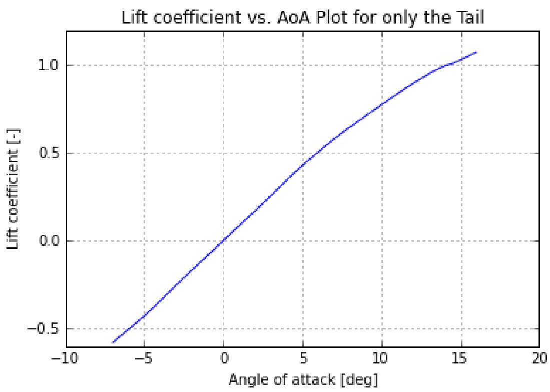

Figure 4.7: 3D Wing $C_L - \alpha$ plot

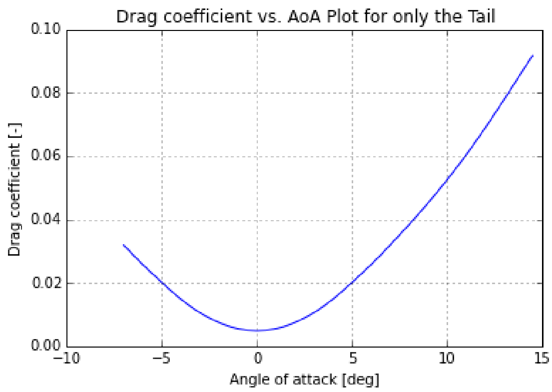

Figure 4.8: 3D Wing $C_D - \alpha$ plot

generate considerable amount of lift and its influence on the moment is negligible, the $C_L - \alpha$ and $C_m - \alpha$ can be easily generated by adding the lift and moments coefficients together using eq. (4.11) and eq. (4.12), where S_h is the horizontal area of the tail, S is the surface area of the wing and $(V_h/V)^2$ is the squared ratio between the speed of the air at the location of the tail and the speed at the position of the wing. This term is found from literature to be 0.85 [1]. The terms c_h and c in eq. (4.12) are the chords of the tail and of the wing respectively.

$$C_{L_{UAV}} = C_{L_{wing}} + C_{L_{tail}} \cdot \frac{S_h}{S} \cdot \left(\frac{V_h}{V}\right)^2 \tag{4.11}$$

$$C_{m_{UAV}} = C_{m_{wing}} + C_{m_{tail}} \cdot \frac{S_h}{S} \cdot \left(\frac{V_h}{V}\right)^2 \cdot \frac{c_h}{c} \tag{4.12}$$

Another important aspect is the downwash angle caused by the wing, which has to be taken into account when computing the angle of attack of the tail. This is calculated using eq. (4.13) from [1], where A is the aspect ratio. This term has to be subtracted from the angle of attack of the tail.

$$downwash = \frac{2 \cdot C_{L_{wing}}}{\pi \cdot A} \tag{4.13}$$

The procedure of computing the drag coefficient is described in the following lines.
Firstly, with the C_{D_0} of each main component computed in the subsections 4.3.1 to 4.3.3. These terms are

added up in order to obtain the total C_{D_0} of the whole UAV. Afterwards, the induced drag is computed using the drag polar described by eq. (4.14), where C_L is the lift coefficient, the e is the Oswald factor and AR is the aspect ratio. It is important to mention that these terms are specific for wing and the tail respectively.

$$C_{D_i} = \frac{C_L^2}{\pi \cdot e \cdot AR} \tag{4.14}$$

For the wing the aspect ratio was fixed to a value of 20 in the midterm report [3]. For the tail, a value of 2.5 was found for the aspect ratio in section 4.4. The estimate of the Oswald factor is based on the elaborate discussion of [31]. Equation (4.15) was used to calculate the Oswald factor of the wing to a value of 0.8432. This is a more accurate estimate than the value of 0.9 considered in the mid-term report [3] due to the fact that this is based on the actual layout of the UAV.C_{L_α} is the slope of the $C_L - \alpha$ graph, the AR is the aspect ratio and the R is the leading edge suction parameter defined in [31].

For the Oswald factor of the tail, another equation, more adequate for low aspect ratio wings, is used. It is taken from [31] and offered in eq. (4.16). Its main advantage is its dependence only on the aspect ratio, which is a parameter already determined. From eq. (4.16) a value of 0.937 was found for the Oswald factor of the tail. By inspecting Fig.1 from [31] and considering the small aspect ratio of the tail together with the low C_{D_0} caused by the tail, it can be concluded that this value can be considered reliable for further calculations.

$$e_{wing} = \frac{1.1 \cdot (C_{L_\alpha}/AR)}{R \cdot (C_{L_\alpha}/AR) + (1-R) \cdot \pi} \tag{4.15}$$

$$e_{tail} = \frac{1}{1.05 + 0.007 \cdot \pi \cdot AR} \tag{4.16}$$

With these terms computed the drag can be finally calculated for the whole UAV. Its formula is given in eq. (4.17), where $C_{D0_{UAV}}$ is the parasite drag of the whole UAV, C_L is the lift coefficient of the component, AR is the aspect ratio, e is the Oswald factor, S_h is the horizontal area of the tail, S is the surface area of the wing and $(V_h/V)^2$ is the squared ratio between the speed of the air at the location of the tail and the speed at the position of the wing. The latter term is again approximate from literature ([1]) to a value of 0.85.

$$C_{D_{UAV}} = C_{D0_{UAV}} + \frac{C_{L_{wing}}^2}{\pi \cdot AR_{wing} \cdot e_{wing}} + \frac{C_{L_{tail}}^2}{\pi \cdot AR_{tail} \cdot e_{tail}} \cdot \frac{S_h}{S} \cdot \left(\frac{V_h}{V}\right)^2 \tag{4.17}$$

With the drag computed, the new graphs can be generated. They consist in $C_L - \alpha$, $C_D - \alpha$, $C_L - C_D$ and $C_m - \alpha$. They are offered in figures 4.9 to 4.12 and briefly described in the following lines.

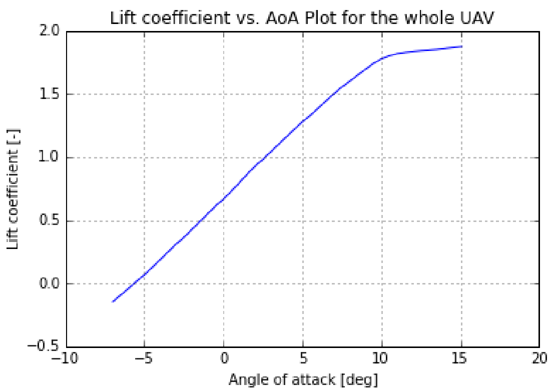

Figure 4.9: $C_L - \alpha$ plot for the whole UAV

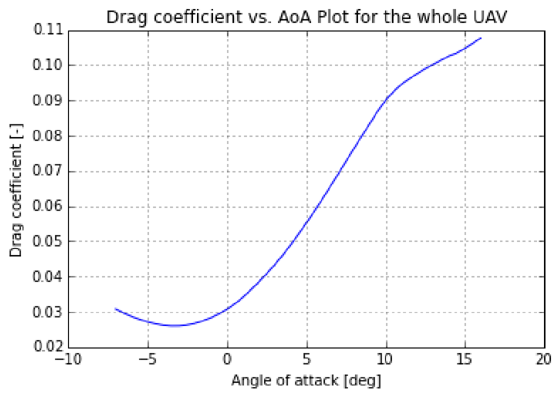

Figure 4.10: $C_D - \alpha$ plot for the whole UAV

By inspecting figure 4.9, it is noticed that for the whole UAV the lift coefficient is increased with respect to the "Wing Only" values. The reason for that lies in the positive lift generated by the tail which slightly increases the overall lift produced by the UAV. However, the increment is considerably small due to the scaling factor which must be taken into account when adding up the lift component of the tail (the second part of eq. (4.11)). Analysing figure 4.10 and figure 4.11, it can be observed that the C_{D_0} of the whole UAV increased to a value of 0.026. This is a considerable rise (30%) with respect to the assumption of 0.2 in the mid-term report [3]. The difference would reflect to the endurance and range factors which decrease considerably. For the endurance factor a value of 21.76 was now found, while for the range factor 23.13 is computed. This change will reflect in the design of the UAV which loses its aerodynamic efficiency, needing a higher amount of fuel to perform

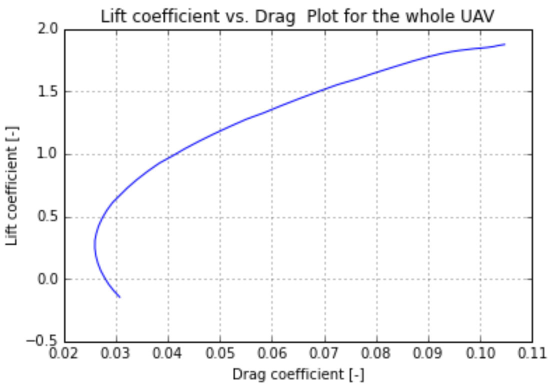

Figure 4.11: Drag Polar ($C_L - C_D$) plot for the whole UAV

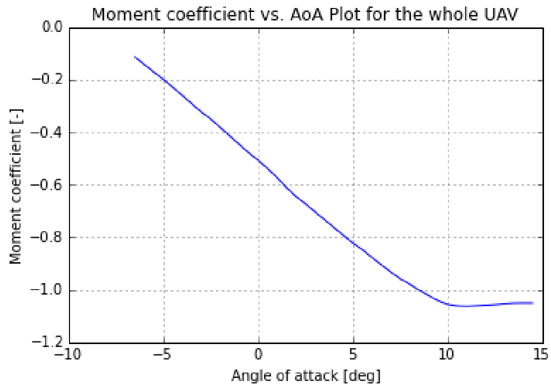

Figure 4.12: $C_m - \alpha$ plot for the whole UAV at the location of the MAC along the span

the same mission. By analysing figure 4.12 it can be observed that the graph keeps the same negative slope revealing a stable behaviour up to 10 degrees. Also, the issues noticed in section 4.3.1 regarding the stability for the angle of attacks higher than 10 is solved by adding the tail. For the whole UAV, the C_m kept constant in this region, so it will not cause any problem from a stability perspective.

4.4 TAIL DESIGN

Based on the analysis performed in the Stability& Controllability chapter an initial estimate for the size of the horizontal surface of the tail is obtained. This is just one of the parameters of the tail design. A discussion on the configuration and size of the tail, completed by its aerodynamic analysis will be treated in the following lines.

The first step in the tail design is choosing its configuration. This is based on the elaborate discussion of chapter 11 from [32]. A trade-off was performed between different tail concepts. For a better visualisation, a complete summary of the trade-off is offered in table 4.4. The scores are offered from 1 to 5 where 1 is the worst and 5 is the best grade.

Table 4.4: Trade off performed on nine tail configurations. The grades are given from 1 to 5

Criteria	Weight	Conventional Tail	Cruciform Tail	T-Tail	V-Tail	Inverted V-Tail	Y-Tail	H-Tail	A-Tail	U-Tail
Reliability	15	2.9	1.9	1.9	4.1	3.1	2.4	2	2.4	3
- Used in existing UAVs	*(70%)*	*(2)*	*(1)*	*(1)*	*(5)*	*(4)*	*(3)*	*(2)*	*(3)*	*(3)*
- Used in manned planes	*(30%)*	*(5)*	*(4)*	*(4)*	*(2)*	*(1)*	*(1)*	*(2)*	*(1)*	*(3)*
Structural loads	15	5	4	3	3	3	3	3	3	3
Weight	15	4	3	2	3	3	3	2	3	2
Wing wake effect	15	2.6	3.2	2.8	4	4	3	4	3	
- On the rudder	*(40%)*	*(2)*	*(2)*	*(4)*	*(4)*	*(4)*	*(4)*	*(3)*	*(4)*	*(3)*
- On the elevator	*(60%)*	*(3)*	*(4)*	*(2)*	*(4)*	*(4)*	*(4)*	*(3)*	*(4)*	*(3)*
Drag Interference	15	3	2	4	5	5	4	2	4	2
Stability	15	3	2	4	4	4	4	3	4	3
Allow TO and landing	15	4	4	4	5	2	3	4	3	4
Manufacturing	15	4	2	3	3	3	3	3	2	2
Weighted Average	100	**2.93**	**2.30**	**2.30**	**3.02**	**2.69**	**2.64**	**2.13**	**2.52**	**2.22**

There are eight criteria which were considered during the trade off. The first one is reliability. This offers an estimate on the popularity of the concepts on the existing air-vehicles. As the choice has to be implemented for an UAV, a higher weight was offered to the subcategory of "use in existing UAV designs". This is a very important category as it offers the designer a feeling on the existing trend on tail configurations. For example, the V-tail is the most popular among the UAV concepts. Examples of UAVs with this tail configurations are the General Atomics Avenger, Northrop Grumman RQ-4 Global Hawk or TAI Anka-A. On the other extreme are the cruciform and the T-tail tails which were rarely used in UAV concepts. One of the few examples of UAVs using one of these conformations is the Ion Tiger UAV which has a cruciform tail and Mantis UAV with a T-tail configuration. The second criteria regards the structural loads. Even if at this point, the final layout of the tail is not known, from previous used designs it is known which choices cause higher structural loads. The conventional tail is the best from this point of view, followed by cruciform. T-tails have to accommodate the horizontal stabilizer at the tip of the vertical tail. V and Y-tails cause higher stresses due to their high dihedral. For a more detailed description of the advantages and disadvantages of each configuration the reader is advised to refer to the sub-chapter 11.3 of [32].The weight is directly related to the structural loads as higher stresses requires further reinforcement which is going to increase the weight of the tail. Therefore, it can be observed in table 4.4 the second and the third criteria are correlated (the grades for these criteria are almost the same). One of the known issues regarding the tail design consists in determining the angles of attack in which it enters in the wake of the wing. For both vertical and horizontal tail, this is very dependent on the configuration of the tail. For example, the T-tail is sensitive to this aspect. There is a wide range of angle of attacks (at stall or post-stall), when the whole tail enters in the wake of the wing. This is a critical condition that can make the air vehicle incapable of recovering from stall. For grading the drag interference criteria, a deeper look has to be given to the aerodynamic advantages of each configuration. The results from [33] provided to be very helpful in concluding that the V-tail configuration (both normal and inverted) has the lowest drag interference. Chapter 11.3 of [32] was used in grading the rest of configurations. Also, the elaborate discussion on stability from [32] was used as the main tool of grading for the 6th criteria. The 7th category is dependent on the shape of tail. If it is pointing downwards (as the Y-tale or the inverted V-tail) the score is lower, as changes have to be implemented to the takeoff and landing systems in order to accommodate the additional tail elements which are prone to touch the ground. For the manufacturing criteria, the grading is based on both the number of elements required for the specific tail configuration together with the complexity of its shape.

4.5 TAIL AIRFOIL SELECTION

The tail is supposed to generate as little lift as necessary during the flight phase to reduce the amount of induced drag. It should just generate lift when the original trim position is disturbed, for example due to a wind gust. If this happens, it generates a moment which brings the aircraft back in the original position.
Following from this, the tail airfoil has to be symmetrical and thick enough to provide a sufficient C_{L_α} to counteract disturbances. From reference aircraft it was deduced that all of them use NACA0009 [1]. Amongst others the reference aircraft are the Beech Bonanza, Beech Queen Air B80, Beech Skipper, Beech Duchess, Cessna 210 Centurion, Cessna T-37, Cessna 337 Skymaster, Cessna 500 Citation, Piper PA-23 Aztec, Piper Pa-31T Cheyenne and the Lockheed 1329-25 Jetstar. For this reason it was decided to select this airfoil for further aerodynamic and stability analysis.

5 | STRUCTURAL DESIGN

This chapter aims at obtaining the shape, thickness, material and position of the structural parts in order to cope with the loads the drone needs to withstand.

In shaping the outer load carrying components of airplanes aerodynamics plays a major role as it defines the outer shape of the drone. Due to this, compromises may be needed between structural efficiency and aerodynamic performance. The main components to be designed are the fuselage and the wings.

5.1 MATERIALS AVAILABLE

The number of materials available to an engineer is between 40,000 and 80,000 and growing [34]. Material selection of each component is based on function, shape and production process. The last will not be considered for this design. Four material families exist: Ceramics, Metals, Polymers and Composites. Each has its own characteristics which may be mechanical, chemical, thermal or electrical. Other relevant aspects are the cost, availability and environmental impact. Material indices measure performance. For the design of the WiFly drones, specific strength (σ/ρ) and specific stiffness (E/ρ) are the most important due to the need of a strong and stiff, yet lightweight design.

- **Ceramics** are hard, brittle and corrosion resistant. In aerospace they are mostly used for their resistance to high temperature. In tension and compression they suffer from brittle failure (although the compression strength is still much higher then the tension strength). The biggest issues with ceramics arises from the lack of ductility which does not allow them to redistribute the load when concentration factors are present (such as cracks or holes). This limits the possibility of having attachments or cutouts. This material shall not be use for any critical component.
- **Metals** are ductile, tough and can conduct electricity. In combination with another metal (alloying) or by heat treatment, one can control their properties. The high strength and ease of manufacturing are important benefits of metals. On top of that, since plastic deformation always occurs before failure, possible damages can be seen without the need of special instruments. A major downside of metals, which arise from their ductility is fatigue. Furthermore, unless surface treatments are carefully applied, metals can corrode. Because of the communication systems within the drones special attention should be given to radio transparency. Most metals do reflect or absorb radio waves, thus those metals can not be used as casings around the antennas.
- **Polymers** can achieve high strengths, but they have very low elastic modulus. They tend to creep at relatively low temperatures and can dramatically change their properties depending on the surrounding temperature. Since the WiFly mission needs to perform in environments ranging between +40° and -40° careful attention needs to be given to polymeric parts.
- **Composites** have the most attractive properties of all the engineering materials. They can provide very high stiffness, strength and toughness while keeping the weight minimal. On the downside, the raw materials are very expensive. Due to their complexity and maturity manufacturing and joining are difficult and costly. They will only be used if the extra performance they provide can be justified [35].

5.2 ANALYZED LOAD CASES

One of the first steps in designing a structure is analyzing the loads. There are nearly infinite load cases and analyzing all of them would be impossible. To accommodate for the short time in which this project must be completed some assumptions must be made. It was decided to search for worst case scenarios. Normally, the procedure of doing this consists in evaluating all cases as taking off at $MTOW$, at OEW, with(out) flaps, wind wind from different directions etc. This cannot be done for this project but based on engineering intuition the following cases are selected:

1. Take off by catapult.
2. Maneuvering at the maximum allowable turn.
3. Maximum gusts encountered with full fuel.
4. Maximum gusts encountered with no fuel.
5. Landing by means of a skyhook.

An extensive explanation of the cases and the loads will be described in the following subsections. It should be noted that an extra contingency factor of 1.15[1] was used to account for the fact that not all load cases could be analyzed and because this is a preliminary structural design. A safety factor of 1.5 is used on the loads as is common practice in aerospace engineering. Limit loads are the highest loads calculated to occur during operation, thus without contingency and safety factor. Max limit loads are those including contingency but without safety factor, ultimate loads are the loads multiplied with the contingency and safety factor.

5.2.1 TAKEOFF LOADS

It was decided to use a catapult system as a launching mechanism. The plane will be connected to a bungee cord which accelerates the plane up until enough lift is generated and the system flies away. The bungee cord will be connected underneath the wing and accelerates the UAV in x-direction. A smaller force will be exerted by the engine which is powered on to assist in the take off. The total acceleration is expected to be $a_{x:launch} = 68.67\,\mathrm{m\,s^{-2}}$. Sideways forces are assumed to be zero and upwards forces are assumed to be no more than the weight of the plane. The list below shows all assumptions and loads expected.

- The acceleration along the x-axis is $a_{x:launch} = 68.67\,\mathrm{m\,s^{-2}}$.
- The limit force exerted by the catapult is: $F_{catapult} = 10486\mathrm{N}$.
- The limit force exerted by the propulsive system is: $F_{prop} = 851.4\mathrm{N}$.
- The plane is in takeoff configuration.
- The mass of the system is $MTOW = 1295\mathrm{N}$.
- The highest loads act on the drone at the start of launching thus $V = 0\,\mathrm{m\,s^{-1}}$.
- The weight of the drone is counteracted by an upwards acting force exactly on the cg location of the drone.

5.2.2 MANEUVERING LOADS

A manoeuvring load factors from $-1.52 < n_z < 3.8$ was derived. [3, ch.10] This would mean that the maximum bank angle would be 75°. To simplify the calculations a quasi-static case is assumed, during the turn. Starting and ending the turn will not be included in the calculations. The loads during maneuvering are lower than those during gust encounters although they act in the same direction. This means that only the gust loading will be considered during the design of the structural components and the maneuvering loads will be neglected.

- The limit acceleration along the $z-$axis is $n_{y+} = 3.8g$.
- The bank angle during this turn is 75°.
- The assumption of a quasi static case will be made, no difference in lift between the left en right wing and no sideways force is exerted on the vertical tail.
- The loads acting on the tail will scale linearly with the loads on the wing.

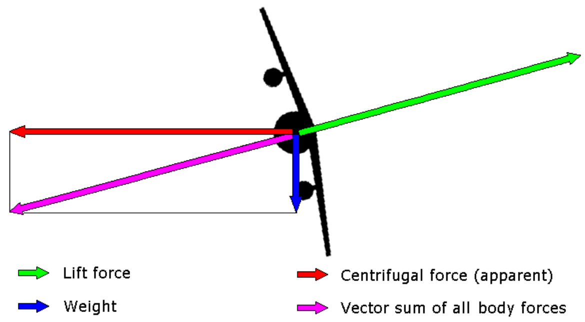

Figure 5.1: The loads on the plane in a turn [2]

5.2.3 GUST LOADS

Gust load calculations proved the limit loads to be $-4.4 < n_z < 6.4$ for the case without fuel and $-3.2 < n_z < 5.2$ in the case of full fuel. These loads occur at cruise speed. For the static calculations the gust is assumed to hit the wing and the tail at the same time although this is not true in reality. (Normally the main wing hits the

[1] A contingency factor of 15% was proposed for the preliminary design in the midterm review. [3]

[2] Adopted from: https://commons.wikimedia.org/w/index.php?curid=10401889 By Deeday-UK, CC BY-SA 3.0. Accessed on May 26, 2016

gust first). Although the loads act in a similar direction as those in the turn, there is an important difference, the gusts loads are dynamic loads, the wing will bend and in this 'spring' part of the energy is stored. This means that only part of the acceleration is experienced by the fuselage. This is way to complicated to model, design and optimize for in the time available for the project. Therefore, the assumption will be that the gusts act on a fully ridged wing. This means that all the loads will be transported to the fuselage as well, Thus that an over-designed fuselage will be produced. Under these assumptions there is no difference between the maneuvering and the gust load except that the load during gusts higher is. For that only the gust case will be treated.

The case with fully loaded fuel tanks consists out of two load cases one for positive n_z and one for negative n_z values:
- The positive limit acceleration along the $z-$axis is $n_{z+} = 5.2$.
- The negative limit acceleration along the $z-$axis is $n_{z-} = -3.2$.
- During the gust the plane is assumed to be stable. The lift increases as does the apparent weight.
- The wing and fuselage are modeled as perfectly ridged body's.
- The aerodynamic forces scale linear with the load factor. Thus lift during gust is $L \cdot n_z$ ect. For aerodynamic forces in the stable situation see table 5.4.

The case with empty fuel tanks consists again out two load cases both for positive and negative n_z:
- The positive limit acceleration along the $z-$axis is $n_{y+} = 6.4$.
- The negative limit acceleration along the $z-$axis is $n_{y-} = -4.4$.
- During the gust the plane is assumed to be stable. The lift increases as does the apparent weight.
- The wing and fuselage are modeled as perfectly ridged body's.
- The aerodynamic forces scale linear with the load factor. Thus lift during gust is $L \cdot n_z$ ect. For aerodynamic forces in the stable situation see table 5.4.

5.2.4 LANDING LOADS

During landing a skyhook will be used. Skyhooks are fundamentally different than other landing mechanisms. A hook on the wing will catch a wire and it allows for landing without a landing gear and runway. Because of the wire restricting the wing to move forward a rotational motion will be started. In the end the plane made a turn of 90° and comes to a hold. In this last moment a pulling force along the main axis will be exerted. This is an unusual load case and will thus be checked. A worked out example can be seen in figure 5.2. For more information see chapter 11.
- The limit acceleration over the $y-$axis is $a_y = 68.6\,\mathrm{m\,s^{-2}}$.
- The speed at approach is $V = 25.4\,\mathrm{m\,s^{-1}}$
- The force acting between the wire and the wing is $F_{Wing} = 6880\mathrm{N}$.
- Lift is weight.
- No gust will be encountered, thus $n_z = 1$.
- A fuel weight of 0.8kg is left (approximately 1 hour of flight).

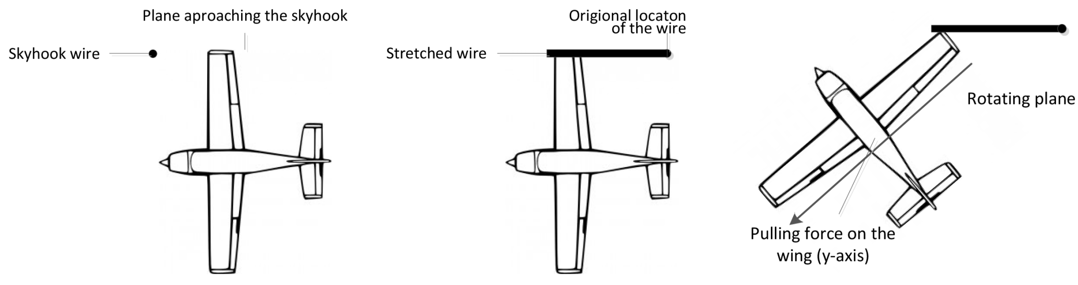

Figure 5.2: How the loads are exerted when using a skyhook for landing.

5.3 FUSELAGE CROSS SECTION DESIGN CONCEPT

The main decision made in this chapter will be about the cross sectional shape of the fuselage. In transporter aviation all fuselages are round but this might not necessarily be the best for this project because no pressurized fuselage is required in a drone. For this trade-off no real fuselage will be designed but several global shapes will be compared. The shapes considered are a circle and square.

To keep things as simple as possible only three trade-off criteria will be used. Structural performance, use full space and aerodynamic performance. For the trade-off the cross sections are assumed to have the same weights, thus area covered by the material and wall thickness. No stiffeners and frames are taken in account.

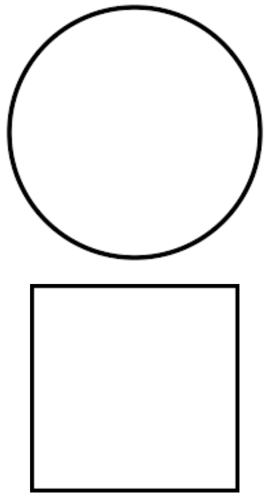

Figure 5.3: The considered cross sectional fuselage shapes, relative in size.

Assuming the shapes have the same weight and the same wall thickness the following ratio between the radius of the circle, (r), and the height and width, denoted as b, of the square. From this it has been calculated that the square height is smaller than the diameter of the circle.

$$b = \frac{\pi}{2} r \tag{5.1}$$

This means that the circle is bigger than the square. When analyzing the enclosed area, which is an important parameter for following calculation but also serves as the parameter to compare the use full space. As calculated the square with the same weight has a 0.8× smaller enclosed area then the circle.

$$A_{e,square} = \frac{\pi}{4} A_{e,circle} \tag{5.2}$$

5.3.1 STRUCTURAL ANALYSIS

To compare the general shapes simple calculations will be performed taking, normal, shear, bending and torsional loads in account. The normal load carried will be similar for all the cases because the material properties σ_{max} and the material area A (which is linear proportional to the weight) are the same for both shapes.

$$N_{max} = \sigma_{max} A_{material} \tag{5.3}$$

$$N_{max,square} = N_{max,circle} \tag{5.4}$$

For bending differences start being visible. In the equation below, eq. (5.5), the beam equation for bending is given.

$$M_{max} = \frac{\sigma_{max} I}{h_{max}} \tag{5.5}$$

$$I = \iint_r y^2 \,\mathrm{d}x\,\mathrm{d}y \tag{5.6}$$

Applying this on both the concepts proves that the circle cross section has higher resistance to moments, applied in the worst case directions, it is 1.9× higher than the moment that can be carried by the square cross section.

$$M_{max,square} = \frac{6}{\pi} M_{max,circle} \tag{5.7}$$

Other differences can be observed for torsional strength of the shapes. Using eq. (5.8) obtained from Megson [36, ch.18]. Because the only changing value is the enclosed area A_E and all the other variables stay constant, τ_{max}, t, it can be calculated that the torsional strength of the square is 0.8× the strength of the circular one.

$$T_{max} = 2 A_e \tau_{max} t \tag{5.8}$$

$$T_{max,square} = \frac{\pi}{4} T_{max,circle} \tag{5.9}$$

To calculate the shear may assumptions where made, most notable is the assumption of symmetry, because symmetry does not only simplify the equations but the location of the shear center is then known ass well. Using Megson [36, ch.17] eq. (5.10) could be derived. Only the loads in the worst location are worked out in the equations. It was derived that a circular cross section can withstand shear loads 2.25× higher than the square one.

$$S_{max} = -\frac{\tau_{max} t I}{\int_0^S t x \, \mathrm{d}s} \tag{5.10}$$

$$S_{max,square} = \frac{4}{9} S_{max,circle} \tag{5.11}$$

	Square	Circle
Normal forces	1	1
Bending moments	1	1.9
Torsional moments	1	1.3
Shear forces	1	2.25

Table 5.1: The structural performance of a square vs a circle, the square is used as a datum.

5.3.2 ENCLOSED AREA

Although the enclosed area was calculated before and it was found that the circular cross section is bigger, this does not mean that more payload could actually fit in there. It is important to note that the circular fuselage will have less effective space if square parts are placed within it and a major part of the space will be lost (around 36%). The shape optimal for this design depends mostly on the shape of the parts that need to be fitted inside. For example if a directional antenna based on a parabolic disc is used in the long range drones the circular shape is better. But as the antenna for mobile phone telecommunication is in the shape of square plates, the flat side needs to be oriented downward and no objects should be placed underneath it. This would fit within the square and circle as well. However, in the circle it only fits halfway and thus the space in the bottom half cannot be used. Using a square fuselage it could be fit in the bottom and more space will be available above it. Because it was decided to use the same design for both type of drones no real preference in shape exist. Other systems for example the propulsive system should fit in either shape.

5.3.3 AERODYNAMIC PERFORMANCE OF DIFFERENT FUSELAGE SHAPES

As presented earlier in this section and shown in figure 5.3 there are two different possibilities for the shape of the fuselage. First one is having a classical cylinder fuselage while the other possibility is to use a frame in a shape of a parallelepiped. In this subsection a small discussion is performed regarding the aerodynamic properties of both candidates. Based on the extensive argument offered by Sadraey [37], the drag coefficient of a parallelepiped is considerable higher, having a value of 1.5 instead of only of 1 of a horizontal cylinder analyzed in the same conditions. This difference of 50% in the drag coefficient would reflect directly in the fuel consumption and due to the snowball effect this will results in a considerable heavier design. Therefore, it is concluded that a fuselage with a cylinder shape would be beneficial for the whole design from an aerodynamics perspective.

5.3.4 COMPARING THE CROSS SECTIONS

Taking all the aspects structure, use-full space and aerodynamics in account it is clear the the circular cross section wins. Structure performance is better in almost all cases. The amount of space that can be used depends mostly on the subsystems that need to fit in and in the end both the circular and square cross section would do. The circular cross section has also proven to be better then the square from an aerodynamic perspective as discussed in the previous paragraph. Thus the circular cross section was chosen in the end. The fuselage will be designed in the next section, section 5.4

5.4 FUSELAGE DESIGN

After deciding on a circular cross section a design was made. For this a program was written in which all the load cases were considered. Due to the lack of time the structure designed will not be fully optimized. The program just calculates the stresses in all locations and this is checked against the maximum allowable stresses. The algorithm is based on the beam theorem approach, which models the the fuselage as a beam.

No local stress concentrations is taken in account. Thus in a future design phase it is recommended to analyze all locations with abrupt changes in dimensions and places where loads are applied.

In appendix B a drawing with the loads on the fuselage is offered. This drawing is used to program the code needed in order to calculate the forces and stresses on the structure. During programming all parameters were kept as variable as possible. Among others the geometry, the weights and even the boundary conditions could be changed. In the following sections descriptions of the theorems used will be given and results will be presented. Section 5.4.1 will threat the external forces and the accelerations due to these forces. Section 5.4.2 threats the derivations of the stresses and section 5.4.3 explains how the buckling strength was calculated. Verification of the code has been done by comparing it to hand calculation results. The error seems to be less than 1%.

5.4.1 EXTERNAL AND INTERNAL FORCES

The forces exist out of three parts; weights, acceleration induced forces and external forces. Because the plane is modeled to be a static object there should be an equilibrium between all these forces. The tables 5.2 to 5.4 list the weights, accelerations and external forces respectively.

Table 5.2: The mass of the subsystems

System	Abbr.	Mass [kg]
Engine mass*	m_e	14.1
Tail mass	m_t	4.85
All else mass	m_{ae}	13.2
Fuselage mass	m_f	25.9
Wing mass	m_w	22.2
Payload mass	m_p	20
Fuel mass**	m_{fuel}	32

Table 5.3: The accelerations in different phases

Phase	Acc. [$\mathrm{m\,s^{-2}}$]
Max takeoff x-direction	62.5
Cruise m_{fuel}=32kg max gust	5.2
Cruise m_{fuel}=32kg min gust	-3.2
Cruise m_{fuel}=0kg max gust	6.4
Cruise m_{fuel}=0kg min gust	-4.4
Max landing y-direction	68.7

Table 5.4: The external forces acting on the plane, rounded off to an integer and do not include the safety factors.

Description	Force	Unit
Max catapult force	10486	N
Max skyhook force	6880	N
Fuselage drag cruise	47	N
Wing drag m_{fuel}=32kg	47	N
Wing lift m_{fuel}=32kg	1527	N
Wing torque m_{fuel}=32kg	-300	N m
Tail drag m_{fuel}=32kg	10	N
Tail lift m_{fuel}=32kg	-133	N
Tail torque m_{fuel}=32kg	33	N m
Wing drag m_{fuel}=0kg	45	N
Wing lift m_{fuel}=0kg	1231	N
Wing torque m_{fuel}=0kg	-316	N m
Tail drag m_{fuel}=0kg	11	N
Tail lift m_{fuel}=0kg	-248	N
Tail torque m_{fuel}=0kg	31	N m

The weights can be converted into forces by using the first law of Newton as shown below. The aerodynamic loads are increased when the load factors are taken in account, these increase all the aerodynamic parameters. For negative n_z this would mean that the aerodynamic forces all became opposite in sign, lift pointing downwards. An exception was made for the drag, which was always pointing to the back and did not changes signs. This is then used to calculate the internal forces.

$$\mathbf{F} = m \cdot \mathbf{a} \tag{5.12}$$

The internal forces are calculated over the length of the fuselage, the x-axis. The z-axis is defined positive. In the figure below, figure 5.4 an example of the internal forces and moments are given. Displayed are the normal forces acting in axial direction (N_x), normal forces acting along the wing (N_y), shear forces acting downwards (V_z) and the moments around turning the plane sideways (M_{yy}). It is important to note that the load case shown is not a leading case. Other cases can be analyzed if required.

The forces in the axial direction are the thrust of the engine which is counteracted by the drag. During take-off the catapult also exerts a force on the system. At that moment the system experiences the highest normal forces. The forces acting downwards which are in clouded in the V_z diagram are positive downwards, which make the internal forces negative, see eq. (5.13). Thus the weights, multiplied with the loads factors, are positive forces while the lift of the wing and the tail are negative. The second graph also displays the moment curve, which was achieved by integrating the shear diagram and adding the aerodynamics moments. For these calculations direct integration of the forces, see eqs. (5.13) and (5.14) was used while adding the appropriate boundary conditions and adding external forces according to the definition of the axis system. A third diagram showing V_y and M_{zz} was made but not shown because it will be zero everywhere in this loading case.

$$V(x) = -\int w(x)\,\mathrm{d}x \tag{5.13}$$

$$M(x) = \int V(x)\,\mathrm{d}x \tag{5.14}$$

As a verification of the code and the external forces the stability of the design can be checked by the boundary at the front of the plane. The boundary condition at that side has not been used in the calculation but should be zero. When this is not the case the code or the forces involved should be revised.

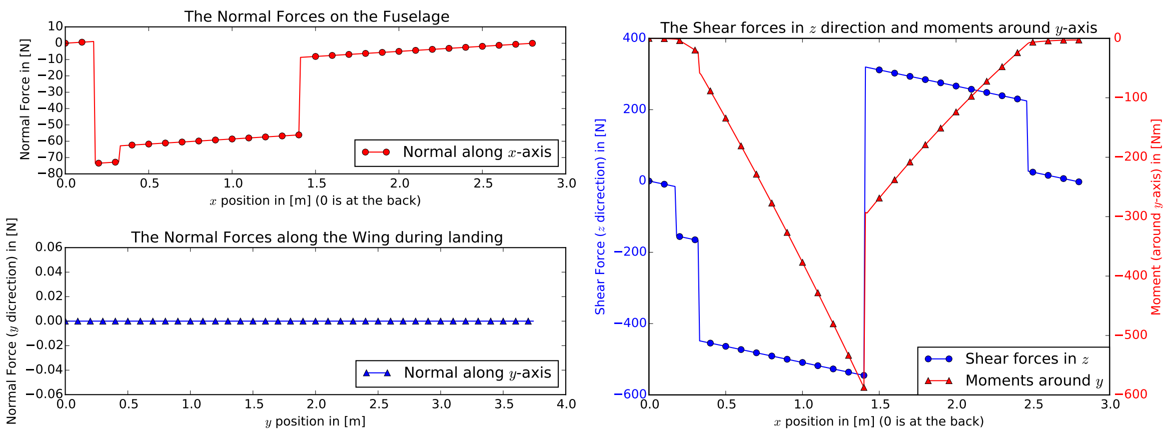

Figure 5.4: The internal forces and moments in cruise flight with no gust and full fuel ($n_z = 1$, $m_{fuel} = 32$kg).

5.4.2 STRESS CALCULATIONS

For the stress calculations several assumptions have been considered. The most important one is that the structure is modeled as a beam. This approach was already explained and it has the following implications: the local load introductions are neglected, the stress concentrations are not taken in account, the structure is assumed to have a constant cross section and no warping occurs. In future phases, it is advised to use FEM or other models which do not use the same simplified assumption. It is also advised to run an analysis on dynamic load cases to verify the load cases used in this report.

The stress calculations was divided into two parts, normal and shear stresses. where the normal stresses exist out of axial tension, compression, the moments M_{yy},& M_{zz}. The shear calculations exist out of V_z, V_y and a torsion calculation although the axial torsion M_{xx} is very small.

The normal stresses due to tension and compression in the fuselage are calculated using eq. (5.15), where σ_x is the normal stress, N_x is the normal force in x direction and A is the cross sectional metal area. This equation assumes that the stress is equally distributed over the cross section of the fuselage. Due to local oads and stress concentrations this might not be the case.

$$\sigma_x = \frac{N_x}{A} \tag{5.15}$$

The normal stress due to tension is calculated by a derivation from the general asymmetric beam bending equation, see eq. (5.16) [36, ch.16] where a simplification was made due to the existence of an axis of symmetry. Therefore, the I_{zy} can be assumed to be 0. In this equation I_{zz} and I_{yy} which are the moments of inertia and y or z are the distances to the center of gravity. These where also calculated, but will not be treated here because it is assumed to be general knowledge. Because σ_x depends on the distance to the center of gravity of the cross section a difference of stresses can be observed over the cross section itself. Assuming $M_{yy} \neq 0, M_{zz} = 0$ the stresses at top and bottom of the fuselage will be highest. For the case $M_{yy} = 0, M_{zz} \neq 0$ the highest stresses can be found in the sides of the fuselage.

$$\begin{aligned}\sigma_x =& \frac{M_{yy}\left(I_{zz}z - I_{zy}y\right)}{I_{zz}I_{yy} - I_{zy}^2} + \frac{M_{zz}\left(I_{yy}y - I_{zy}z\right)}{I_{zz}I_{yy} - I_{zy}^2} \\ =& \frac{M_{yy}}{I_{yy}}z + \frac{M_{zz}}{I_{zz}}y \end{aligned} \tag{5.16}$$

To calculate the total normal stress the stresses due to normal forces and bending moments where added up together. From this the plot in figure 5.5a could be made. Here the fuselage skin stress is displayed on a flat plate. Imagine it to be a fuselage to be formed when the bottom and top of the picture are bend forward meeting each other and creating a cylindrical shape. The loads are low in this example leading cases will be shown in appendix B.

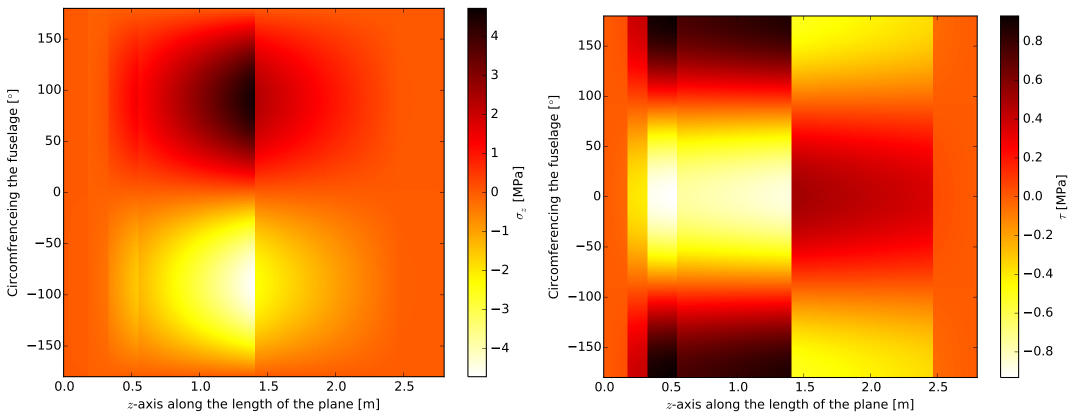

(a) The total normal stresses.

(b) The total shear stresses.

Figure 5.5: Stresses in the skin during cruise flight with no gust and full fuel ($n_z = 1$, $m_{fuel} = 32$kg).

Shear flow due to the shear force and torsion was calculated by using eq. (5.17) [36, ch.17]. Here the simplification of symmetry was made again thus $I_{xy} = 0$. To simplify the calculations it was assumed that the stiffeners do not carry any shear load, which is a realistic assumption. The stiffeners are accounted for in the moments of inertia but not in the integral. The shear flow (q_s) should be divided by the local thickness t to find the stresses. The stresses in the example case are displayed in figure 5.5b the figure can be read in a similar way as the figure of normal stresses (figure 5.5a).

$$\begin{aligned} q_s =& -\left(\frac{S_z I_{zz} - S_y I_{zy}}{I_{zz}I_{yy} - I_{zy}^2}\right)\int_0^s tz\,\mathrm{d}s - \left(\frac{S_y I_{yy} - S_z I_{zy}}{I_{zz}I_{yy} - I_{zy}^2}\right)\int_0^s ty\,\mathrm{d}s + q_{s,0} \\ =& -\frac{S_z}{I_{yy}}\int_0^s tz\,\mathrm{d}s - \frac{S_y}{I_{zz}}\int_0^s ty\,\mathrm{d}s + q_{s,0} \end{aligned} \tag{5.17}$$

$$\tau_{yz} = \frac{q_s}{t} \tag{5.18}$$

With all the stresses known the material properties should be checked next to assure that the structure is strong enough to withstand these stresses. It was chosen to use the von Mises stress criteria, which is also called the octahedral shear stress theory and is described by eq. (5.19) [38, C1.17]. σ_{yield} is the yield strength which can be determined by a simple tension stress test. In figure 5.6 the von Mises stress is shown both 3D and the flat plate layout which was used for the normal and shear stresses. The stress is normalised with

$\sigma_{vonmises}/\sigma_{yield}$ and when this values stays below 1 no yielding occurs.

$$
\begin{aligned}
\sigma_{yield} &= \frac{1}{\sqrt{2}}\sqrt{(\sigma_x-\sigma_y)^2+(\sigma_y-\sigma_z)^2+(\sigma_z-\sigma_x)^2+6(\tau_x y^2+\tau_y z^2+\tau_z x^2)} \\
&= \sqrt{\sigma_x^2+3\tau_{yz}^2}
\end{aligned} \tag{5.19}
$$

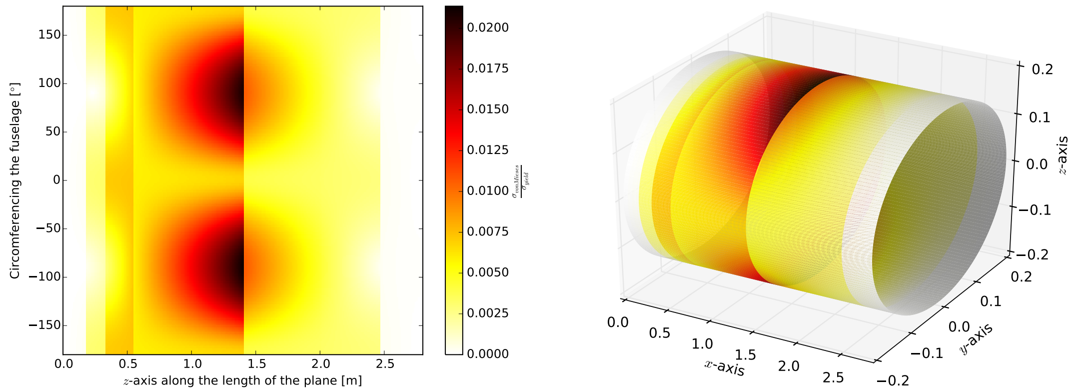

Figure 5.6: The von Mises stress normalized by the yield stress projected on a plane and in 3D, during cruise flight with no gust and full fuel ($n_z = 1$, $m_{fuel} = 32$kg).

5.4.3 BUCKLING CALCULATIONS

Structures know more failure modes than yielding due to stress, one of the general cases is failure due to buckling. Calculating maximum external forces before buckling occurs can be difficult especially for mixed load cases and more exotic structures. Buckling can be calculated by various algorithms and theoretical estimates can be made but reality proves often different. This is because buckling is very sensitive to initial imperfections and real live structures will have these defects.

Due to these imperfections and the fact that applying theoretical algorithms will not be possible in this short time frame, it was decided to use empirical estimates derived from tests. Several approaches can be used. The shell can be modelled as a several curved sheets in between the stiffeners, as a few curved and stiffened plates or as a thin walled cylinder with stiffeners. Because the empirical formulas are based on tests, it requires that a test is done on a similar structure and some dimensionless quantities are used in selecting the appropriate source, r/t, l/r and Z (shown in eq. (5.21)). This was the main argument to select the model with the thin walled cylinder, which is investigated extensively for a.o. missile structures and aircrafts. Because no extensive data can be found on thin walled with stiffeners, it was assumed that the structure without stiffeners should be able to carry the loads. This is a very conservative assumption because stiffeners are generally added to increase the buckling strength more than they are there to decrease the stresses from the former section. Due to this the structure of the fuselage will be over-designed. In the future, a more in depth analysis can be implemented in order to further optimize the structure.

Calculating the buckling strength in mixed load cases is done by treating the cases separately and using interaction equations to check the mixed case. In this section the normal force buckling, moment buckling and shear force buckling will be treated while torsional buckling will be neglected. After that the interaction equations will be explained.

To calculate the normal stresses at buckling ($\sigma_{N,cr}$) when only a compressive force is applied eq. (5.20)[38, C8.2] is used. Here E is the modulus of elasticity, ν the Poisson ratio, t the skin thickness and r the radius of the cylinder. K_c is the buckling coefficient and can both be calculated theoretically and empirically. The empirical value, which is used, depends a.o. on the radius over thickness (r/t) ratio and Z. Z can be calculated accordingly to eq. (5.21) with L being the distance between the closest two frames. When r/t and Z

are known graphs can be used to find K_c, the data provided by Leonard A. Harris in [39] is used. Only the 90% probability design curve is given thus that was used. If available the 99% probability design curve will be used. Boundary conditions are not important for the buckling of the long cylinders, thus for higher values of Z as in the case of this drone.

$$\sigma_{c,cr} = \frac{K_c \pi^2 E}{12\left(1-\nu^2\right)}\left(\frac{t}{t^2}\right) \tag{5.20}$$

$$Z = \frac{L^2}{r\,t}\sqrt{1-\nu^2} \tag{5.21}$$

$$R_c = \frac{\sigma_{N_x,max}}{\sigma_{c,cr}} \tag{5.22}$$

To calculate the normal stresses at buckling while the cylinder is under pure bending eq. (5.23)[38, C8.7] where C_b is obtained from test data produced by Herbert S. Suer [40]. The 99% probability line is used here

$$\sigma_{B,cr} = C_b E\left(\frac{t}{r}\right) \tag{5.23}$$

$$R_b = \frac{\sigma_{N_{yy)M_{zz},max}}}{\sigma_{B,cr}} \tag{5.24}$$

The case of shear buckling is approached in a similar way as has been done in the normal force buckling calculation. The main difference is that the coefficient changed to the torsion coefficient K_t times 1.25 [38, C8.12]. Values for K_t where obtained in a similar way to those of the normal case as well. A graph from George Gerard and Herbert Becker [41] provided then the values. The formula for torsion would only miss the 1.25 at the start. But due to the low torsional stresses torsion has been neglected.

$$\tau_{S,cr} = 1.25\frac{K_t \pi^2 E}{12\left(1-\nu^2\right)}\left(\frac{t}{t^2}\right) \tag{5.25}$$

$$R_s = \frac{\tau_{V_z V_y,max}}{\tau_{S,cr}} \tag{5.26}$$

Adding up the stresses to a total value directly is not possible because of interaction between the different loads. But adding up the fractions R_c, R_b, R_s is possible by eq. (5.27). The rule is that if $R_t < 1$ no buckling occurs.

$$R_t = R_c + \sqrt[3]{R_s^3 + R_b^3} \tag{5.27}$$

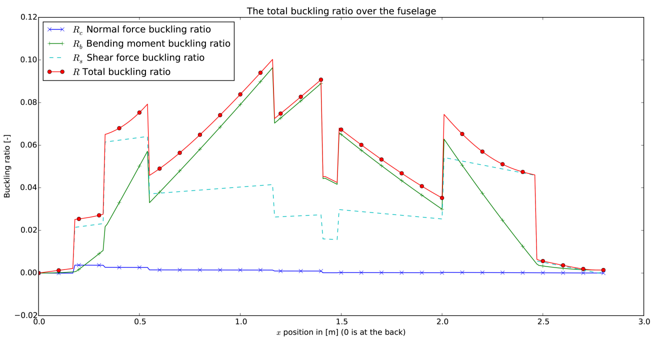

Figure 5.7: The buckling ratio along the length of the fuselage in cruise flight ($n_z = 1$, $m_{fuel} = 32$kg).

5.4.4 INITIAL FUSELAGE DESIGN

A structural design is determined from many requirements, for this design loads and size where decided up and are not variable during the structural design phase. For example the radius is determined from fitting all the subsystems. Some inputs are variable though, for example the wall thickness, and material choice. Soon it became clear that buckling would be leading the design. Buckling due to landing loads at the location closest to the main wing are the highest. However, using a simple design with no stiffeners, aluminum 2024-T6 and a constant skin thickness of 1mm the skin still does not come close to failure because the loads are never high enough. It was thus decided to variate the skin thickness over the length of the fuselage. But having the whole fuselage have a thickness thinner than 1mm is not possible. At least not over the whole length, the chances of damage due to people lifting the plane, or hitting it are too high. Locally it might be possible but 'NO GRIP' warnings should be placed upon those parts.

Because metals blocks the radio waves of the communication systems it was decided to make the front of the plane from composites. As it was noticed that using aluminum would result in an over designed structure, it was chosen to go with a quasi-isotropic composite with less strength and stiffness. Quasi-isotropic E-glass with volume density of 60% was selected. Because the lower density the weight would decrease while it could still withstand all the load cases.

It was chosen to not produce the whole plane from glass fibers due to the major increase in cost. Although glass fiber itself is not expensive, making small structures from fiber composites is expensive. Beside in small parts the fiber are not long enough to give real benefits in strength [35].But other metals where analyzed, and in the end magnesium was selected because its descent strength, good elasticity and low density, $\rho = 1.78\,\mathrm{g\,cm^{-3}}$. One of the main reasons for using no magnesium in aerospace engineering is the combustion risk. The ignition point[3] of magnesium alloys is around 473 °C while burning at a maximum temperature of 3100°C [42]. To reduce the risk of fire 0.5% to 5% calcium can be added to the alloy [43] raising the ignition temperature to 673-773°C[44]. This is above the actual melting temperature of magnesium as well as aluminum. For this although the risk of combustion still exist it only happens after failure due to melting. Because no people are in the drone elevated burn temperatures should not be a problem. Magnesium generates a gray film when corroding, this film protects against further corrosion although some pitting might occur at elevated temperatures in humid environments. Over all, the corrosion resistance of magnesium is very good [4]. The resistance of magnesium in fatigue is poor, tensile tests showing a resistance of 10^7 cycles for an amplitudes of 50MPa [45]. Primarily the fatigue crack propagation is bad, even worse then aluminium 7075-T6. Please keep in mind that the WiFly system will not fly that much, so the amount of cycles will be very low and loads stay generally small. One should note that rolled magnesium AZ31 shows strong anisotropic properties especially in fatigue and thus special attention should be given to this in further phases [46].

Table 5.5: Material properties of magnesium and glass fiber

Property	Magnesium AZ31B-H24	Quasi-isotropic E-Glass 60%	Unit
Elasticity	45	21	GPa
Yield Strength	221	235	MPa
Ultimate Strength	290	235	MPa
Ultimate elongation	15	1.6	%
Poisson ratio	0.35	0.23	[-]
Density	1.78	2.0*	$\mathrm{g\,cm^{-3}}$

* Estimated value

Table 5.6: Skin thickness, $x = 0$ at the back of the plane.

Description	Location range [m]	Thickness [mm]	Material
Back to the engine frame	0-0.324	0.8	Magnesium
Engine frame to rear wing frame	0.324 - 1.16	1.0	Magnesium
Rear wing to front wing frame	1.16 - 1.49	1.1	Magnesium
Front wing frame to comm system	1.49 - 2.00	1.0	Magnesium
Comm system to front of plane	2.00 - 2.81	1.0	E-glass

[3]Source: http://www.engineeringtoolbox.com/fuels-ignition-temperatures-d_171.html Accesed on 15 June 2016
[4]see: http://www.totalmateria.com/Article19.htm accessed at: 20th June 2016.

The thickness changes over the length of the fuselage because the loads in the front and back are lower than those in the middle, thus a thinner skin is allowed. Optimizing a structure would mean that all the points along the fuselage would fail at the same load, the thickness is thus changing continuously. This would be impossible to produce thus discrete changes where introduced. The thickness changes coincide with the frames holding the tail/engine, the wing box front and back frame and the payload frame. In the end the weight of the skin and the frames is 7.9kg.

The fuselage design as presented here is far from complete. Details like mounts, cutouts and local reinforcements still needs to be designed. To account for the increase of weight due to this an factor of 1.4 will be used. This is a little higher than the factor 1.3 which is usually used to estimate the structural weight of a fuselage when only the stiffeners, frames and skin weight are known. The higher factor was chosen because the systems will be packed more densely then in a transportation aircraft. This would mean that the final fuselage structure weight would be 11.06kg. This estimate is a lot lower then the one estimated based on Raymer [2] and shown in section 9.1. The potential reason for that consists in the extensive use of reference aircraft which can also carry passengers. Therefore, the fuselage may include furniture, isolation, a pressurized cabin and more. The designed drone does not have that thus the weight of the fuselage can be further reduced. Considering the limitation of the method of Raymer [2] a fuselage weight of 11.06kg obtained after a complete structural analysis of the fuselage seems to be reasonable.

5.5 ENGINE MOUNT

As was proposed by Raymer [35, p.100-104] and the engine manufacturer a truss system was used as a connection between the engine box, engine with firewall, and the fuselage. This allows for better airflow for cooling, easier detachment for maintenance and for better vibrational damping. A firewall should have a thickness of 9.5mm when made out of plywood. The shape of the firewall should still allow for good airflow around the engine. Because this it was chosen not to install a square plane but a quadrilateral shape which decreases towards the center. An example of this is the black wall visible in figure 5.8.

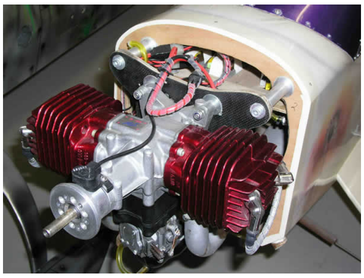

Figure 5.8: Engine mount as adviced by the manufacturer

The truss system behind the engine exist out of four bolds which act as spacers as well. These four spacers carry the thrust and the weight (including inertia) of the engine. Because that this is a proven concept the frame itself will not be calculated. Here the forces exerted on the connection to the frame in the fuselage will be calculated. The load cases used are described insection 5.2 where the following forces where derived, all values are the ultimate forces.

5.5.1 NORMAL OPERATION WITH GUST LOADS

Under normal operations, assuming the maximum gusts at maximum thrust.

- The ultimate thrust provided by the engine $T_E = 851.4$N.
- The ultimate positive load factor $n_{y+} = 6.4$g.
- The ultimate negative load factor $n_{y-} = -4.4$g.
- The weight of the engine is $W_e = 14.042$kg, including engine mount weight
- The center of gravity of the engine is assumed to be between the two cylinders.

Because of symmetry along the xz-plane it was assumed the the loads in y direction is spread out evenly over the all the four bolds. This symmetry assumes that the spacers are similar in all corners. In table 5.7 the loads are described for this case.

5.5.2 TAKE OFF SITUATION

The following assumption for take off are listed below. The resulsts of the calculations can be seen in table 5.8

- The limit thrust provided is $T_E = 851.4$N.
- The acceleration is $a_x = 62.5\,\mathrm{m\,s^{-2}}$.
- The weight of the engine is $W_e = 14.042$kg.

Bolt	Fx	Fy	Fz	Unit
Top Left	-14.54	0	344.53	N
Top Right	-14.54	0	344.53	N
Bottom Left	440.24	0	344.53	N
Bottom Right	440.24	0	344.53	N

Table 5.7: The loads of the engine mount on the frame in the fuselage during a gust.

- The center of gravity of the engine is assumed to be between the two cylinders.

Bolt	Fx	Fy	Fz	Unit
Top Left	-204.80	0	59.40	N
Top Right	-204.80	0	59.40	N
Bottom Left	-126.39	0	59.40	N
Bottom Right	-126.30	0	59.40	N

Table 5.8: The loads of the engine mount on the frame in the fuselage during take off.

5.5.3 LANDING SITUATION

The following assumption for take off are listed here below. The resulsts of the calculations can be seen in table 5.9

- The limit thrust provided is $T_E = 229\text{N}$.
- The sideways acceleration is $a_y = 10\text{m}\,\text{s}^{-2}$.
- The weight of the engine is $W_e = 4.1\text{kg}$.
- The center of gravity of the engine is assumed to be between the two cylinders.

Bolt	Fx	Fy	Fz	Unit
Top Left	55.97	59.40	415.99	N
Top Right	330.52	59.40	415.99	N
Bottom Left	95.18	59.40	415.99	N
Bottom Right	369.73	59.40	415.99	N

Table 5.9: The loads of the engine mount on the the frame in the Fuselage during landing.

5.6 WING DESIGN

Special attention was directed towards the design of the wing as it is supposed to carry the strongest aerodynamic loads acting on the UAV. Three loading situations were assessed as critical and will be used in this chapter to size the wing structure. Those are: takeoff, flying through a strong wind gust and the landing. First, the methods used (coded) will be described and afterwards the results will be presented.

As in most airplanes today, the wings of the drone contain a wing box which is meant to carry all the loads. This is placed as seen in figure 5.9 inside the LA203A airfoil. The inner shape represents the simplified skins of the wing box (straight lines). Since the moment of inertia of the simplified structure is slightly smaller than that of the real one the assumption is conservative. In order to mitigate the risk of a bird strike it was decided to design the wing box such that it can carry all loads. In an event similar to the collision with a foreign object the leading edge of the wing is usually destroyed. If the wing box can maintain the structural integrity by itself a catastrophe may be avoided.

5.6.1 GENERAL SHAPE AND ASSUMPTIONS

The wing box will reduce in size towards the tip together with the wing. Since the wing taper ratio is 0.361 the wing box dimensions at the tip will be about three times smaller than at the root. The cross section of the wing box is symmetric about the x-axis (shown in figure 5.9). The following assumptions and simplifications are included in the analysis.

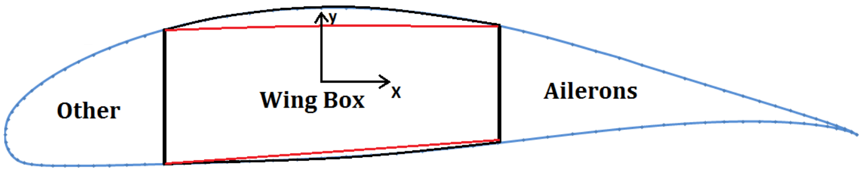

Figure 5.9: LA203A Composition

- The analysis will be done for only half of the wing box, that is, one wing. For symmetry reasons it is expected that the stress distribution will be identical for the other half of the wing box.
- Stringers on the upper skin and ribs will be used to help maintain the shape of the wing upon loading as well as to preventing buckling. Each stiffener has a cross sectional area of 30 mm^2.
- The wing box is passing straight through the fuselage and it will carry the fuel needed for the mission. On top of that, it has to be detachable for transportation (See figure 5.10). The attachment method has not been designed but the connection with the fuselage occurs inside the fuselage
- All the considered loads are static or quasi static.
- Buckling on the front and rear panels (AD and BC in figure 5.20) is not considered. This is not needed as the two walls will act as the flanges of the wing and are thus sufficiently thick.
- In this design phase bonding methods and the failure mechanisms associated with them have not been analyzed.
- To prevent strong stress concentration areas, all the stringers will be used throughout the entire span of the wing box (no interruptions).
- The fuel level is at all times uniformly distributed in the wing. The quantity of stored fuel at each cross section decreases with the span.
- One 22 g antenna is placed at the wing tips of each wing on a support made out of a materials which does not disturb the propagation of electromagnetic waves. The support will not be analyzed.
- Upon launching, the wing produces no lift or drag
- During cruise, the effect of the tangential force of the wing is small in comparison to the normal force
- Upon landing, the hook will introduce force in one of the wings acting in the direction in which the wing is pointing. This force results in a pure normal stress. It is assumed that the load is uniformly introduced on the cross sectional area of the tip.
- Thin wall assumption holds, allowing the use of shear flow.

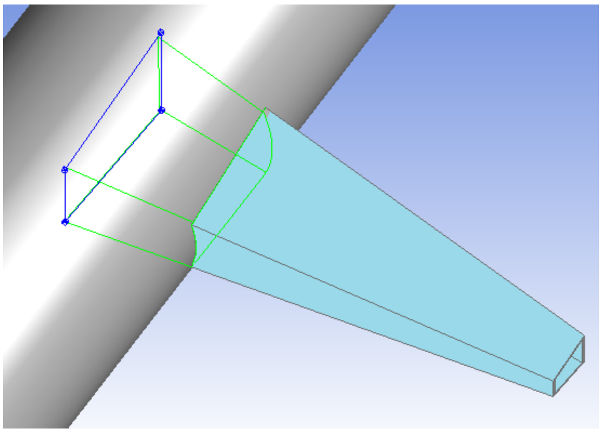

Figure 5.10: Wingbox-Fuselage connection

5.6.2 MOMENT OF INERTIA

The moment of inertia of the wing box was calculated at every span-wise location. Both I_{xx} and I_{yy} had to be computed as they are relevant for analyzing the flight through a gust and the takeoff loads respectively. They can be seen in figure 5.11 and figure 5.12.

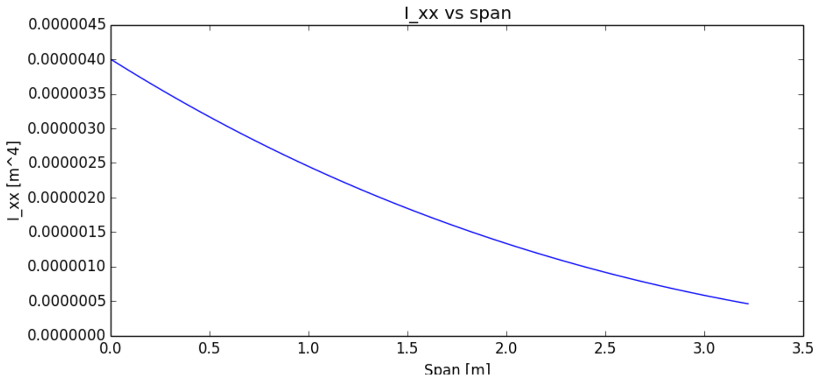

Figure 5.11: I_{xx} vs. span

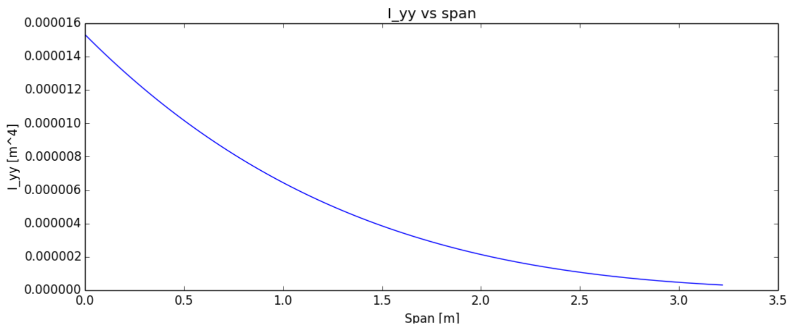

Figure 5.12: I_{yy} vs. span

5.6.3 Span-wise Moment and Force

The three load cases to be analyzed are displayed in figure 5.13.

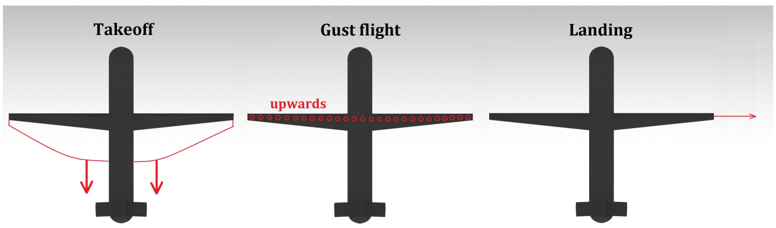

Figure 5.13: Load cases analyzed for the wing

Takeoff

It is known that the launching system will accelerate the UAVs forward with approximately 63 m/s^2. Due to the mass of the wing and of the fuel inside it, an inertial force will tend to push the wing backwards. In order to determine the magnitude of this force, each wing has been divided into 100 span-wise sections. For each section the mass of the structure and the fuel inside it has been determined. The mass of the 22 g antenna has been added to the last element at the wing tip. It is assumed that 31.8 kg of fuel are stored in the wings. In the piece of software used, the total mass attributed to each section has been stored in an array which was then multiplied by the takeoff acceleration. The force distribution can be seen in figure 5.14. Mind that the force is acting towards the rear of the airplane, opposite to the launching direction (x-direction). The sudden increase in force at the wing tip is due to the mass of the antenna placed at the wing tip.

The moment (about y) created by this force was determined by calculating the moment caused by all the forces acting between the point considered and the nearest wing tip. This is needed for calculating the normal stress in the structure for this loading case. The distribution can be seen in figure 5.15.

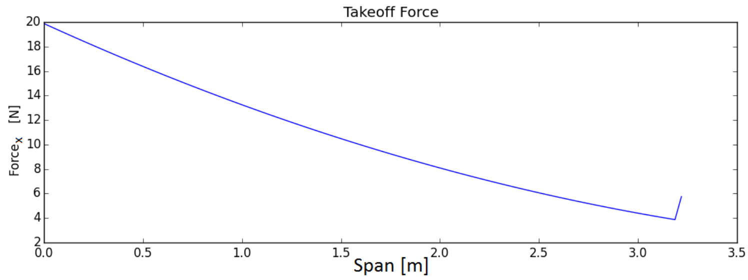

Figure 5.14: Force distribution on the wing during takeoff. Force acting opposite to the flying direction

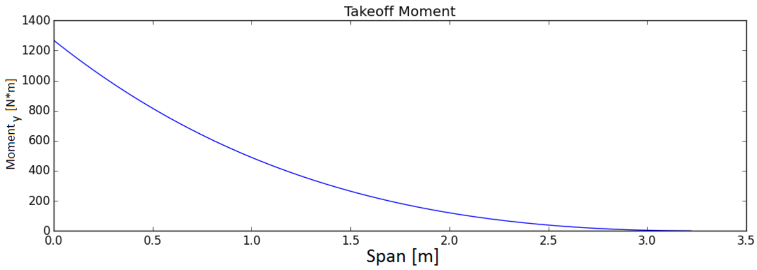

Figure 5.15: Moment distribution on the wing during takeoff

Gust flight
The span-wise moment was obtained using XFLR5 for a number of points along the span (chosen by the aerodynamics group). Since those do not correspond with the 100 span-wise points at which the structure is analyzed, information needs to be derived from the given points. A cubic interpolation was done based on the given points. The span-wise moment distribution is shown in figure 5.16.

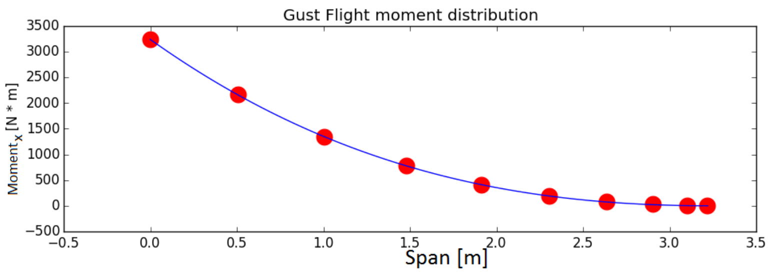

Figure 5.16: Moment distribution on the wing during gust (dots are the data points)

Based on the moment distribution, the vertical force (lift) at every span-wise location was determined (from the wing tip towards the root). It was assumed that the moment at every location along the span consists of the moments induced by the forces applied between the point considered and the wing tip. Starting from the second to last point along the wing, where only one force (unknown) contributes to the moment, and moving on towards the root, one can determine the force distribution (if a low resolution was used, the results would have high errors, but the 100 points used introduce sufficient accuracy as the shape of the force curve in figure 5.17 would not change for higher resolutions). This force (shown in 5.17) represents the lift distribution along one wing. Together with the location of the center of pressure, they will be used to determine the shear stress in the wing (center of pressure at certain span-wise locations is determined from XFLR5 and interpolated like it was done for the moment distribution).

Landing Load
As mentioned earlier, the sky-hook landing mechanism will only produce a force acting at the wing tip of the captured wing in its pointing direction (load uniformly distributed on the cross section of the wing tip). The force is equal to the deceleration induced (-69 m/s^2) multiplied by the Operative Empty Weight (OEW) plus the payload weight of the vehicle (in total 100.2 kg). This results in a force of 7605 N (assuming landing at

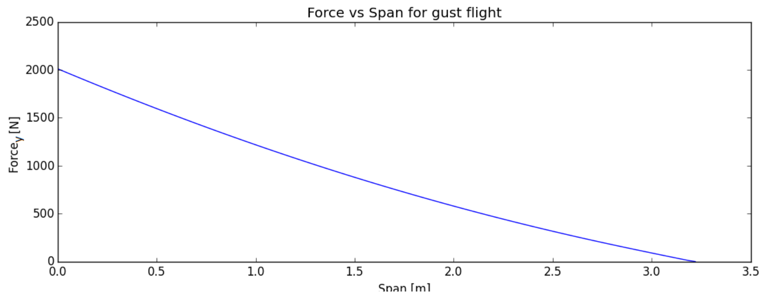

Figure 5.17: Force distribution on the wing during gust. Force acting upwards

1.1 OEW as some fuel still needs to be in the tanks), which can be considered constant towards the first half of the span (fuselage is the mass main contributor). No moment is introduced in the structure of the wing in this case.

5.6.4 Normal Stress

The normal stresses considered are acting in the span-wise direction. They are induced by bending moments for gust flight and takeoff and by a normal force for the landing.

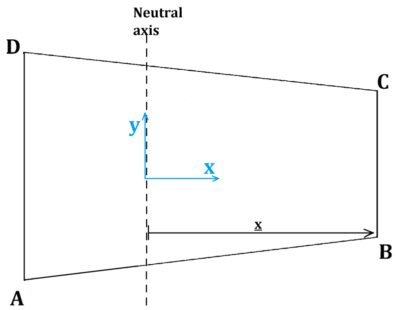

Figure 5.18: Neutral axis and the distance $\underline{x}$ to the edges (upward bending)

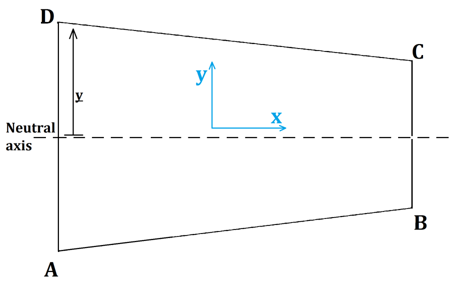

Figure 5.19: Neutral axis and the distance $\underline{y}$ to the edges (rearward bending)

$$\sigma_z = \frac{M_y \cdot \underline{x}}{I_{yy}} \tag{5.28}$$

$$\sigma_z = \frac{M_x \cdot \underline{y}}{I_{xx}} \tag{5.29}$$

$$\sigma = \frac{F}{A} \tag{5.30}$$

Takeoff
The stress induced by the moment is calculated using equation (5.28). Here M_y is the local moment about the y-axis, $\underline{x}$ is the distance along the x-axis to the point where the stress is being calculated (see figure 5.18).
Gust
Using equation (5.29) one can calculate the normal stress the normal stress due to the gust. Here M_x is the moment about the x-axis, $\underline{y}$ is the vertical distance from the neutral axis to each of the points on the structure. (see figure 5.19)
Landing
For landing, the constant force is simply divided by the local cross sectional area to find the normal stress.

5.6.5 Shear

In order to find the shear stress, the shear flow had to be computed first. As shear flow is only defined for thin walled structures such walls need to be assumed. The shear flow of a closed cross section is divided into an open section component with a force acting through the shear center and a closed section component which accounts for the position where the shear force is acting. This can be seen in figure 5.20. Here, one can see that the cross section has been divided into four elements: AB, BC, CD, DA. It is assumed that the stiffeners do not carry any shear stress and only influence the moment of inertia of the structure. Since the shear force changes in magnitude and position along the span and the moment of inertia differs, every cross section needs to be analyzed. In the next lines, the procedure applied to each span-wise location is described. Since during landing no shear force is present, a shear stress analysis will not be performed for the landing load.

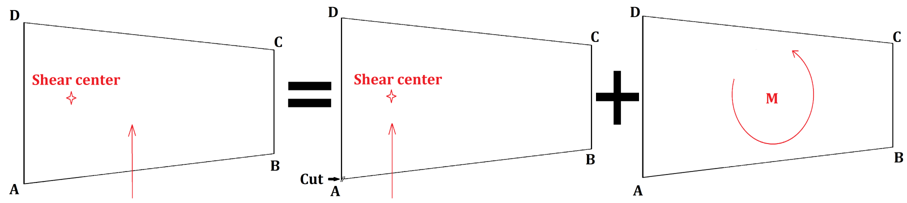

Figure 5.20: Shear Flow components

$$q_s = -\frac{I_{xx}S_x - I_{xy}S_y}{I_{xx}I_{yy} - I_{xy}^2}\int_0^s txds - \frac{I_{yy}S_y - I_{xy}S_x}{I_{xx}I_{yy} - I_{xy}^2}\int_0^s tyds \tag{5.31}$$

Gust

As a first step, the structure will be cut at point A (first section on the right hand side of figure 5.20). This will result in a null value of the shear flow at that point. The general shape of the shear flow equation of an open cross section (q_s) can be seen in equation (5.31). Since one axis of symmetry exists I_{xy}=0. Also because the tangential force is very small in comparison to the normal force for this loading scenario, only S_y will be kept and S_x is set to 0. The equation can be rewritten as (5.32).

$$q_s = -\frac{S_y}{I_{xx}}\int_0^s tyds \tag{5.32}$$

$$q_{s_{BC}}(s) = Q_{s_{AB}}(B) - \frac{S_y}{I_{xx}}\int_0^s tyds \tag{5.33}$$

In equation (5.32) I_{xx} is the moment of inertia of the cross section, s is a variable representing the distance along an element from its starting point (e.g. distance from A along AB). Every time a new element is analyzed, its contribution is added to the last value of the proceeding element. See for example 5.33 in the case of BC.

Once the open section shear flow is determined one can close the section and add q_0 which is constant throughout the cross section. Moment equilibrium then needs to be performed about a point (point A). The open section shear flow is obtaining by solving equation (5.34). In this equation, A_{encl} represents the area enclosed by wing box, AM is the distance from point A to CD, AB_x is the horizontal distance from A to BC, F is the force and d_{FD_x} is the horizontal distance from A to the location where the vertical force F acts.

$$2q_0 A_{encl} + \int_0^{AB} q_{b_{AB}} AMds + \int_0^{BC} q_{b_{CD}} AB_x ds + F \cdot d_{FD_x} = 0 \tag{5.34}$$

Takeoff

Since the only force acting in this scenario is inertial, the force is acting through the center of mass. Because the structure is symmetric about the x axis (shown in figures 5.18 and 5.19) the center of mass and shear center of the wing box will lie at an equal distance from the upper and lower skins. This means that the shear force will produce no torque in the cross section and only q_s contributes to the shear flow. Similarly to the gust loading, some elements in equation (5.31) can be dropped. This becomes equation (5.35) for element DA and equation (5.36) for element AB. The approach for the next segments (BC, CD, AD) is the same.

$$q_s = -\frac{S_x}{I_{yy}}\int_0^s txds \tag{5.35}$$

$$q_{s_{AB}}(s) = Q_{s_{DA}}(B) - \frac{S_x}{I_{yy}}\int_0^s txds \tag{5.36}$$

To obtain the total shear shear flow in the structure one needs to add q_0 (if not null) to the open section shear flow of each element. Shear stress is the shear flow divided by the thickness. (See equation (5.37))

$$\tau = \frac{q}{t} \tag{5.37}$$

5.6.6 VON MISSES STRESS

With the normal and shear stress determined at each node one needs to combine the two in order to get an idea of how far from failure the wing box structure is. Von Misses failure criteria states that permanent deformation of a structure is expected when the equality in equation (5.38) holds. Where σ_y is the yield stress of the material used.

$$\sigma_y = \sqrt{\sigma^2 + 3\tau^2} \tag{5.38}$$

5.6.7 WING BUCKLING

Another important failure mode is buckling. Defined as a mathematical instability leading to failure, buckling is a science on its own. In this design phase, an accurate buckling analysis can not be performed. Instead, an empirical method for flat plates will be used in order to approximate the stress values at which this failure type is expected. The method used is described more in depth in [38].

Since it only concerns larger surfaces which are in compression, only the upper skin is analyzed. The variables in hand are the number of stringers on the upper side, their position as well as the location of the ribs. The compressive stress at which buckling is expected is given by equation (5.39).

$$F_{c,cr} = K_c \eta_c E \left(\frac{t}{b}\right)^2 \tag{5.39}$$

Where K_c is the flat plate buckling coefficient for in-plane compression loads, η_c is the plasticity reduction factor in compression load (assumed 1), E the Youngs Modulus, b the width of the loaded side of the plate and t is the thickness of the plate.

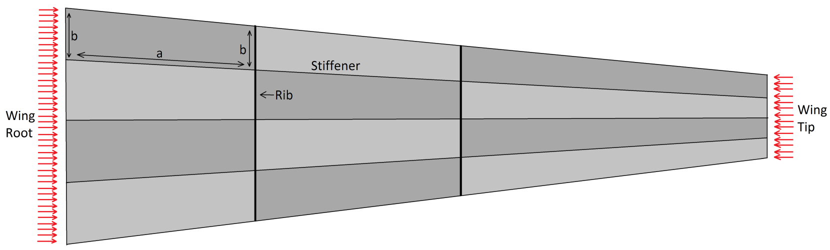

Figure 5.21: Top view of wing showing stringers and ribs

From figure 5.22 one can see that the buckling coefficient depends on the aspect ratio of the considered element as well as the way in which its edges are fixed (hinged or clamped). From figure 5.21 one can see how a and b are defined in figure 5.22 as well as how the wing box is divided for this buckling analysis (ribs and stringers).

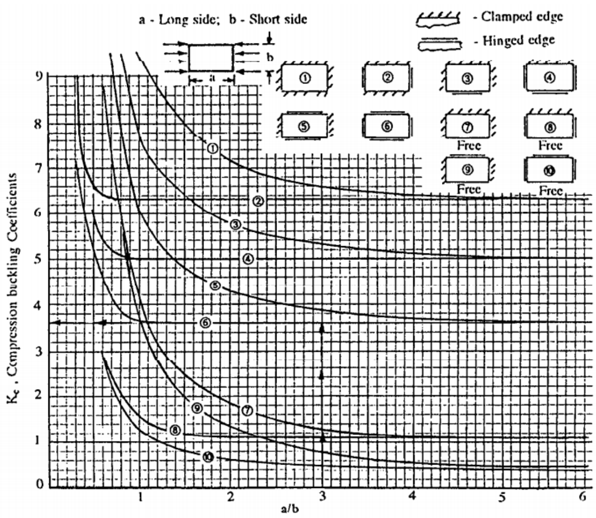

Figure 5.22: Buckling coefficient graph

Table 5.10: Aluminium 6061 properties

Density [kg/m^3]	Tensile Yield Strength [MPa]	Modulus of Elasticity [GPa]	Melting Point [°C]	Fatigue Strength [MPa]
2700	276	68.9	582 - 652	96.5

It is assumed that the margins of each section are hinged (model 6 in figure 5.22). This is not entirely true, since the ribs and the stringers prevent rotation and in plane expansion to a certain extent. However those are not rigid enough to consider the edges of the sheets in-between the stringers clamped. Since for an a/b ratio bigger than 1 the buckling coefficient for model 6 converges towards the value of $K_c = 3.7$, this will always be used.

5.7 WING BOX RESULTS

In this section the results obtained numerically will be presented or discussed. The geometry of the wing box will also be presented. One should bare in mind that the results presented are not the most optimum as refinement involves a time consuming iterative process. The process was halted the moment a design that met the performance requirements was found while having a weight inferior to what was predicted. In a further design stage the structural performance could be improved.

5.7.1 MATERIAL SELECTION WING BOX

Earlier in this chapter (section 5.1) a short description of all the engineering materials available was made. In this section a further trade-off precess will be performed for choosing a material for the wing box specifically.

Since the wing box carries large loads and it is long and slender, it is crucial that the deformation experienced is not very big. That calls for a material with high stiffness and strength. With this criterion one can eliminate the possibility of using polymers as they tend to have a low E-modulus. As cutouts will be made throughout the wing box, for fuel lines, rivet holes, electric cables, etc., one needs to consider the effect of concentration factors in the design. One class of materials performs particularly bad with concentration factors, ceramics. Due to this weakness they will be discarded.

Composites and metals are the viable options left. Since composites are much more expensive, they shall only be used if the design turns out to be unreasonably heavy [35].

In what concerns metals, four are used in aerospace structural applications: steel, aluminium, titanium and magnesium. From those, steel should only be used if very high strength is needed for a certain part. Titanium is very expensive to buy and to process and should therefore be avoided. Magnesium on the other hand is light and reasonably priced, its main downside is its flammability which poses a great danger in this case especially as the fuel will be stored inside the wing box. Another downside is the risk of a sudden increase in cost (see risk chapter 19). Aluminium remains the preferred choice as it provides a good compromise between strength, stiffness, mass and cost. Unless really necessary, titanium and steel will not be used.

The selection of the best aluminium alloy is a complex task due to the very high number of options available. A trade-off selection procedure is not the best method of picking an alloy in this case as it is not known whether the maximum allowed strength is a limiting parameter for the design (a simulation is needed). Thus the selection process used will be an iterative one. As price and availability are very important for the production and commercialisation of the product, the simulation will begin with one of the less expensive aluminium alloys used in aerospace, aluminium 6061. This is a cheap and popular material for aerospace. It offers excellent joining characteristics and good acceptance of applied coatings. On top of that it combines relatively high strength, good workability, and high resistance to corrosion [47]. If this material does not posses sufficiently good properties the simulation will be made for another, more expensive material. The properties of aluminium 6061 are displayed in table 5.10. Fatigue is not expected to be a problem for this type of UAV. The material is certified for 500,000,000 cycles with completely reversed stress with a Moore machine and Moore specimen. On top of that due to the low chances of a disaster severe enough to damage the communication sub-system it is expected that the fleet will not go through more than 50 cycles. Welded joints will not be used as they weaken the structure and make it more susceptible to corrosion. On top of that, welded joints can not be disassembled which would make the product less sustainable.

Table 5.11: Location of the center of pressure along the span for C_L

Span-wise location [m]	0	0.51	1	1.48	1.91	2.3	2.64	2.9	3.1	3.22	Average
X cp (% chord Loiter)	31.9	31.8	31.8	35.2	35.1	35	34.9	34.8	34.4	37.5	34.3

5.7.2 WING BOX POSITION

Before the analysis is started one must make sure that the wing box analyzed fits inside the wing and that it maximizes the efficiency. One must account for the presence of ailerons and the actuators powering them in the rear of the airfoil. Those can be seen in figure 5.23. The ailerons occupy the last 20% of the chord (as the chord varies along the span, the dimensions are given relative to the local chord). A further 10% of the chord is assumed to be occupied by the aileron hinge and actuators.

As a rule of thumb, the flanges (vertical walls) of the wing box are most efficient when they are long, as they

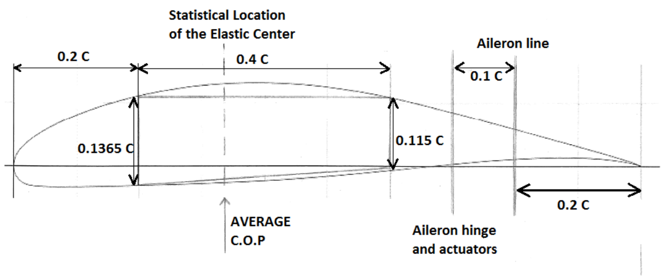

Figure 5.23: Wing box position inside the airfoil

greatly increase the moment of inertia about an axis parallel to the chord line. However the spacing between them should be sufficiently high as a volume of 44 liters is needed inside the box for fuel. Other constraints for the position of a wing box inside a wing are aero-elastic instabilities. Though such an analysis has not been performed in this design stage, it is known that the coupling between pitching moment and bending moment is what leads to the catastrophic aero-elastic failures. Wing divergence is a static phenomena which results in a self increasing angle of attack of a part of a wing. Upon a small disturbance that increases the angle of attack the wing twists further increasing the angle of attack (the center of pressure (c.o.p.) moves towards the leading edge as the angle of attack increases). One way to prevent the wing from diverging is to have the wing box placed such that c.o.p. will always be behind the elastic axis. The c.o.p. is most forward when the angle of attack is high and thus this is the most critical scenario. However, c.o.p. is not at the same location along the span for a given angle of attack. In table 5.11 one can find the position of the center of pressure at different span-wise positions. The average value of the c.o.p. is at 34.3 % of the length of the chord.

The typical location of the elastic center of a wing is located at 35% of the wing [48]. As only the wing box is assumed to be load carrying, it will be assumed at 35% of the length of the box.

Having all the before mentioned constraints in mind the wing box has been positioned as seen in figure 5.23. One can see there that the elastic axis and the average location of the center of pressure coincide for the maximum angle of attack achievable. The wing box can not be made any smaller as its inner volume is 46.3 liters (compared to the 44 that are needed). Placing the front flange more forward or the rear one more towards the back would results in a less efficient design as the dimensions of the two flanges would decrease (airfoil is less thick).

The wing box configuration chosen can be seen in table 5.12. The points A, B, C and D are defined in figure 5.20. The given total mass accounts for the wing box as well as the skin of the airfoil (assumed 0.7 mm thick).

5.7.3 WING BOX STRENGTH

The methods described in section 5.6 are applied for the three scenarios discussed (Takeoff, Gust and Landing). The stress at every location has been divided by the yield stress to find how far from failure the structure is according to the Von Misses Failure criteria. The arrows in the picture indicate the direction from which the airflow is coming from. The relatively low stresses would be in a real life situation amplified locally by stress d

Table 5.12: Wing box dimensions and results

AB/chord [-]	tAB/chord [-]	BC/chord [-]	tBC/chord [-]	CD/chord [-]	tCD/chord [-]
0.4	1.667E-3	0.11	1.85E-3	0.4	1.667E-3
DA/chord [-]	tDA/chord [-]	Stiffeners Upper skin	Stiffeners Lower skin	Area Stiffener [mm^2]	Ribs location [m]
0.14	3.7E-3	5	1	30	[0.2, 0.8, 2]
Mass skin +ribs [kg]	Mass Stiffeners [kg]	Mass rest of wing [kg]	Total wing mass [kg]	Expected wing mass [kg]	Volume inside wing [liters]
7.6	4.58	8.76	21	22.2	46.3

concentration factors such as cutouts. The reference concentration factor, for a circular hole is 3.

Takeoff

In figure 5.24 one can see the distribution of Von Mises stress along the bottom skin (the top skin is symmetric to the bottom skin w.r.t. the acting force, and is thus identical). One can see that the maximum stress is found at the root of the trailing edge flange.

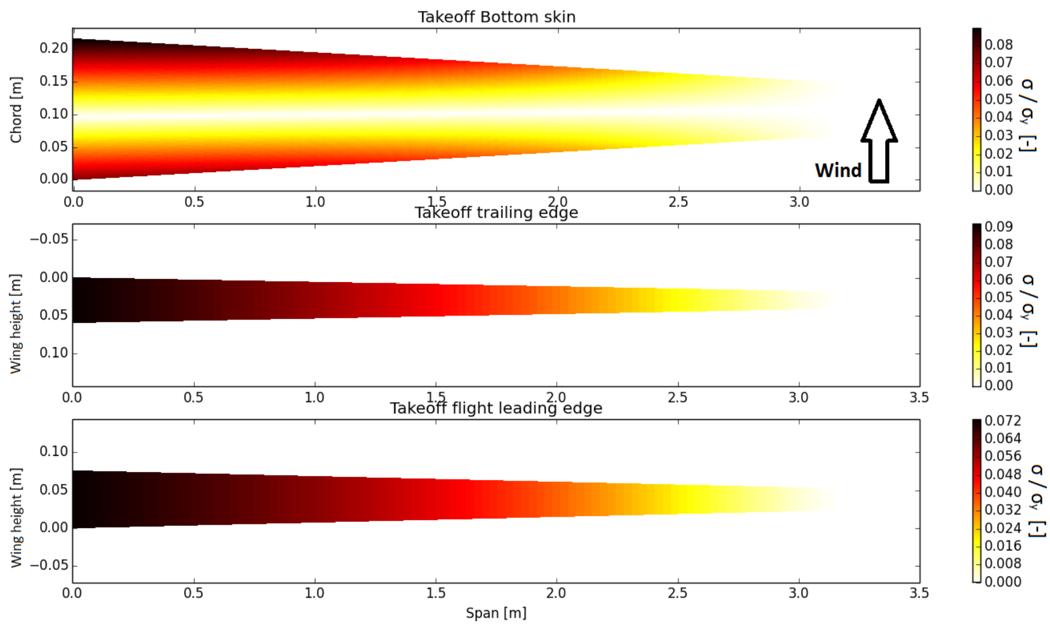

Figure 5.24: Stress distribution along 3 faces during takeoff

Gust

In figures 5.25 and 5.26 the Von Mises stress distribution during a gust can be seen. The maximum stress occurs at the leading edge. That is expected since the front flange is slightly longer than the rear one, thus allowing a smaller deflection upon an upward force such as the one induced by the gust. The maximum stress experienced, without any load concentration factor, is 8 times smaller than the failure stress predicted.

Landing

Unlike in the other two load cases, during landing, the maximum stress is experienced at the tip (see figure 5.27). That is expected since there is the smallest cross sectional area. None of the three analyzed load cases is close to failure according to the Von Misses failure criteria. Out of those, the highest load is experienced during a gust and is located at the front flange.

Buckling

Another type of failure that is analyzed is buckling. In figure 5.28 the normal stress experienced on the top skin

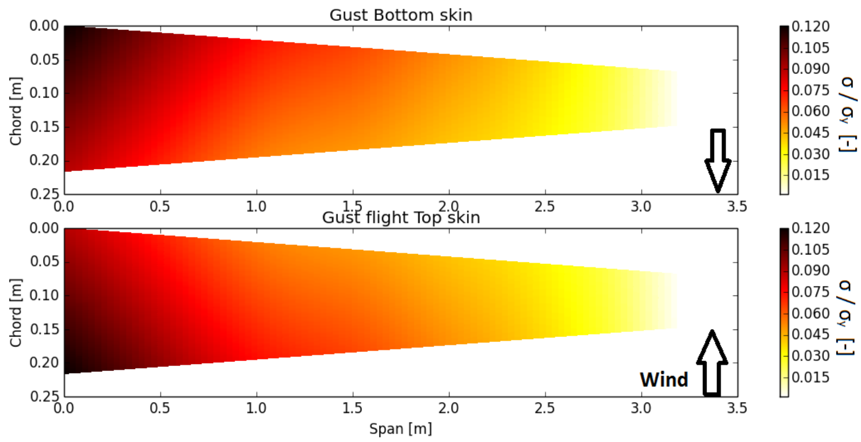

Figure 5.25: Stress distribution along the top and bottom faces of the wing box while flying through a gust

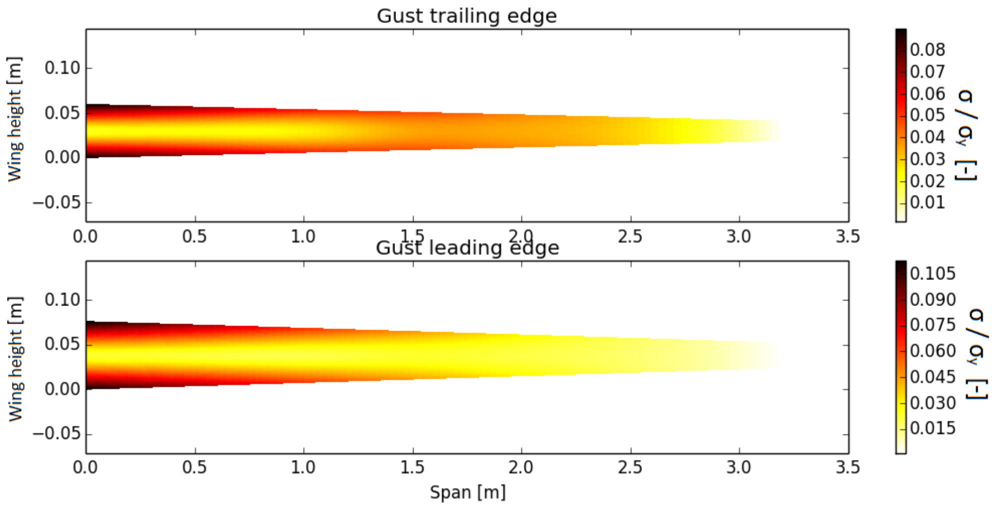

Figure 5.26: Stress distribution along the front and rear faces of the wing box while flying through a gust

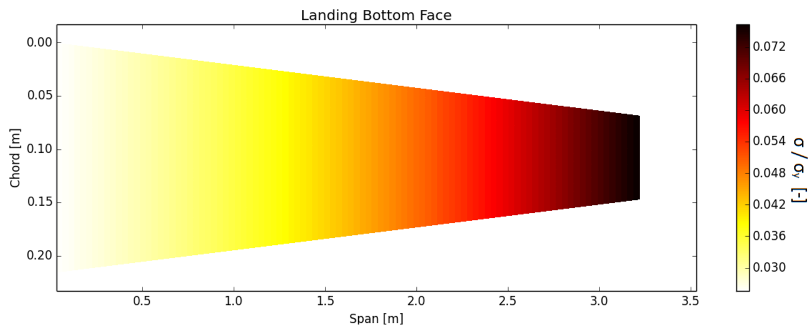

Figure 5.27: Stress distribution along the bottom face of the wing box during landing

during a gust (the strongest compressive force is expected in this situation) is plotted at 64 different locations along the width of the wing box. Underneath that, the stress at which buckling is expected in every span-wise segment is plotted (segments delimited by ribs). Thus, by a shorter margin, buckling is not expected to occur with the ribs and stringers described in table 5.12.

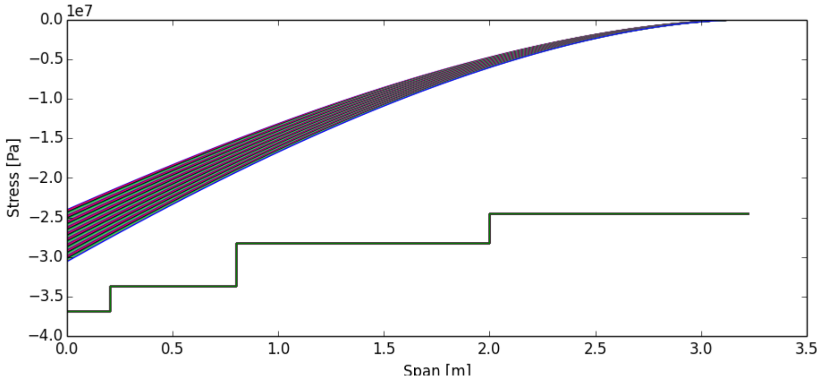

Figure 5.28: Compressive normal stress on the top sking of the airfoil vs buckling stress

5.7.4 WING BOX COST

The cost of aluminium T6061 is 1.8115 euro/kg (June 2016, London Metal Exchange) per kg under the form of an extrusion billet. Due to the material losses experienced during manufacturing it is safe to assume that about 20% of the material bought will be lost. This leads to a material cost of 44.55 euro. The manufacturing costs can‘t be approximated as they are highly dependent on the company and complexity of the product. From [49] one can see that for military aircraft the cost of engineering fabrication and assembly is about 4 times the cost of the materials. This results in a very rough estimate of the wing cost of 223 euro (just the wing shell). To this price one should add the cost of other components fitted in the wings such as fuel tanks, pumps, anti icing, etc.. Those components have not been chosen yet and thus can not be added to the price estimate. Capital Recovery, another significant part of the cost is not included in the cost provided as the working hours of the engineers and mechanics are not included. In this situation, an empirical estimation would make for a better cost estimation. From [50] one can find the cost of the wing of a UAV is about 90% of the total cost of the UAV airframe. That is understandable as the fuselage of a UAV usually has little complexity (no passengers). With a total airframe cost estimated from UAVs of the same size, a price of 5k€ for the airframe. This results in a cost of 4.5 k€ for the wing.

5.8 FURTHER STEPS IN STRUCTURAL DESIGN

The fuselage design from section 5.4.4 and wing design from section 5.7 are not complete, some parts still need to be designed (such as the clamp). A more accurate analysis would also be required before the airframe is put into production, this new analysis should include extra failure types such as those related to joints. This subsection will give an insight into the future steps to be taken.

First of all the modeling of the load cases needs be improved. Such an example are the aerodynamic forces on the tail which need to be modeled more accurately and also the trim forces during all flight conditions. Further the weights in the fuselage design should be modeled as actual distributions instead of the force through the cg. Beside this it would be beneficial to analyze dynamic loads as being dynamic and not as the static cases which are assumed for now. This would make a difference especially in the gust and landing loads. One should also take the elasticity in account then.

Improvements of the stress calculations can be made by taking stress concentrations and elasticity in account. This can for example being done by using FEM analysis. For this an even more detailed information on the aerodynamic forces should be known. Before this can be modeled accurately more should be know about the wing fuselage integration, other mounts and cutouts. The results could for example lead to local reinforcements.

Optimization has only been performed to a certain extent. A lighter airframe can be achieved but such an optimization poses the risk of delaying the project. Structural optimisation takes a lot of time and should not be done until more a detailed structural analysis is performed.

6 | PROPULSION AND POWER

The propulsion and power subsystem is presented in this chapter. It is divided in several sections, each containing the procedures for sizing and results for the design. Elements and parts have been chosen to fulfill the requirements and will be discussed where possible. The engine selection, location and maximum thrust is treated in section 6.1. The sizing of the propeller is added to this section to complete the powerhouse section. The fuel section discusses the fuel type, the fuel system architecture and fuel tank sizing. This is presented in section 6.2. The air inlet sizing procedure has been added to this section to complement these topics. This chapter is concluded with the electrical system, including the electrical architecture and power budgets in section 6.3.

6.1 ENGINE

Propeller engines are the most suitable engine type for the WiFly mission UAVs, as can be concluded from the trade-off performed in the midterm report [3]. The driving principle behind this kind of propulsion is the modest acceleration given to a relatively large mass of matter, contrary to the large acceleration given to a relatively small mass, as described by the general theory of thrust generation [51]. The larger the acceleration, the greater is the amount of chemical energy that needs to be converted to mechanical energy. The propeller is thus the most efficient propulsive option currently available for airplanes when the mission is limited to low subsonic applications. In addition to this apparent advantage for propeller based thrust generation, manufacturing and maintaining propeller engines is far less expensive and complex than for jet engines for example.

The engine selection and location will be presented in section 6.1.1 and section 6.1.2, respectively. Reference vehicles and their respective mission requirements indicate that propeller engines are used in aircraft with a wide range of applications and flight conditions, bridged only by the design of the propeller [51]. This section is concluded with the design of the propeller and determination of fundamental sizing parameters in section 6.1.3.

6.1.1 ENGINE SELECTION

A list of commercially available piston-prop engines was compiled (see appendix D) and an engine that complied with the mission requirements at the lowest weight was selected from this list. However, the engine selection must be rectified since the results from wing and power loading calculations have changed with respect to the conceptual design and also because the loss of power due to lower air density at higher altitudes was not taken into account. Sadraey [52] provides the following empirical relationship to estimate this loss:

$$P_{max} = P_{max_0}\left(\frac{\rho}{\rho_0}\right)^m \tag{6.1}$$

In the above equation, P_{max_0} and ρ_0 represent the maximum engine power and the air density, respectively, at sea level, whereas the same symbols without subscript denote their values at an arbitrary altitude. The power m is a correction factor to account for the advancement of technology; a value of 0.9 is suggested in the case of Otto cycle engines. Using the International Standard Atmosphere [29], one finds that at a cruise altitude of 4 km this power loss equals 30%.

The highest value for power required for the propulsion system is 8.64 kW (in cruise) and the power reserved for all other subsystems is 1.4 kW. The sum of these is the P_{max}. Applying eq. (6.1), this results in a total power required of 14.02 kW at sea level conditions. Based on these values, the most appropriate UAV engine considered for the WiFly system is the Rotron RT300 EFI LCR. This engine has 32 HP, a mass of 11.9 kg and a P_{max_0} of 20.3 kW. It has a length of 268 mm, a width of 170 mm and a height of 200 mm.

An advantage of the Rotron engine is that it runs on conventional aviation gasoline (avgas), as opposed to Aspen fuel which is used in the 3W International engines considered before. Avgas is widely available at airports all around the globe, whereas Aspen fuel is not as widely available. Furthermore, Aspen is generally sold in small quantities (5L jerrycans and 200L barrels) and is, partly due to this small scale, a lot more expensive per liter than avgas. Since it was decided to have a pusher configuration and engine cooling is more of a problem, the fact that the Rotron engine has liquid cooling is beneficial as well. Finally, Rotron provides many optional accessories that are fine-tuned for use on this specific engine, such as generators and radiators, which will not be elaborated upon due to the lack of reliable product data. These elements are planned to be treated in further design steps.

6.1.2 ENGINE LOCATION

The location for the single engine will be on the plane of symmetry of the UAV. A pusher configuration is used to allow for clearance in the nose of the UAV to accommodate the complex communication system [53]. Furthermore this has been identified as the location with the least negative aerodynamic interference due to the aerodynamic skin drag reduction resulting from an undisturbed flow around lift inducing surfaces [52]. Flow separation on the body is suppressed, even at high angles of attack, as the streamtube in front of the propeller is energized [51]. Raymer states that this allows for a lower wetted area or a shorter fuselage, leading to a positive effect on the drag properties [2]. Pusher configurations however, are known to have a lower net thrust compared to tractor configurations since the incoming flow has been disturbed mainly by the presence of the main wing and fuselage [52]. Concerning propeller efficiency, the net result for the two configurations is about equal [54], as the drag reduction is compensated by a lower net thrust.

According to Sadraey, longitudinal controllability is improved with a pusher configuration, a preferable property considering the given wind conditions. The presence of propwash is stabilizing for pusher prop and inherently destabilizing for tractor prop configurations [54]. This will reduce the amount and sizes of high lift devices and control surfaces, indirectly lowering the weight of other subsystems. However, to comply with the CS-23.905 certification [55] for pusher propellers, the WiFly UAV needs a proper exhaust system and fire prevention system such as firewalls. This will introduce additional weight, but an overall weight advantage is still gained from using a pusher configuration. The choice of the engine has a build in liquid cooling system, simplifying the design of the propulsion subsystem.

The engine will be buried in the rear of the fuselage. This limits the available space inside the fuselage while at the same time allows for a smaller wetted area [52]. Compared to podded engines, this configuration will be lighter and therefore preferred. The diameter of the propeller determines whether the engine may or may not be placed on the fuselage center line. This is due to the ground clearance requirements set by CS-23.925b, which states that the propeller must not contact the runway surface when the airplane is in maximum pitch attitude during normal takeoffs and landings.

The heat from the engine exhaust gases are potentially discharged into the pusher propeller disc. Paragraph CS23.905 states that the propeller must demonstrate by tests that it is capable of continuous safe operation when this occurs. The same requirement holds for potential accumulated ice and any removable item from the airplane. This problem can be contained by proper cowl design and use of a minimal number of removables.

6.1.3 PROPELLER DESIGN

Thrust generated by the propeller is the consequence of a complex interaction between the forward motion of the propeller, its rotational speed and geometry. Two fundamental sizing parameters are commonly used in propeller design. The diameter of the propeller disk, D, the virtual disk formed when a propeller rotates, and the geometric pitch, or pitch distance P_D, the distance the propeller would travel along its axis of rotation per revolution of the propeller. Both parameters are commonly presented in inches and are to be calculated at different phases in the flight profile, at corresponding power settings. A custom propeller will be designed to comply with all mission requirements. The mission profile dictates two main flight phases, cruise at 4000m altitude and loiter at 2000m altitude. Designing a propeller for these phases ensures optimal performance in the mission. Development and production costs are limited because the amount of propellers needed is reasonably high.

The material of the propeller can be based on different criteria. The rotational tip speed limit for metal and advanced composite propellers is 15% higher than for wood propellers [51]. When tip velocities approach Mach 1, unwanted shockwaves occur at the tip, which have a negative effect on thrust generation. The sound produced by the propeller increases significantly because of the same reason. Metal propellers are therefore preferred over wood propellers (smaller diameter needed), as a high limit for the rotational tip speeds directly influences the speed of the gusts it is capable of dealing with before reaching sonic tip velocities.

The design process for the propeller is described by Gudmundsson [51] and will be used for determining the diameter and pitch distance. Stinton has presented a method of calculating the diameter of the propeller based on the intended cruise speed, effective engine power, RPM and material [56]. Effective engine power refers to the maximum engine power corrected for the altitude. From the operation manual of the engine manufacturer [57], an efficiency of 88% and an optimal RPM of 5000 can be found. It has been decided that an engine efficiency η_e of 85% is used to obtain a conservative value for the propeller diameter.

$$P_{BHP} = \eta_e \cdot P_{max} \tag{6.2}$$

With a maximum power of 32 HP and an efficiency of 85%, the Brake Horse Power (BHP) of the engine is 27.2 BHP, calculated using eq. (6.2). Equation (6.3) and eq. (6.4) present the equations by Stinton for two and three bladed metal propellers respectively. Equation (6.5) is derived by Raymer [2] and is indifferent for different material types. K_p is based on the number of blades and equals 20.4 and 19.2 for two and three bladed propellers, respectively. The results are presented in table 6.1. The diameter for three bladed propellers is lower than for two bladed propellers, mainly because the same surface area is formed by more blades, decreasing the required length of each individual blade. A diameter of 45" and a diameter of 39" will be used for selection process for two and three bladed metal propellers respectively.

$$D = 22 \cdot \sqrt[4]{P_{BHP}} \tag{6.3}$$

$$D = 18 \cdot \sqrt[4]{P_{BHP}} \tag{6.4}$$

$$D = K_p \cdot \sqrt[4]{P_{BHP}} \tag{6.5}$$

Table 6.1: Propeller diameter

Method	#Blades	Diameter [in]
Stinton	2	44.67
Stinton	3	36.55
Raymer	2	41.42
Raymer	3	38.98

The pitch distance can be calculated by considering the distance it has to travel per revolution. It has to be evaluated at different velocities in the flight envelop with corresponding RPM, taking into account the efficiency of 0.85. This can be quantified with eq. (6.6). An RPM of 5000 revolutions per minute has been used, as this allows for the lowest specific fuel consumption. The results are presented in section 6.1.3. A pitch distance of 46.3" for cruise and a pitch distance of 24.2" for loiter has been determined.

$$P_D = \frac{V}{\frac{RPM}{60} \cdot \eta} \tag{6.6}$$

As the largest section of the mission encompasses loitering the mission area at a low speed, it can be rationalized that the propeller needs to be able to perform efficiently at this condition as well. However, it can be concluded from the calculations from aforementioned equations that the current description of the propeller will be overdesigned for the loiter stage. Therefore it was chosen to have a constant speed, controlling pitch propeller to fly efficiently at both the cruise and loiter phase; a low pitch for low-speed operations, and a large pitch for high-speed operations. The pitch distance varies with the pitch angle β given by the relation described in eq. (6.7). This will also increase the propeller performance in case of an engine failure, as fixed-pitch propellers will windmill, increasing the drag.

$$\tan\beta = \frac{P_D}{2 \cdot \pi \cdot r_{ref}} \tag{6.7}$$

The results are presented in section 6.1.3. Both the cruise and loiter phases are evaluated for both the two and three bladed propellers. The reference radius, r_{ref}, is taken as 0.75 of the maximum radius R.

A 39" feathering three bladed constant speed controllable pitch propeller, capable of attaining pitch angles of at least 30 ° has been chosen as the optimal design for the propeller for the UAV. A feathering propeller will decrease the drag and improve the UAVs gliding performance in case of a One Engine Inoperative situation (OEI). It prevents windmilling, which reduces the probability of structural failure due to this phenomenon. It has been decided that a three bladed propeller is used to reduce the diameter of the propeller disk, increasing the ground clearance to comply with the CS-23.905 certification. Constant speed to ensure the most optimal

Table 6.2: Pitch distances and angles for different flight phases

Flight mode	**#Blades**	**Velocity** [$\mathrm{m\,s^{-1}}$]	**Pitch Distance [in]**	**Pitch Angle** [°]
Cruise	2	55.56	46.3	25.3
Cruise	3	55.56	46.3	28.3
Loiter	2	37.18	24.2	13.9
Loiter	3	37.18	24.2	15.6

Specific Fuel Consumption (SFC) state and a controllable pitch mechanism to operate most efficiently in both the cruise and loiter phases.

6.1.4 MAXIMUM THRUST

Maximum thrust generated by propeller aircraft is dependent on the rotation speed of the propeller, its forward speed and geometry. It is generally given by eq. (6.8), with P_{BHP} given in kW. This expression indicates an infinite thrust at zero airspeed, which is physically impossible. This expression can still be used to evaluate the thrust of determined flight conditions.

$$T = \frac{\eta_p \cdot P_{BHP}}{V} \tag{6.8}$$

The maximum thrust at zero forward airspeed is determined with the cubic spline method for constant-speed propellers as given by Gudmundsson [51]. Equation (6.9) is used in this cubic spline method to determine the static thrust. Sea level atmospheric conditions and a spinner spanning from the origin to 0.15R of the propeller disc are used to complete the equation. This value for the spinner radius has been taken from reference propellers, which all have a spinner spanning between 0.1R and 0.2R. The results are presented in section 6.1.4.

$$T_{static} = 0.85 \cdot P^{2/3} \cdot (2 \cdot \rho \cdot A)^{1/3} \cdot \left(1 - \frac{A_{spinner}}{A}\right) \tag{6.9}$$

Table 6.3: Maximum thrust for different flight phases

Flight mode	**Airspeed** [$\mathrm{m\,s^{-1}}$]	] **Maximum Thrust** [N]
Cruise	55.56	386.7
Loiter	37.18	577.9
Takeoff	0	851.4

6.2 FUEL SYSTEM

The fuel system is a subsystem in itself, with its own requirements and design principles. An analysis of the fuel type, the corresponding fuel feed system architecture and fuel tank sizing make up the largest part of this section. This is complemented by the sizing of the air inlet. The fuel type considered will be discussed in section 6.2.1. As the fuel type dictates the fuel system layout, it is important to consider all aspects that can affect the design of the fuel system in section 6.2.2. The fuel tank sizing, based on engine performance data, is presented in section 6.2.3. Since fuel alone cannot make the engine run, the air intake sizing is presented in section 6.2.4.

6.2.1 FUEL TYPE

Currently, the most-used fuel type in piston-prop engines is aviation gasoline 100 Low Lead (avgas 100LL) [51], where 100 refers to the octane rating of the fuel. A higher octane rating means better knock-free engine performance. Engine knocking, or uncontrolled fuel detonation, happens when part of the air/fuel mixture ignites spontaneously outside the normal combustion front. Tetraethyl lead (TEL) is added to avgas because it is an effective anti-knock additive as it stops the chain reactions that cause autoignition, and thereby helps in providing a smooth and reliable engine operation [58].

A downside to this fuel type is the fact that it contains lead, which is detrimental to both the environment and people's health. Despite several efforts, no widely available unleaded avgas has been developed yet. The Federal Aviation Administration (FAA) has announced its desire to make a type of unleaded avgas widely available by 2018, and has issued a report that recommends processes and criteria for identification and approval of unleaded avgas [59]. As long as an unleaded avgas is not yet sufficiently developed and widely applied, avgas 100LL will be used since this is the fuel type recommended by the engine manufacturer and because it is available at airports all over the globe.

6.2.2 FUEL SYSTEM LAYOUT

This section provides the fuel system layout. There will be two fuel tanks, one in each wing and extending into the fuselage. The fuel tanks have vents to allow air in and relieve vacuum as fuel is drawn from them. They also have gas caps that can be opened for refueling when the UAV is on the ground. Furthermore, fuel probes (DC capacitance sensors) in the tanks measure the fuel level. These probes should be properly calibrated and located within the fuel tanks to account for the irregular geometry of the tanks, in order to provide a reliable and consistent measure of the fuel level. [60] Since the design is a mid-wing configuration, gravity-feed fuel tanks cannot be used. Instead, pumps will have to be used. [61]

The fuel system layout can be found in figure 6.1, in which the solid lines indicate "normal" operation and the dashed lines indicate "abnormal" operation. From the fuel tanks, the fuel first goes through a check valve, which ensures one-directional flow (i.e. the fuel will not be able to flow back into the tanks), to the selector valve. This valve has the options LEFT, RIGHT, or OFF, meaning fuel can be supplied by only one tank at a time. The fuel is then collected in the collector tank, ensuring steady fuel flow to the engine. It then flows to the fuel strainer, from where it can supply the engine primer. Two pumps are used because it creates redundancy, i.e. failure of one pump will not cause failure of the entire fuel system. The engine-driven pump is the main pump, the electric one mainly serves as a back-up should the other fail (hence the dashed lines). The pumps draw fuel from the tanks and delivers it to the fuel injection system, where air is added to the fuel. In case it is necessary during flight, fuel can be dumped from the fuel collector tanks. [62]

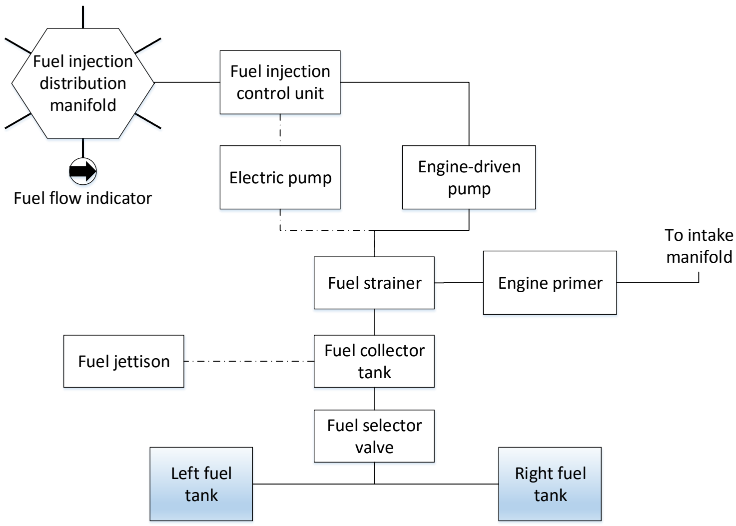

Figure 6.1: Fuel system layout

6.2.3 FUEL TANK

The fuel tank, commonly placed in the wing of an aircraft, is used to store the fuel. Due to lift generated by the wing, an upward bemanding of the wing is to be expected. By placing fuel tanks in the wing, part of these bending loads are compensated, and the wing is relieved for these kinds of loads. The size and shape of the wing determine the final fuel tank design. The fuel volume for which it is designed can be calculated from the required fuel weight and fuel density.

The main flight phases in the mission are the 3h cruise phase and the 24h loiter phase. These are steady flight conditions, resulting in a constant altitude, velocity and orientation. Although the weight changes during both phases, influencing aerodynamic and structural parameters, sizing is based on the initial values at the start of each phase to allow for a margin of contingency for e.g. maneuvering. The thrust required in both phases is equal to the drag of the UAV in that particular flight phase. The equation is a combination of eq. (6.1), eq. (6.2) and eq. (6.8). It can be calculated using eq. (6.10).

$$T = D = \frac{\eta_p \cdot \eta_e}{V} \cdot P_{max_0} \cdot \left(\frac{\rho}{\rho_0}\right)^m \tag{6.10}$$

The values for drag in cruise and loiter are determined in chapter 4. By rewriting eq. (6.10) for P_{max_0}, the sea level power required can be determined based on the drag and velocity of that phase. Compensating for altitude to translate the power required to sea level conditions, and incorporating the propeller and engine efficiency results in the power required by the engine. The results are presented in section 6.2.3.

Table 6.4: Power required for cruise and loiter

Flight mode	**Density** [$\mathrm{kg\,m^{-3}}$]	**Airspeed** [$\mathrm{m\,s^{-1}}$]	**Thrust** [N]	**Power** [kW]
Cruise	0.8191	55.56	74.7	8.64
Loiter	1.006	37.18	61.4	4.70

The power obtained from this equation is the power needed for propulsion. The total power required at sea level is obtained by adding the power required for the payload and other subsystems. Figure 6.2 presents the specific fuel consumption and maximum power generated for different RPM settings. The minimum value for SFC is 0.5 lbs/kWh (or 0.2268 kg/kWh) at 5000 RPM. The maximum power that can be delivered by the engine at sea level then equals 20 HP (or 14.91 kW), allowing the WiFly UAV to fly at this setting.

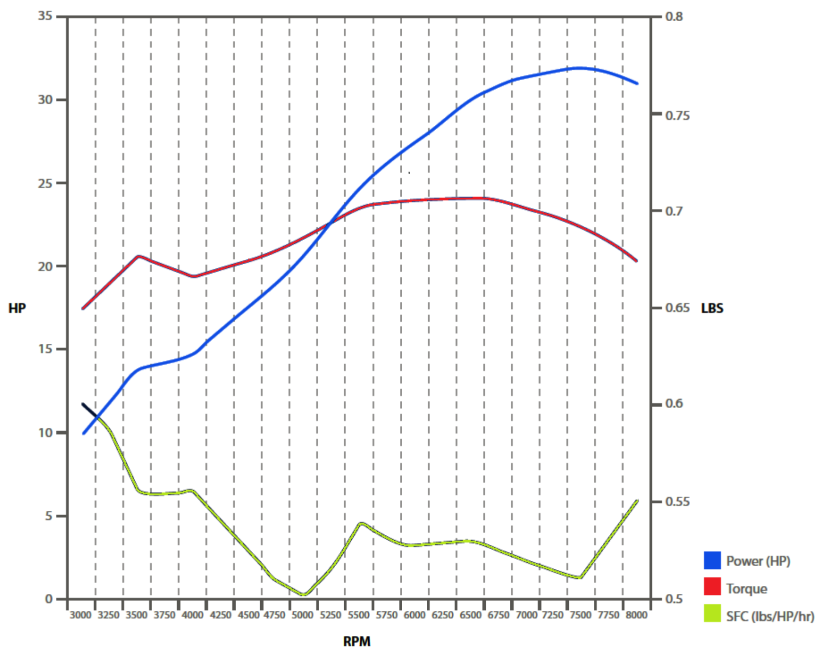

Figure 6.2: Specific Fuel Consumption for Rotron 300 EFI LCR

The mass of the fuel needed for both the cruise and loiter phase can now be determined with eq. (6.11). The results are presented in section 6.2.3. The total fuel mass is 31.5 kg. An average density of 0.721 $\mathrm{kg\,m^{-3}}$ has been found for avgas, resulting in a fuel volume required of 0.04361 m^3, or 43.61 liters.

$$W_{fuel} = SFC \cdot t \cdot P_{req} \tag{6.11}$$

Table 6.5: Fuel mass required for cruise and loiter

Flight mode	**Duration [h]**	**Power required** [kW]	**Fuel mass** [kg]
Cruise	3	8.64	5.88
Loiter	24	4.7	25.6

6.2.4 AIR INLET SIZING

The inlet sizing is based on the amount of air needed for the engine to work. In general, the amount of air needed is based on the Air-to-Fuel Ratio (AFR), which is the mass ratio between air and fuel used in the combustion process. A stoichiometric AFR is a ratio when there is perfect combustion, i.e. no exhaust gases besides water and carbon dioxide. A rich mixture refers to when this ratio is lower, so relatively less air per unit mass of fuel, while a lean mixture refers to a ratio when there is relatively more air per unit mass of fuel compared to the stoichiometric ratio.

$$\dot{m}_{air} = \rho \cdot A \cdot V \tag{6.12}$$

The amount of air in kilograms passing through a surface per second can be calculated with eq. (6.12). This equation has to be used for every flight condition, as density and airspeed differ per mission phase. Using eq. (6.12) and the AFR, it possible to determine the inlet area using eq. (6.13). The results are presented in section 6.2.4.

$$A_{inlet} = \frac{AFR \cdot \dot{m}_{fuel}}{\rho \cdot V} \tag{6.13}$$

Table 6.6: Inlet area for different AFR and flight modes

Flight mode	**Density** [kg m^{-3}]	**Velocity** [m s^{-1}]	**AFR** [-]	**Inlet area** [m^2]
Cruise	0.819	55.56	15	$1.89 \cdot 10^{-5}$
Cruise	0.819	55.56	14.7	$1.85 \cdot 10^{-5}$
Cruise	0.819	55.56	13	$1.63 \cdot 10^{-5}$
Loiter	1.006	37.18	15	$1.19 \cdot 10^{-5}$
Loiter	1.006	37.18	14.7	$1.16 \cdot 10^{-5}$
Loiter	1.006	37.18	13	$1.03 \cdot 10^{-5}$

A lean mixture of air and fuel will lead to high temperatures, while a rich mixture will lead to a reduction in temperature. This is due to the fact that the excess fuel will absorb part of the heat. By using a rich mixture, detonation is avoided, up till a point where knocking starts to occur. An AFR of 13 is used as it is recommended by the FAA for avgas rich mixtures [59]. This determines the minimum required inlet area of $1.63 \cdot 10^{-5} m^2$ in all phases.

6.3 ELECTRICAL SYSTEM

In recent years, the use of electricity as a means to power subsystems in aircraft has become preferable over the use of hydraulic or pneumatic systems. A higher dependence on electrical power requires a reliable and efficient way of both generating the power as well as transporting it. However, before one can go into designing the electrical system, the electrical loads need to be mapped; that is, at least a preliminary estimate needs to be made of what systems/appliances require what amount of power. This investigation is performed in section 6.3.1. The layout of the electrical system is provided in section 6.3.2.

6.3.1 POWER LOADS

This section provides the power requirements for the different appliances installed on the UAVs. The power breakdown can be found in table 6.7. The power requirements of the communication subsystem (in the table, "payload" is for communication with the ground and "communication" for with the base station) and the avionics are explained in more detail in chapter 3 and chapter 8, respectively. The power requirements of appliances that have not been selected yet (such as the fuel pumps and the anti-icing system) were estimated conservatively. [62]

Table 6.7: Power requirements of appliances

Component	Power [W]
Payload	398
Communication	303
Mission computer	15
Flight computer	2.5
Transponder	15
Camera	6
Actuators	48
Fuel pumps	25
Fuel sensors	1.5
Pitot tube	5
Lights	50
Anti-icing system	100
Total	**969**

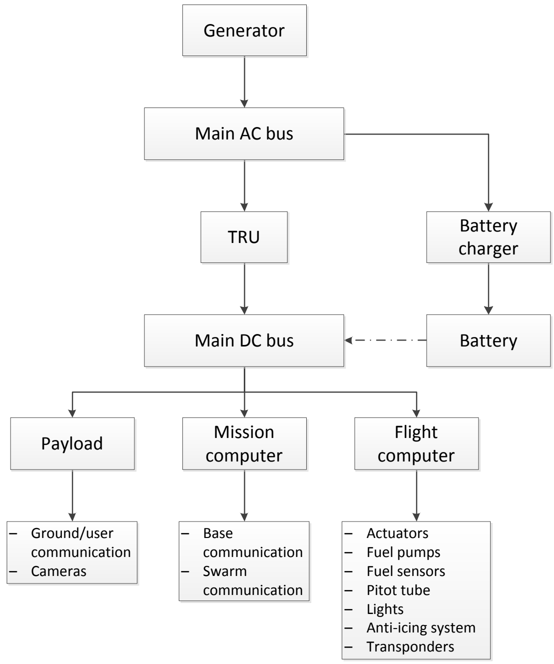

Figure 6.3: Electrical system layout

6.3.2 ELECTRICAL SYSTEM LAYOUT

In the most general sense, an electrical system consists of an electrical power source, a power distribution system (including power converters) and the electrical loads connected to the system. [63] The layout of the electrical system can be found in figure 6.3. The complete wiring of the system has not yet been designed, but the diagram does include all components that will be installed.

Due to the relatively small size and low power requirements of the UAVs, only one AC generator (or alternator) will be used that will supply all subsystems with electrical power. The AC generator converts the mechanical energy provided by the engine into electrical power. DC generators could be used instead of AC generators, however the voltage is higher with alternators, which means they experience lower current and hence lower power losses. Moreover, the complete power generation system has a lower weight when AC generators are used, despite the better insulation that is required because of the higher voltage. [64] The engine manufacturer, Rotron, can supply the engine with an alternator that can generate up to 3 kW of power.

Additionally, a battery will be installed as backup power source in case of engine or generator failure. The Tattu 30000mAh lithium polymer (LiPo) battery was selected for this purpose. After engine failure, the communication with the people on the ground will be discarded and only the communication with the base station will be maintained. The selected battery can supply 666 Watt hours, which is sufficient to power all other appliances for over one hour after engine failure. Ideally, the battery will be powered by an external source when the UAV is on the ground, such that charging the battery will not require power provided by the generator. Keeping in mind the likely hectic circumstances in which the system will be used, the battery charger will also be linked up to the generator such that it can be charged during flight should this be necessary.

As explained in chapter 8, most appliances will be powered through the mission or flight computer. These computers, as well as the payload for ground communication, require DC power. Therefore, the AC power generated by the alternator will need to be converted to DC by a transformer rectifier unit (TRU). It is possible that some of the appliances that are powered through the computers actually require AC power, in that case an inverter should be installed to convert the DC power supplied by the computers.

7 | Stability and Control

7.1 Control Surfaces

An aircraft needs control surfaces in order to be maneuverable and controllable. The control surfaces change the airflow around the wings and the tail resulting in a change in forces and moments, making the aircraft steerable. Most common control surfaces are the ailerons on the main wing for roll control and elevator and rudder on the tail for pitch and yaw control. A V-tail configuration was chosen for the WiFly UAV which means that the elevator and rudder are combined into one control surface called ruddervator.

7.1.1 Horizontal Tail Surface Sizing

In this subsection the horizontal tail will be sized following the same steps that were used in the mid-term report [3]. First the loading diagram will be constructed, secondly a center of gravity range will be made based on that, thirdly the scissorplot is constructed and finally the tail is sized.

The loading diagram is constructed for three different positions of the wing. For all of these positions the UAV is loaded in the same way. For this loading it is assumed that the fuel is stored in the wing. Therefore, its x-coordinate changes equivalent with the wing. The mass and their x-coordinates w.r.t. the nose can be found in table 7.1. The position of the wing, X_{LEMAC}, is at 1.303m. All these values were calculated in the iteration process of section 9.1 and presented in figure 9.3.

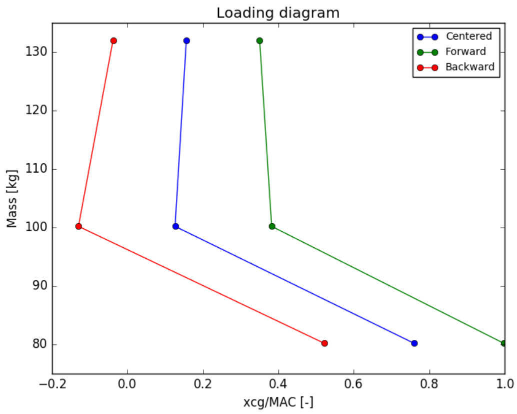

Figure 7.1: Loading diagram conventional configuration

Table 7.1: Mass of components and their x-coordinates

Component	mass [kg]	x-location [m]
Wing	22.2	1.404
Tail	4.85	2.483
Fuselage	25.9	1.404
Engine	14.042	2.635
All else	13.2	0.916
Fuel	31.8	1.404
Payload	20.0	0.347

The following approach was used for generating the loading diagram. The loading of the UAV was done in three steps, operational empty weight ($80kg$), payload ($20kg$) and fuel ($31.8kg$). At each of these steps the center of gravity was determined w.r.t. the X_{LEMAC}. After this was done the center of gravity was divided by the mean aerodynamic chord. This process was done for three wing positions, 10% more forward, centered and 10% more backward. The results can be found in 7.1.

Based on the loading diagram a c.g. range can be determined. This c.g. range will represent the maximum and minimum c.g. location of the UAV for the different wing positions. However, the center of gravity location is plotted against the positions of X_{LEMAC} divided by the fuselage length. This is done to visualize the influence of the wing placing with respect to the fuselage length, rather than only the X_{LEMAC} w.r.t. c.g. location, which on itself is not meaningful. The result is presented in figure 7.2.

To check if the UAV can be stable and controllable for a specific configuration a scissor plot has to be made. A scissor plot puts a limit on the c.g. range and gives a corresponding value for the ratio of horizontal tail plane surface area to main wing surface area. The limits are set by the stability line for the most aft c.g. location

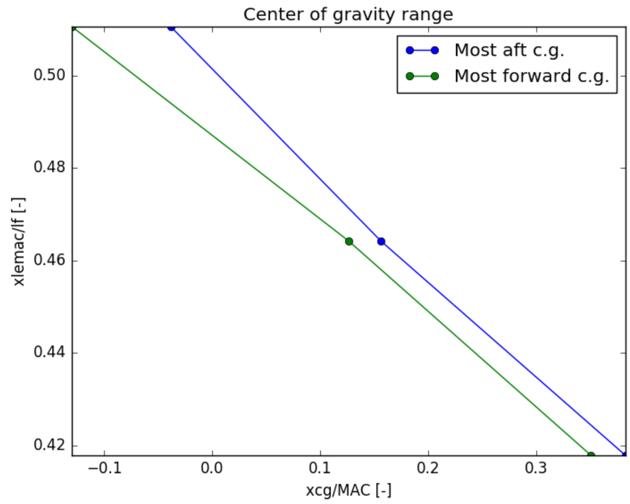

Figure 7.2: Center of gravity range conventional configuration

and by the controllability line with the most forward c.g. location. The equation used for stability is the stick-fixed static stability eq. (7.1) and for controllability eq. (7.2) is used. The values of all the parameters and coefficients that were used and determined can be found in table 7.2[65] [66]. Here the parameter $\frac{V_h}{V}$ is based on statistical data and others are found through analysis. It was decided to have a stability margin of $0.05\bar{c}$. The plot is shown in figure 7.3.

$$\bar{x}_{cg} = \bar{x}_{ac} + \left(1 - \frac{d\epsilon}{d\alpha}\right) \frac{S_h l_h}{S\bar{c}} \left(\frac{V_h}{V}\right)^2 - \frac{x_{lemac}}{\bar{c}} - 0.05 \tag{7.1}$$

$$\bar{x}_{cg} = \bar{x}_{ac} - \frac{C_{m_{ac}}}{C_{L_{A-h}}} + \frac{C_{L_h}}{C_{L_{A-h}}} \frac{S_h l_h}{S\bar{c}} \left(\frac{V_h}{V}\right)^2 - \frac{x_{lemac}}{\bar{c}} \tag{7.2}$$

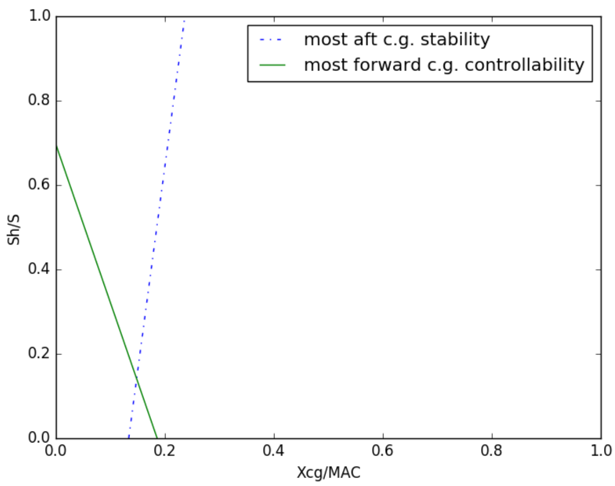

Figure 7.3: Stability and control lines conventional configuration

Table 7.2: Relevant parameters stability and control

Parameter	Value	Unit
$\bar{x}_{ac}$	3.540	[-]
$\frac{d\epsilon}{d\alpha}$	0.256	$[rad^-1]$
l_h	1.081	[m]
$\bar{c}$	0.396	[m]
$\frac{V_h}{V}$	0.85	[-]
$C_{m_{ac}}$	-0.0179	[-]
$C_{L_{A-h}}$	5.909	[-]
C_{L_h}	2.978	[-]
l_{fn}	1.227	[-]

The UAV should be stable and controllable for the whole c.g. range. If this is not the case, the design should be reconsidered. Now that the c.g. range and stability plot are known it is possible to estimate an optimal tail size and a corresponding X_{LEMAC}/l_f. This can be done by plotting both in one figure with the same x-axis and different y-axes. Analyzing the plot in figure 7.4 it can be seen that the optimal $\frac{S_h}{S}$ is 0.217 for a X_{LEMAC}/l_f of 0.4642.

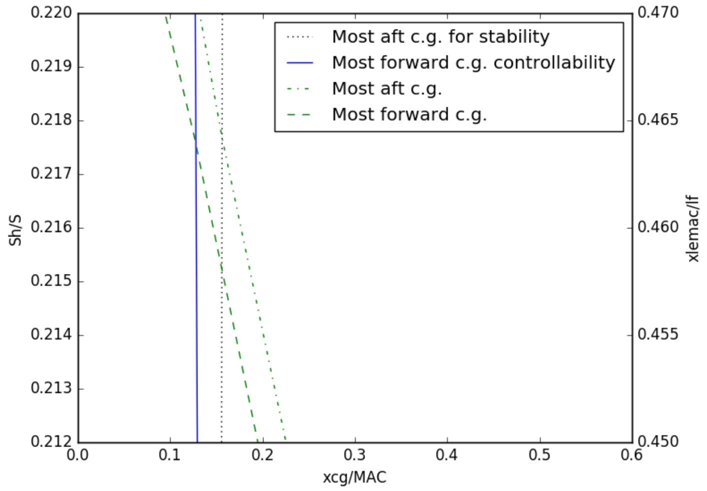

Figure 7.4: c.g. range combined with scissor plot

7.1.2 AILERONS

The first estimations for the control surface areas are based on statistical relations found in [56, Table 11-4]. Where it can be seen that for ailerons the fraction of aileron surface area over the total wing area should remain between 0.08 and 0.1. Knowing the total wing area of 2.143 m^2 it can be found that the area of ailerons per wing should approximately be 0.0536 m^2. The chord length of the aileron over the chord of the wing should remain between 0.2 and 0.3. Value of 0.2 is used in order to leave more room for the wingbox which results in an aileron mean chord of 0.0655 m and a length of 0.82 m. For the ailerons the same taper ratio is applied as is for the main wing. The ailerons are used for rolling the aircraft and in order to check if the size of the ailerons is sufficient the achieved roll rate needs to be calculated. From CS-23 regulations it can be found that the aircraft needs to be able to roll 60 degrees in 4 seconds when approaching for landing. For this an approximation for the mass moment of inertia around the roll axis is needed. For this eq. (7.3) from [2] can be used.

$$I_{xx} = \frac{b^2 W R_x^2}{4g} \tag{7.3}$$

Here R_x is the radii of gyration with an average value of 0.25 for single engine propeller aircraft. [2] This way it can be calculated that the required angular acceleration generated by the ailerons is 15 °s^{-2}. With this acceleration the roll can be completed in time and without any angular velocity in the end because the first half of the roll the aircraft accelerates and the other half it decelerates. It was assumed that the deflection of the ailerons gives an increase in lift ΔC_L of 0.1 over the affected area and when placing the center of the aileron at 1.5 m from the root this results in an acceleration that is 2.6 times higher than the required. Even though it is higher than required it is decided to use this sizing for the ailerons in case the actual moment of inertia changes.

7.1.3 RUDDERVATOR

In order to estimate the size of the ruddervator first estimations are made for the horizontal and vertical areas needed for the tail which are then converted into the necessary area for the ruddervator. Using again the statistical values from [56, Table 11-4] which states that the horizontal tail area must be around 0.16 to 0.2 of the main wing area. In addition from the scissor plot it was found that for the UAV to be stable and controllable the ratio needs to be larger than 0.217. Thus a value of 0.217 was used which results in a required horizontal area of 0.233 m^2. Similar analysis was made for the vertical part where the area must be within 0.075 to 0.085 of the main wing. This would result in an vertical area of 0.091 m^2. In a V-tail configuration the vertical and horizontal surfaces are combined into one surface at an 45 degree angle. This means that the projected area of the ruddervator needs to be the size of the required horizontal and vertical areas. Because the horizontal area requirement is larger it will also be used to size the ruddervator resulting in an area of 0.329 m^2. The control surface is required to be between 0.5 to 0.55 of the ruddervator surface area. Using the value of 0.5 this will result in an area of 0.164 m^2.[56, Table 11-4] In order to get estimates for the span and chord of the ruddervator and the control surface the aspect ratio needs to be known. It is advised to avoid using vertical surfaces with high aspect ratios because they can suffer fin stalls at moderate angles of yaw. An aspect ratio of 2.5 is assumed based on the average of the rudder and elevator statistical data. [56, Table 11-4] This results in a span for the ruddervator of 0.907 m and for the control surface 0.641 m. The chord of the ruddervator is 0.363 m and 0.256 m for the control surface. These values are also presented in table 7.3 where all values are given per wing. The control surface itself is positioned at the tip of the ruddervator in order to increase its effectiveness and to provide room for the actuators at the root of the ruddervator.

Table 7.3: Aileron and Ruddervator parameters

Parameter	Aileron	Ruddervator	Controls	Units
Area	0.054	0.329	0.164	m^2
Span	0.82	0.907	0.641	m
Chord	0.066	0.363	0.256	m

Table 7.4: Control surface maximum distributed loading

Parameter	Value	Units
Aileron	1006.33	$N\,m^{-2}$
Horizontal	1383.01	$N\,m^{-2}$
Vertical	1176.90	$N\,m^{-2}$
Ruddervator	1810.14	$N\,m^{-2}$

7.1.4 CONTROL SURFACE FORCES

In order to size the actuators that control the movement of the ailerons and ruddervators it is necessary to estimate the forces and moments acting on those surfaces. For this statistical estimations were used that provide the maximum distributed control surface loading based on the design maneuvering wing load. The equations for the aileron, horizontal tail and vertical tail are presented in eq. (7.4), eq. (7.5) and eq. (7.6) respectively.[67] All the equations are based on data in imperical units and the inputs and outputs needed to be converted.

$$\bar{w}_{aileron} = 0.466 \cdot n \frac{W}{S} \tag{7.4}$$

$$\bar{w}_{horizontal} = 4.8 + 0.534 \cdot n \cdot \frac{W}{S} \tag{7.5}$$

$$\bar{w}_{vertical} = 3.66 \cdot \sqrt{n \cdot \frac{W}{S}} \tag{7.6}$$

For the design wing loading the value of 568.3 $N\,m^{-2}$ was used and for the maneuver load a value of 3.8 is used. Because for the WiFly UAV a V-tail configuration is used, the horizontal and vertical loads were converted to a 45 ° angle to get the load for the ruddervator. These results are presented in table 7.4.

Assuming that the total force acts in the middle of the control surface the moment generated at the hinge could be found. For the aileron this is 1.77 Nm and for the ruddervator this is 38.16 Nm. It can be seen that the moment for the aileron is much lower and this is because the aileron has almost half the area and a much higher aspect ratio compared to the ruddervator control surface leading to a much smaller moment arm and moment.

7.2 STABILITY SIMULATION

In order to estimate the stability of the entire WiFly UAV a simulation was generated. For this the Athena Vortex Lattice (AVL) program was used [68]. This program has numerous features and is intended for rapid aircraft configuration analysis. The program uses the vortex lattice method to estimate the stability parameters of an aircraft configuration. Thin lifting surfaces with a low angle of attack and sideslip must be used in order to have accurate results from the vortex lattice model. In addition Mach number below 0.7 is recommended to use but even at cruise conditions the WiFly UAV is operating far from that limit. For the simulation the basic geometry of the UAV was implemented consisting of the main wing and the V-tail. Next the flying conditions together with the UAV mass, moments of inertia and center of gravity were added to the model. Estimates for mass moments of inertia around all axises were found using similar formulas as eq. (7.3) from

[2]. After the simulation the different eigenmodes and corresponding eigenvalues were obtained. With these eigenvalues parameters like time to half amplitude, natural frequency, the period and damping ratio could be calculated. These values are presented in table 7.5 which correspond to the loiter flight condition. It must be noted that these results are based on a simplified model shown in figure 7.5 and are used as a rough first estimate for the stability of the WiFly UAV.

Table 7.5: Stability simulation results

Parameter	Short Period	Phugoid	Dutch Roll	Aperiodic Roll	Spiral
Eigenvalue	-2.14 + 8.12i	-0.045 + 0.12i	-0.47 + 2.99i	-5.58+0.0i	0.089+0.0i
$T_{\frac{1}{2}}$ [s]	0.324	15.403	1.475	0.124	7.788*
P [s]	0.774	52.360	2.101	-	-
ω [Hz]	8.397	0.128	3.027	-	-
ζ [-]	0.255	0.352	0.155	-	-

* This mode is unstable and the value shown here is the time required to double the amplitude

There are three periodic eigenmodes - short period, phugoid and Dutch roll together with two aperiodic modes - aperiodic roll and the spiral. It can be seen that all eigenmodes are well damped except for the spiral. The $T_{\frac{1}{2}}$ in table 7.5 shows the time to half amplitude and because spiral is unstable for that mode it represents time to double amplitude instead. In the table P stands for the period of the motion, ω is the frequency and ζ is the damping ratio. As expected the short period, dutch roll and aperiodic roll motions are dampened very quickly and only the phugoid takes long time to die out. Although the spiral motion is unstable it is still fairly slow and can be actively controlled using the flight computer and can be avoided. Therefore this unstability does not pose a threat to the operation of the WiFly UAV.

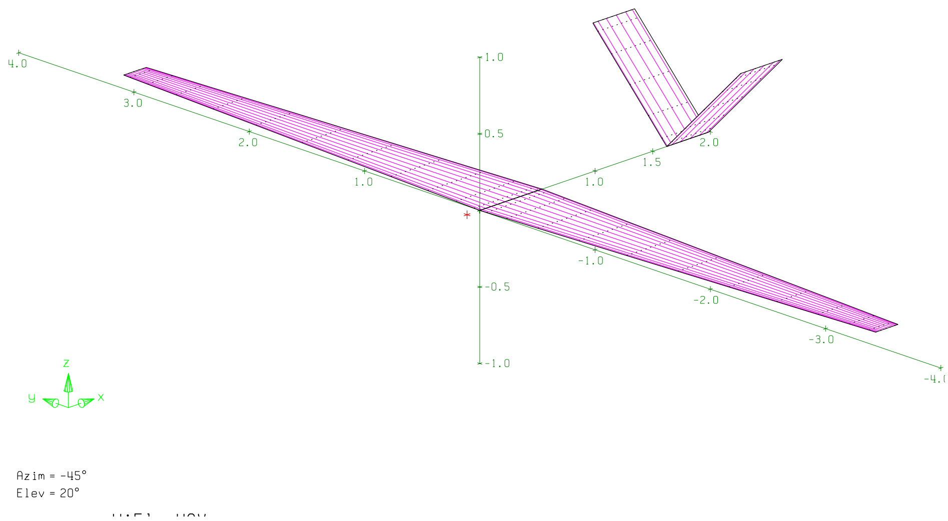

Figure 7.5: UAV model in AVL

8 | AVIONICS

For a successful operation of the UAV several instruments are needed on board and these must interact together. First the general architecture of the on board hardware is presented in figure 8.1.

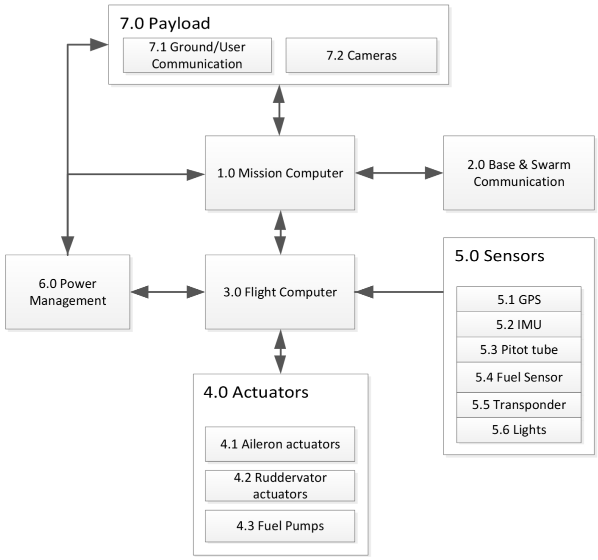

Figure 8.1: WiFly hardware architecture and Data Handling

8.1 MISSION COMPUTER

The most important element in the architecture is the mission computer which is central to all processes. It connects and processes information between the payload, base and swarm communication and the flight computer. For the WiFly UAV the DuraCOR 311 mission computer was chosen.[69] It is a mission computer specifically designed for unmanned vehicles, has high reliability and supports many connections. This all is provided at a low weight of 0.68 kg and low power of 15W. Because of the high importance of the mission computer redundancy needs to be added in order to avoid single point of failures. For this reason two mission computers are installed on the UAV.

8.2 FLIGHT COMPUTER

The mission computer connects to the base and swarm communication module which is further described in section 3.6.6. From that module commands containing the operation tasks and instructions for the mission are passed into the flight computer. The flight computer is responsible for the navigation of the UAV and it acts as an autopilot. For the WiFly UAV the Vector flight computer by UAV Navigation is used.[70] This system among other features supports automatic takeoff and landing, flight plan execution and return to base in case of communications failure. All of these features are essential in the WiFly mission. It also includes GPS, an inertial measurement unit and other attitude sensors. In total the flight computer weighs 0.18kg and consumes 2.5W. Due to its mission critical nature this system also needs to be doubled for redundancy. The flight computer is also responsible for controlling the fuel flow into the engines and the power it generates.

8.3 ACTUATORS

The flight computer is responsible of controlling the UAV's flight and it achieves this through the control of servos that move the control surfaces of the UAV. There are two types of actuators that are used in UAVs. These are the hydraulic and the electromechanical actuators. It was decided to use electromechanical actuators because they offer a high efficiency and accuracy together with easy maintenance. In section 7.1.4 the loads on the control surfaces were determined resulting in required torques of 1.77 Nm for the aileron and 38.16 Nm for the ruddervator. For the aileron it was decided to use PA-RR-260-8 actuator that can provide a maximum of 5.0 Nm torque and 3.0 N m continuous torque and consume 16 W.[71] For the ruddervator it was decided to use the same actuator together with a 13:1 ratio gear transmission. This way it is still possible to provide the high torque but at a slower turn speed. For the ruddervator this still means a turn speed of $7.7\,^{\circ}\mathrm{s}^{-1}$ which is sufficient for its operation. The PA-RR-260-8 actuators have redundancy built in for the actuation and also for receiving the signals which means it is not necessary to use extra actuators and space. Having the same type of actuators for both the ailerons and ruddervators also makes maintenance easier and quicker.

8.4 SENSORS

The flight computer can take additional inputs from various sensors in order to operate more accurately or to increase the reliability. In addition to the integrated GPS it was decided to use a pitot tube in order to measure the airspeed. The pitot tube measures the difference between the static and dynamic air pressure and from that derives the airspeed. It is important to place the pitot tube at a location where the airflow is undisturbed to get precise measurements. For that reason the pitot tube is placed at the front of the fuselage. In addition the pitot tube needs to be heated in order to avoid it freezing and blocking the measurements. The results of the pitot tube are meant to complement the GPS data. Next a sensor to measure the fuel level was necessary to add in order to accurately estimate the weight of the aircraft at any point in flight and to know the amount of fuel left in the tanks. For this a lightweight sensor by Gill Sensors & Control is used [72] which has a weight of 36 g and consumes only 0.5W.

From the year 2020 onwards it is required for the UAVs to have a transponder on board. [73] Transponders are used in order to keep track of all the aircraft in the airspace and to avoid collisions. For the WiFly UAV a MX transponder by Sagetech is used which is a mode S transponder with ADS-B in/out capability [74] meaning it can broadcast its own location and determine the locations of nearby aircraft. This way each UAV in the swarm knows the location of other UAVs and also other aircraft are aware of the swarm and can avoid possible collisions. The transponder has a weight of 150g and requires a maximum power of 15W. The CS-23 regulations also require for the UAV to have external lights [55]. A red colour light is placed on the tip of the left wing and a green light on the tip of the right wing. A white light is mounted in the back of the UAV. These lights also help to avoid collision when the visibility is low.

8.5 POWER AND PAYLOAD

Next module in the hardware architecture is the power system. The power is generated by the engine of the UAV and is the connected with the mission computer, flight computer and payload modules that distribute the necessary power to instruments connected to them. The electrical power generation and distribution is discussed in detail in section 6.3.

The final module is the payload. This consists of the system for communication with the users and cameras to assess the disaster area. The communication with the users is described more in depth in section 3.4.3. In order to assess the area different types of cameras can be used based on the necessity. For this purpose the JZC-N51820L camera module was selected. This camera provides the ability to take pictures with 1920x1080 pixel resolution and has a 18x optical zoom capability. This means that at an altitude of 6km without zoom each pixel would correspond to 3.3 m on the ground and 15.8 cm with full zoom. At 2km altitude these values would be 1.1 m and 5.3 cm respectively. The camera module weighs 220g and consumes a maximum of 6W.[75] This provides the ability to assess disaster area at the beginning of the mission and if necessary provide updates throughout the mission.

The selected instruments and sensors are summarised in table 8.1 together with their individual weights and power consumptions.

Table 8.1: Hardware components summary

Type	Component	Nr	Individual Weight [kg]	Individual Power [W]
Mission computer	DuraCOR 311	2	0.68	15
Flight computer	Vector	2	0.18	2.5
Fuel sensor	Gill	6	0.036	0.5
Transponder	MX Mode S	2	0.15	15
Camera	JZC-N51820L	1	0.22	6
Actuators	PA-RR-260-8	3	0.52	16

9 | Design Iteration Process

In this chapter the weight estimation is implemented for chosen design. From [3] an initial estimate of the weight was found for each component. This approximation has to be iterated again in order to obtain a more accurate estimate. The iteration process is presented in section 9.1. This subsection is presenting the whole iteration procedure, offering a complete overview on the design process. The section 9.2 is offering the complete layout of the UAV together with a brief reasoning on the selection of some important parameters.

9.1 Weight Estimation

From the midterm report [3] an initial estimate of 58.5 kg was found for the MTOW of UAV. At that stage of the design this was a fair estimate and it was known that it has to be iterated again for the final design. The complete iteration process is described in figure 9.1 and figure 9.2. The reason for variation is due to the more accurate estimates for the subsystems parameters which influence considerable the elements of the weight computation tool. Firstly, more precise aerodynamics parameters are computed using the procedure described in chapter 4. As it can be seen in figure 9.1, the next step is to calculate the power required and select an engine which can provide this amount of power. Also, based on the technical data of the engine provided by the manufacturer, an initial estimate of the fuel weight can be calculated. This whole process is described fully in chapter 6.

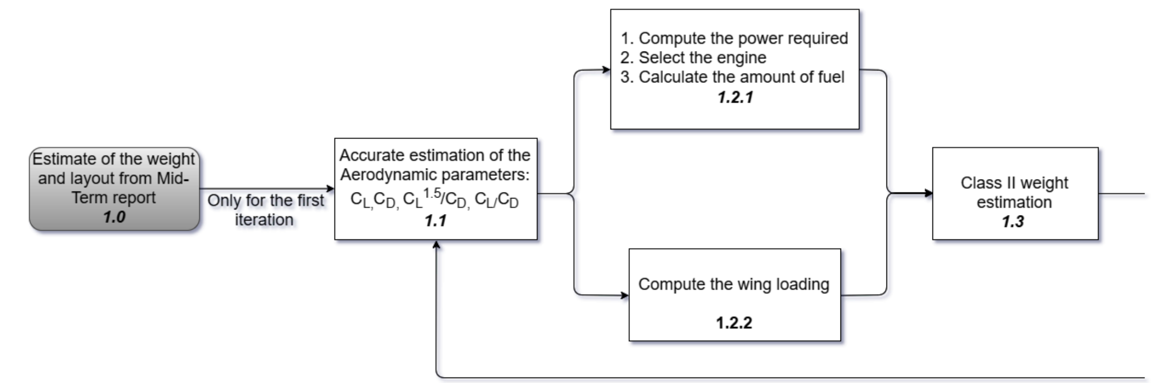

Figure 9.1: The first part of the iteration process, offering all the steps up to the output of Class II weight estimation

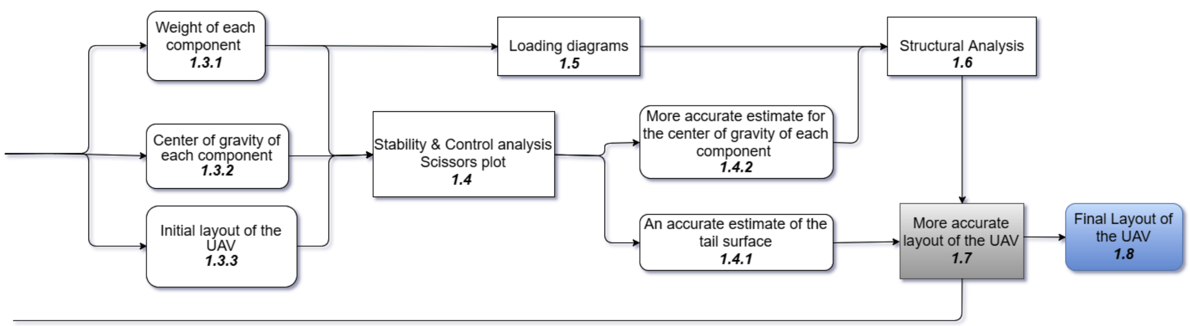

Figure 9.2: The second part of the iteration process, offering all the steps from the output of Class II weight estimation up to the final layout

Afterwards, the class II weight estimation can be performed. The approach used for calculating the component weights follows the method from Reymar [2]. This procedure allows the weight estimation of the wing, horizontal tail, vertical tail, fuselage, landing gear, installed engine and a group called "All-else empty" which includes the weight of all components not mentioned before. The method uses the mass per m^2 of wetted area of the corresponding component. These values are given in table 9.1 and are taken from table 15.2 from [2].

Table 9.1: Factors for weight estimation [2]

Item	Factor	Unit	Multiplier	Unit
Wing	12	$\frac{kg}{m^2}$	$S_{exposed_{planform}}$	m^2
Horizontal tail	10	$\frac{kg}{m^2}$	$S_{exposed_{planform}}$	m^2
Vertical tail	10	$\frac{kg}{m^2}$	$S_{exposed_{planform}}$	m^2
Fuselage	7	$\frac{kg}{m^2}$	S_{wetted}	m^2
Installed Engine	1.4	-	Engine weight	N
"All-else empty"	0.10	-	TOGW	N

The issue of using this method is to find the exposed and wetted areas as the geometry of the aircraft changes at each iteration. The approach used for computing these values consists in the following steps. Firstly, the wing area is determined using the wing loading eq. (9.1) and the latest estimate for the MTOW as the weight input. In the formula, the ρ is the density at sea level, the V_{stall} is the stall speed taken from requirements and the $C_{L_{max}}$ is an output of the aerodynamics analysis.

$$\frac{W}{S} = \frac{1}{2}\rho \cdot V_{stall}^2 \cdot C_{L_{max}} \tag{9.1}$$

Afterwards, using an estimate for the aspect ratio of 20, the span and the chord size can be found. The choice of 20 for the aspect ratio is discussed extensively in the mid-term report [3] and a summary of that discussion is presented in section 9.2. With the span and chord computed, the approach for calculating the other lengths is based on a reference UAV. The main reference was MQ-1 Predator and the lengths are scaled with the conversion factor obtained by dividing the computed span length by the reference one. However, if the subsystems (communication, propulsion, etc.) demand specific dimensions for the size of the fuselage, these quantities will be used as geometrical inputs. With the specific areas determined, the components weights can be estimated. The outcome of the Class II weight estimation is the empty weight and center of gravity of each component together with an initial layout of the UAV. By adding up the components weight the new operational empty weight is found. Using this parameter the loading diagrams can be generated, which will be used as principle input in the structural analysis. All the outputs of the Class II estimation are used for performing the stability and control analysis. The results consist in more accurate estimates for the center of gravity of each component and for the size of the tail. With the area of the tail and with the confirmation that the structure can cope with all loads, a more accurate layout of the UAV is fixed. This will be further iterated until the whole process converges. This is equivalent of saying that the difference between two consecutive outputs of the iteration process becomes so small that there is no need for entering the loop again. For this design, it was decided to use a maximum discrepancy of 0.5 kg. So, if the difference between the MTOW values of two successive iterations is less than 0.5 kg, it is concluded that the design process converged and the last output is kept as final design. With the complete layout of the UAV fixed, more elaborate analysis can be conducted.

9.2 GEOMETRICAL PARAMETERS

An important parameter which has to be considered at the very early stage of the design is the aspect ratio of the wing. A value of 20 for the aspect ratio was already decided in the mid-term report [3] and is kept also for the final design. The reasoning behind this number is offered in the following lines. From ([30]. p.111) a range between 10 and 30 is found specific for the aspect ratio of the high endurance aircraft. For example the Schweizer SGS 1-35 has an aspect ratio of 23.3, while Lockheed U-2 has one of 14.3 [[30]. p.111]. When analysing high endurance UAV's, a value of 25 for the aspect ratio is common for IAI Heron [76] or the RQ-4 Global Hawk [77]. However, taking into consideration that the altitude at which the system is flying is relative low (around 3000 m), a decrease in aspect ratio with respect to the reference UAV's may be considered. The reduce can be implemented because due to the low altitude, the density of the air is high. Therefore, enough lift would be generated by flying at a reasonable C_L. As C_L is not too high, the induced drag coefficient would

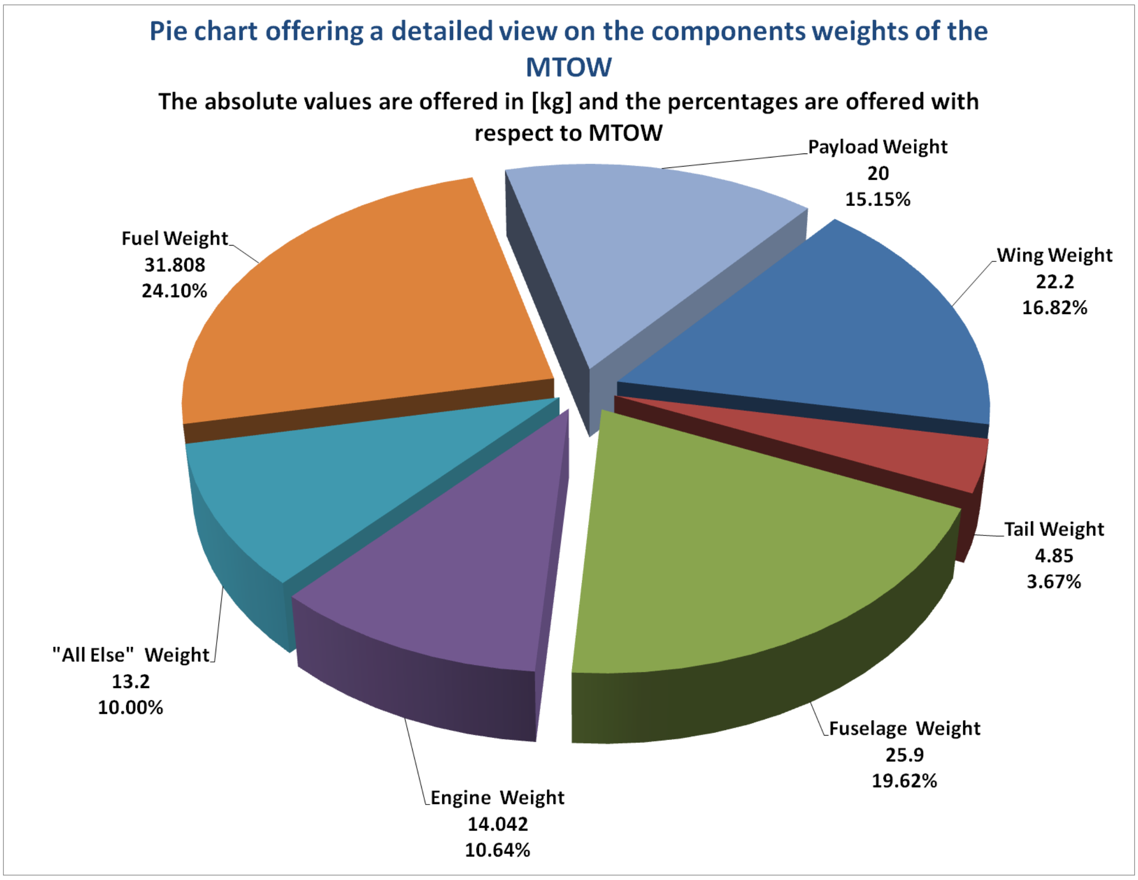

Figure 9.3: A Detailed View on the Weight Components of the MTOW for the UAV as obtained from Class II weight estimation

be relatively small (in comparison with the ones flying at higher C_L), so a smaller aspect ratio can be considered to decrease the second term of the drag polar. Therefore, a value of 20 for the aspect ratio is a fair consideration. In chapter 14, the sensitivity of the UAV design to this parameter is analysed and discussed extensively.

Based on the extensive reasoning given in [3], it was decided to use a mid-wing configuration. Its main advantage is the low drag generation with respect to the low or high-wing choices. The primary drawback of this configuration is the need to transfer the moment due to the wing lift through the fuselage. This is problematic for passenger aircraft because it is unacceptable to have a structural element passing through the middle of the fuselage [30]. For the WiFly UAV this will not be a problem because the wing box is extended straight through the fuselage.

For the geometrical layout of the wing, it was decided in the mid-term report [3] to use no sweep and a moderate taper. Wing sweep is used when the aircraft is operating at supersonic or high-speed subsonic velocities. However, as the WiFly UAV is flying at low Mach numbers (up to 0.3), far from the supersonic regions, there will be no benefits in having a sweep angle. Regarding taper ration, a value of 0.361 was considered based on the primary reference MQ-1 Predator [78], which was also confirmed using a graph from [30, Figure 2.39] showing that the induced drag is also minimised around that value.

As explained in section 9.1 the span and chord are found such that the wing loading requirement are met. For the other parameters the reference Predator MQ-1 is used scaled down to the dimensions of the designed UAV. However, if a system demands higher dimensions for the fuselage (radius, length) in order to fit it, these values are chosen instead. An overview of the UAV layout is offered in table 10.1. Also, a detailed view on the components weight distribution is offered in figure 9.3.

10 | Configuration and Layout

This chapter gives an overview of how the final design looks like. It will have the wing positioned in front of the tail which is in V-shape. Furthermore, the fuselage has a circular cross section and a bulge in the front of the UAV. An illustration of the external layout is given in section 10.1 which consists of a technical drawing showing the external dimensions of the UAV and a 3D rendering. Section 10.2 will show all the components in the interior of the UAV by means of an exploded view and a sketch which proofs that all components fit in the fuselage and wings.

10.1 External Layout

A 3D rendering of the WiFly UAV's can be found in figure 10.1 to get a general impression of how the UAV design looks like.

Figure 10.1: 3D rendering of the WiFLy UAV's

Figure 10.2 shows a technical drawing of the UAV exterior. The wing span, root and tip chord, fuselage diameter at different positions can be retrieved from this technical drawing. Furthermore, the main geometric parameters of the exterior are summarized in table 10.1 .

10.2 Internal Layout

In this section an exploded view is give in figure 10.3 to show which components are located in the interior of the UAV. It shall be noted that this is done to a level of detail of main components. This implies, that wires and very small components like a light are not shown. In this exploded view, the components are numbered. The allocation of the component names to the numbering can be found in table 10.2
Figure 10.4 and figure 10.5 shows the outline of the fuselage and the relative positioning of interior components in a front and side view, respectively. This way it can be proven that all components actually fit in the fuselage and the wings.
A block diagram which shows how electrical components carried on board are connected to each other is shown in section 6.3.1.

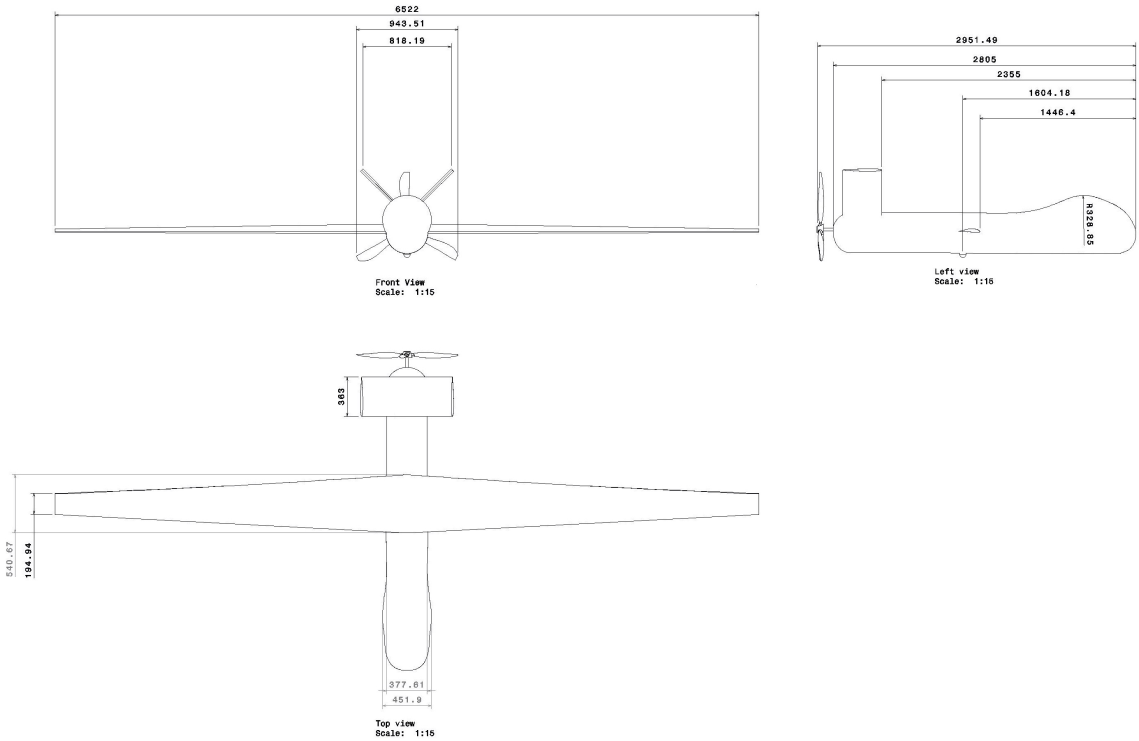

Figure 10.2: External dimensions of the UAV

Table 10.1: Main geometric dimensions

Dimension	Value [mm]
Wing span	6522
Root chord	541
Tip chord	195
Fuselage diameter	378
Fuselage length	2807

Table 10.2: Table of components

Number	Component
1	Fuselage
2	Wing
3	Wingbox and Fuel tank
4	Aileron actuators
5	Ruddervator actuators
6	V-Tail
7	Main UAV communication antennas
8	Telecommunication antenna
9	Camera
10	Tranceivers
11	Mission computer
12	Mesh node hardware
13	Battery
14	Flight computer
15	Amplifiers
16	Engine
17	Generator
18	Propeller blades
19	Emergency UAV communication antennas
20	Engine intake
21	Radiator

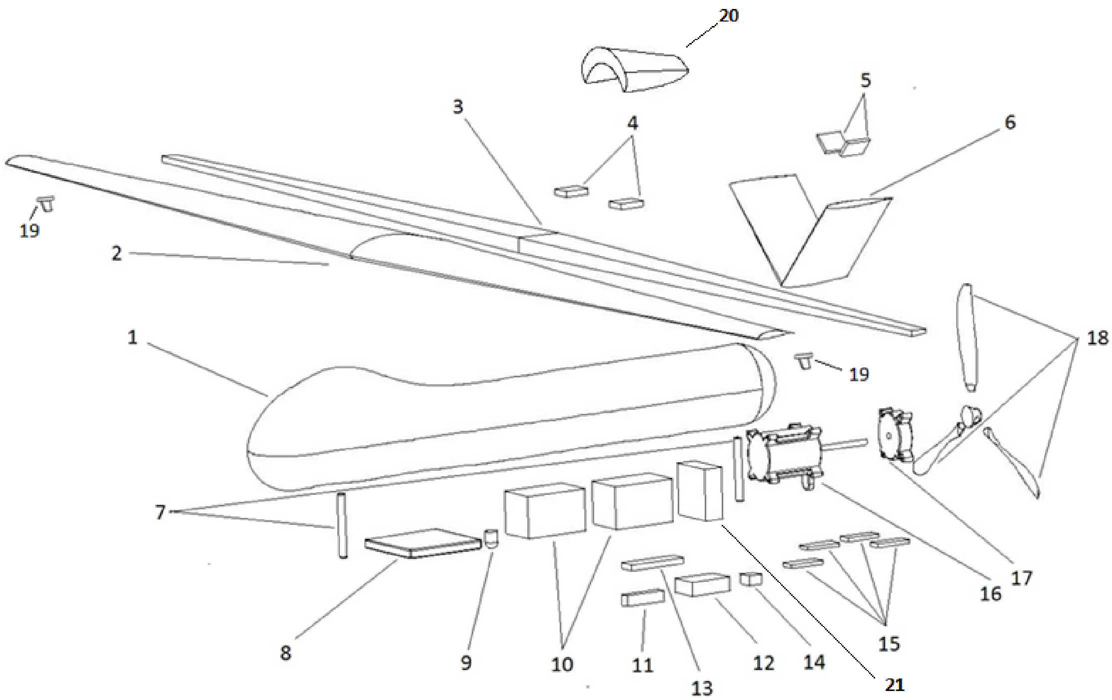

Figure 10.3: Exploded view of all components

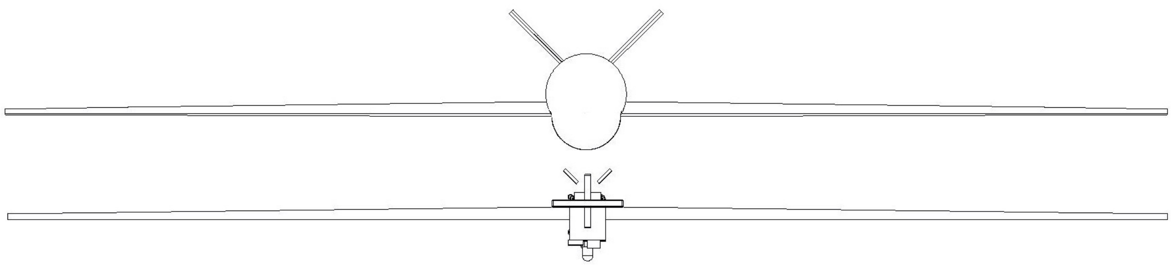

Figure 10.4: Proof of fit (front view)

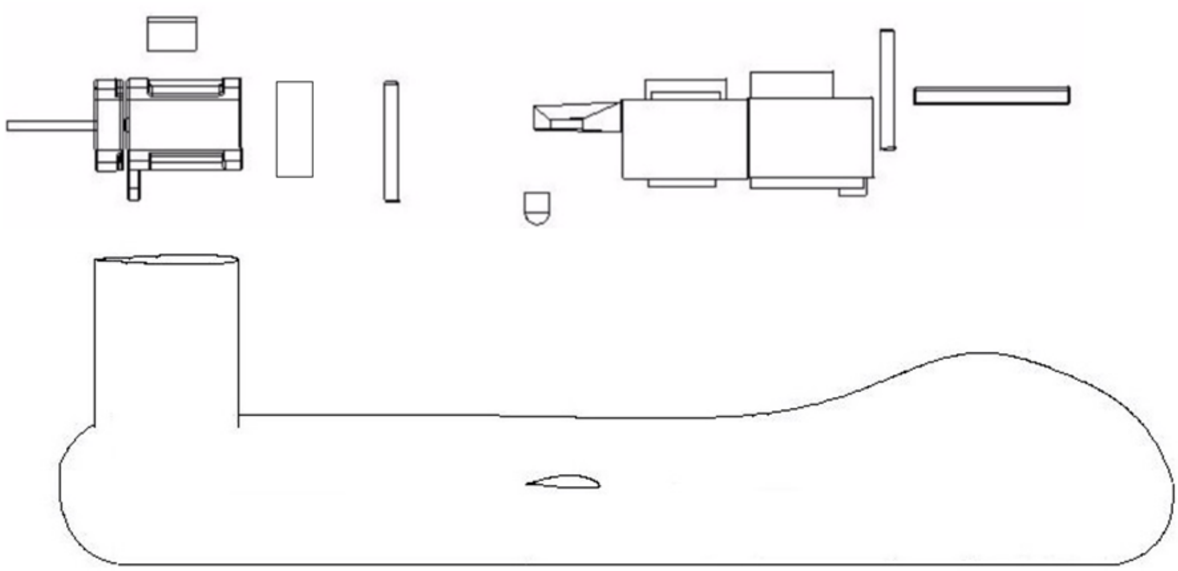

Figure 10.5: Proof of fit (side view)

11 | TAKEOFF AND LANDING

Take-off and landing are both very important phases in the operation of the UAVs. In this chapter the take-off system is described in section 11.1 and the landing system is described in section 11.2.

11.1 TAKEOFF SYSTEM

In the mid term report[3] a trade-off was done which resulted in a bungee launch system for the UAV. In this section the launch system is designed based on references and calculations. The takeoff shall be able to operate with minimal personnel and must have small storage volume. Small being at maximum the size of a container so it can be move around in case the base station needs to be reallocated.

To make clear what kind of system will be used a functional drawing is shown in figure 11.1. The UAV is placed on a cradle to prevent interference between the propeller and the launching system. Expressing the system in a mathematical model can be done based on the free body diagram in figure 11.2. Based on this free body diagram the equations of motion can be expressed as in eq. (11.1). Based on the analysis done in [79] it can be assumed that a simplified model is sufficient to estimate the velocity and acceleration.

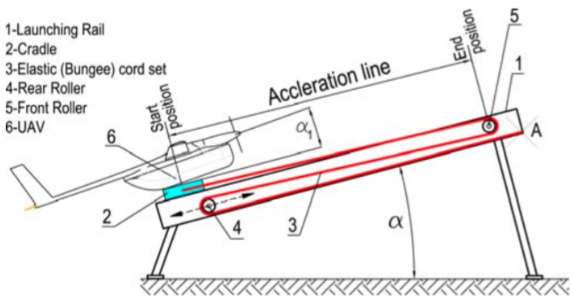

Figure 11.1: Functional drawing takeoff[79]

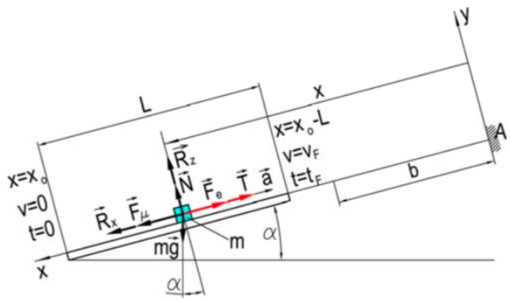

Figure 11.2: Free body diagram takeoff[79]

$$m\ddot{x} = -F_{\mu} - mgsin\alpha + F_e + T \tag{11.1}$$

The equation of motion can be rewritten to a second order differential equation. The solution for the non-homogenous equation leads to the derivatives for velocity in eq. (11.2) and acceleration in eq. (11.3). By applying the final values $t = t_F$, $x(t_F) = x_0 - L$ the time it takes from releasing the UAV to lift off can be calculated. The acceleration and velocity are plotted in figure 11.4. As can be seen, the maximum acceleration occurs at the beginning and is $62.49 m/s^2$. The takeoff velocity is 1.1 the stall velocity and is determined to be $25.33 m/s$. For the design, bungee cables made by Sandow Technic are used. These cables have linear force for elongation from 20% to 80% [1] and are therefore easy for calculations. The final launch system has a launch distance $L = 7.1m$ so it will easily fit in a container.

$$\dot{x}(t) = \left(x_0 + \frac{T}{q} - \frac{mg}{q}(\mu\cos\alpha + \sin\alpha) - b\right)\sqrt{\frac{q}{m}}\sin\sqrt{\frac{q}{m}}t \tag{11.2}$$

$$\ddot{x}(t) = \left(x_0 + \frac{T}{q} - \frac{mg}{q}(\mu\cos\alpha + \sin\alpha) - b\right)\sqrt{\frac{q}{m}}\cos\sqrt{\frac{q}{m}}t \tag{11.3}$$

$$t_F = \sqrt{\frac{m}{q}}\arccos\frac{x(t_f) - \frac{mg}{q}(\mu\cos\alpha + \sin\alpha) - b\frac{T}{q}}{x_0 + \frac{T}{q} - \frac{mg}{q}(\mu\cos\alpha + \sin\alpha) - b} \tag{11.4}$$

[1] http://www.sandowtechnic.com/html_en/product_en_Sa_9.php,accessedon:12thofJune,2016

Figure 11.3: Mark 3 Skyhook by Insitu

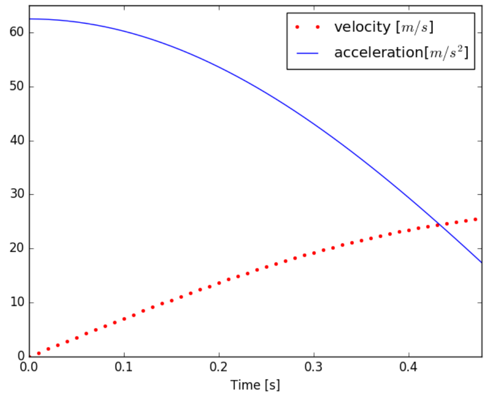

Figure 11.4: Velocity and acceleration w.r.t time

11.2 LANDING SYSTEM

In order to recover the UAVs a dedicated landing system needs to be selected. Since it was decided not to use a landing gear on the UAV in order to save weight and have the system operational even when airports are not nearby. Other landing systems that were considered are net recovery and systems using parachutes. For net recovery it became clear that for the WiFly UAV the net for landing would have a size around 10m x 10m and would require large cranes at the mission site making it unfeasible. The parachute options were discarded because of their bad controllability in strong winds. Because of these reasons the landing system that obtained the best score in a tradeoff was the Skyhook concept.

The Skyhook concept consists of a deployable crane with a cable hanging from the top as can be seen in figure 11.3. Using accurate GPS data the UAV will make its approach and fly its wing into the cable which then slips into the hook on the tip of the wing. The cable is connected to springs in order to slow the aircraft and bring it to a stop. The Skyhook landing system is developed by Insitu company which is owned by Boeing. The system is used to capture the ScanEagle and RQ-21 Blackjack UAVs. The RQ-21 Blackjack has an operational empty weight of 36 kg with a maximum payload of 18 kg compared to the WiFly UAV with an OEW of 71.7 kg and payload of 18.8 kg as found in table 15.2.[80] It is not known what is the maximum UAV weight the Skyhook can recover and because the WiFly UAV is around 35 kg heavier than the RQ-21 Blackjack it might be necessary to strengthen the Skyhook structure and/or use a stronger cable.

Due to its relatively simple design the system is very reliable and has a low reload time making it suitable for swarm operations. The UAVs can be lowered onto a special trolley which removes the need for rescue workers to lift and carry the heavy UAVs. In order to reduce the landing time of the whole swarm two Skyhooks are used. The size of the system is 5.8m x 2.2m x 1.9m when ready to be transported and 8.8m x 5.3m x 17.67m when deployed. The system has a weight of 1896 kg. [81] There is no information available indicating the loads on the UAV during landing so an assumption was made that the UAV will become to a stop within 0.5s from its approach speed that would be 1.1 times the stall speed. This results in an average deceleration of approximately 7g. Similarly there is no indication about the cost of a Skyhook landing concept. For this it is for now assumed that it would remain within the budget of 150k euros or otherwise a similar system can be developed that can meet that budget.

12 | Swarm Formation Flying

This chapter will elaborate on formation flying during the WiFly mission and consists of three sections. In section 12.1 the formation in which the UAV's are flying during cruise is described. Section 12.2 explains the swarm concept at the disaster site. During loiter, it is important to know, which area is covered on the ground by one antenna. This shape is assumed to be circular or hexagonal. This assumption is finally discussed and proven in section 12.3.

12.1 Formation in Cruise

When the system is launched, the first part of the mission is to cruise at most 300 km to the disaster area. During this phase, the UAVs are not building up a mesh network which connects people at the disaster site to the ground station. Therefore, the formation of the UAVs can be optimised for efficiency. This can be mainly achieved by drag reduction. One of the best possibilities to do this is suggested by birds in nature. They fly in V shaped formations to reduce the energy needed to fly. This can also be applied to aircraft flying in a V shape as seen in figure 12.1. It shall be noted that this formation is not limited to three UAVs but it can be expanded theoretically to an infinite amount of UAVs [82].

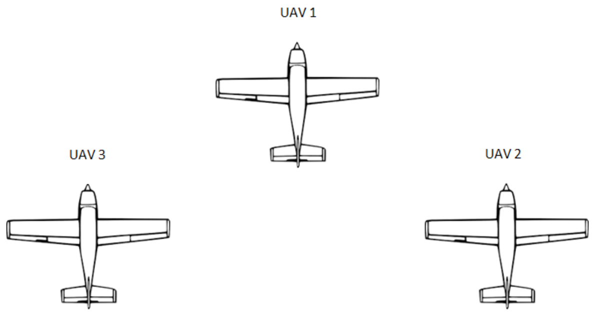

Figure 12.1: Illustration of three aircraft flying in V-formation

The aerodynamic advantage of the V-shape swarm configuration is the so called wing tip vorticity. Since the pressure at the top of the wing is lower than the pressure at the bottom of the wing, the air is sucked to the upper side of the wing around the wing tip. This phenomenon is called wing tip vorticity and the flow pattern in the vertical plane can be seen in figure 12.2 [82].

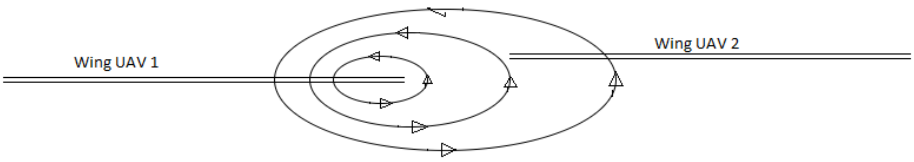

Figure 12.2: Impact of wing tip vorticity on other aircraft

The type of drag which can be reduced by flying in this formation is the so called induced drag, which is a function of the downwash produced by a lift generating wing. This implies that, if the downwash is reduced, the induced drag will decrease as well. Through the V-formation, every aircraft apart from the leading aircraft is able to fly in the upwash part of the vorticity created by the aircraft in front. This upwash cancels part of the downwash created by its own wing and thus the induced drag is decreased significantly. In this way it is possible to reduce the drag up to 50 % [82]. This effectively saves fuel which is an important aspect for the WiFly mission as it increases the endurance of the system.

12.2 SWARM FORMATION IN LOITER

In general the UAVs will circle at a constant turn radius above the disaster site. The main reason for this is that the communication system works most reliable if the connection of the user at the ground is restricted to as few UAVs as possible. This is explained in section 3.4.2.

12.2.1 CONTROL SYSTEM DESIGN PHILOSOPHY

There are three core principles for a successful swarm control. They are the usage of digital pheromones, path planning and collision avoidance. The idea behind these three design principles are suggested by Sauter and Matthews [82] and described as follows:

- **Usage of digital pheromones**: The principle of digital pheromones is adapted from nature. Animals expel pheromones in areas they have visited and other animals know that some peer has moved to this area already and can navigate themselves. This is a way of communicating in a swarm which can be adapted to a swarm of UAVs as well.
- **Path planning**: Depending on where the digital pheromones are located and which action they require from the swarm, UAVs have to switch position with respect to each other in order to perform as well as possible with the given resources. These paths shall be as short as possible as this contributes to a fuel efficient manner to complete the mission.
- **Collision avoidance**: When the digital pheromones are very dynamic in position, this might require a lot of movement of the single UAVs. Therefore, it is of out most importance that collision avoidance between UAVs is guaranteed at any time during the mission.

12.2.2 IMPLEMENTATION OF CONTROL SYSTEM DESIGN PHILOSOPHY

The swarm behavior at the disaster site consists of two phases. In phase one, all the UAVs will set up a homogeneous network at an altitude of 2 km. This first layer of UAV's will access the distribution of the people in the disaster area by mapping the number of connections on the ground. An example for a homogeneous UAV distribution in phase one is shown in figure 12.3 for a 10 by 10 km example disaster area. The probability that the distribution of the people on the ground is not homogeneous is very high and therefore, a swarm control algorithm has to be developed for optimal distribution. This algorithm will order the UAV's in multiple layers at different altitudes and is based on digital pheromone mapping, path planning and collision avoidance. Their implementation for WiFly is explained hereafter.

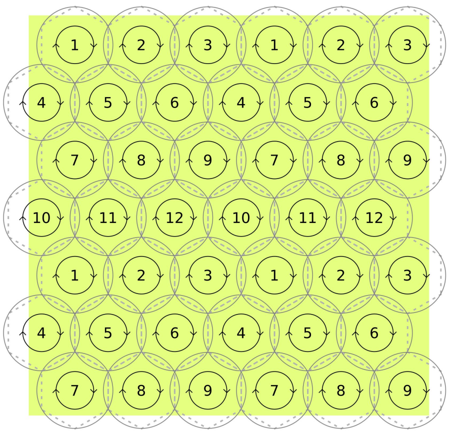

Figure 12.3: Initial swarm formation and its projected ground coverage (Number in centre represents the frequency used by this UAV)

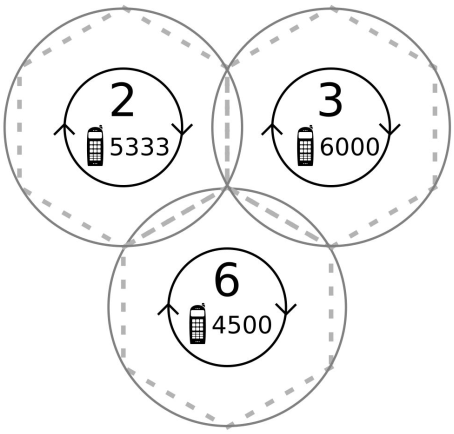

Figure 12.4: Pheromone map

Digital pheromone mapping: In case of the WiFly system, the digital pheromone is the number of phones connected to the UAV. A pheromone map will be generated for every layer of the swarm with different resolutions, since the area covered by one UAV differs with altitude. The maps will provide a valuable overview of the distribution of people on the ground which will serve as a basis for the path planning of the swarm. An example pheromone map is shown in figure 12.4. If the pheromone value of a UAV is above 5333 it is assumed to be overloaded because the communication system of one UAV was designed for 5333 connections as discussed in section 3.3. To clarify, in figure 12.4, the upper left cell is not overloaded but also not underloaded. The upper right cell is clearly overloaded and the bottom cell has still available capacity.

Path Planning: The digital pheromone map will give the control system the opportunity to see where more UAVs are needed and will also show where too many UAVs are located. Based on this, the UAV's of the swarm will change their positions. The algorithm for repositioning the UAV's is shown in figure 12.5.

To explain the algorithm properly, some variables and concepts have to be defined, namely:

- **Layer concept and its labelling**: The layers will be 100 meters apart in altitude.The most upper layer is called L1 and the layer 100 m below is called L2 and so on. A 2D demonstration with 5 layers is given in figure 12.6.
- **Counter variables in most upper UAV layer**: The upper layer has a counter variable "i" to identify the UAV in this layer.
- **Variable for distance between two adjacent UAV's**: There will be a variable "d" for every UAV which measures the distance to the most adjacent UAV.
- **Pheromone variable for every UAV**: There will be a pheromone variable for every UAV which shows how many people are connected to this particular UAV. If the value of the variable is greater than 5333, the UAV is said to be overloaded.

It is easier to explain the algorithm in figure 12.5 when splitting it in multiple parts. The parts are numbered from 1 to 3. Every part is explained hereafter:

Section 1: This section makes sure that the whole area of the disaster site is assessed at any time. If the upper layer is not covering the whole disaster area, the layer will ascend until it covers the whole area again.
Section 2: This part checks if the i'th UAV in the most upper layer is overloaded or not. If the i'th UAV is not overloaded, the next one is checked. If it is overloaded, all UAV's which are not overloaded and also not adjacent to the i'th overloaded UAV ascend for 100 m. The overloaded UAV stays at the same altitude with its adjacent UAV's. The adjacent UAV with the least amount of connections will move in direction of the overloaded UAV until the minimal distance between two UAV's of two times the turn radius is reached. If the i'th UAV is still overloaded, the next adjacent UAV is moved as close as allowed to the i'th UAV until it is not overloaded anymore. If it is not possible to avoid overloading with the adjacent UAV's, it will be moved forward to section 3.
Section 3: In case the adjacent UAV's do not have enough capacity to offer enough connections, it needs assistance from the layer above. Therefore, the UAV with the least amount of connections from the layer above will descend again and will locate itself as close as allowed to the UAV with the highest number of connections. This process repeats until the i'th UAV is not overloaded anymore.
It shall be noted that the algorithm can be optimised further, however this was not possible due to time constraints, considering that swarm control is an active area of research.

Collision avoidance: When reordering the swarm pattern especially in layers with a huge amount of UAV's, the risk of collision between two UAVs is given. This needs to be avoided since otherwise, UAV's would crash and stop working and the reliability of the system is greatly decreased. Therefore, three principles for collision avoidance are presented in the following:

- UAVs are not allowed to cross the path of another UAV which is forecasted in the next 30 seconds.
- In case one UAV has to cross another UAVs future path, it does so by crossing it at an right angle to reduce the amount of time the paths overlap.
- The minimum distance between every two UAVs is at least two times the minimum turn radius of the UAV.

If these principles are worked into the control algorithm, the risk of collision is tending towards zero.

12.3 CELL POINTING

As is mentioned before the UAVs will circle with constant radius above the disaster area. So far the shape of the cell on the ground has either been assumed a circle or a hexagon depending on the context. This section

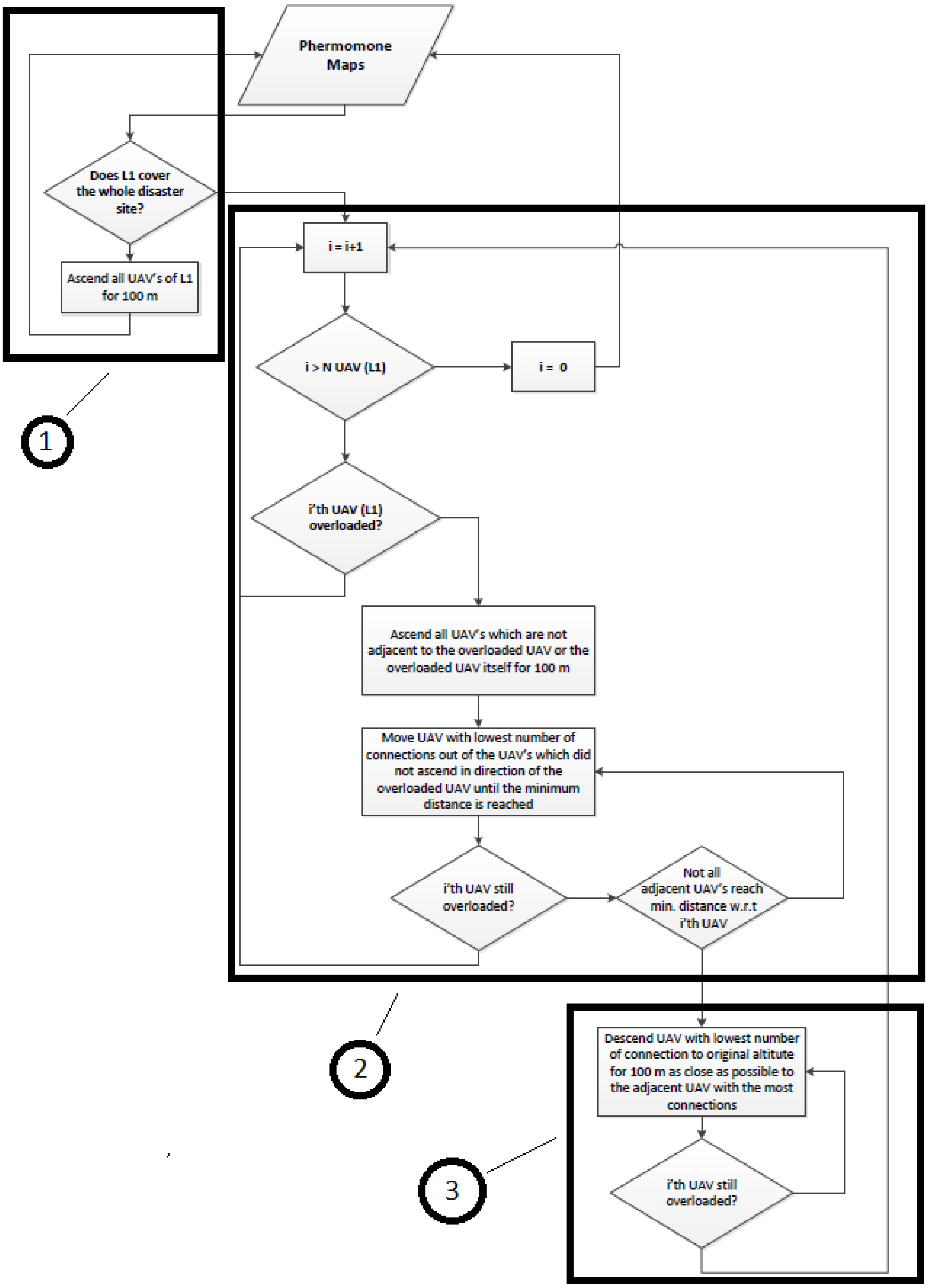

Figure 12.5: Swarm control algorithm in loiter (rectangle is a change in formation, diamond is a decision (if the arrow leaves to the right, the statement in the diamond is answered with yes, otherwise when it is answered with no, the arrow leaves to the bottom.))

will show that with the selected antenna and correct antenna pointing that assumption is valid.

For the analysis that is done here it is assumed that the antenna radiates in a cone. The angle selected for the cone is the beam width of the antenna, 42°. This is actually the half power beam width of the antenna.

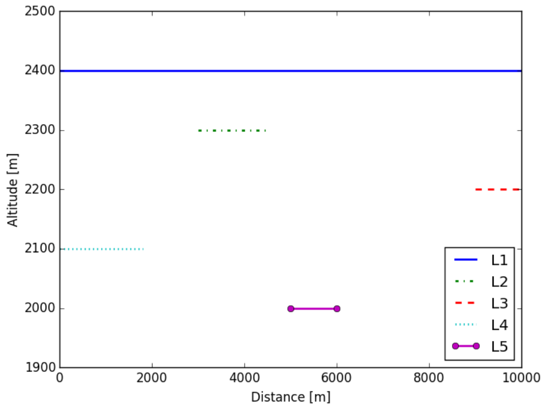

Figure 12.6: Layer Concept

This is often used during analysis as the boundary of the radiated signal. In reality some power will still be radiated outside the cone. If the UAV hovers above the center of its cell and the antenna radiates downwards the radiated pattern on the ground will be exactly circular (assuming the ground is flat). A 2D version can be seen in figure 12.7, the gray triangle. Unfortunately the fixed wing UAV is unable to hover above the cell center. Instead it will circle around the cell center with a certain radius, R. This means that the antenna will have to be tilted. This tilts the radiated cone and the the pattern on the round will turn into an ellipse. The antenna has to be tilted in such a way that the center of the ellipse coincides with the center of the cell. The solution for the antenna tilt angle, δ, can be found by constructing another triangle in figure 12.7, the black triangle. Now simple expressions can be found for R_{C1} and R_{C2}. These are the lengths of the ellipses major axis on both sides of the cell center. If the cell center and the ellipse's center coincide the two values will be equal. This is stated in eq. (12.1). This equation is numerically solved and plotted in figure 12.8. It shows the antenna tilt angle for a range of turn radius's. It also shows the increase in length of the major axis compared to the diameter of the ideal circular cell. This is a measure for the distortion of the cell. At a turn radius of 600m the deformation of the cell is only 5%.

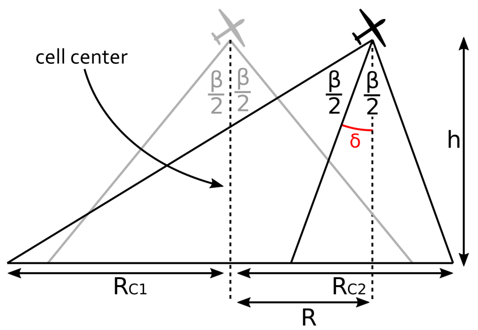

Figure 12.7: Radiated cell geometry during a turn. (Ideal hovering situation is depicted in grey)

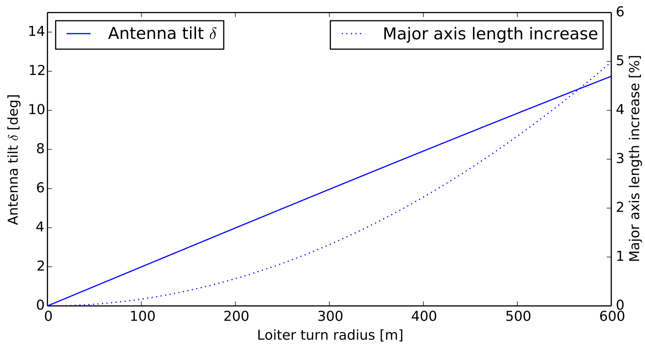

Figure 12.8: Effect of turn radius on the antenna angle and radiated ellipse size. ($h = 2500$ [m], $\beta = 42°$)

$$
\begin{aligned}
R_{C1} &= h \cdot \tan\left(\frac{\beta}{2} + \delta\right) - R \\
R_{C2} &= h \cdot \tan\left(\frac{\beta}{2} - \delta\right) + R \\
R_{C1} &= R_{C2}
\end{aligned}
\tag{12.1}
$$

13 | Flight Performance

In this chapter the flight performance of the UAV will be analysed. The flight performance is useful to get an overview of the standard maneuvers the UAV will perform during its mission. The topics that will be discussed in this chapter are climbing flight 13.1, gliding performance 13.2 and turning performance 13.3.

13.1 Climb

After takeoff the UAVs will have to climb to cruise altitude. Performance analysis wise, this action can be divided into two main parts. The first one being the rate of climb and the second is the time to climb to the specific altitude. Using the rate of climb also the service and absolute ceiling can be determined. All this will be discussed in this section.

The rate of climb can be derived from the equations of motions of an aircraft in unsteady climbing flight. The free body diagram and kinetic diagram for this flight phase can be seen in figures 13.1, 13.2.

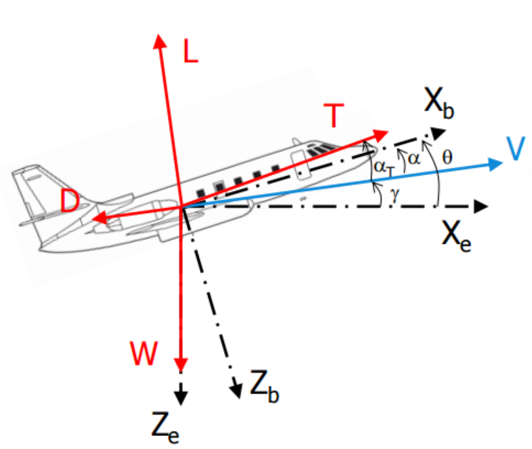

Figure 13.1: Free body diagram climbing flight slides [83] lecture 2

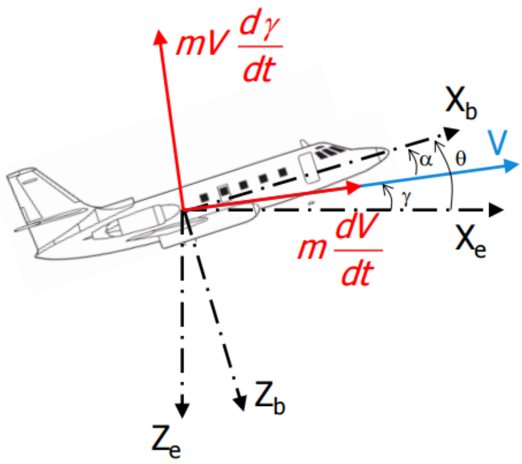

Figure 13.2: Kinetic diagram climbing flight [83]

Since the UAV can be considered a low speed aircraft, the rate of climb is the same as for steady flight.[83] This greatly simplifies The simplified equation is shown in (13.1). This consists of the power available P_a, power required P_r and the weight. It is assumed that $\alpha_T = 0$, so the thrust works in exactly the opposite direction of the drag. Both the power available and power required are influenced by the density and thus altitude. How the powers change with altitude is shown in figure 13.3. From this figure it can be concluded that the excess power, difference in P_a and P_r, becomes smaller with increasing altitude and with that the rate of climb will decrease. The equation for the rate of climb, with density and velocity effects included, is eq. (13.2) [83].

$$RC_{st} = \frac{TV - DV}{W} = \frac{P_a - P_r}{W} \tag{13.1}$$

$$RC = \frac{P_a}{W}\left(\frac{\rho}{\rho_0}\right)^m - V\left(\frac{\rho C_{D,0} S V^2}{2W} + \frac{W}{\pi e A (2S\rho V^2)^2}\right) \tag{13.2}$$

Now in order to have the most optimal climb, in terms of time to climb, there is an optimal climb velocity. This velocity is defined as the point where the power required is at a minimum with respect to the velocity. Unfortunately this optimal velocity is lower than the stall speed at every phase in flight. Therefore, it is decided to climb at 1.1 times the stall speed in order to keep a certain safety margin. Taking all the aforementioned into account the rate of climb with respect to altitude and the corresponding climb angle are plotted in the figures 13.4 and 13.5. By using the changing rate of climb the required time to cruise altitude is determined

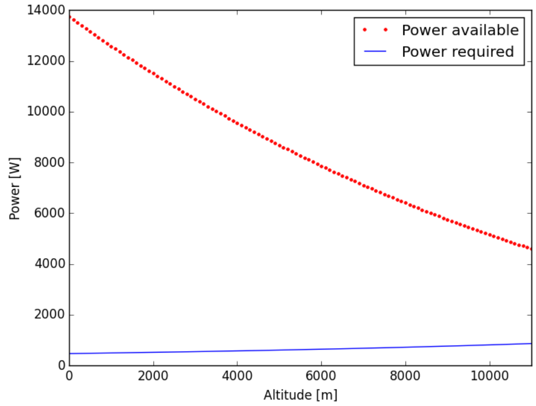

Figure 13.3: Power change with altitude

to be 19.2 minutes.

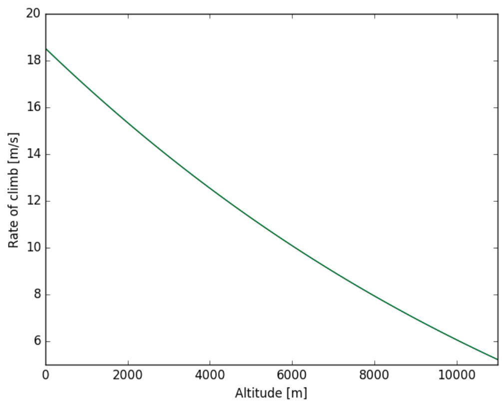

Figure 13.4: Rate of climb w.r.t. altitude

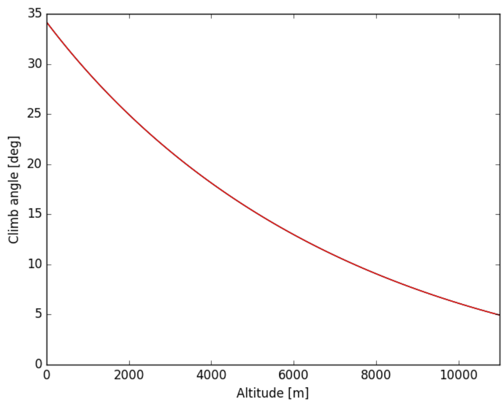

Figure 13.5: The climb angle w.r.t. altitude

Following the same approach to higher altitude could lead to the determination of the service and absolute ceiling. The service ceiling is the altitude at which the UAV can no longer climb at least 30.48 meter per minute. At 11km the climb rate is still as high as 313.14 meter per minute, since this altitude is already way out of the flight envelope the service ceiling is not determined. The absolute ceiling is the altitude at which the rate of climb is 0 meters per second which will also be too far out of the flight envelope and thus of none interest.

13.2 GLIDE

Gliding performance of the UAV can be crucial in the case of an engine malfunction. Gliding performance ask for the maximum $\frac{C_L}{C_D}$ in order to achieve maximum range. This maximum range is useful when an emergency landing spot has to be selected in the area. The maximum endurance is achieved for $\frac{C_L^{\frac{3}{2}}}{C_D}$ and can be useful if landing spot is too crowded.

The free body diagram and kinetic diagram are shown in figures 13.6 and. The corresponding equations of motion are as in eq. (13.3) and eq. (13.4).

$$-D + W sin\theta = 0 \tag{13.3}$$

$$L - W\cos\theta = 0 \tag{13.4}$$

In this free body diagram θ is the gliding angle, defined as the angle that the velocity makes with the horizontal. This angle can be calculated by dividing both equations which leads to eq. (13.5). Based on this equation two conclusions can be drawn. The first being the fact that the glide angle solely depends on the maximum lift over drag ratio and is completely independent of the weight. The second is the higher the maximum lift over drag ratio the flatter the glide angle can be.

$$\tan\theta = -\frac{1}{\frac{L}{D}} \tag{13.5}$$

Now the choice is either between maximum range or maximum endurance. Both cases will be discussed since different situations can require different optimum settings. If an UAV suffers engine power loss, but the landing site is not prepared yet, loiter time rather than range is important. On the other hand if a suitable landing spot is further away, maximum range becomes more important.

The glide angle can also be calculated in the way it is expressed in figure 13.7. The difference in height divided by the range can be used to calculate the glide angle. Now rewriting this as eq. (13.6) gives the maximum range. The maximum range for cruise altitude is 92.51km and for the loiter altitude it is 46.25km.

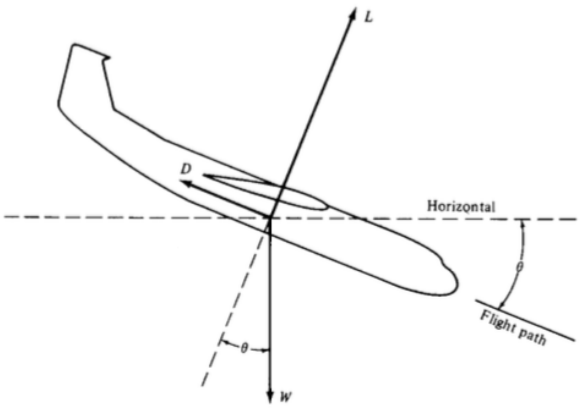

Figure 13.6: Free body diagram gliding flight[84]

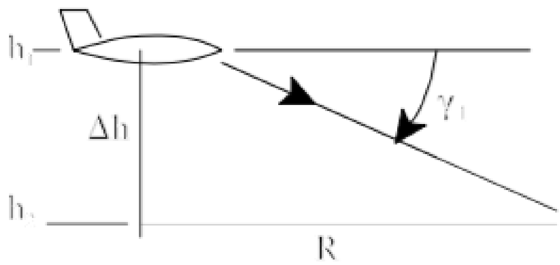

Figure 13.7: Glide range[84]

$$R = \frac{h_1 - h_2}{\tan\gamma_1} = \frac{L}{D}\left(h_1 - h_2\right) \tag{13.6}$$

The maximum endurance can be calculated using the rate of climb, which is negative in this power-off scenario. The rate of climb, or in this scenario rate of sink, can be computed based on figure 13.7 as in eq. (13.7). This can be further rewritten using the small angle assumption which makes $\sin\gamma \approx \tan\gamma \approx \frac{1}{\frac{L}{D}}$

$$SR = -V\sin\gamma = -V\frac{C_D}{C_L} = -\sqrt{\frac{2WC_D^2}{\rho S C_L^3}} \tag{13.7}$$

As can be seen the sink rate, just like the climb rate, is influenced by the density. The change of sink rate with respect to altitude is plotted in figure 13.8.

13.3 MANEUVERING

The performance of the UAV in terms of maneuverability can be expressed in several ways depending on what is desired. High turn performance can be seen as being able to make the tightest turn, the fastest turn or the steepest turn. All require different settings and are limited by maximum power, load or aerodynamic properties.

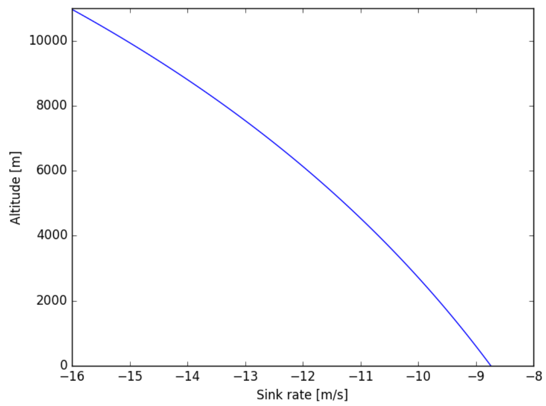

Figure 13.8: Sinkrate w.r.t. altitude

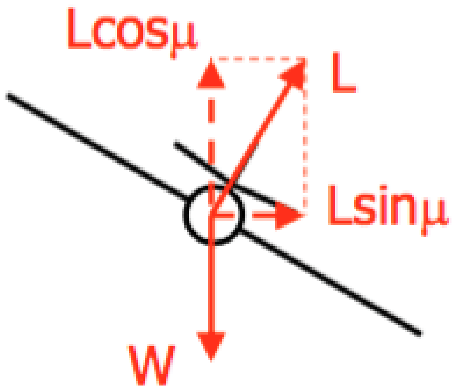

Figure 13.9: Free body diagram horizontal sustained turn

13.3.1 STEEPEST TURN

The steepest turn represents the largest bank angle the UAV can cope with. This is on one side limited by the lift generated and on the other side by the maximum maneuvering load. The steepest turn will be calculated for several altitudes, bank angles and load factors.

The lift generated by the UAV puts a limit on the bank angle for low velocity flight. This can be explained by the free body diagram in 13.9. At a certain angle the UAV will no longer generate enough lift to maintain a steady horizontal turn. This represents the steepest bank angle at low velocity and is determined to be 34°. The corresponding minimum velocity with respect to altitude is shown in 13.10.

On the other hand there is the maximum maneuver load which was determined to be $n_{+} = 3.8$. This load factor corresponds to a bank angle, for steady horizontal turn, following eq. (13.8) which is based on the free body diagram of figure 13.9. Using the value for n_{+}, a bank angle $\mu = 75.74°$ is calculated. In order to achieve a steady horizontal turn the velocity can be calculated with eq. (13.8), this is again dependent on the altitude. Since the velocity plotted in figure 13.11 is lower than the maximum achievable velocity of the UAV, it can be concluded that the UAV is able the achieve the velocity needed for the steepest turn possible.

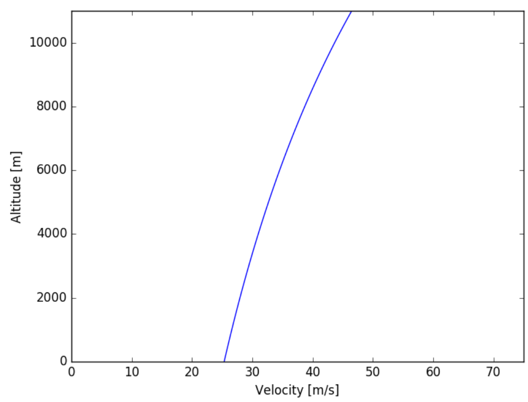

Figure 13.10: Velocity w.r.t. altitude $\mu = 34°$

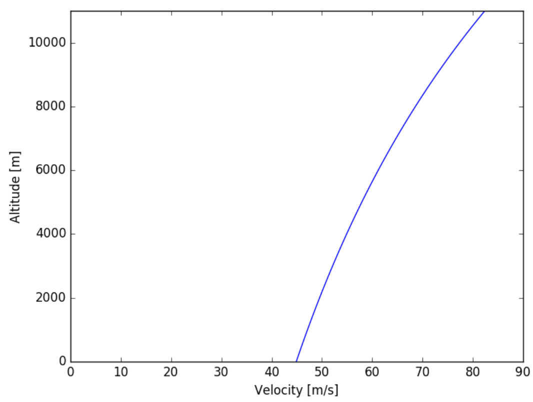

Figure 13.11: Velocity w.r.t. altitude $\mu = 74.74°$

$$n = \frac{L}{L cos\mu} = \frac{1}{cos\mu} \tag{13.8}$$

13.4 TIGHTEST TURN

The second, more important, turning performance is the tightest turn. The tightest turn is the smallest radius required to make a turn. This will be very useful for the loiter phase since based on these calculations the distance required between the UAVs can be determined.

To derive an equation for the turn radius, the kinetic diagram of figure 13.12 and the free body diagram of figure 13.9 are used. Summing up the forces in the lateral direction and rewriting leads to eq. (13.9). It can be seen that for a given n, R decreases when V decreases. Vice versa if the V is fixed and the n increases the same will happen. As explained in the aforementioned section 13.3.1 the n is directly related to the bank angle which will be fixed during loiter. It is more beneficial to fly at smaller radius with lower speed and therefore lower drag.

$$R = \frac{V^2}{g\sqrt{n^2 - 1}} \tag{13.9}$$

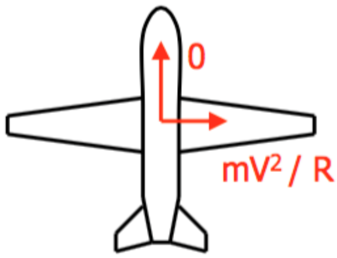

Figure 13.12: Kinetic diagram horizontal sustained turn

Since the velocity is dependent on the flight altitude the turn radius will change with altitude. Since loiter takes place at a fixed velocity of $35.9 m/s$. Turning during loiter will take place at a bank angle of 20° which gives a load factor of $n = 1.064$. These values are fixed and this will result in a turn radius of $384 m$ for every altitude. Furthermore, the tightest turn, which is achieved at the lowest velocity possible is plotted against the altitude in figure 13.13. For the tightest turn a bank angle of 32.26° is required.

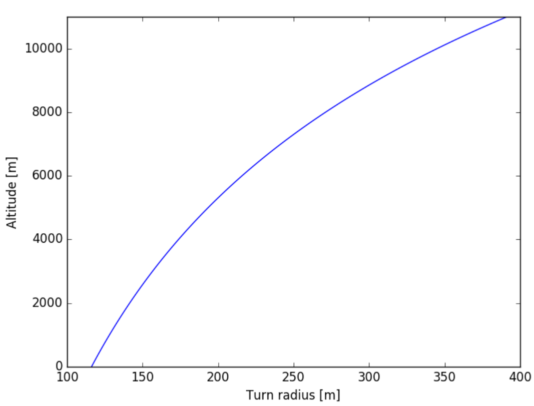

Figure 13.13: Turn radius w.r.t. altitude

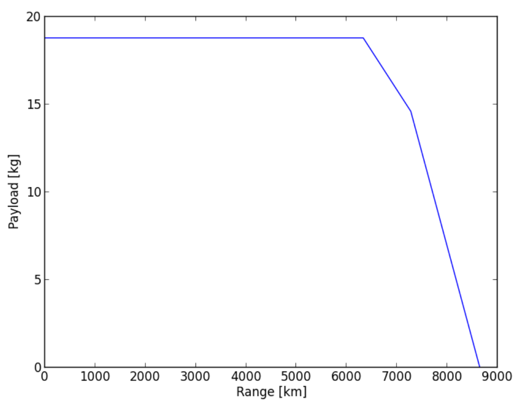

Figure 13.14: Payload-Range diagram for WiFly UAV

13.5 PAYLOAD-RANGE

The payload range diagram was updated for the latest WiFly UAV configuration and is presented in figure 13.14. It can be seen that with full payload the UAV has a range of around 6500 km. When the payload weight is reduced there is up to 10% extra room for fuel in the tanks extending the range. When no payload is on board the UAV it has a range of 8600 km.

14 | SENSITIVITY ANALYSIS

At the end of each design process, it is very important to analyze the flexibility of the final product. This must be done in order to ensure that possible changes in parameters in more advanced stages of the design process do not affect the feasibility of the design. The chapter is divided in three parts, each one treating a change in one parameter of the design. The discussion starts in section 14.1, in which the cruise speed is modified and the impact on the design is discussed. Afterwards, the variation of the payload mass is treated and the results are discussed in section 14.2. The last part deals with the change in aspect ratio and it is presented in section 14.3. The chapter finishes with a small conclusion in which the degree of design feasibility is examined based on the variations previously analyzed.

14.1 CRUISE SPEED SENSITIVITY

The first parameter that is changed in order to analyze its effect on the overall design is the cruise speed. The choice of considering the variation of this parameter is based on issues identified during the design process. It was observed that keeping the initial requirement of 300 km/h cruise speed drove the design to an unrealistic extent (an MTOW of almost 200 kg). Therefore, in order to better identify the impact on the design when the initial requirement of 300 km/h is kept, this value was considered in the sensitivity analysis of the design. Also, an intermediate value of 250 km/h was considered in order to observe what happens when the designed cruise speed of 200 km/h is moderately increased. Both changes are presented in table 14.1, including the difference with respect to the designed value offered both in absolute magnitude and percentage.

Table 14.1: Sensitivity of various parameters to a change in cruise speed (+25%, +50%)

			Absolute Value		Relative Change	
Parameter	**Unit**	**Original**	V_c = **250**$\mathrm{km\,h^{-1}}$	V_c = **300**$\mathrm{km\,h^{-1}}$	**+25%** V_c	**+50%** V_c
V_c	$\mathrm{km\,s^{-1}}$	200	250	300	25%	50%
$MTOW$	kg	132	150	193	13.64%	46.21%
OEW	kg	80.2	88.7	117.2	10.6%	46.13%
W_f	kg	31.8	41.3	55.8	29.87%	75.47%
Span	m	6.52	6.95	7.88	6.6%	20.91%
$\bar{c}$	m	0.326	0.347	0.394	6.44%	20.96%
S	$\mathrm{m^2}$	2.13	2.42	3.11	13.63%	46.22%
P_e (cruise)	kW	8.64	19.63	33.9	127.3%	292.5%
P_e (loiter)	kW	4.7	5.13	5.98	9.2%	27.3%
n_+	[-]	5.19	6.24	7.29	20.23%	40.4%
n_-	[-]	-3.19	-4.24	-5.29	32.92%	65.86%

As can be seen in table 14.1, the design is sensitive to cruise speed especially due to the power required. This doubles when increasing the cruise speed to $250 km/h$ and almost quadruples when it is increased further to $300 km/h$. In the latter case, also the MTOW increases dramatically due to the fact that another (heavier) engine must be selected to provide enough power. As expected, the fuel required almost doubles while the geometrical dimensions such as the span and chord increase by a fifth of their original values. Also, the load factors are sensitive to cruise speed, increasing greatly when the UAV is flying faster. This will have a considerable impact on the structure of the aircraft, which has to be reinforced in order to cope with higher loads.

14.2 PAYLOAD WEIGHT SENSITIVITY

The second parameter that was analyzed is the payload weight. This is an important, mission-dependent parameter of the design. Therefore, it is interesting to analyze the impact of changing the payload on the UAV design. This analysis can be used in the future, when for example a new generation of the system will be considered, which might have a lighter communication system (due to the development of technology) or performs a slightly different mission that requires a heavier payload. The difference of 2 kg between the payload values was selected such that the analysis will also be relevant for determining the impact of the more accurate estimate of the payload, which was recalculated to a value of almost 18 kg.

Table 14.2: Sensitivity of different parameters to a change in payload weight (±10%)

Parameter	Unit	Original	Absolute Value		Relative Change	
			W_p = **18** kg	W_p = **22** kg	**-10%** W_p	**+10%** W_p
$MTOW$	kg	132	127.5	137	-3.41%	3.79%
OEW	kg	80.2	78	82.3	-2.74%	2.62%
W_f	kg	31.8	31.5	32.7	-0.94%	2.83%
W_p	kg	20	18	22	-10%,	10%
Span	m	6.52	6.47	6.64	-0.76%	1.88%
$\bar{c}$	m	0.326	0.324	0.33	-0.73%	1.91%
S	m^2	2.13	2.09	2.21	-1.52%	3.78%
P_e (cruise)	kW	8.64	8.4	8.81	-2.76%	1.98%
P_e (loiter)	kW	4.7	4.69	4.91	-0.23%	4.48%
n_+	[-]	5.19	5.27	5.2	1.54%	0.19%
n_-	[-]	-3.19	-3.27	-3.2	2.51%	0.31%

Due to the small difference in the payload weight (2 kg) between the new and the original concepts, the difference in weight, geometrical parameters and power required is moderate. Only the power needed in loiter increases by a value of 5%, however this does not influence the design since the driving factor for sizing the engine is the power required during cruise. It is important to notice that no other parameters change by more than 4% when increasing or decreasing the payload weight by 10%. This means the design is flexible to a change in payload weight. Therefore, the design will not require extensive changes when the payload weight will be further decreased due to the development of communication technology.

14.3 ASPECT RATIO SENSITIVITY

The last term treated in the sensitivity analysis is the aspect ratio. The reason for analyzing the impact of this parameter is the fact that the value of 20 was considered at an early stage of the design process, and was confirmed by the sensitivity analysis performed in the mid-term report [3]. However, at this stage, the design tool is more complete and the results of changing the aspect ratio are more reliable and the discussion on the impact of this variation is more relevant. As in [3], the analyzed aspect ratios have a value of 15 and 25 respectively. The changes on the design are shown in table 14.3 and discussed in the following lines.

Table 14.3: Sensitivity of different parameters to a change in aspect ratio (±25%)

Parameter	Unit	Original	Absolute Value		Relative Change	
			AR = **15**	AR = **25**	**-25%** AR	**+25%** AR
AR	[-]	20	15	25	-25%	25%
$MTOW$	kg	132	123	152	-6.8%	15.2%
OEW	kg	80.2	70	98	-12.7%	22.2%
W_f	kg	31.8	33	34	3.8%	6.9%
Span	m	6.52	5.51	7.8	-15.6%	19.6%
$\bar{c}$	m	0.326	0.37	0.31	12.6%	-4%
S	m^2	2.13	2.02	2.45	-4.9%	15.1%
P_e (cruise)	kW	8.64	8.83	9.68	2.2%	12.1%
P_e (loiter)	kW	4.7	4.85	5.13	3.2%	9.2%
$C_L^{1.5}/C_D$	[-]	21.76	20.57	21.8	-5.5%	0.2%
C_L/C_D	[-]	23.13	22	22.8	-4.9%	-1.4%

As can be observed in table 14.3, the impact of a change in aspect ratio is quite significant, especially regarding the operational empty weight of the UAV. It can be seen that by decreasing the aspect ratio to a value of 15, the reduction in operational weight is almost 13%. This is mainly due to the fact that the structure becomes lighter. This decrease is lower in the values of MTOW due to the slight increase in fuel weight caused by the drop of aerodynamic efficiency. However, reducing the MTOW by 7% would be an important achievement that will decrease the price of the whole system. Therefore, in future versions of the design, it would be wise to consider a smaller aspect ratio. The value of 15 would be a more appropriate candidate, resulting in a lighter UAV of 123 kg. No benefit is observed when increasing the aspect ratio to a value of 25. The endurance and range factors remain almost unchanged due to the fact that the decrease in induced drag is compensated by the profile drag, which slightly increases due to the enlargement of the whole UAV. The rise in MTOW when considering such a big aspect ratio is significant (more than 15%), which proves that a further increase in this parameter would be unnecessary.

14.4 CONCLUSION ON SENSITIVITY ANALYSIS

This section sums up the conclusions of the previous paragraphs and provides a discussion on the feasibility of the whole design. Based on table 14.1, it is concluded that the design is very sensitive to a change in cruise speed. This limits the flexibility of the system in the sense that it would require major modifications in order to be able to perform a mission which demands a higher cruise speed. In that case, the engine will have to be changed in order to provide the required power. This drastic change will lead to an unrealistic modification of the design.

Based on the discussion of section 14.2, it can be concluded that the design is more flexible to a change in payload weight. No big changes must be made to the design if the payload is slightly increased or decreased. This aspect directly reflects on the feasibility of the design in that it is able to perform a wide range of missions (requiring different payload weights). However, the reader should be aware of the limitation of the analysis as it was implemented for a relative small difference in payload weight (±10%). If for other missions the required payload exceeds or is lower than this amount, another study regarding the impact of the change on the design shall be performed.

From the analysis performed in table 14.3, it was found that a change in the geometry of the wing has limited influence on the feasibility of the design. It was observed that an aspect ratio of 15 would be beneficial for the design, however if the mission would require a higher endurance, the benefit of modifying the aspect ratio would be diminished. As the aspect ratio is fixed at an early stage in the design process, changing it for future versions of the UAV would be unrealistic since then the entire architecture of the aircraft must be redeveloped.

15 | Budget & Contingency Allowance

In the beginning of the design process budgets were defined for driving design parameters like weight, power and cost. These values were based on statistical methods and reference data but are now updated with values obtained during the detailed design together with selected components for subsystems. Before the design is finalized the budgets are always estimations. Overshooting a budget might lead to failure of the mission within the specified requirements and in order to minimize this risk contingencies are introduced for the budgets. As the design maturity increases, the contingency factors become less until they are zero and the prototype stage is reached. The contingency factors are shown in section 15.2.

15.1 Budget Break Down Structure

Budget break downs are divided into mission related and UAV related break downs. UAV related budget break downs are shown in tables 15.1 to 15.3 and they cover the cost, weight and power. Mission related break downs consist of cost and endurance, which cover the main requirements that have to be fulfilled by the WiFly concept. These are shown in tables 15.4 and 15.5.

15.1.1 UAV Related Budget Breakdown

Tables 15.1 to 15.3 show the cost, mass and power budgets per UAV. These budgets are generated using subsystem component weights and power requirements. For the component costs rough estimations were made because for majority of the components no cost data is available and is only given after requesting a quota from the supplier. In addition, ordering a large number of components for the entire swarm can have a significant effect on the cost per unit.

Table 15.1 shows the cost of a single UAV. It can be seen that the requirement of 50k€ per UAV has increased to 64.1 k€ instead. This is mainly due to the high cost of the telecommunications components which are crucial for fulfilling the mission and cheaper components either do not exist or do not come close to providing the needed performance.

Table 15.1: Budget break down of cost resources

Cost resource per UAV: 64.1 k€	
Propulsion system	8k€
Payload	38.1k€
Avionics & Actuators	10.2k€
Airframe	5k€
Communications system	2.8k€

Table 15.2: Budget break down of mass resources

Empty mass resource per UAV: 90.53 kg	
Propulsion system	20.39 kg
Payload	18.8 kg
Airframe (tail+wing+fuselage)	37.04 kg
Avionics & Actuators	4.02 kg
Communications system	3.88 kg
All Else	6.4 kg

Comparing the values for each subsystem's weight with the class II weight estimation it can be noted that the propulsion system weight has increased by around 6 kg. This can be explained by the fact that the propeller weight and generator weight were added. After selecting all components for payload its weight dropped from 20kg to 18.8kg. In addition the structural weight dropped by 15.9 kg. This was achieved because the initial weight estimation equations are not specific for UAVs which have a much simpler and lighter fuselage. This leads to a total empty weight of 90.53 kg and OEW of 71.73 kg. From the total weight savings 6.4 kg will be budgeted as a reserve in case any subsystem weight increases and 10 kg can be used as an extra fuel. This extra fuel can cover the climbing flight phases of the mission that were not considered in the initial fuel calculations and extend the loiter phase.
Table 15.3 presents maximum power usage of each subsystem. Here the avionics part includes the mission computer, flight computer and the transponder power consumptions. In total all subsystems require 789 W when working on full capacity.

15.1.2 MISSION RELATED BUDGET BREAKDOWN

Tables 15.4 and 15.5 contain the cost and endurance budgets for the whole mission. In the requirements it is specified that the whole system should not cost more than 3M€ and the UAVs need to loiter at the mission site for at least 24h.

Table 15.3: Budget break down of power resources

Power resource per UAV: 789 W	
Payload	398 W
Avionics	40 W
Actuators	48 W
Communications	303 W

Table 15.4: Budget break down of WiFly project

Cost resource of WiFly project: 3.38M€	
Launch mechanism	150k€
Landing mechanism	150k€
UAVs	2.88M€
Ground station	200k€

Table 15.4 presents the cost of the entire WiFly system. From UAV budgets it can be seen that the cost of a single UAV that could fulfill the mission is 64.1 k€ and with the selected number of 45 UAVs in total this results in a cost of 2.88 M€. For the launch and landing systems it was not possible to find the costs for the selected systems and therefore rough estimates are given for those. Similarly, a detailed design of the ground station is planned as a future development and only a rough estimate is given at this point. With these values the entire system would have a cost of 3.38 M€.

For the WiFly UAV the loiter and cruise times were set as design parameters based on the requirements for the system. The takeoff time represents the time it takes for the UAV to go from launch to the cruise altitude. When the UAV has returned from cruise it will take 20 min for landing. The return of the UAVs must be scheduled such that there is no overloading of the landing system which would result in a too long wait time.

15.2 CONTINGENCY MANAGEMENT

Contingency management is a very important part of project management since some budgets are crucial for the success of the mission. If the project becomes too expensive or does not fulfill a driving requirement, it would lead to fatal failure in the development of the product or system. To control the risk of failure, so-called contingency factors are applied to the elements of the budgets. These indicate the uncertainty in design and act as a safety margin. As the design maturity increases, certainty grows and the contingency factors can be decreased without risking the success of the project. At the very last stage, a prototype is built and no contingency is applied anymore as the product size and weight are final. The contingency factors applied to the budgets given in tables 15.1 to 15.5 throughout this project are shown in table 15.6, taking into account different project stages.

Table 15.5: Endurance break down of WiFly system

Endurance resource per mission: >24h	
Takeoff	19min
Cruise	3h
Loiter	>24h
Landing	20min

Table 15.6: General contingency factors for all budgets per design phase

Design maturity	**Contingency factors (%)**
Conceptual design estimate	20
Preliminary design	15
Released drawings	10
CAD Model & Simulations	5
Prototype	0

In case design options contain new and non-proven technology, higher contingencies shall be applied to that certain component since the risk of it to exceed the limit is much higher than for proven technology. Therefore, the contingency factors in table 15.6 are just an indication in what range the contingency factors shall be picked, but it does not show final values. Those are dependent on the design choice. In case a component exceeds the budgeted resource with the applied contingency factors, action has to be taken in the project progress to prevent the project from being cancelled. In this case, the team has to meet and create a new budget break down. In case the chosen option does not allow to find a suitable solution for the budget problem, the design options have to be revised and thus a new configuration has to be chosen. This change might be minor or major, depending on how much the budgets were diverging.

16 | Market Analysis

A market analysis must be conducted in order to investigate the competitiveness of the product and the added value it has in the market. The market analysis begins by analyzing the potential customers and competitors of the product in section 16.1 and 16.2, respectively. Then, in section 16.3, projections are made regarding the development of the market, the expected market share the WiFly system will obtain, the target cost of the system and the key success factors. The chapter is concluded with a SWOT analysis in section 16.4.

16.1 Customer Analysis

A customer analysis is needed to identify potential buyers or operators of the system. Once the customers' needs have been identified, it is important to analyze how they want their needs to be fulfilled and how the WiFly system can provide this. By narrowing down the possibilities of potential buyers, constraints can be drafted for the design process.

Initially, as outlined in the baseline report [4], it was expected that search and rescue organizations will be the main customers. However, upon consultation with the Dutch USAR team (a summary of which can be found in appendix E), it was found that the budget of any such team is far too low to allow for them to purchase the system themselves. Rather, governments and militaries (specifically those in areas susceptible to disasters) will be the main potential customers. Their requirements for the system are in many aspects the same as those of search and rescue organizations, as they want a quick and efficient rescue operation after their country has been hit by a disaster. Besides local governments, intergovernmental organizations such as the UN and NATO are also potential customers. The International Search and Rescue Advisory Group (INSARAG) of the UN aims at worldwide standardization and optimization of rescue operations after collapsed structure disasters. Even if the UN itself is not interested in purchasing the system, INSARAG can play an important role in the promotion of the product by recommending it to its members once it is tested and proven to work.

From the meeting with a representative of the Dutch USAR team, it became clear that the main requirement of such teams would be for the system to arrive at the disaster area as fast as possible, preferably earlier than any other organization. The reason why this is so important is because the search and rescue teams, just after arriving, have very limited overview of the situation in the disaster area. The WiFly system should therefore aid in assessing the situation. It can do this by taking pictures of the area and by creating a map of safe/unsafe areas. Furthermore, the rescue teams initially have limited knowledge of where to look for people under the rubble, based on reports from locals/survivors, and the assessment takes a lot of time. Ideally, the WiFly system can pinpoint phone locations on a map such that the teams have a better idea of where to search. Finally, search and rescue teams currently use satphones to communicate, which is very expensive. Hence, it would be beneficial for the rescue teams if the system allowed them to make phone calls to each other.

16.2 Competitor Analysis

A competitor analysis is conducted to identify and assess the competitors to create a competitive advantage. Although currently there is no product that provides the exact services the WiFly system will provide, some financially strong corporations are working on similar projects that use (swarms of) UAVs to provide internet connectivity in remote areas.

Google is working on two projects that employ drones for the purpose of providing internet in all corners of the Earth. The first is Google Loon, which uses stratospheric balloons to provide a network to rural and remote areas. The second is Google Skybender in which drones are used to provide 5G Internet access all over the globe. Another wealthy corporation that uses drones to provide Internet access is Facebook with its Aquila drone. Each of these projects is however still in the early stages of development and, in contrast to the WiFly system, none of them aim to aid in search and rescue operations. On the other hand, the projects are run by two very wealthy companies that will be a threat to the success of the WiFly project should they decide to develop products that more closely resemble the WiFly mission.

16.3 PROJECTIONS

This section provides projections of the market in order to investigate the potential success of the WiFly system. A prediction of future markets can be found in section 16.3.1. The expected market share is covered in section 16.3.2. The target cost and key success factors are covered in sections 16.3.3 and 16.3.4, respectively.

16.3.1 PREDICTION OF FUTURE MARKETS

The UAV market is rapidly evolving and experiences an upward trend in its net worth. Its net worth was estimated to be $500 million over 2014 and is expected to have grown to $2 billion by 2022, which is an average annual growth of approximately 17%. Military applications still prevails as top contributor to this, but civilian applications are predicted to grow steadily over the coming years as well. [85] This is in agreement with what was reported during the meeting with the Dutch USAR member, where it was mentioned that there is a recent trend in using UAVs to aid in search and rescue operations.

16.3.2 EXPECTED MARKET SHARE

The market is still new and open for companies to enter. However, as mentioned before, two financially strong companies are working on projects that include Internet-providing UAVs, although not specifically designed to aid in search and rescue operations. In order to obtain a large market share, it is therefore essential to quickly undertake action and produce a working system before competitors enter the new market. The use of drones in rescue operations is growing and the WiFly system can benefit from this trend.

16.3.3 TARGET COST

In chapter 15, the total cost of the system was estimated to be 3.38M€. However, the price of some of the components, such as the landing and takeoff system, were a very rough estimate. Since the exact costs for building the system are not known yet, it is hard to accurately predict a realistic target cost at this stage. For now, it is expected that the full WiFly system will be sold for anywhere between 4M€ and 4.5M€.

16.3.4 KEY SUCCESS FACTORS

Key success factors are the specific elements needed for the project to be successful from a marketing point of view. They are related to resources, design, production, operation, maintenance, logistics and technology. It should be noted that key success factors can change throughout the life cycle of the product.

The WiFly system has many different features, each with its strengths and weaknesses. Two key success factors have been identified. The first of these is the major weakness, being that it is only useful when there is a disaster. The second one is the fact that it operates in a swarm, thereby automatically building in redundancy and allowing for economies of scale.

Disasters

The WiFly system is designed for disaster situations, where it creates a temporary network to aid search and rescue teams, pinpoint phone locations and allow data transfer. To assess the added value of this system, a disaster has to take place and the WiFly system has to be available for the location where it occurs. This might pose problems as an initial purchase of the WiFly system before it has shown its worth is unlikely. After it has operated successfully on different missions, it will move up the reliability scale and more purchases are inbound. Other applications of the WiFly system are possible with different configurations of the UAVs, but since it has been designed for disaster situations, it is most likely overdesigned and its added value for those missions is low.

Economies of scale

Economies of scale are cost advantages that a company obtains due to the scale or size of the operation. Generally, this means that the cost per unit decreases as the amount of products increases. The swarm feature is the driving force behind this key success factor. Once the swarm is set up, virtually an infinite amount of drones can be added to the system. The larger the swarm of UAVs, the lower the average cost per unit.

16.4 SWOT ANALYSIS

The SWOT analysis, as can be found below, summarizes the observations made in the previous sections. It provides a quick overview of the Strengths, Weaknesses, Opportunities and Threats of the system and the services the system provides. The strengths and opportunities can counter the weaknesses and threats, while the opposite can endanger the success of the project.

Strengths

- The system operates autonomously.
- It is reliable, as using a swarm of UAVs creates redundancy.
- It is innovative.
- It is deployed fast and reaches the disaster site quickly.
- Shortly after a disaster it provides the victims with emergency information.
- By pinpointing phone locations, it can offer a quick insight into what areas are (un)safe.
- It complements existing rescue operations and thereby helps saving lives.
- It requires minimal crew once the system is up and running.
- The entire system is reusable, and hence sustainable.

Weaknesses

- It is a complex system.
- It is expensive.
- It has a very specific potential customer base (governments, humanitarian organizations etc.).
- It is only useful when there is a disaster.
- It is a new and untested concept.
- The effectiveness depends on many factors.
- It requires that the victims of the disaster have phones and the phones must be switched on in order to be able to localize them.

Opportunities

- There are not many competitors for this purpose.
- The market for UAVs/drones is growing.
- The system is attractive for governments of areas that are susceptible to (natural) disasters.
- It is attractive for network provider companies to join the project.
- An infrastructure can be grown when the system is present at multiple locations all over the globe.
- The market is still open to innovation.
- UN/NATO and similar organizations might be interested in supporting/subsidizing it.
- Global warming might increase the number of natural disasters.
- In the future, the system may be updated to include more functions besides providing an emergency mobile network.

Threats

- It should operate during disasters, which might cause damage to the system.
- Alternative ways to provide network in disaster areas.
- Big companies like Google and Facebook are already working on providing Internet in remote locations.
- (Autonomous) UAVs require authorizations from governments to fly.
- The UAVs might interfere with flight paths from other aircraft.
- Rapid development in UAV technology makes it a hard to predict market.

17 | Verification and Validation

This chapter covers the verification and validation of the different calculations and numerical models that are used during the design. Each subsystem will be discussed and analyzed on both the subjects separately. This section will present the procedures to be performed during and after the detailed design phase.

17.1 Verification

Verification is performed in order to check whether the imposed requirements for the mission are met and is done both at system and subsystem level.

For each program that was generated first a unit test was performed to make sure that it worked as required and does not contain any errors. In order to check a unit of code the results of hand calculations were compared with the outputs of the program for the same inputs. Once all the errors were eliminated the models could be used for the detailed design.

Aerodynamics

In order to increase the reliability of the aerodynamic analysis, a parallel computational approach was used in determining the specific parameters. This means that two independent procedures were used and the outputs were verified with each other. This is a very powerful method to verify the results and to find mistakes in the computational tool. In table 17.1 the output of these two methods are offered and the difference is given in percentage in the third column. The specific parameter computed in the table is the parasite drag (C_{D_0}). The first procedure uses XFLR5 while the second one uses the method proposed by Roskam in [1]. The reader is advised to refer back to chapter 4 for a complete analysis of these parameters and a complete discussion regarding the difference between the estimates. Unfortunately, for modeling and integrating the fuselage,

Table 17.1: A comparison between the values of the C_{D_0} [-] calculated through two independent methods

Component	XFLR5	Roskam [1]	Difference relative to each other (%)
Wing	0.014	0.0123	12.1%
Tail	0.00486	0.01226	152.2%

XFLR5 was found to be not suited for the present application. This was concluded after the first simulation of the whole UAV with the XFLR5, whose results were qualified as unreliable due to the fact that they contradict the laws of physics. The program predicted a negative drag, which is impossible in a real situation. Therefore, for the whole UAV the XFLR5 was not used as a tool for verifying the results. A reliable method for verifying was to compare the results with parameters of reference aircraft offered by Roskam [1] in various graphs and tables. If the difference was unexpectedly big and no explanation was found to justify its occurrence, the computational software was rechecked for bugs. In the post-DSE phase of the project, a complete CFD model can be used to verify the results.

Propulsion

The amount of fuel needed for the mission and the power produced by the engine was verified using data sheets provided by the engine manufacturer. The value for the WiFly UAVs power loading of 0.054 was compared with a UAV with similar mission and parameters, specifically the MQ-9 Reaper which has a power loading of 0.069. This verifies that the design power loading can be considered feasible.

Communication

All the link budgets that were calculated were compared against existing communication solutions to see if the calculated budget was not too optimistic and leading to a design that could not exist in reality. For the calculation of the data rates and the network capacity no material was found to perform a comparison. Also no models could be found to compare the results against. Strictly speaking the methods used for sizing the payload are currently not validated nor verified. After an initial deployment of the system data can be gathered to aid in the validation of the model, which in turn can be used to design the next version of the WiFly system with the knowledge that was unavailable at this stage.

Stability and Control
The control surfaces were designed using statistical relations that should result in a stable aircraft. The stability of the UAV was then verified with a simulation using the AVL program which has been validated to give accurate results for Mach numbers less than 0.6 and is therefore also applicable for the WiFly mission [86]. The performance of control surfaces for roll maneuvers was computed analytically to verify the compliance with regulations.

Structures
For verification specific points on the fuselage were selected and for these points the numerical model results were compared with analytical results.

17.2 VALIDATION

Validation demonstrates that the right product has been designed. Validation is very important to prove the stakeholders that the product accomplishes their expectations. In this section plans for final system validation are presented.

Aerodynamics
The most reliable way of validating the results of the aerodynamics analysis is to perform a full scale wind tunnel testing of the UAV. This will ensure that all the parameters are accurately computed and that the aircraft will perform as expected. Another less reliable way of validating the data would be to use a pre-tested and pre-validated computational software. The advantage of this approach is the price of the evaluation which is considerably lower than a full wind-tunnel testing. However, the designing team should be aware of the limitations of the computational program and shall treat its results with prudence. In the post-DSE stage of the design project, the output of the wind tunnel testing can be used also to validate the results of a potential CFD model.

Propulsion
In order to validate the propulsion system the aircraft is flown to its maximum endurance and range capabilities. The atmospheric conditions are simulated to demonstrate that the mission objectives can be accomplished in real life. This will correct the estimated parameters used in the design process, based on manufacturer datasheets.

Communication
Communication system will be validated through demonstration. For that, the components of this system will be placed in an anechoic chamber where the connections between the system and users are established. The long range capabilities need to be tested in a remote area such as a desert and the performance in rough weathers with strong rains are to be tested as well. The components selected for the UAV were checked and based on their manufacturer's tests they achieve level of performance similar to the WiFly requirements.

Structures and materials
To validate the structure of the UAV it will be loaded under a load 1.5 times the maximum load it will experience. Any load above that should result in a structural failure of the UAV.

Stability and Control
One needs to check that the 10 Bft requirement is sufficient to prove the good functioning of the system in harsh conditions. Stability and controllability shall be validated by flying at different fuel loadings and altitudes performing all the necessary maneuvers. The Skyhook landing system is also used for RQ-21 BlackJack UAV with similar mission and characteristics as the WiFly.

18 | RAMS Analysis

Reliability, Availability, Maintainability and Safety (RAMS) is a method complementing the Systems Engineering process used in the project and design phases to ensure satisfying all customer needs. It addresses several non-technical topics that are derived from the design, and concern the logistic support phase. Several tools of this analysis have been used before such as the FMECA, block diagrams and breakdown trees, although the application of the tools differ.

A general description followed by the effect on the design for the four topics is presented in the following paragraphs. The procedure and definitions as described in the Systems Engineering and Technical Management Techniques guide [87] will be used to evaluate each topic. Design for reliability is performed in section 18.1. Availability is derived from reliability and maintainability, therefore maintainability will be presented first in section 18.2. Availability and Safety will be treated in section 18.3 and section 18.4 respectively.

18.1 Reliability

Reliability is defined as the probability that a system will perform in a satisfactory manner for a given period of time when used under specified operating conditions. Reliability, failure density and hazard functions are typically used to model reliability behaviour of components, subsystems and systems. Although these would provide tools to quantify reliability, this will not be treated because reliability data is not available for all components, and too many assumptions will have to be made. Instead, the application of these functions, and their effects on the design will be elaborated upon.

Systems and subsystems can be decomposed into components, which are connected to each other either in series or in parallel, or a combination of both. A series network is the simplest type of network in which all components must operate in a satisfactory manner for the system to function properly. This connection is modeled in figure 18.1a. Each component can be considered critical, as a failure of any of the components will lead to improper functioning of the system. This is not preferred for the autonomous WiFly UAVs, where direct corrective measures cannot be performed due to absence of a pilot. Parallel redundant configuration models are models where a number of the same components are connected in parallel. Total system failure can then only be achieved when all parallel components fail. Parallel networks can be divided into active and standby redundancy models, presented in figure 18.1b and figure 18.1c respectively.

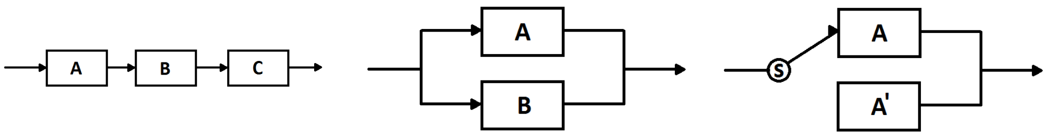

(a) Series network **(b)** Active parallel network **(c)** Standby parallel network

Figure 18.1: Possible network configurations

The effect on design due to reliability considerations can be elaborated upon per subsystem. The main focus will be the level of redundancy in design and damage control when the component or subsystem fails.

- **Aerodynamics** The main aspect that needs to be examined for reliability is the ability to generate lift by the lift inducing surfaces, which can perform their function with near absolute reliability. All lift inducing surfaces are sized for conditions exceeding the ones stated in the mission requirements, ensuring proper functioning during non-nominal operation. This can be seen as applying a safety margin on the mission conditions. No redundancy is present when this fails, but the design is based on mitigation, i.e. high glide performance minimizes damage to the UAV and ground conditions in case failure occurs.
- **Structures** The structure needs to be able to cope with all the load conditions described in the mission requirements and conditions. Both the fuselage and lift inducing surfaces have been designed for multiple load paths, and safety margins have been applied where appropriate to increase the reliability of

the structure. Multiple load paths can be seen as designing for active redundancy.

- **Propulsion** The single-engine propulsion system has no build in redundancy regarding thrust generation due to weight considerations. This subsystem has therefore also been designed based on mitigation. Windmilling and excessive noise generation have been mitigated by using a feathering propeller, which also allows for better glide performance in a OEI situation.
- **Power** The power subsystem is to provide electric power to the other subsystems. This is done using a generator attached to the engine, which also charges the battery. In case the generator fails, the charged battery is able to take over the functions of the generator. The battery will not be used to power other subsystems during nominal operation and is therefore categorized as standby parallel.
- **Fuel** The fuel feed subsystem has two pumps, one driven by power generated by the engine generator, and one driven by the battery. The battery driven pump is an example of standby redundancy. The engine driven pump will be sufficient to operate during nominal conditions. Only during failure of this pump will the battery driven pump be used, such that the engine can operate nominally and the UAV can continue the mission.
- **Stability & Control** Considering the stability of the UAV, the center of gravity range allowed has been sized for worse-case scenarios, ensuring stability in all flight conditions considered. The actuators for control surface deflections have been designed for UAV safety-critical systems, including multiple levels of redundancy within each component [71].
- **Avionics** Two mission computers, two flight computers and two transponders have been used to improve the reliability of the system. This active redundancy is important for UAV systems, especially autonomous UAVs like the WiFly system, which has minimal human interference.
- **Communication** Four radio cards have been used, double the amount that is needed for nominal operation. Two high power antennas and two low power antennas have been used to transfer data between UAVs. All of them are active at the same time, but a single high power antenna would suffice for the mission, depending on the line of sight of the single antenna. A high level of active redundancy is achieved, mainly due to line of sight considerations.
- **Payload** A passive antenna has been used, improving the reliability of the single antenna. Four transceivers are used in parallel, but all of them are needed to comply with all requirements of the mission. However, in case of a transceiver failure, the only thing affected is the capacity i.e. the amount of people that can connect to a single UAV. In most cases, not all UAVs will be loaded up till their maximum. The computer used has a Mean Time To Failure (MTTF) of 100k hours, or around 11 years of continuous operation. The ethernet switch used is connected in series to the transceivers, and therefore categorized as a critical component. However, it will not affect the UAV itself or the flight conditions. A quick calculation has shown that it is cheaper to fly back to base to repair the component and fly back than to include a second switch.

18.2 MAINTAINABILITY

Maintainability is defined as the ability of an item to be maintained. Topics such as ease of access, accuracy, safety and economy related to maintenance actions fall under this category. The definition is therefore often changed to the probability that a system to be maintained, will be ready after a defined period, under stated conditions.

Maintenance actions can be split into preventive and corrective maintenance, as presented in figure 18.2. The time needed for maintenance is the addition of all maintenance action times of both categories. Factors such as Mean Corrective Maintenance Time (MCMT), Mean Preventive Maintenance Time (MPMT), Mean Time To Maintain (MTTM) and Mean Down Time (MDT) will not be elaborated upon because these are dependent on logistic support and human factors. When the MTTM is known, the amount of labor hours and the costs associated with them can be calculated. Costs, both for equipment and labor, can only be properly estimated once the logistic support has been determined. This includes spare and repair parts, personnel, test and support equipment, documentation, computer software and facilities. Anthropometric factors were analyzed but based on the total size of a single WiFly UAV, these requirements will not pose any challenge.

The Mean Time Between Maintenance (MTBM) is not prevalent for the WiFly system, as it will only be operating during disasters. The availability of the system is influenced by this parameter, but it is unlikely that disasters severe enough to render the existing communication system useless, occur twice in the same region in a short period. The main focus of maintenance will be preventive maintenance, to ensure quick deployment in case of a disaster.

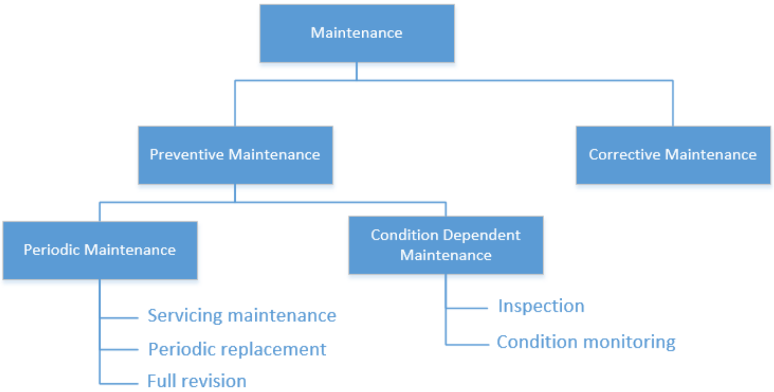

Figure 18.2: Maintenance actions

18.3 Availability

Availability is defined as the degree that a system will be ready or available when required for use. It is a result of reliability and maintainability and is often expressed as a fraction or percentage. The relation between reliability, availability, maintainability and safety is presented in figure 18.3. Three types of availability are defined. Inherent availability, achieved availability and operational availability. In the case of the WiFly system, operational availability is most prevalent, as it has to be able to perform properly in disaster areas on a short notice.

Availability for the WiFly system has to be high since disasters and their consequences that require the WiFly system will be severe. However, it has to be realized that when no disasters occur, the system has enough time for preventive maintenance procedures. Also, the swarm of UAVs can be sized for different scenarios, as not all disasters will require the full system to be launched. By using the swarm concept, availability is inherent, unless it is expected that the full system is needed to perform the mission. In all other situations, spare UAVs will ensure availability of the WiFly system.

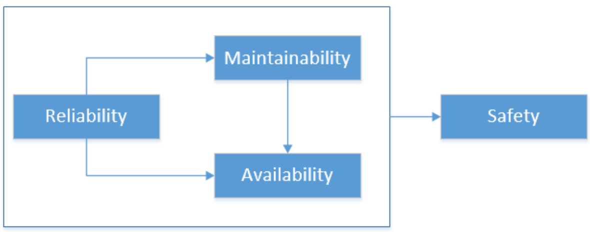

Figure 18.3: Relation between R, A, M and S

18.4 Safety

Freedom from hazards to humans and equipment is defined as Safety. Safety engineering is used to prevent or minimize loss or damage to humans, equipments, the design and the environment. Most of these considerations however are included in the design by considering the airworthiness requirements such as FAR CS-23. Technical risks outside the scope of the airworthiness requirements are discussed in chapter 19. Issues related to the environment are elaborated upon in chapter 20. The sensitivity analysis performed in chapter 14 will determine the sturdiness of the design.

19 | Risk Assessment

In order to quantify the uncertainty of the mission, a risk assessment needs to be performed. Though risk is always present, it is crucial that one aims at achieving the mission needs while minimizing the possible threats. For the safety of the project, risk assessment needs to be done at every step in the mission development. A too high risk may lead to the cancellation of the project. Moreover, greater losses may occur (like bankruptcy of the company) if the risk is not identified, or assessed incorrectly. At the current design stage all the components that the UAVs will have are known, therefore the risks can be analyzed in more detail compared to the previous report.

Risk Types

There are four types of risks: technical, cost, schedule and programmatic. One must keep in mind that the different risk categories are related. That is, a technical problem may delay the project and increase its cost while a tight schedule and low budgets will result in high technical risks. Since the design of the WiFly system is directly influenced by the technical risks, and all others are interdependent, these risks are the only ones elaborated upon.

Approaching Risk

Risk management involves five main phases: 1. Planning, 2. Risk Identification, 3. Risk Assessment, 4. Risk Analysis, 5. Risk Handling. Standard methods for dealing with risk exist, for example FMECA introduced in 1940s by the U.S. military is used for risk identification [88], Risk Map for assessing and risk item tracking for risk control. This chapter will treat identification and assessment of the system in section 19.1 and of the project in section 19.2. Risk control is achieved using among others the contingency allowance described in chapter 15.

19.1 System Risks and their Handling

A procedure called Technical Performance Measurement has been performed for the most important performance parameter of the WiFly system, the maximum takeoff weight (MTOW). This has been tracked since the design configuration was fixed at the end of the mid-term phase. Large variances of this parameter occurred.

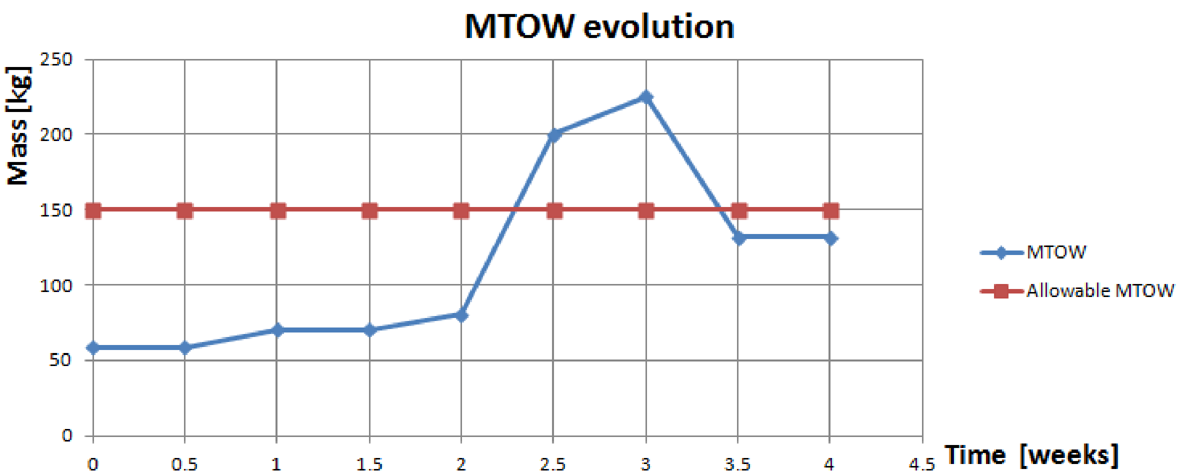

Figure 19.1: MTOW evolution since the beginning of the final report

As one can see in figure 19.1, the MTOW estimation just after the design was picked was just 58.5 kg. However that estimation relied on the aerodynamic properties estimated by Roskam [1]. When an XFLR 5 software simulation was performed, one could see that the initial estimation of the aerodynamic parameters was too optimistic. The new design would require more fuel and would weigh 70.3 kg. With this new weight a new, more powerful engine was needed to satisfy the requirements. This lead to a MTOW of 80.5 kg. When a power-plant was chosen, one could see that the performance levels provided by the engine data sheet were significantly inferior to those predicted. The MTOW spiked to 200 kg when the information on the engine data sheet has been used. After another iteration the MTOW increased to 230 kg. At this point if the weight was not decreased, totally new takeoff and landing systems had to be picked (catapult and sky-hook). To solve this issue the team decided to relax one of the requirements of the mission. Namely the cruise speed of the drones decreased from 300 km/h to 200 km/h allowing for a lower flight altitude (from 6000 m to 4000 m). The requirement change therefore lengthens the response time of the system.

System risks concern all risks related to the life cycle of the system. This includes the mission, operation and maintenance. This chapter will treat the identified mission risks. The technical risks are placed in a risk map in figure 19.2.

1. Factors such as severe rainfall or volcanic ash will decrease the connection quality between the UAVs and the ground, leading to a possible loss of communication. To mitigate this risk the system was designed to operate in 99% of the rains in Indonesia, as these are classified as the worst rains on earth.
2. The communication link (UAV to Base) is lost due to banking with a bank angle exceeding 25°. The mission has been adapted to limit the required bank angle.
3. Due to the minimum distance between two drones of twice the turn radius, dense locations on the ground (dense with people) may not be perfectly covered as only a limited number of drones could survey one region.
4. Overloading of the Random Access Channel, resulting in bad connection quality between the UAVs and the mobile phones on the ground.
5. Outside system reading or modifying the data transmitted between the UAV and the base. This risk has been mitigated by using an the encryption method used by the MD4000 hardware.
6. No authorization for the 900 MHz frequency band used by the payload.
7. Interference between the transmitting cells of the payload subsystem of different UAVs, resulting in an inferior link budget.
8. Loss of aerodynamic performance, controllability and means of propulsion due to ice formation.
9. Jammed flight controls during flight, possibly resulting in total loss of controlability. Mitigated by a high level of redundancy in component selection of related subsystems.
10. Loss of position and attitude determination, due to sensor instruments failing. This risk has been mitigated by using heated triple redundant pitot tubes and angle of attack sensors.
11. Reduced lift and aeroelastic instability due to having long and slender wings. This risk has been mitigated by designing the wing with such and event in mind.
12. Magnesium fuselage ignites or catches fire, resulting in total loss of a drone. This risk has been mitigated by using a special alloy with thermal properties similar to conventional aluminum.
13. Engine failure, resulting in loss of thrust and power generation. By using a feathering propeller and a battery, the impact of this risk is severely reduced.
14. Blocked inlet area, resulting in insufficient air for the engine to work. This has been mitigated by using a larger inlet than required, and a liquid cooling system to reduce the required air needs.
15. Bird strike, resulting in damage to the UAV, possibly leading to failure of the UAV itself. To mitigate this risk, the structure of the wing is designed such that only the wing box can carry all the load.
16. Collision between UAVs, resulting in damage or loss of one or more UAVs. This risk is reduced by fitting the system with transponders that provide their location.

19.2 PROJECT RISK

A project declared to have a high risk may be low on budget or time, or simply in danger of not achieving the imposed technical performance. That is, "the Systems Engineering Universe is established by technical performance, cost and schedule. All three dimensions are interconnected via risk" [89, slide 4].

Events that may pose a risk to the project are numerous. The risks do not end once the product is built and tested. Political factors play a significant role especially as the regulations on the use of drone are expected to change in the nearby future. Another possible political risk would be the sudden increase in the price of magnesium if products originating countries with poor working conditions are no longer allowed in Europe. This is a particular high risk as more than half of the world's magnesium resources are in China, Russia and

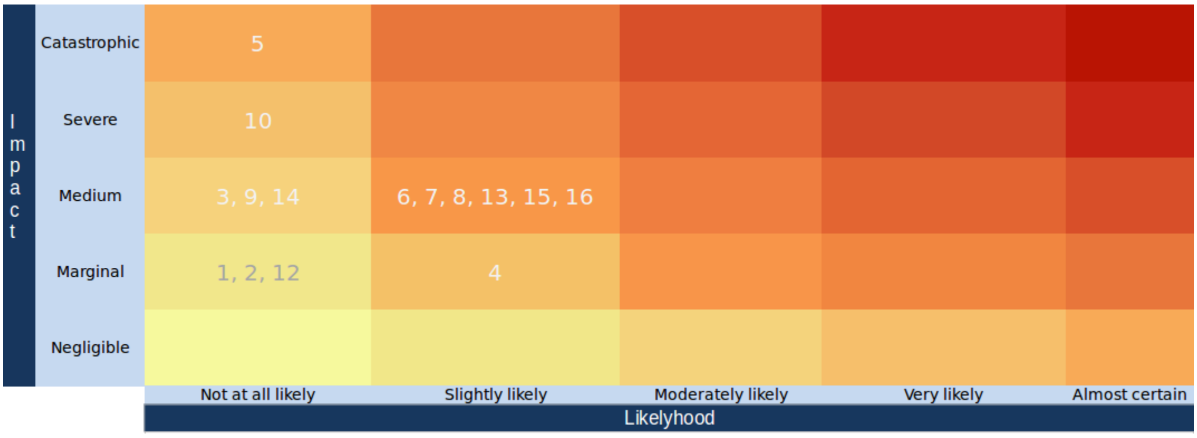

Figure 19.2: Technical Risks Map

North Korea. China supplies more than half of the world's magnesium. [1]. A non political risk that may occur after the launch of the product is the improper maintenance given by customers which want to do their own maintenance and service.

[1] see http://metalpedia.asianmetal.com/metal/magnesium/resources&production.shtml accessed on 17-jun-2016

20 | Sustainable Development

In this chapter the sustainable development strategy of the WiFly project is discussed. During all phases of development the system is being optimized for a circular economy, in other words a recyclable system. This is explained in section 20.1. After that the environmental impact of the system during operation is assessed. The noise produced by the aircraft is analyzed in section 20.2. Finally the emissions of the engine are discussed in section 20.3.

20.1 Circular Economy

The three points concerning the mid-term report will be discussed in this section. As stated in the mid-term report [3], the WiFly system should be designed with circular economy in mind. This new "way of thinking" is increasing in popularity throughout the market. The founding principles of circular economy are: non-existent waste (it is driving new cycles), modularization of the product (flexibility), renewable energy and design for systems. [90]

Today's economy is linear. The life of the product begins with the extraction of the raw material, undergoes transportation, manufacturing, use and disposal (waste). In order to close this loop, one would like to eliminate the disposal phase and have the product or its materials re-enter the economy. For that to happen a thoughtful initial design is required as well as a good business model.

The initial design must be made with circular economy in mind. The WiFly system should be durable (long lifetime), it must be easy to maintain and repair as well as easy to be dis-and re-assembled. Material hygiene (uniform use of materials) is needed to improve the level of recyclability. Modularity is another key element as it adds value to the product (multipurpose) and also increases its usability, while at the same time reducing the amount of units needed to operate in all mission scenarios. Ideas for modularization can be: having a payload compartment where different systems can be included depending on the need, e.g. an infra-red thermometer if the disaster is a wildfire, a Geiger counter in case of nuclear disasters, etc. Since disasters are rare, part of the system could be used for surveillance.

20.1.1 Materials

For the structural design, apart from designing a structure that is able to withstand the loads, the environmental aspects were of great concern. In this subsection the materials used and their environmental impact will be discussed.

The number of different materials used should be kept as low as possible. The amount of materials has an influence on several parts of the project. First of all, the complexity increases vastly when different types of materials are used, which decreases the material hygiene. Material hygiene is one of the 10 Golden principles on sustainability. To have a high material hygiene mixing of materials should be avoided and a clear and obvious structure should be adopted. Furthermore, the transportation pollution increases with increasing amount of material. More materials have to be transported to the production site leading to more cost and higher environmental impact. The materials used for the structural components are aluminum, magnesium and E-glass.

Aluminum is widely available so the transportation costs to, for example Europe, will be very low. Adding to that the recycling benefits, it approximately saves 95% of the energy required for primary aluminium production[1], thereby avoiding corresponding emissions, including greenhouse gases.

Magnesium is mainly produced in China, Russia and Canada so the transportation cost will be a bit higher, however, this is compensated by the fact that the lighter structure (due to the usage of magnesium) results in less pollution by the UAV itself. By using die casting for recycling the demand on primary magnesium can be

[1] see: http://recycling.world-aluminium.org/uploads/media/fl0000217.pdf accessed on: 17th of June, 2016

reduced up to 50%[2].

E-glass is produced all over the world including Europe. Therefore, transportation costs will be low. However, E-glass can not be recycled and used to produce new E-glass, but has to be decomposed. Even though no new E-glass can be produced, it can still be recycled into other (functional) materials. Cement manufacturers can use the E-glass to save on the use of primary materials. Recycling 1000 tonnes of E-glass in cement saves up to 450 tonnes of coal, 200 tonnes of chalk, 200 tonnes of sand and 150 tonnes of aluminum oxide[3].

20.2 NOISE

Today aircraft noise has become an aspect that has to be kept in mind during design more than ever. Noise emissions could potentially be harmful for humans when exposed to noise levels exceeding 80 dB [3]. The duration of exposure directly influences the severity of the harmful effect on humans and animals. Shortening the exposure time is not possible however, since the emergency network will be most useful during the first 72 hours a disaster has taken place. The noise emissions will therefore have to be limited to levels that are not harmful to humans. Noise levels of under 80 dB are not harmful for humans, no matter the exposure time. Three sources of noise emission have been identified for the UAVs in flight. They will be elaborated upon in the following paragraphs. Takeoff from the catapult system and retrieval with the Skyhook have not been taken into account. The duration for these phases are insignificant compared to the cruise and loiter phases.

Aerodynamic noise is the noise that arises due to aerodynamic perturbation of air. An example of this is the sound perceived when an aircraft reaches sonic speeds, i.e. breaking the sound barrier. The WiFly UAVs are flying at low subsonic speeds in the loiter phase, so such effects are not prevalent. CFD simulations and wind tunnel tests need to be performed to get accurate values for aerodynamic noise.

Control surface noise is the noise that arises due to perturbation of air due to control surface deflection. This is very similar to the aerodynamic noise and will follow the same procedure to obtain accurate values for the noise due to control surface deflections.

Engine noise is the noise caused by the engine and propeller. Rotary engines do not differ too much from piston engines when comparing noise values. A disadvantage to rotary engines is that when knocking occurs, it will continue knocking as only a single combustion chamber is present, indicating a fuel mixture that is too lean. This is countered by using a rich mixture, as described in section 6.2.4. Propeller noise is generally within acceptable limits when tip velocities do not approach sonic speeds [51]. The Republic XF-84 Thunderscreech has earned its nickname because the outer half of the propeller blades would travel at airspeeds higher than Mach 1. The propeller has been sized to counter this, which is elaborated upon in section 6.1.3.

Windmilling propellers, in a OEI situation, are known to produce excessive noise levels as well. This has also been addressed in section 6.1.3, by considering a feathering propeller for OEI situations. This will reduce structural damage, contribute to a favorable glide ratio and reduce noise levels.

20.3 EMISSIONS

As global warming gains more and more attention, it is important to consider the environmental impact of the system. Therefore, an estimate should be made of the expected emissions of the UAVs. It is however difficult to accurately estimate this, since there are many factors that influence the (ratios of) products that are formed in the combustion process. Among other parameters, the installed engine, engine setting, flight phase and air-fuel ratio all influence the amount and ratio of the greenhouse gases that are released.

Ideal combustion takes place when the air-fuel ratio is the stoichiometric ratio (for avgas 100LL this is approximately 15:1). In that case, all reactants are present in the perfect ratio and the fuel is burnt such that only CO_2 and H_2O are formed. In reality the combustion is never ideal, and other pollutants will be formed as well. When the air-fuel ratio is too rich, i.e. there is less air than required for the stoichiometric reaction

[2] see:https://www.dropbox.com/s/fw49oxxn8e8ie3j/Screenshot$%$202016-06-18$%$2023.32.14.png?dl=0 accessed on: 17th of June, 2016

[3] see:https://fiberline.com/news/miljoe/breakthrough-recycling-fibreglass-now-reality accessed on: 17th of June, 2016

to take place (oxygen deficiency), part of the fuel cannot react completely to CO_2 and H_2O and a complex mixture of CO and hydrocarbon molecules (generically denoted by C_xH_y) will form. Another cause for the production of pollutants is when the combustion temperature and pressure are high while the reaction time is short. Then, nitrogen (which makes up 78% of the volume in ambient air) and oxygen react in the combustion chamber to form nitrogen oxides (NO_x). Other pollutants include soot and lead bromides (due to the presence of lead in avgas 100LL). [91]

No indications of the emissions of UAVs that use the Rotron engine, which will also be installed on the WiFly system, are publicly available at this time. However, the composition of exhaust gases of other aircraft that run on avgas 100LL has been researched. Based on data for three single-engine piston aircraft, table 20.1 provides an estimated range of the expected emissions. The three aircraft for which data was found have a heavier engine (150-300 hp) and other factors such as efficiency and air-fuel ratio may differ substantially from those of the WiFly UAVs. Therefore, the values in the table serve as indications only. Usually, the value given for the expected CO_2 emissions is the ideal one obtained from stoichiometric analysis. The reason for this is that most of the CO and C_xH_y react to CO_2 (and H_2O) once it enters the atmosphere, and these two pollutants are therefore commonly considered part of the exhaust CO_2 mass.

Table 20.1: Avgas 100LL estimated emissions per kg of burned fuel, based on data from [92]

Compound	**Landing & Takeoff** [$g\,kg^{-1}$]	**Cruise** [$g\,kg^{-1}$]
CO_2	3170	3170
CO	700-1100	250-600
NO_x	2-9	15-45
C_xH_y	12.5-25	5-15
Soot	0.05	0.05
Lead	0.79	0.79

21 | Future Project Plan

Although this is the final report that concludes the DSE, the project itself can proceed further. Therefore, a schedule for further process will be presented in this chapter. It contains a short discussion on future tasks, project design and development logic, a Gantt chart and cost analysis.

21.1 Further Tasks and Development Logic

In this section the tasks left for development are discussed. From literature the following phases where discovered: updated detailed design, part prototyping and testing, prototyping, validating, optimizing, certifying, production, marketing, implementation, support and maintenance.

21.1.1 Updated Detailed Design

A small discussion will be provided for each system and subsystem provided in this report on what should be performed during the detailed design phase.

The communication payload that is responsible for the communication with mobile phones was mainly analyzed for its capacity. Reference components have been picked, but they are not optimal for use on the UAV. The first thing that will have to be done is the design of the transceivers based on the reference models. This will most likely also lower the cost that is budgeted for them. Once the transceivers have been designed the software can be written based upon the open source GSM stacks that are available. The reference model also makes use of the open source stack. The code will have to be modified to support features that are specific to the WiFly system for example the SMS credit system and cached web portal. With the transceiver and software completed the system can be tested and verified. After that the selection of the antenna can be reconsidered with a more thorough analysis and simulation. Then the combiner/splitter needs to be researched and designed to find an optimal configuration with the lowest weight and power loss. Once that is all done the packaging of the system for installation in the UAV can be designed including the tilting mechanism that contains the mounting point for the antenna. In parallel with the design activities it is advised to organize a meeting with the government to see if a permit can be obtained for transmission on the 900MHz band in exceptional circumstances like disasters. Potential customers would like to have certainty that there are no legal hurdles to take when the system has to be deployed.

For the stability and control subsystem the next steps involve developing the software around the UAV control and swarm movements. The autopilot that can control all the UAV maneuvers needs to be implemented and in parallel the swarm positioning algorithms need to be worked out. Finally, the interface for the ground system is required that connects the swarm positioning and UAV autopilot with commands from the swarm operators.

In order to guarantee that an accurate and complete aerodynamic analysis was performed on the UAV, the approach used has to be redefined. Firstly, with the CAD model of the UAV finished, a complete CFD model shall be implemented. This kind of simulation was impossible to perform during the DSE as it would have required a tremendous amount of time. This advanced simulation would offer accurate estimates of the aerodynamic parameters as the lift, drag and moment coefficient, which would influence the flight performance of the whole swarm considerably. Later on, in order to achieve even more reliable estimates for the aerodynamic parameters, a full model of the UAV should be placed in a wind tunnel and a complete test should be performed. This will offer the actual values for the aerodynamic parameters, so no more contingency factor would be used. With these terms fixed, the flight performance of the whole swarm is accurately defined and it can be completely predicted.

Using the datasheets from the engine manufacturer has resulted in a solid baseline for detailing the propulsion and power subsystem. Getting more accurate data from the engine manufacturer would improve this. Designing the fuel lines, heat transfer mechanisms and designing a propeller with a dedicated propeller manufacturer are the next steps in the design phase to be performed. Testing the engine and monitoring actual fuel consumption is a crucial step to be performed, as the required fuel needs to be accurately calculated. Maximum thrust and propeller performance can also be determined in a test setting.

In order to complete the design of the electrical system, first all parts should be selected. For example, at this stage no specific fuel pumps and anti-icing systems have been selected yet. Once this has been done, the wiring of the system can be designed. It would be helpful to obtain a detailed data sheet of the generator such that its power output and behavior is better understood. The choice of battery could be reconsidered as for example there may be reasons to choose another type than a LiPo battery.

The structural analysis could be improved in many ways as was described in section 5.8. It mostly consists of generating more load cases, generate dynamic load cases, designing the mounts, model the force introductions, model the stress concentrations and modeling elastic effects. In the end optimization needs to be performed.

Lastly the ground base should be designed, this has barely been done until now. The base station includes the command and control center and operational objects like catapults and skyhook and a bigger fuel tank. It can also be recommended to include some repair facilities. It should be noted that the ground station should be designed in such a way that operations can be done independent from existing local facilities because they might not be available after the disasters.

21.1.2 PART, SYSTEM PROTOTYPING AND TESTING

The part, system prototyping and testing starts halfway during the detailed design. At first not a whole drone and ground station system will be built but parts and systems will be produced. These parts can then be used for testing as it is a lot cheaper to test parts than to test the whole system. Aerodynamics can be tested in a wind-tunnel with a mock-up. The telecommunication can be tested by connecting phones with it while adding for example rain or frequency interference. Control and stability can be tested by simulation or implementation in existing (smaller) drones.

21.1.3 PROTOTYPING AND VALIDATION

This phase consists of building a real size prototype so that the performance of the design can be tested. Then the results should be discussed with the stakeholders and changes might be required. Here not only the performance with respect to the requirements are made but the performance will be compared with the needs and expectations of the customers. Because the system is not certified by the authorities yet, these tests should be performed on specific test tracks where it cannot pose a threat to others. After this phase a choice should be made on whether the design should change or whether it is good enough to enter the production phase. If this is the case the following phase can be started.

21.1.4 CERTIFICATION

Certification might be a major problem for our project. It is a small project that needs to be certified for almost all countries in the world. Certification takes a lot of time and money. With the rules as they currently are, the product will have to be certified in all EU countries separately. EASA does not test search and rescue drones, but the regulations in most countries will resemble the CS-23 [55] and FAR part 23 regulations. However, it has been announced that the regulations will change in the foreseeable future. A lot remains unknown about the new regulations and making accurate estimations on the time and budget is not possible at this point.

21.1.5 PRODUCTION

When certification has been completed and the required changes have been implemented and tested, production can start. During production not only the drones and ground systems will be produced but also spare parts. The production costs are €64,100 per piece section 15.1.1 and estimating the time required is hard to estimate. More should be known about the production methods and scale before this estimate can be made accurately.

21.1.6 MARKETING

This phase is started at the beginning of the project and continues throughout the whole project, and before the production starts at least one customer should be known otherwise the risks are too high. Marketing consists first of all out of brand awareness. This can be achieved by presenting our project and its benefits to rescue teams and organizations all over the world. During these presentations feedback can be given on the functionality of the product and this could then be implemented in the design. This would help to fit the product more to the customer's needs.

21.1.7 IMPLEMENTATION, SUPPORT AND MAINTENANCE

These phases take place after selling the product. Implementation is helping the teams who are going to work with the product. Support consists of training personnel, executing small design changes if required and performing maintenance. It is not yet known whether this phase is done by the WiFly team or by external organizations.

21.2 PROJECT DESIGN & DEVELOPMENT LOGIC

In this section a flow diagram will show the next phases of the project including the tasks that will have to be done. The flow diagram is depicted in figure 21.1.

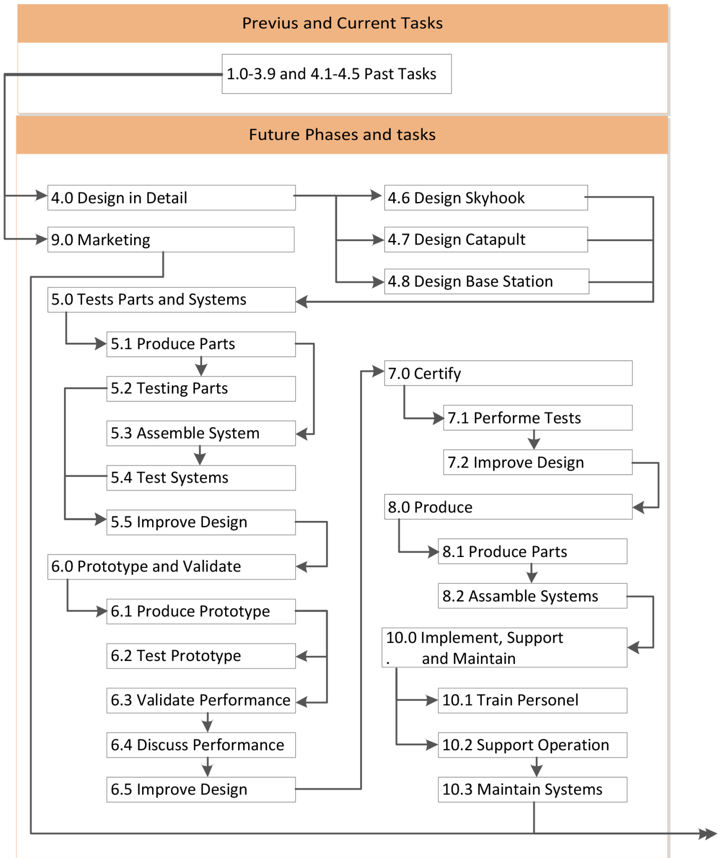

Figure 21.1: The work flow diagram for the next steps of the WiFly project

21.3 GANTT CHART

From the phases explained before, a small Gantt chart was made. The durations of the phases in the Gantt chart are based on crude estimates. The engineering time estimates come from the engineering teams, the other time estimates were taken from existing projects.

22 | Conclusion

An emergency communication network for disaster areas is provided by an autonomous swarm of 45 Unmanned Aerial Vehicles. These UAVs are capable of providing victims with emergency information, locating and mapping mobile telephones, while also providing Search and Rescue teams with an initial assessment of the situation. This is most crucial in the first 24 hours after a disaster has taken place, as most people will be in need for rescue and medical services.

The system has been designed for an area of 100 km^2, in which 300 thousand people are affected by a disaster. To fulfill the need for a communication network, a communication system has been designed that is able to perform the following for at least 24 hours:

- **SMS Service** SMS is the most reliable type of communication that works with the old GSM standard to ensure communication for all mobile phones. The amount of SMS that can be sent is throttled to prevent overload in case all victims try to connect at the same time.
- **SMS Broadcast** To quickly provide emergency information, a cell broadcast function is added to the communication system. This allows the operators, in collaboration with the rescue services, to quickly distribute safety and medical information.
- **Emergency Web Portal** More elaborate first aid and safety information is provided by the Emergency Web Portal. This will mostly be text based information with the addition of maps of the affected area for the victims. This portal is cached on the UAV to limit traffic loads.

Based on the design for the communication system, a mission for the swarm of UAVs is drafted. The two main functions that the system has to fulfill from a technical point of view is to arrive quickly (3 hour cruise phase, 200 km/h at 4000m) at the disaster area and fly for a long time (24 hour loiter phase, 108 km/h at 2000m) above the disaster area itself. These functions differ fundamentally, resulting in different altitudes, power requirements and load cases. A swarm of UAVs is designed to comply with the required altitudes, range, endurance and performance. An overview of the main subsystem design choices and their effect on the mission is provided below:

- **Aerodynamics** The LA203A airfoil, a high endurance airfoil, has been used to comply with the 24 hour communication network providing loiter part of the mission. A V-tail, based on the NACA 0009 airfoil, was found to be the most appropriate tail to comply with the technical requirements. An in-depth aerodynamic analysis using XFLR5 and emperical Roskam methods provides all aerodynamic parameters to be used in other subsystems.
- **Propulsion** The Rotron 300 EFI LCR, 32 HP engine is used in a fuselage buried pusher configuration. This engine and configuration allows for lower aerodynamic drag characteristics, whilst decreasing the net thrust. This adverse effect is countered by the design of a three bladed 39 inch feathering constant speed controllable pitch propeller, which is adjustable for different flight phases.
- **Power** An AC generator is installed to convert part of the power provided by the engine to electrical power, which powers the payload, flight computer and mission computer. These computers in turn power all other appliances on the UAVs. A battery is installed as a backup power source in case the engine or generator fails, to not worsen the situation on the ground.
- **Structures** A load case analysis identified flying through a gust to be the critical scenario from a structural point of view. A wingbox made out of cheap aluminium 6061 is able to cope with all these loads, while enclosing enough volume to be used as a fuel tank.
- **Stability and Control** Ruddervators on the V-tail and ailerons on the main wing have shown through stability analysis that they are able to stabilize and control the UAV in all flight phases with the worst case perturbations.
- **Communication** The communication between UAVs and communications with the base is sized based on the set of different links that will be encountered during the mission. The radio cards, mesh node hardware, antennas and amplifiers chosen ensure a communication range of 20 km between UAVs, and 200 km range between UAVs and base.
- **Avionics** A flight computer is used to control the UAV and provides autopilot functions. A mission computer and transponder are used to increase the level of autonomy. These components will be placed

twice in the UAV to increase the reliability of the autonomous UAV.

An analysis of different disaster types and areas results in many scenarios the WiFly system has to be able to operate in. Furthermore the behaviour of the swarm, its opportunities and threats, must be accounted for in the design of the UAV. An overview of the choices made for the takeoff, landing and swarm operation is provided below:

- **Takeoff** A bungee chord catapult system, using linear force bungee cables by Sandow Technic, is used to takeoff no matter the environmental situation due to the disaster. It is sized to accelerate the UAVs to 10% above the stall speed in a situation with 10 Bft headwinds.
- **Landing** To complement the fact that no landing system has been used for takeoff, a Skyhook will be used as the aerial retrieval system. It shares the same set of advantages as the bungee chord system, enabling retrieval indifferent of the environmental situation.
- **Swarm** The V shaped flight formation in cruise allows for fuel savings by utilizing the wing tip vorticity. Path planning, collision avoidance and usage of digital pheromones are used as design principles to create a draft version of the control system for autonomous swarm flight.

Affirmation of the design choices made is provided by a performance analysis on both the UAVs and the design itself. Results of this analysis are used to evaluate whether the WiFly system complies with all stakeholder requirements, and thus fulfill the mission.

- **Flight performance** The rate of climb, glide and maneuvering performance are evaluated to obtain an understanding of the capabilities and behaviour of the designed UAV. Cruise altitude is reached within 20 minutes. In a One Engine Inoperative situation, all WiFly UAVs are able to glide nearly 50 km at loiter altitude, double at cruise altitude. A turn radius of 384 meter, with a bank angle of 32 degrees influences the choice of hardware used for the payload communication subsystem.
- **Design performance** The sensitivity of the design to changes in input parameters presents an idea of how sturdy design is. The design is very sensitive to the chosen cruise speed, due to its effect on the required fuel mass. This effect snowballs through the design, increasing the maximum takeoff weight greatly. Miminum cruise velocity is therefore preferred, and determined to be 108 km/h. The sensitivity to payload weight is minimal, allowing for modular design. A relative change in aspect ratio would decrease the performance in loiter and/or cruise.

The risks accompanied with, and due to, the design, operation and environment of the WiFly system are evaluated to rationalize the feasibility of the system. Verification and validation has been performed to ensure the precision of the used computational tools. A Reliability, Availability, Maintainability and Safety analysis is performed to address non-technical design principles. Technical risks identified in earlier design stages are reevaluated, and appropriate contingency actions are taken where needed to decrease the risk. Most of the risks are mitigated or avoided by using parallel redundant design where possible, to ensure a high level of reliability and availability.

Adopting a circular economy and keeping up a high level of material hygiene will decrease the cost of the system over its lifetime. The noise and fuel emissions have been determined to estimate the impact of the WiFly system on the environment. The design choices made by the propulsion subsystem minimizes the negative impact of the system. Steps to be performed for detailed design are part prototyping and testing, system prototyping, validation tests and design optimization. Most of these steps include testing and advanced computational models, which for this stage are outside the scope of the project. Once the design is optimized, certification, production, marketing, implementation, support and maintenance needs to be designed and performed to complete the life cycle.

It can be concluded that technically, this project is feasible. The main issue for all subsystem designs is the fact that the UAV has two crucial, but fundamentally different phases. Flying somewhere fast (cruise) requires a different design compared to flying for a long time (loiter). On the other hand, creating a emergency communication network with a swarm of UAV's, capable of flying in worst case conditions in disaster areas is difficult to realize within a budget of 3 million Euro, due to the current technology and prices of the communication system. Advancement of technology in this sector would greatly reduce the price of the WiFly system, increasing the feasibility of the final product.

BIBLIOGRAPHY

[1] J. Roskam and C.-T. E. Lan, *Airplane Aerodynamics and Performance.* DARcorporation, 1997.

[2] D. P. Raymer, *Aircraft Design: A Conceptual Approach*, 2nd ed. Washington, D.C.: American Institute of Aeronautics and Astronautics, Inc., 1992, ISBN-10: 0930403517.

[3] L. Bermel, H. F. C. Hendrikx, A. Jürisson, A. J. J. Lagerweij, G. H. M. Lebesque, V. T. Mateescu, N. V. Meima, T. Nguyen, A. A. Prodan, and C. A. M. Socci, "Midterm Report, WiFly: An emergency communication network for disaster areas," May 2016, DSE-Project.

[4] ——, "Baseline Report, WiFly: An emergency communication network for disaster areas," May 2016, DSE-Project.

[5] G. Association. (2015) The Mobile Economy. GSM Association. [Online]. Available: http://www.gsmamobileeconomy.com/GSMA_Global_Mobile_Economy_Report_2015.pdf

[6] *Digital cellular telecommunications system (Phase 2+); Technical realization of the Short Message Service (SMS)*, 3rd Generation Partnership Project (3GPP) Std., Rev. ETSI TS 100 901 V7.5.0, December 2001, 3GPP TS 03.40 version 7.5.0 Release 1998.

[7] (2001, August) Riding the lightwave down and back up. B&C Consulting Services.

[8] *Digital cellular telecommunications system (Phase 2+); Technical realization of Short Message Service Cell Broadcast (SMSCB)*, European Telecommunications Standards Institute Std., Rev. Version 5.3.0, July 1996, GSM 03.41.

[9] M. Sauter, *From GSM to LTE: An Introduction to Mobile Networks and Mobile Broadband.* Wiley, 2011.

[10] (2015, November) Bevolking; kerncijfers [dataset]. Centraal Bureau voor de Statistiek. [Online]. Available: http://statline.cbs.nl/Statweb/publication/?DM=SLNL&PA=37296ned&D1=52-56&D2=0,10,20,30,40,50,(l-1)-l&VW=T

[11] E. Salomon and E. Beaumont. (2002, January) Sdcch usage and dimensioning. Alcatel.

[12] *Digital cellular telecommunications system (Phase 2+); Radio Transmission and Reception*, 3rd Generation Partnership Project (3GPP) Std., Rev. ETSI TS 100 910 V8.20.0, November 2005, 3GPP TS 05.05 version 8.20.0 Release 1999.

[13] *SatSite Model 142*, SS7ware, 2016. [Online]. Available: http://yatebts.com/products/satsite/satsite_datasheet

[14] A. Cervone. (2014, September) AE2111-II Lecture 04: Spacecraft Telecommunications. TU Delft. [Online]. Available: https://blackboard.tudelft.nl/bbcswebdav/pid-2259460-dt-content-rid-7890359_2/courses/32552-141501/AE2111-II%20Lecture%2004_Telecommunications.pdf

[15] International Telecommunication Union, "Attenuation by atmospheric gases," ITU, Place des Nations 1211 Geneva 20 Switzerland, Report, 2013, Report ITU-R P.676-10.

[16] ——, "Specific attenuation model for rain for use in prediction methods," ITU, Place des Nations 1211 Geneva 20 Switzerland, Report, 2005, Recommendation ITU-R P.838-3 .

[17] Rain fade calculations. [Online]. Available: http://www.philsrockets.org.uk/Rain%20Fades.pdf

[18] S. Heppe, *Handbook of Unmanned Aerial Vehicles - (Chapter) Problem of UAV Communications.* Springer Science, 2015.

[19] Peter Joseph Bevelacqua. Polarization of plane waves and antennas. Website. . [Online]. Available: http://www.antenna-theory.com/basics/polarization.php

[20] Meshdynamics INC. (2009, May) Mesh dynamics md4000 overview. Presentation. Meshdynamics INC.

[21] Meshdynamics INC. Meshdynamics md4000 brochure. Meshdynamics INC. [Online]. Available: http://meshdynamics.com/documents/MD4000_BROCHURE.pdf

[22] Ubiquiti Networks. Xtremerange2 technical sheet. Ubiquiti Networks. [Online]. Available: https://dl.ubnt.com/xr2_datasheet.pdf

[23] ——. Xtremerange4 technical sheet. Ubiquiti Networks. [Online]. Available: https://dl.ubnt.com/xr4_datasheet.pdf

[24] ——. Xtremerange5 technical sheet. Ubiquiti Networks. [Online]. Available: https://www.fratec.net/pdf/xr5_datasheet.pdf

[25] T. R. Systems. Ttrm1004-d02 technical specifications. [Online]. Available: http://triadrf.com/pdf/TTRM1004-D02.pdf

[26] Cobham Antennas. Oa4-2.5v/9205 technical sheet. Cobham Antennas. [Online]. Available: http://www.european-antennas.co.uk/media/1261/ds9205.pdf

[27] E. A. Ltd. Oa4-2.5v/9205 technical specifications. [Online]. Available: http://www.european-antennas.co.uk/media/1261/ds9205.pdf

[28] Cobham Antennas. Aba-2.3v/1964 technical sheet. Cobham Antennas. [Online]. Available: http://www.european-antennas.co.uk/media/1328/ds1964ra.pdf

[29] U. G. P. Office, "U.s. standard atmosphere 1976," National Aeronautics and Space Administration, Washington D.C., United States, Investigation and analysis report, 1976, NASA-TM-X-74335.

[30] J. John D. Anderson, *Aircraft Performance and Design.* Singapore: WCB McGraw-Hill, 1990, ISBN-10: 0071160108.

[31] D. S. M. Niță, *Estimating the Oswald factor from basic aircraft geometrical parameters.* 20099 Hamburg, Germany: Hamburg University of Applied Sciences, Hamburg, 1990.

[32] S. Gudmundsson, *General Aviation Aircraft Design*, 1st ed. The Boulevard, Langford Lane, Kidlington, Oxford OX5 1GB, UK: Elsevier, 2014, ISBN-13:: 9780123973085.

[33] O. E. Vatandas and A. Anteplioglu, "Aerodynamic performance comparison of v-tail and conventional tail for an unmanned vehicle," in *Recent Advances in Space Technologies (RAST), 2015 7th International Conference on.* IEEE, 2015, pp. 655–658.

[34] K. G. Budinski and M. K. Budinski, *Engineering Materials: Properties and Selection (9th Edition).* Pearson, 2011.

[35] D. P. R. Ph.D, *Simplified Aircraft Design for Homebuilders.* Design Dimension Press, 2002, ISBN-10: 0972239707.

[36] T. Megson, *Aircraft Structures for Engineering Students, Fifth Edition (Elsevier Aerospace Engineering).* Butterworth-Heinemann, 2012.

[37] M. Sadraey, *Aircraft Performance.* VDM Publishing, 2009. [Online]. Available: https://books.google.nl/books?id=7m8LQgAACAAJ

[38] E. F. Bruhn, R. J. H. Bollard, L. E. Hackman, G. Lianis, W. F. McCombs, A. F. Schmitt, C. R. Smith, and J. A. Wolf, *Analysis and Design of Flight Vehicle Structures.* Tri-State Offset Company, June 1973.

[39] L. A. Harris, H. S. Suer, W. Skene, and R. Benjamin, "The stability of thin-walled unstiffened circular cylinders under axial compression including the effects of internal pressure," *Journal of the Aeronautical Sciences (Institute of the Aeronautical Sciences)*, vol. 24, no. 8, pp. 587–596, August 1957. [Online]. Available: http://dx.doi.org/10.2514/8.3911

[40] H. S. Suer, W. Skene, R. Benjamin, and L. A. Harris, “The bending stability of thin-walled unstiffened circular cylinders including the effects of internal pressure,” *Journal of the Aerospace Sciences*, vol. 25, no. 5, pp. 281–287, may 1958. [Online]. Available: http://dx.doi.org/10.2514/8.7639

[41] G. Gerard and H. Becker, “Handbook of structural stability, part iii - buckling of curved plates and shells,” National Advisory Committee for Aeronautics/NASA, NACA Technical Note 3783, 1957, ISBN-13: 978-1-68015-628-7. [Online]. Available: http://app.knovel.com/hotlink/toc/id:kpHSSPIII5/handbook-structural-stability/handbook-structural-stability

[42] E. L. Dreizin, C. H. Berman, and E. P. Vicenzi, “Condensed-phase modifications in magnesium particle combustion in air,” *Combustion and Flame*, vol. 122, no. 1-2, pp. 30–42, jul 2000. [Online]. Available: http://dx.doi.org/10.1016/S0010-2180(00)00101-2

[43] T. Satoh, H. Ueno, and Y. Ogawa, “High-strength non-combustible magnesium alloy,” Oct. 29 2009, uS Patent App. 12/439,601. [Online]. Available: http://www.google.com/patents/US20090269237

[44] K. Masaki, Y. Ochi, T. Kakiuchi, K. Kurata, T. Hirasawa, T. Matsumura, Y. Takigawa, and K. Higashi, “High cycle fatigue property of extruded non-combustible mg alloy AMCa602,” *MATERIALS TRANSACTIONS*, vol. 49, no. 5, pp. 1148–1156, 2008. [Online]. Available: http://dx.doi.org/10.2320/matertrans.MC2007108

[45] K. TOKAJI, “Fatigue behaviour and fracture mechanism of a rolled AZ31 magnesium alloy,” *International Journal of Fatigue*, vol. 26, no. 11, pp. 1217–1224, nov 2004. [Online]. Available: http://dx.doi.org/10.1016/j.ijfatigue.2004.03.015

[46] F. Lv, F. Yang, Q. Duan, Y. Yang, S. Wu, S. Li, and Z. Zhang, “Fatigue properties of rolled magnesium alloy (AZ31) sheet: Influence of specimen orientation,” *International Journal of Fatigue*, vol. 33, no. 5, pp. 672–682, may 2011. [Online]. Available: http://dx.doi.org/10.1016/j.ijfatigue.2010.10.013

[47] Aerospace Specification Metals Inc., *Structural Alloys Handbook*. John M. (Tim) Holt, 1996 edition.

[48] J. I. C. Olivier A. Bauchau, *Structural Analysis: With Applications to Aerospace Structures*. Springer, 2009.

[49] R. Martin and D. Evans, “Reducing Costs in Aircraft: The Metals Affordability Initiative Consortium,” *JOM*, pp. –, - 2000.

[50] P. Thokala, “Life cycle cost modeling of uavs,” School of Engineering Sciences University of Southampton, NACA Technical Note 3783, 2016. [Online]. Available: http://www.southampton.ac.uk/assets/schools/ses_posters/62$%$20life$%$20cycle$%$20cost$%$20modelling$%$20of$%$20uavs.pdf

[51] S. Gudmundsson, *General Aviation Aircraft Design: Applied Methods and Procedures*. Oxford, England, UK: Butterworth-Heinemann, 2013, ISBN-10: 0123973082.

[52] M. H. Sadraey, *Aircraft Design: A Systems Engineering Approach*. Chichester, England, UK: John Wiley & Sons, 2012, ISBN-10: 1119953405.

[53] V. Shmyrov, R. Tsukanov, A. Ryzhenko, and V. Pehterev. (2010, February) Airplane Power Plants Systems Designing. Kharkiv Aviation Institute. [Online]. Available: http://smolenskcrash.com/smol_conf/dane/airplane_powerplant_design.pdf

[54] F. Hitchens, *Propeller Aerodynamics*. AUK Academic, May 2015.

[55] *Certification Specifications and Acceptable Means of Compliance for Normal, Utility, Aerobatic, and Commuter Category Aeroplanes CS-23*, European Aviation Safety Agency (EASA) Std. ED Decision 2015/018/R, Rev. Amendment 4, July 2015.

[56] D. Stinton, *The Design of the Aeroplane*. Bsp Professional Books, 1985.

[57] R. P. Limited, *Engine Manual Rotron EFI 300*, 2015th ed., Rotron Power Limited, Dorset, UK, mar 2015.

[58] E. Goodger and R. Vere, *Aviation Fuels Technology*. London: Palgrave Macmillan, 1985, ISBN-10: 0333357876.

[59] Unleaded AVGAS Transition Aviation Rulemaking Committee, "FAA UAT ARC Final Report Part I: Unleaded AVGAS Findings & Recommendations," Federal Aviation Administration, U.S. Department of Transportation, Washington, D.C., Tech. Rep., 2012.

[60] R. Langton, C. Clark, M. Hewitt, and L. Richards, *Aircraft Fuel Systems*. Chichester, England, UK: John Wiley & Sons, Ltd., 2009, ISBN-10: 047005708.

[61] Federal Aviation Administration, *Aviation Maintenance Technician Handbook—Airframe: FAA-H-8083-31*. Newcastle, Washington, USA: Aviation Supplies and Academics, Inc., 2012, vol. 2, ISBN-10: 1560279508.

[62] I. Moir and A. Seabridge, *Aircraft Systems: Mechanical, electrical, and avionics subsystems integration*. Chichester, England, UK: John Wiley & Sons, Ltd., 2013, ISBN-10: 0470059966.

[63] ——, *Design and Development of Aircraft Systems*. Chichester, England, UK: John Wiley & Sons, Ltd., 2013, ISBN-10: 1119941199.

[64] ——, *Civil Avionics Systems*. London: Professional Engineering Publishing, Ltd., 2003, ISBN-10: 1563475898.

[65] E. K. A. Gill, G. La Rocca, and V. W. J. C. (2016, February) Course Organization & System Engineering for Aerospace. Delft University of Technology Aerospace Engineering Faculty. Kluyverweg 1 2629HS Delft, the Netherlands. Blackboard non public. [Online]. Available: https://blackboard.tudelft.nl/bbcswebdav/pid-2524909-dt-content-rid-9118932_2/courses/35051-151603/AE3201-L01-SEforAerospace-V09.pdf

[66] ——. (2016, February) System Engineering Methods. Delft University of Technology Aerospace Engineering Faculty. Kluyverweg 1 2629HS Delft, the Netherlands. Blackboard non public. [Online]. Available: https://blackboard.tudelft.nl/bbcswebdav/pid-2524910-dt-content-rid-9122763_2/courses/35051-151603/AE3201-L02-Methods-V10.pdf

[67] C. K. W.A. Timmer, R. De Breuker, *AE2111-I Systems Design, Project Reader - Aircraft*. TU Delft, 2014.

[68] M. Drela, "Athena vortex lattices program," Sebtember 2004, 29 Jan 15 MacOSX executable for AVL 3.35 (courtesy of Harold Youngren).

[69] FAA. (2016, June) Parvus duracor 311. Curtiss Wright. [Online]. Available: https://www.curtisswrightds.com/products/electronic-systems/rugged-mission-computing/duracor-mission-computers/duracor-311.html

[70] U. Navigation. (2016, June) Vector technical specifications. UAV Navigation. [Online]. Available: http://www.uavnavigation.com/support/kb/autopilots/vector/vector-technical-specification

[71] P. Actuators. (2016, June) Pa-rr-260-8 redundant servo actuator. Pegasus Actuators GmbH. [Online]. Available: http://www.pegasus-actuators.com/products/redundant-actuators/pa-rr-260-8

[72] Gill. (2016, June) Gslevel-4223. Gill Sensors & Control. [Online]. Available: http://www.gillsc.com/assets/Uploads/GSlevel-LD4223-Iss-3.pdf

[73] FAA. (2016, May) Ads-b faq. Federal Aviation Administration. [Online]. Available: https://www.faa.gov/nextgen/programs/adsb/faq/

[74] Sagetech. (2016, June) Mx transponder. Sagetech Corporation. [Online]. Available: http://sagetechcorp.com/mx-transponders.html

[75] H. X. Technology. (2016, June) Jzc-n51820l. Hangzhou Xiongmai Technology Co. [Online]. Available: http://www.xiongmaitech.com/en/index.php/product/product-detail/27/104/65

[76] A. Nagel and M. Shepshelovich, "Development of High-Lift UAV Wings," *24th Applied Aerodynamics Conference*, pp. 10–14, June 2006.

[77] N. Grumman. (2006, October) Global Hawk, Integrated Risk Management. U.S. Air Force. Distribution Unlimited. [Online]. Available: http://www.dtic.mil/ndia/2006systems/Thursday/atkin.pdf

[78] Deputy Assistant Secretary for Budget. (2010, February) Fiscal year 2011 budget estimates: Aircraft procurement. Presentation. United States Air Force.

[79] Z. Novaković, N. Medar, and L. Mitrović, "Increasing launch capability of a uav bungee catapult," *Scientific Technical Review*, vol. 64, no. 4, pp. 17–26, 2014.

[80] Insitu Inc. (2015, August) Rq-21a blackjack. Insitu Inc. [Online]. Available: https://insitu.com/images/uploads/pdfs/RQ-21ABlackjack_v2_ProductCard_PR120115.pdf

[81] I. Inc. (2015, August) Mark 3 skyhook. Insitu Inc. [Online]. Available: https://insitu.com/images/uploads/pdfs/SkyHook_Mark3_ProductCard_PR051915.pdf

[82] Gopalarathnam, "Aerodynamic benefit of aircraft formation flight," *Encyclopedia of Aerospace Engineering*, 2010.

[83] M. Voskuijl. (2011, April) Lecture 02 Climb and Decent Performance. Delft University of Technology Aerospace Engineering Faculty. Kluyverweg 1 2629HS Delft, the Netherlands. Blackboard non public. [Online]. Available: https://blackboard.tudelft.nl/bbcswebdav/pid-2210970-dt-content-rid-7454900_2/xid-7454900_2

[84] Aerospace and Ocean Engineering - Virginia Polytechnic Institute and State University, "Gliding flight (steady state) perfromance," Online, 925 Prices Fork Rd,Blacksburg, VA 24060,Verenigde Staten, March 2003.

[85] Grand View Research, Inc., "Commercial UAV Market Analysis By Product (Fixed Wing, Rotary Blade, Nano, Hybrid), By Application (Agriculture, Energy, Government, Media & Entertainment) And Segment Forecasts To 2022," Grand View Research, Inc., Tech. Rep., 2015.

[86] Ramón López Pereira. Validation of software for the calculation of aerodynamic coefficients. Linköpings Universitet Tekniska Högskolan. [Online]. Available: http://www.diva-portal.org/smash/get/diva2:329418/fulltext01.pdf

[87] v. T. M. Hamann, R.J. (2006, January) Systems engineering & technical management techniques part 2. Delft University of Technology Aerospace Engineering Faculty. Blackboard non public. [Online]. Available: https://blackboard.tudelft.nl/bbcswebdav/pid-2691330-dt-content-rid-9278491_2/courses/35047-151604/AE3-S01%20-%20Systems%20Engineering%20%26%20Technical%20Management%20-%20Part%202.pdf

[88] P. Hopkin, *Fundamentals of Risk Management: Understanding, Evaluating and Implementing Effective Risk Management*, I. of Risk Management, Ed. Kogan Page, 2012, vol. 2, ISBN-10: 0749465395.

[89] W. J. C. Verhagen, R. Curran, E. K. A. Gill, and L. R. G. (2016, March) Risk Management & Reliability Engineering. Delft University of Technology Aerospace Engineering Faculty. Kluyverweg 1 2629HS Delft, the Netherlands. Blackboard non public. [Online]. Available: https://blackboard.tudelft.nl/bbcswebdav/pid-2524917-dt-content-rid-9170170_2/courses/35051-151603/AE3221-L08-Risk%20%26%20Reliability%20%282015-2016%29.pdf

[90] K. Habermann. (2015, September) MF2032 Eco Design Business Models. KTA Bilda. Non public. [Online]. Available: https://bilda.kth.se/courseId/12732/node.do?id=24020515&ts=1441614309425&u=-4773342

[91] M. G. Zanin, "The green airport concept and the international flight academy on biofuels," Master Thesis, Baylor University, December 2007.

[92] T. Rindlisbacher, "Aircraft piston engine emissions summary report," Federal Office of Civil Aviation (FOCA) Switzerland, Technical Report, 2007.

A | Functional Diagrams

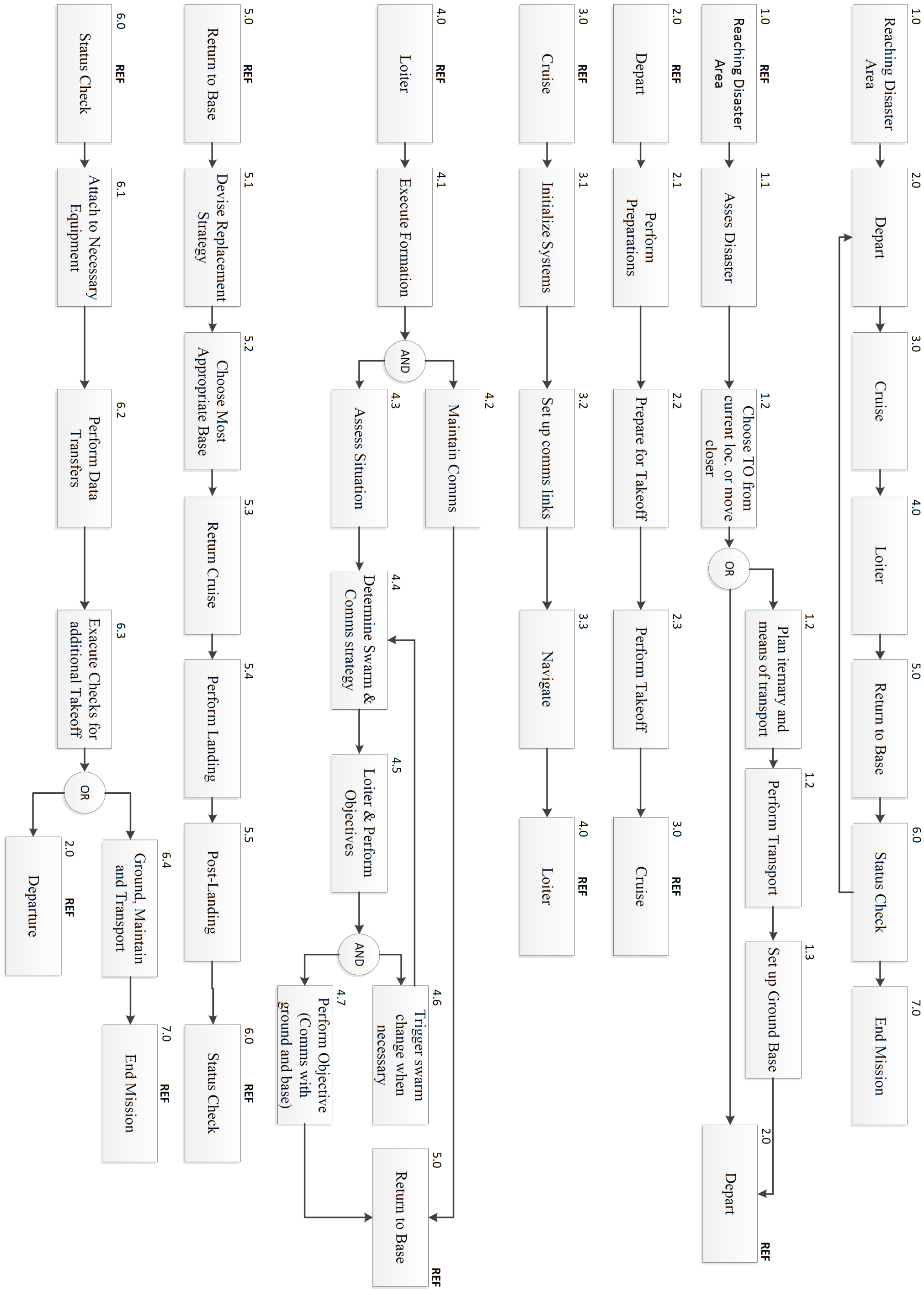

Figure A.1: Functional Flow Diagram

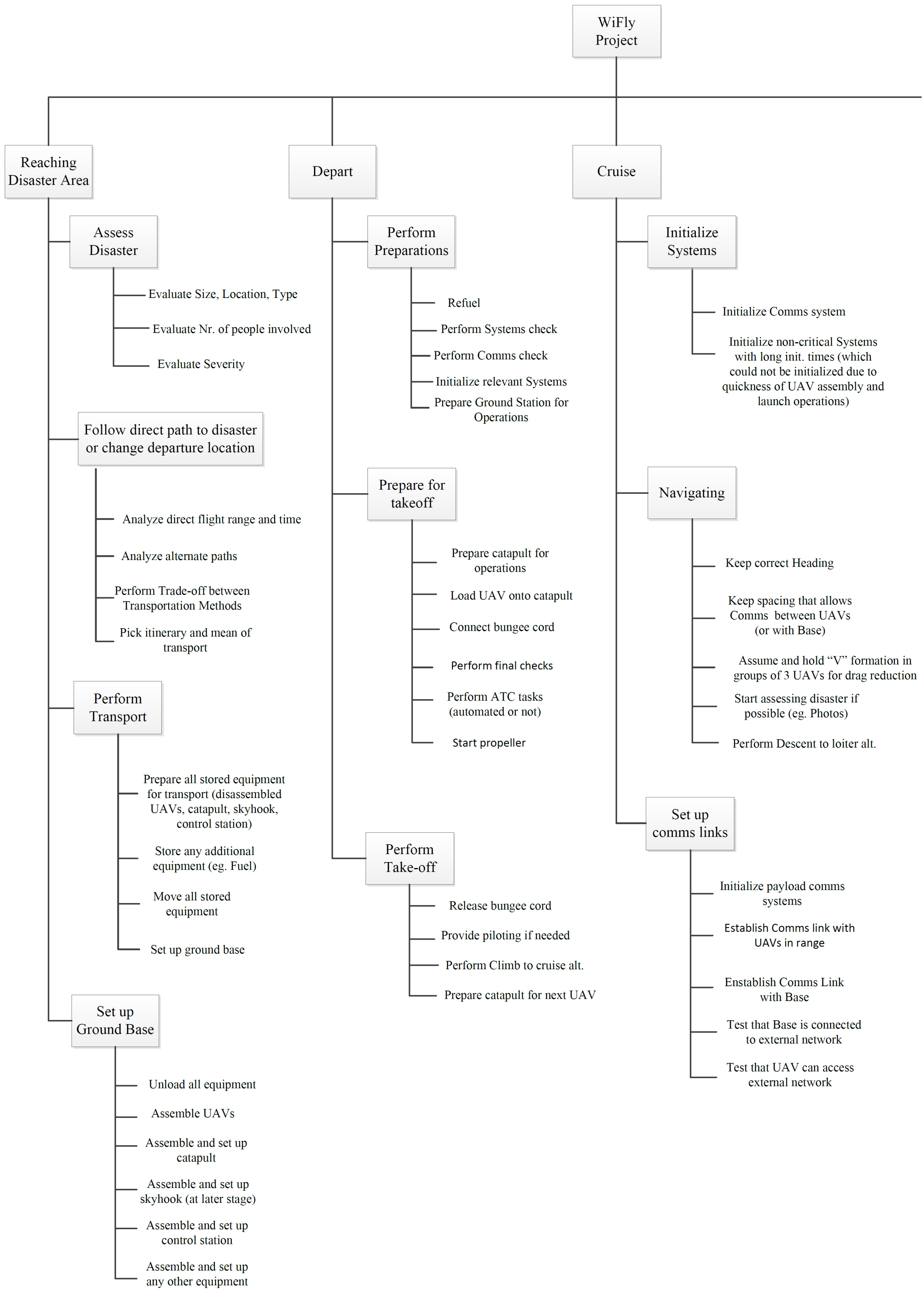

Figure A.2: First part of the Functional Breakdown Diagram

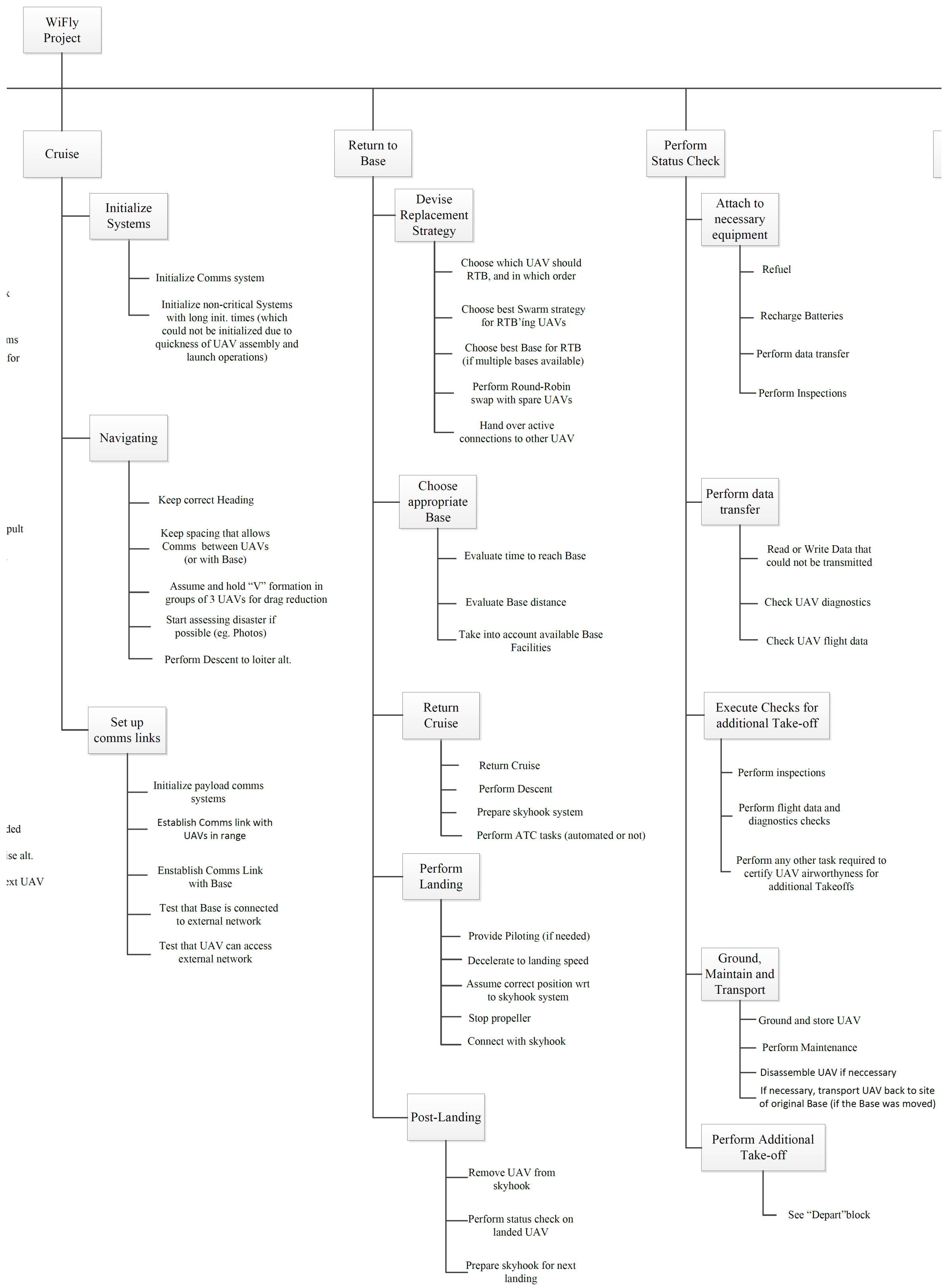

Figure A.3: Second part of the Functional Breakdown Diagram

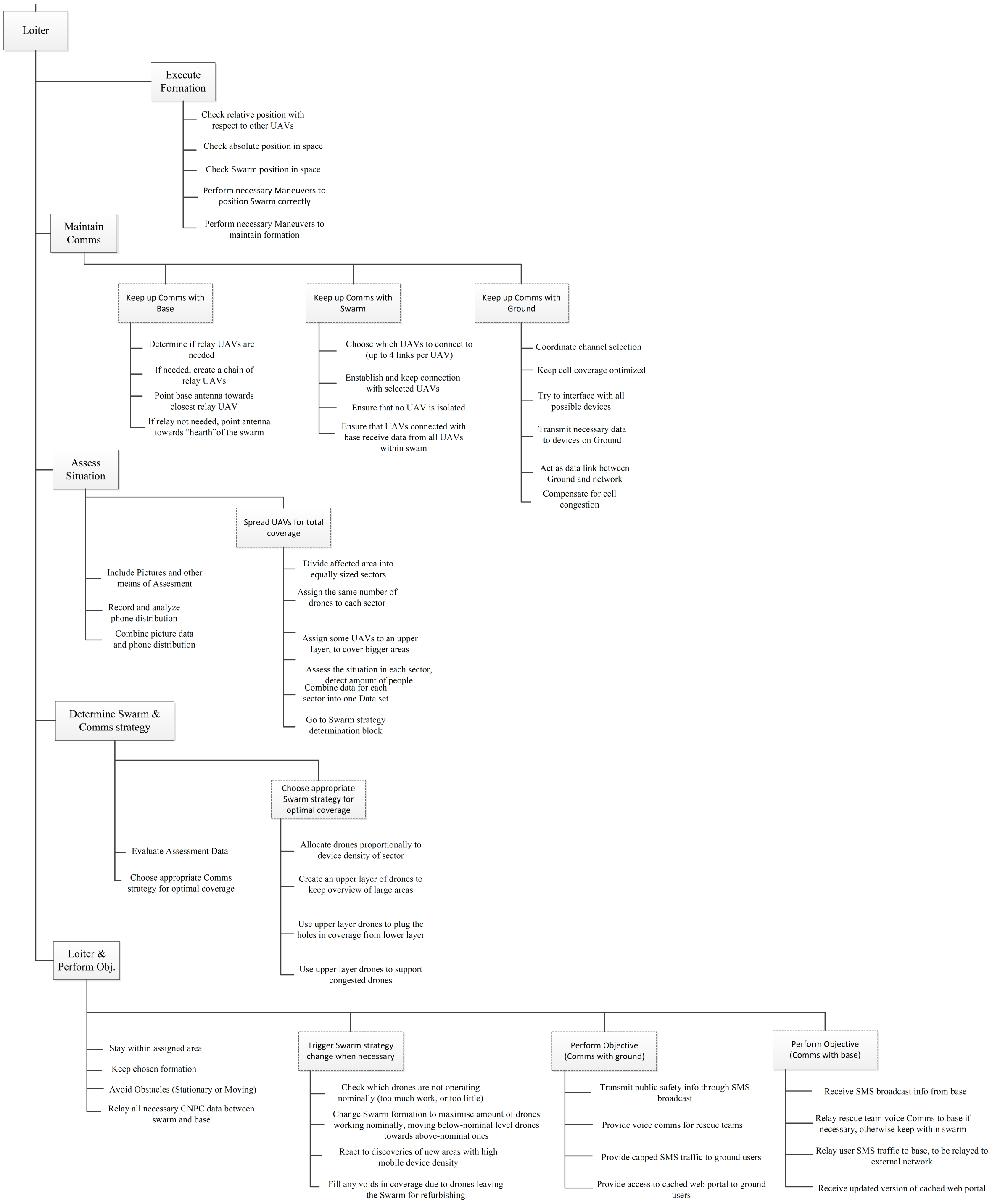

Figure A.4: Third part of the Functional Breakdown Diagram. The "Loiter" block is directly under the "WiFly Project" one

B | LOADS ON THE FUSELAGE

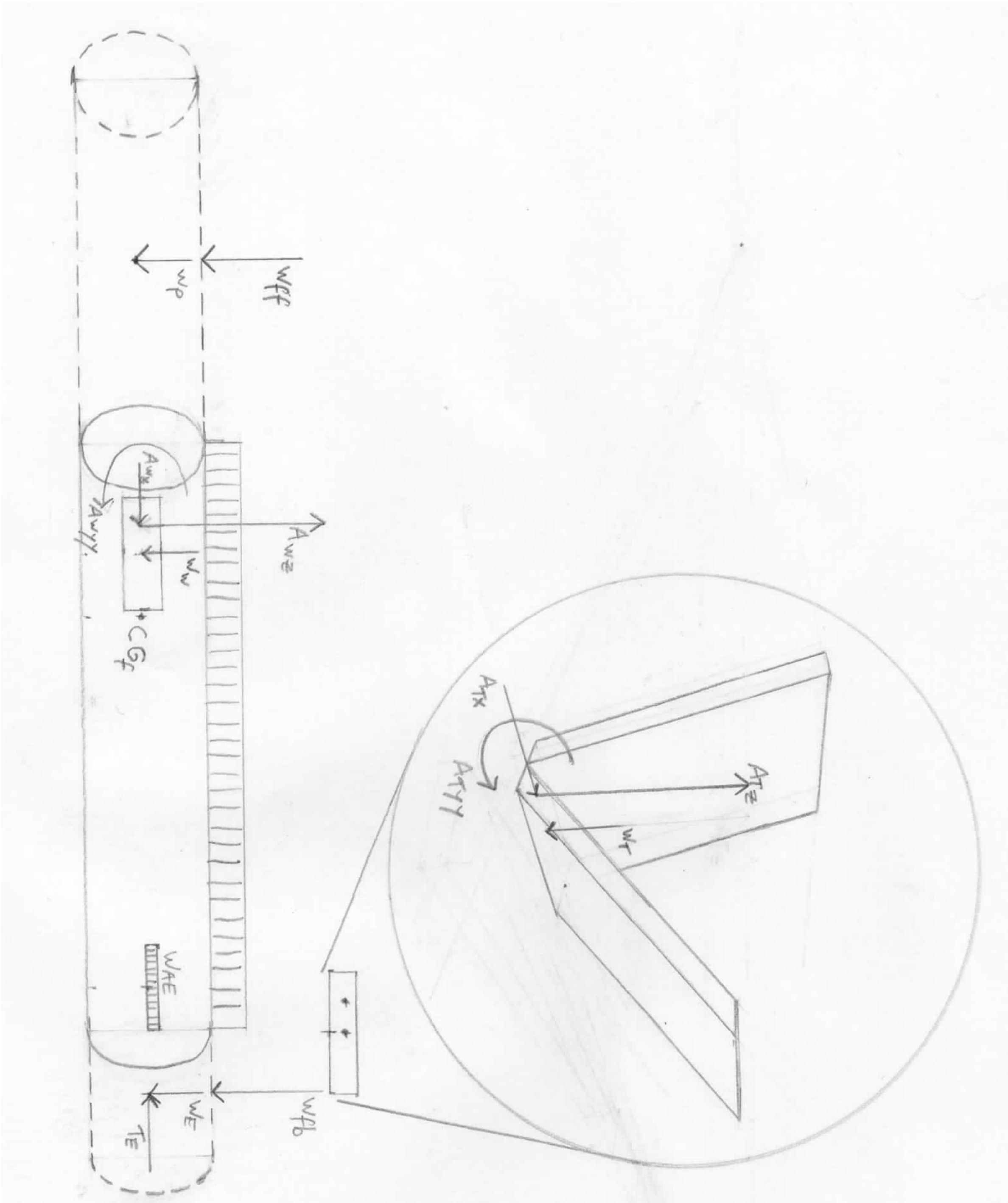

Figure B.1: The Loads on the fuselage due to a gust.

C | Communication system Appendix

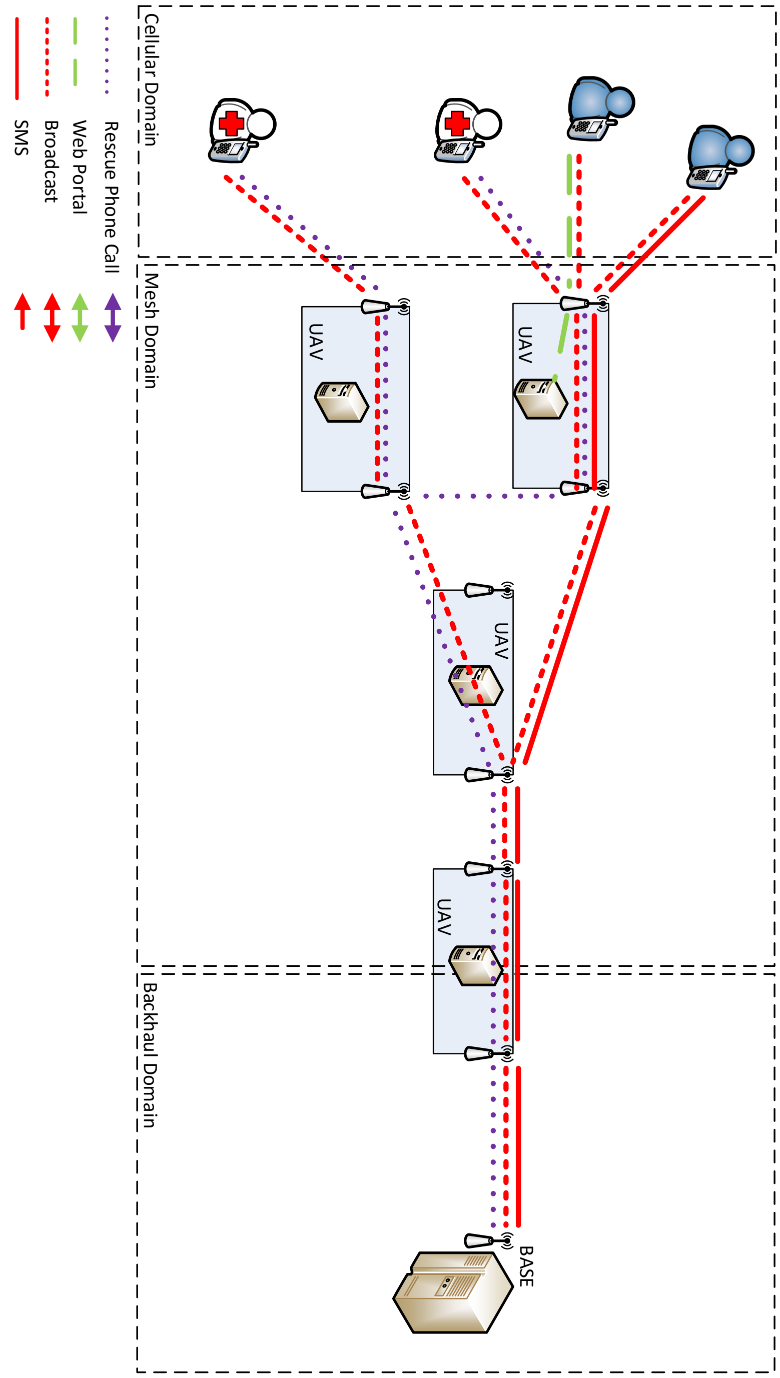

Figure C.1: Diagram showing how the users can interact with the different communication services, as well as the path followed by the data belonging to each different mode.

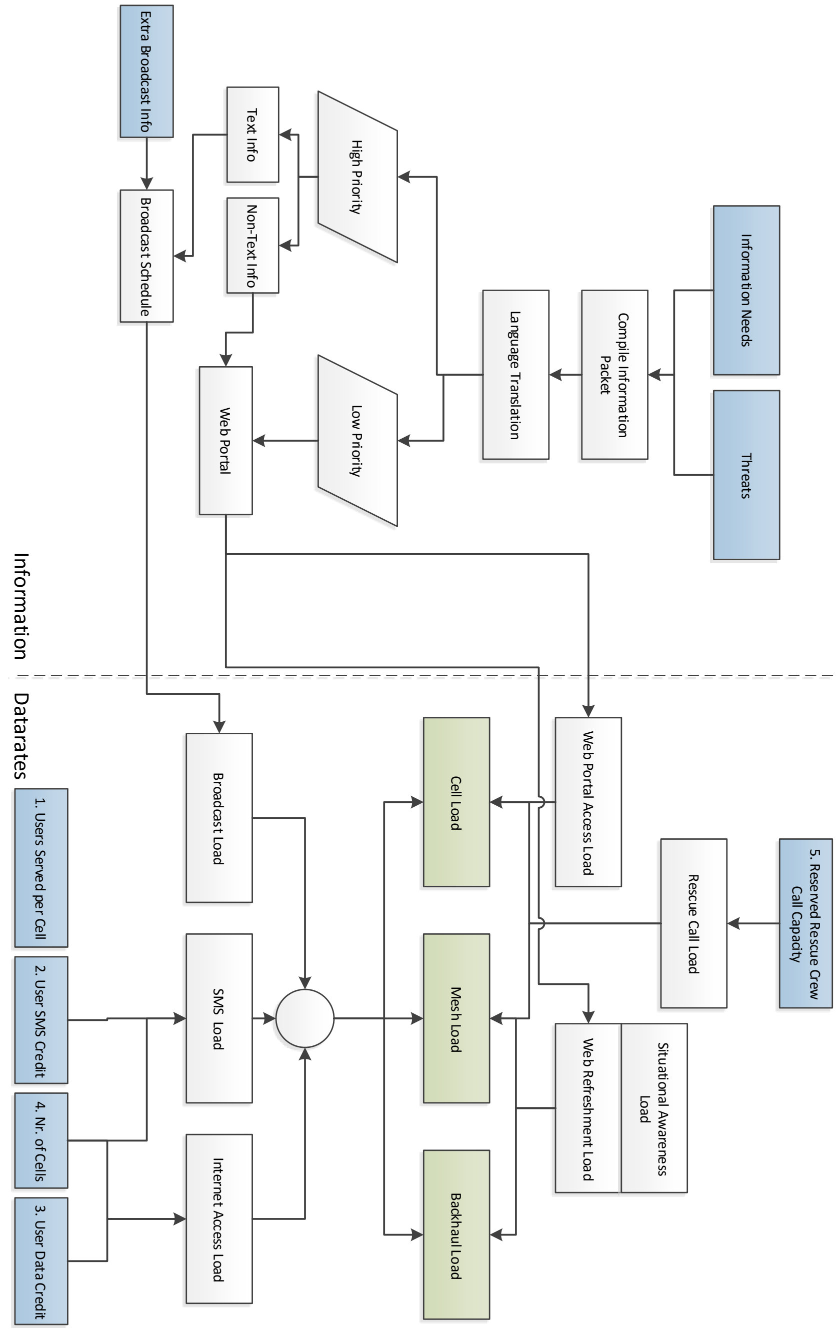

Figure C.2: Influence of each type of information on the data rates of the different communication links.

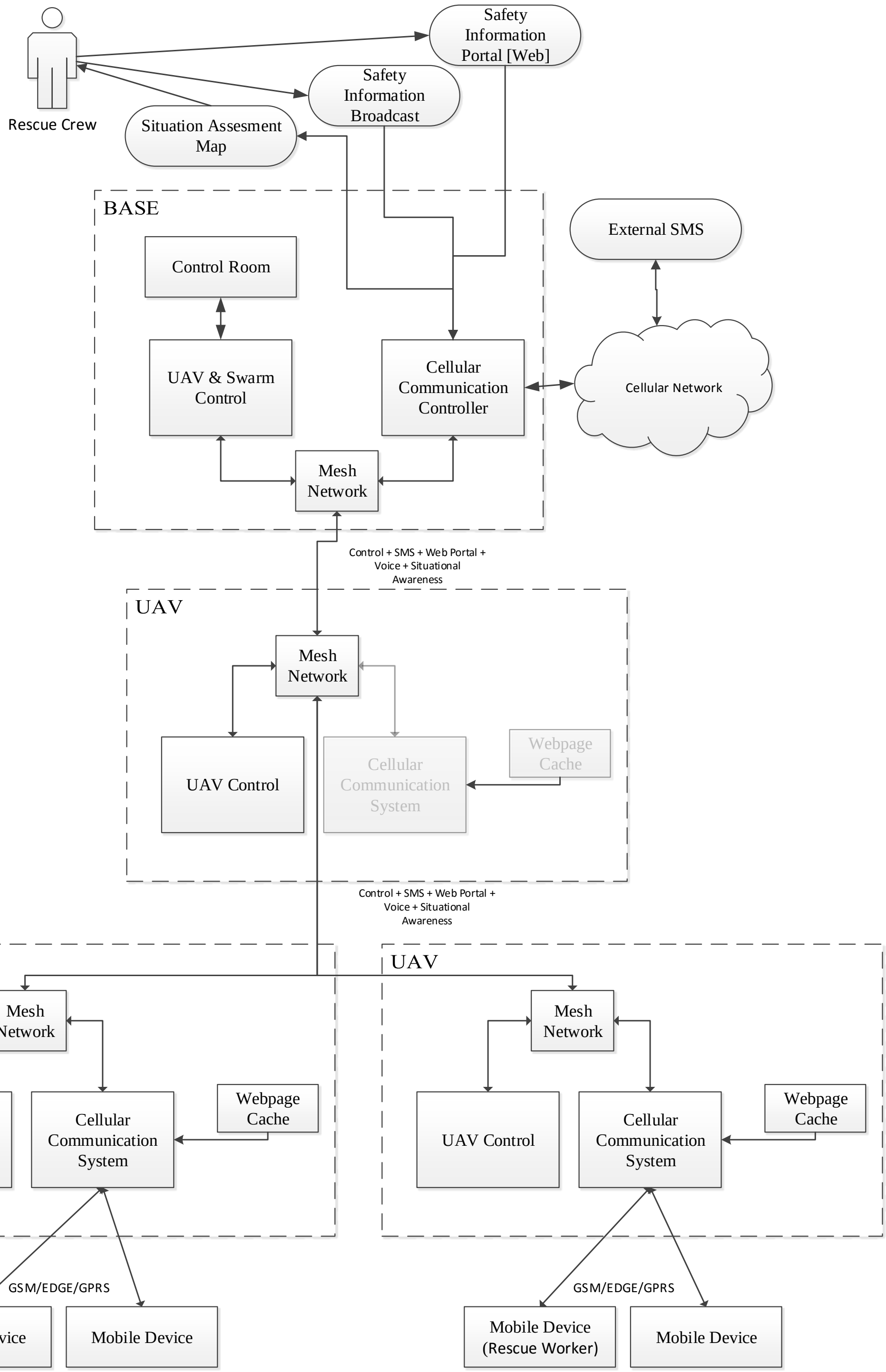

Figure C.3: Communication flow diagram.

D | List of Engines

Table D.1: List of possible engines

Manufacturer	Type	Fuel type	m [kg]	P_{max} [kW]	RPM	FC[1] [kg/h]	Price[2]
3W International	110i B2	Aspen 2	3.1	8.17	7850	4.69	€1343
3W International	157xi B2 TS	Aspen 2	4.1	14.06	6400	6.67	€1624
3W International	170xi B2 TS	Aspen 2	4.1	9.43	5650	5.42	€1785
3W International	210xi TS	Aspen 2	5	13.42	6450	6.80	€2293
3W International	275xi B2 TS	Aspen 2	7	18.92	7050	9.91	€2879
3W International	342i B2 TS	Aspen 2	8.8	23.53	7050	10.82	€4221
Advanced Innovative Engineering	125CS	Avgas 100LL/gasoline	7	15	8000	5.25	?
Hirth	2702 V	min. 95 octane	31	29.4	5500	12.28	€2944
Hirth	F 23 LW AS	min. 95 octane	22	36.7	6500	12.28	€3725
Hirth	F 33 A	min. 95 octane	12.7	18.1	6000	8.73	€2292
Hirth	F 33 AS	min. 95 octane	12.7	20.6	6500	10.37	€2755
Hirth	F 33 B	min. 95 octane	12.7	18.1	6200	9.01	€2292
Hirth	F 33 BS	min. 95 octane	12.7	20.6	6500	10.37	€2755
Hirth	F 33 ES	min. 95 octane	12.7	20.6	6200	9.55	€2755
Hirth	F 36	min. 91 octane	9.4	11	6000	6.55	€1719
Limbach	L 275 E	Avgas 100LL	7.2	15	7200	7.58	€2378
Limbach	L 550 E	Avgas 100LL	16	37	7500	16.52	€8642
Limbach	L 550 EF	90 oct. gasoline	15	37	7000	14.89	€8910
Rotax	582 UL	Avgas 100LL	29.1	48	6500	19.47	€5638
Rotron	300EFI	Avgas 100LL	11.9	22.4	6500	7.22	?
Rotron	300HFE	Jet A1/JP5/JP8	11.8	22.4	6600	7.90	?
Rotron	600HFE	Jet A1/JP5/JP8	21	38.8	6500	15.34	?
Rotron	600LCR	Avgas 100LL	21.2	40.3	6500	14.59	?

[1] This is the fuel consumption of the engine at maximum power.
[2] The prices were obtained from different retailers and not necessarily from the manufacturer, thus they serve as an indication only.

E | USAR.nl Meeting summary

On the 31st of May, a meeting with the head coordinator of USAR.nl, Martijn Boer, took place at 11:00. The main purpose of the meeting was to gain insight in the operation and logistics of a search and rescue team, while presenting the current design to see whether it complies with real-life operation. Urban Search And Rescue Netherlands (USAR.nl) is the only Dutch self-sufficient non-military search and rescue team, with their headquarters located in Zoetermeer. USAR.nl is a UN classified 'Heavy Team' and deal with cases in the Netherlands and abroad.

Martijn Boer starts the presentation by stating that the entire SAR process is very politically oriented. This becomes apparent when teams do not cooperate with each other due to geopolitical reasons. With help from USAR.nl, the operation and logistics in Nepal has been taken care of, since the Dutch are deemed neutral. The airport of Kathmandu was overloaded with the 76 different SAR teams arriving and leaving at the same time. It appears this was not unique to the Nepal, but occurs often in rescue operations as every team is trying to be the first (for reputation sake). NGOs will always be faster as they do not require permission from its governmental body.

Communication problems are present in disaster areas. However, the main reason is not what was expected at first. A communication network is usually operative, but overloading peak traffic loads during the first 72 hours hinder teams from using it. Communication through satellite is possible but expensive (€18k for 10 days), and channels are bought by commercial parties, mostly media. An international platform called vOSOCC by Global Disaster Alert and Coordination System (GDACS) is used to report any activities performed. However, it has been found too slow to be useful, and efficiency is still lost due to double work. SMS seems to be a reliable medium that always works and is nearly instant.

The most important features that would be useful in rescue operations are all based on the initial assessment of the area. Having maps with locations and hotspots of people and pictures or maps of the affected area would decrease the time spent on the assessment. Nowadays, most rescue operations are based on local information. Also it is important to keep in mind that during the first 72 hours, which are deemed to be the most important when saving people, an overloading of the system is to be expected. Telephones are still charged and everyone is contacting relatives and emergency services. After these 72 hours, this overload will have passed, but so will the most important timeframe for saving lives. This is mostly due to batteries running empty, rendering the WiFly system itself useless.

Although drones and their possibilities are heavily looked into, most teams have a different opinion of what would be useful in such a situation. Modular drones might be the solution for this, as this can cover all functions deemed useful in such operations. Search and Rescue teams however, have limited budgets. According to Martijn, maintaining 4 SAR teams including equipment and base costs 1.8M€ per year, with 500k€ for deployment. This is excluding the transport aircraft, which needs to be eithered purchased, rented or borrowed.

F | GANTT CHART

WBS	Task Name	Work	Duration	Start	Finish	Predecessors
1.4.6	**Finalise Detailed Desing**	**22.380 hrs**	**255 days**	**Wed 15-6-16**	**Tue 6-6-17**	
1.4.6.1	**Base station**	**3.000 hrs**	**26 wks**	**Wed 15-6-16**	**Tue 13-12-16**	
1.4.6.2	Base commnunication	0 hrs	4 wks	Wed 15-6-16	Tue 12-7-16	
1.4.6.3	Mobile communication	500 hrs	4 wks	Wed 15-6-16	Tue 12-7-16	
1.4.6.4	Propulsion	200 hrs	2 wks	Wed 15-6-16	Tue 28-6-16	
1.4.6.5	Electric	200 hrs	2 wks	Wed 15-6-16	Tue 28-6-16	
1.4.6.6	(Swarm)Control and Stability	6.000 hrs	51 wks	Wed 15-6-16	Tue 6-6-17	
1.4.6.7	Avionics	480 hrs	4 wks	Wed 15-6-16	Tue 12-7-16	
1.4.6.8	Aerodynamic	6.000 hrs	51 wks	Wed 15-6-16	Tue 6-6-17	
1.4.6.9	Structures	6.000 hrs	51 wks	Wed 15-6-16	Tue 6-6-17	
1.5	**Tests Parts and Systems**	**4.100 hrs**	**330 days**	**Wed 29-6-16**	**Tue 3-10-17**	
1.5.1	Produce Parts	1.000 hrs	51 wks	Wed 29-6-16	Tue 20-6-17	68
1.5.2	Test Parts	600 hrs	3 wks	Wed 21-6-17	Tue 11-7-17	74
1.5.3	Assemble System	500 hrs	4 wks	Wed 21-6-17	Tue 18-7-17	74
1.5.4	Test System	1.000 hrs	5 wks	Wed 19-7-17	Tue 22-8-17	76
1.5.5	Redsign	1.000 hrs	6 wks	Wed 23-8-17	Tue 3-10-17	77
1.6	**Prototype and Validate**	**31.000 hrs**	**350 days**	**Wed 4-10-17**	**Tue 5-2-19**	
1.6.1	Produce Prototype	12.000 hrs	26 wks	Wed 4-10-17	Tue 3-4-18	78
1.6.2	Test Prototype	8.000 hrs	26 wks	Wed 4-4-18	Tue 2-10-18	80
1.6.3	Validate Performance	6.000 hrs	30 wks	Wed 4-4-18	Tue 30-10-18	80
1.6.4	Discuss Performance	200 hrs	2 wks	Wed 31-10-18	Tue 13-11-18	82
1.6.5	Improve Design	4.800 hrs	12 wks	Wed 14-11-18	Tue 5-2-19	83
1.7	**Certify**	**30.000 hrs**	**315 days**	**Wed 6-2-19**	**Tue 21-4-20**	**79**
1.7.1	Performe Test	20.000 hrs	51 wks	Wed 6-2-19	Tue 28-1-20	79
1.7.2	Improve Design	10.000 hrs	12 wks	Wed 29-1-20	Tue 21-4-20	86
1.8	**Produce**	**120.000 hrs**	**509 days**	**Wed 22-4-20**	**Mon 4-4-22**	**85**
1.8.1	Produce Parts	60.000 hrs	51 wks	Wed 22-4-20	Tue 13-4-21	85
1.8.2	Assamble Parts	60.000 hrs	51 wks	Tue 13-4-21	Mon 4-4-22	
1.9	**Implement, Support and Maintain**	**0 hrs**	**1887 days**	**Tue 13-4-21**	Wed 5-7-28	
1.9.1	Train Personel	0 hrs	51 wks	Wed 14-4-21	Tue 5-4-22	
1.9.2	Support Operations	0 hrs	300 wks	Thu 6-10-22	Wed 5-7-28	88
1.9.3	Maintain systems	0 hrs	300 wks	Thu 6-10-22	Wed 5-7-28	88

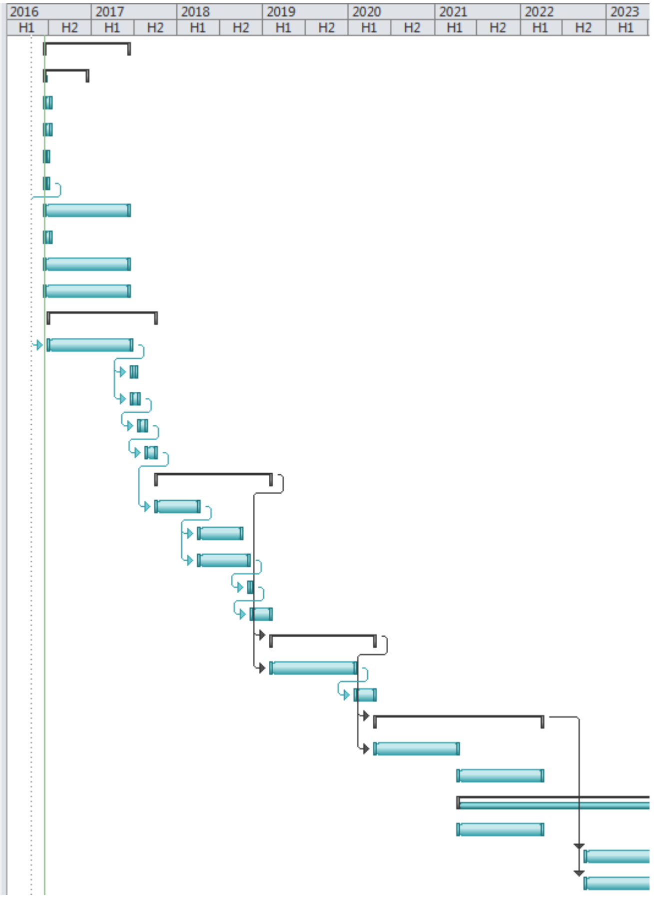

Figure F.1: The Gantt chart furture of the project, all times are estimated on other projects.